NUREG/CR-3569
PNL-4915

Spectral and Dosimetric Measurements of Photon Fields at Commercial Nuclear Sites

Prepared by P. L. Roberson, G. W. R. Endres, R. A. Fox,
D. L. Haggard, K. L. Holbrook, L. A. Rathbun

Pacific Northwest Laboratory
Operated by
Battelle Memorial Institute

Prepared for
U.S. Nuclear Regulatory Commission

GPO Printed copy price: $6.00

NUREG/CR-3569
PNL-4915

Spectral and Dosimetric Measurements of Photon Fields at Commercial Nuclear Sites

Manuscript Completed: December 1983
Date Published: August 1984

Prepared by
P. L. Roberson, G. W. R. Endres, R. A. Fox,
D. L. Haggard, K. L. Holbrook, L. A. Rathbun

Pacific Northwest Laboratory
Richland, WA 99352

Prepared for
Division of Facility Operations
Office of Nuclear Regulatory Research
U.S. Nuclear Regulatory Commission
Washington, D.C. 20555
NRC FIN B2419

ABSTRACT

Spectral and dosimetric measurements of photon fields were performed at seven commercial nuclear reactor sites. Revisions in 10 CFR 20 that specify exposure-to-dose conversion factors (C_x) much greater than unity for photons between 40 keV and 200 keV could impact personnel monitoring practices. Monitoring at effective depths of 1 cm of tissue and shallower could underestimate doses received from high-energy photon fields (>3 MeV).

No locations with large C_x factors (approximately 1.5 rad/R) were found. The most significant production of low-energy photons was found to be due to photon scattering. The scatter continuum has an effective C_x factor of approximately 1.2 rad/R. One location was found with a nearly pure scatter spectrum. Other locations contained significant contributions from medium-energy photons due primarily to radioactive decay of cobalt and cesium isotopes. Monitoring requirements at 0.007-cm and 1.0-cm depths in tissue were found to be adequate for estimating dose received in radiation fields containing high-energy photons. Enhanced surface doses attributed to high-energy knock-on electrons were measured in all locations monitored. Personnel monitoring techniques may provide inaccurate results in high-energy fields.

CONTENTS

FIGURES

TABLES

ACKNOWLEDGMENTS

The authors acknowledge the help of many support groups at the Pacific Northwest Laboratory and of the health physics groups at the reactor sites. We thank Fred Eichner, Virginia Tews and Chuck Souder for the preparation and the analyses of the TL dosimeters. We thank Mark Johnson for assistance during the site measurements. We thank Marianna Cross for word processing services and Jan Baer for editing services. We also acknowledge the help of Lori Bisping and Janet Rhodes for trip scheduling and typing of progress reports. Jack Prewett and the Pacific Northwest Laboratory graphics section did an excellent job on the many line drawings and spectra. We extend a special thanks to Chris Simonen for assistance with the computer analysis of the data.

1. INTRODUCTION

Current personnel monitoring practices may be inappropriate for radiation areas with significant contributions from photons with energies less than 200 keV. The use of an exposure-to-dose conversion factor of unity for all photon energies is specified in Title 10, Part 20 of the Code of Federal Regulations (10 CFR 20). Experimentally measured and calculated conversion factors are significantly greater than unity for energies between 40 keV and approximately 200 keV, with a maximum of 1.5 at approximately 60 keV, as listed in Table 1 (American National Standards Institute [ANSI] 1983). Revisions of 10 CFR 20 to include improved conversion factors could have a significant impact on personnel monitoring practices. In extreme cases, radiation zones may have to be monitored to determine the appropriate conversion factors.

TABLE 1. Conversion Factors for Computing Dose Equivalent from Exposure for the ICRU[(a)] Sphere (ANSI N13.11-1983, Appendix C)

Photon Energy (keV)	Conversion Factor ($rem \cdot R^{-1}$)[(b)] to Dose Equivalent in the ICRU Sphere at a Depth of		
	1.0 cm ("Deep")	0.3 cm	0.007 cm ("Shallow")
15	0.28	0.67	0.90
20	0.58	0.79	0.94
30	1.00	1.07	1.11
40	1.28	1.29	1.34
50	1.46	1.46	1.50
60	1.47	1.46	1.50
70	1.45	1.45	1.50
80	1.43	1.43	1.48
90	1.41	1.41	1.45
100	1.39	1.39	1.43
110	1.37	1.37	1.40
120	1.35	1.35	1.36
130	1.33	1.35	1.34
140	1.32	1.32	1.32
150	1.30	1.30	1.30
662	1.03	1.03	1.03

(a) ICRU = International Commission on Radiation Units and Measurements.
(b) 1 rem = 10^{-2} Sv; 1 R = 2.58×10^{-4} $C \cdot kg^{-1}$.

The presence of low-energy photons[(a)] in radiation areas is due not only directly to the decay of radioactive atoms, but also to photon scattering in shielding material. Shielding attenuates the primary photon field, scatters photons in all directions and shifts the spectral distribution to lower energies primarily through the Compton interaction (Fenyves and Haiman 1969). In heavily shielded areas, maximum fluxes of photons are expected between 50 keV and 150 keV, just above the rise in the photoelectric cross section for the atoms making up the shielding material.

Current personnel monitoring requirements may also be inadequate for dose estimations in fields with a significant contribution of high-energy photons, such as from ^{16}N (6.1 MeV). Doses deposited by high-energy photons at tissue depths of 1 cm or shallower are significantly less than those deposited at the depth of maximum dose, which is approximately 3 cm for 6-MeV photons (Johns and Cunningham 1978). Depth-dose curves presented in Figure 1 for ^{60}Co and 6-MeV photons show the reduced surface dose for the higher energies. While an "ideal" dosimeter monitoring the deposited dose at 1 cm would underestimate the actual deep dose by only approximately 20%, many practical dosimeters can underestimate the dose received by a greater amount. Dosimeters using less filtration on the deep-dose element to improve the response to x rays or to monitor at 0.3 cm for dose to the lens of the eye can indicate a dose of about half of the maximum received.

To help assess the impact of proposed changes in regulatory requirements for low-energy photon dosimetry and of current regulatory requirements for high-energy photon dosimetry, spectral and dosimetric measurements were performed at representative commercial nuclear sites. The spectral measurement equipment included intrinsic germanium (Ge) detectors, lithium-drifted germanium [Ge(Li)] detectors, and sodium iodide [NaI(Tl)] detectors. The Ge and Ge(Li) detectors were used because of their high spectral resolution. The NaI(Tl) detector measurements were performed in several locations for comparison. The dose measurement equipment consisted of ionization chambers and thermoluminescent dosimeters (TLD) embedded in a plastic material (phantom) or covered with various aluminum filters. Dose rate as a function of depth in phantom was used to assess relative dose to deep-seated organs, to estimate the spectral composition and beta-to-photon ratio, and to perform measurements using source geometries in work environments.

(a) For the purposes of this report, energies below 200 keV are referred as low energies, energies between 200 keV and 3 MeV as medium energies, and energies above 3 MeV as high energies.

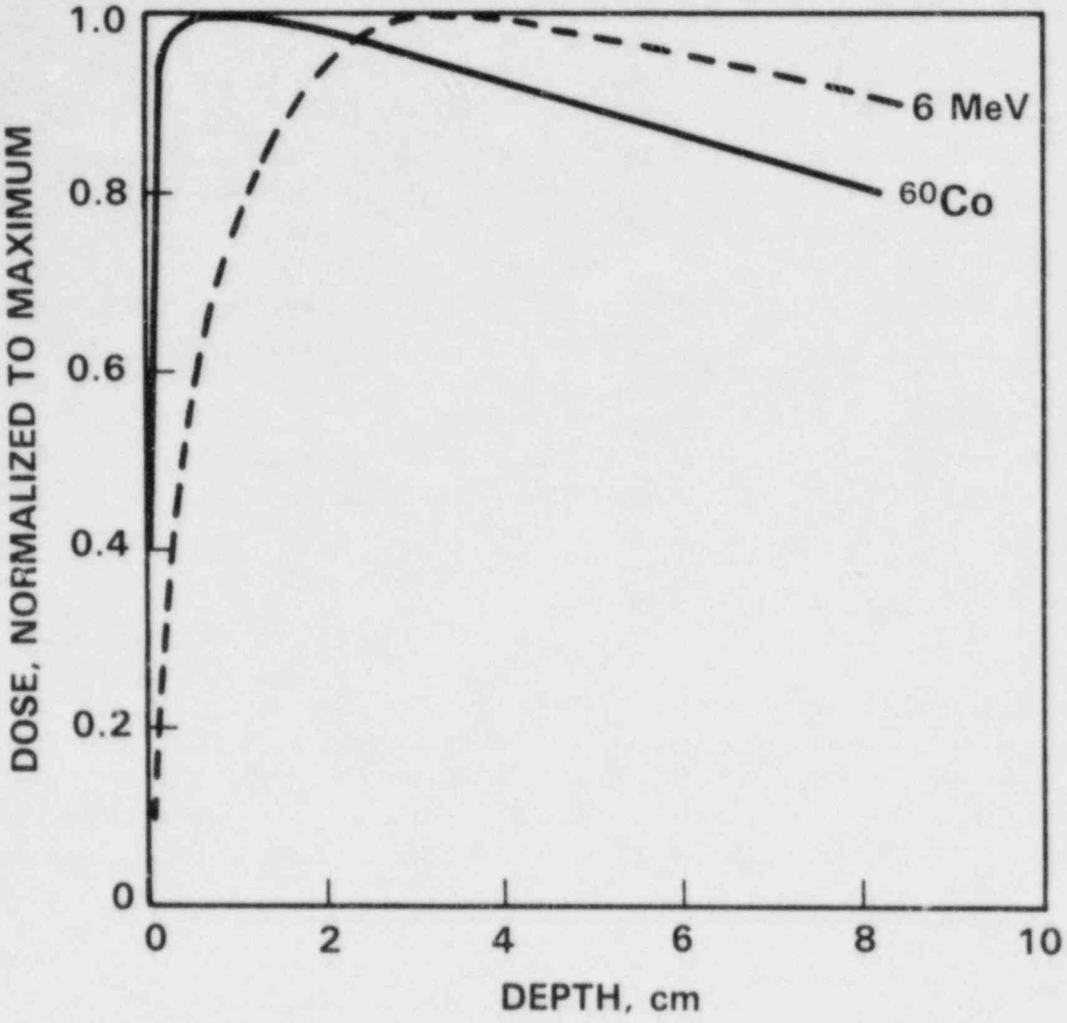

FIGURE 1. Depth-Dose Dependence on Photon Energy

Spectral measurements were performed in radiation fields of up to approximately 10 mR/h without a collimator on the detector. For fields up to 50 to 100 mR/h, a collimator was necessary to reduce the data collection rate and allow spectral data to be gathered. Ion chambers were used for greater radiation fields (above approximately 100 mR/h). The TLDs were used in areas with small and large exposure rates, overlapping with rates for both the spectral and ion chamber measurements.

Measurements were performed at seven commercial nuclear reactor sites (Table 2). These included four pressurized-water reactors (PWRs) and three boiling-water reactors (BWRs). Measurements were performed at PWRs three times while at power (operating) and three while in refueling or maintenance

TABLE 2. Measurement Sites

Site	Type	Operating Age, y	Status	Data
G	PWR	6	Operating	1/82*
K	PWR (twin)	1/2	Operating	3/82
		5	Shutdown	
B	PWR	8	Shutdown	4/82
			Operating	9/82
M	BWR	8	Operating	9/82
			Shutdown	3/83
Q	BWR	7	Operating	11/82
P	PWR	21	Shutdown	11/82
N	BWR	10	Operating	3/83

* Equipment checkout.

conditions (shutdown). All three BWRs were visited while operating and one while shutdown. One BWR and one PWR were visited during both operating and shutdown conditions for comparison. One twin PWR was visited. Operating plant ages ranged from one-half to ten years. Shutdown plant ages ranged from 5 to 21 years. The site measurements were performed between January 1982 and March 1983. Photon spectra are compiled in Appendix A.

Dose in rad and dose equivalent in rem are used synonymously in this report. The quality factor for photons is assumed to be unity.

2. MEASUREMENT PROCEDURES AND ANALYSIS TECHNIQUES

The methods of data collection for the photon spectrometers, the tissue-equivalent extrapolation chamber and the TL dosimeters are given below. Details of photon field measurement techniques are given in Appendix B.

2.1 PHOTON SPECTROSCOPY

Data accumulated with the photon spectrometer system were analyzed to determine spectral composition and radioisotope identification. Figure 2 contains an example block diagram of the equipment arrangement. The Ge, Ge(Li) or NaI(Tl) detectors required high voltage input. The Ge and Ge(Li) detectors also required preamp power. The signal was input to the amplifier, which was typically built into the multichannel analyzer system. Data were stored on magnetic tape cassettes, and were transferred to the analysis computer after measurements were completed.

Raw data were in the form of pulse-height distributions. The detector did not collect the full energy for most photons because of the escape of scattered photons. The pulse-height distributions were corrected for detector efficiency and scattering losses to yield energy spectra. The analysis procedure is outlined in Figure 3. Using source geometry constraints, the detector was calibrated for efficiency and response (scattering loss) as a function of energy. During data analysis this information was used to convert the pulse-height distributions to energy spectra.

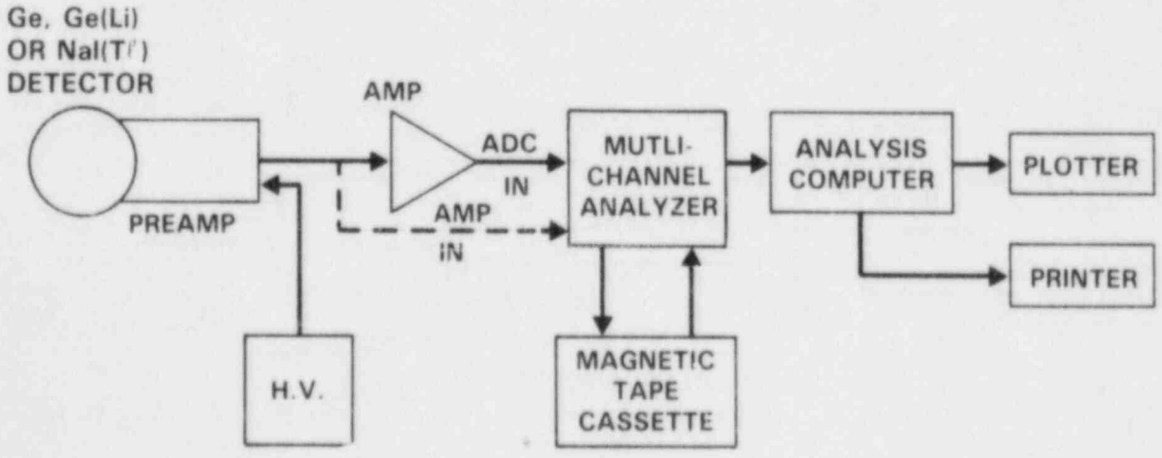

FIGURE 2. Equipment Arrangement for the Photon Spectrometer

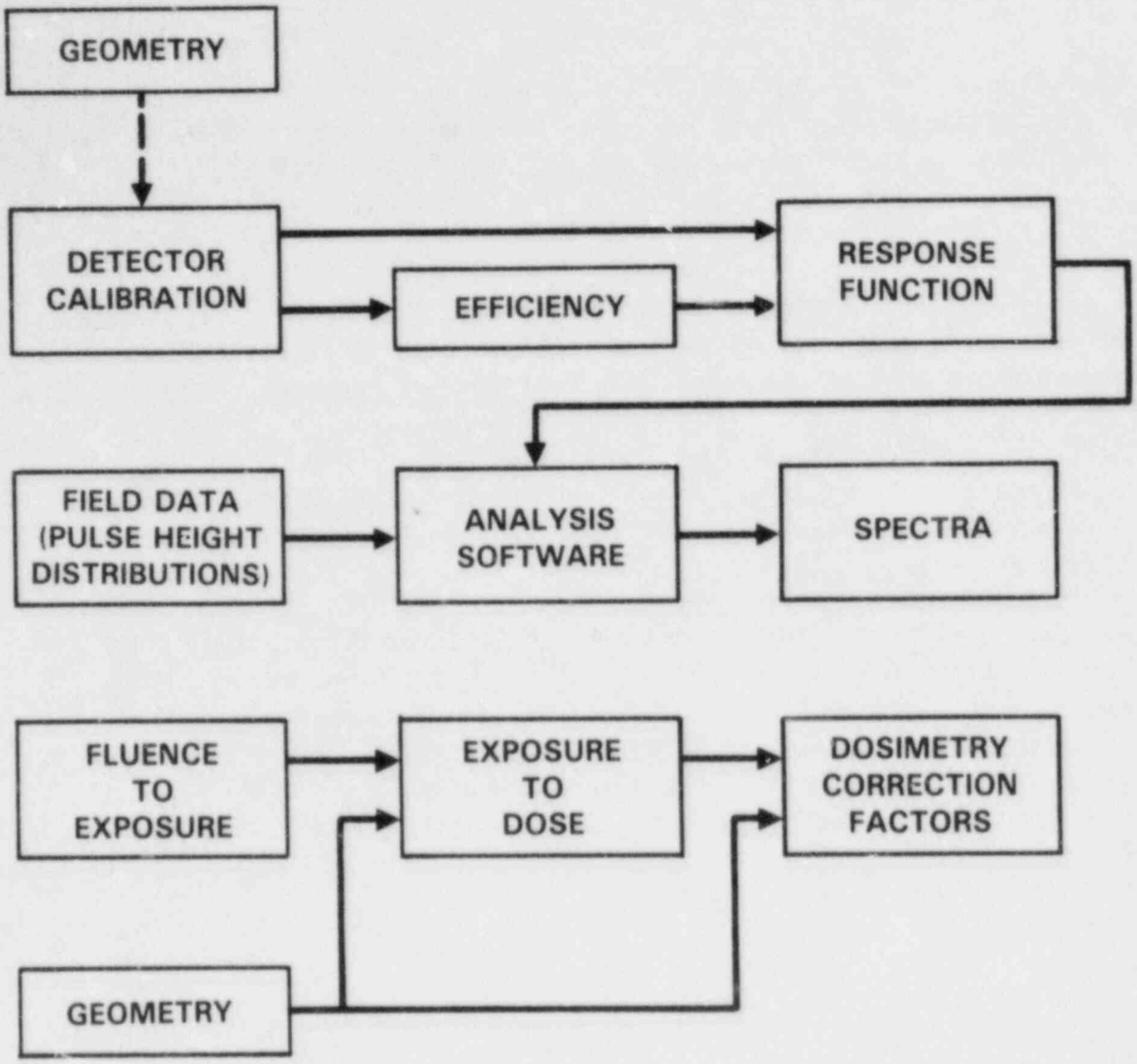

FIGURE 3. Block Diagram of Data Analysis Procedure for the Spectral Measurements

The efficiency curve for the intrinsic Ge detector used for most of the measurements is presented in Figure 4. The low-energy decline of efficiency is due to the thickness of the detector window. The high-energy decline is due to the increase in the penetrating power of photons at the higher energies. The efficiency was measured using radioisotope mixtures with known relative

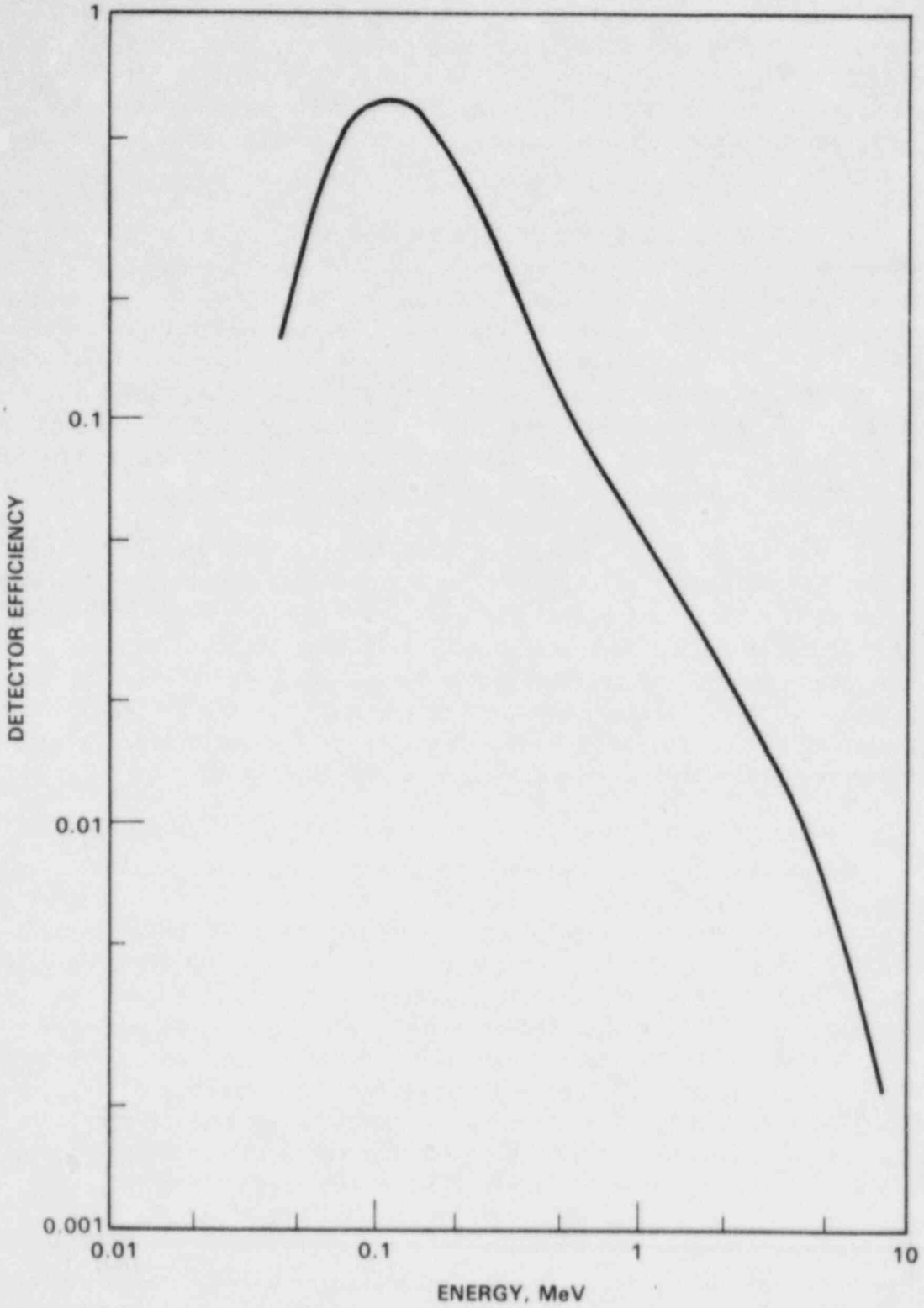

FIGURE 4. Efficiency Curve for a Ge Detector

photon intensities up to about 2 MeV. A smooth curve was drawn through the measured points using a semi-empirical model (Hajnal and Klusek 1974). The extrapolated efficiency curve above 2 MeV was checked using a ^{16}N field at a reactor site. Differences in efficiency as a function of photon entrance angle were measured to be small compared to other uncertainties of the data analysis.

The detector response function included the full-energy peak, single and double escape peaks at the higher energies, a continuum due to the loss of Compton-scattered photons, and low-energy counts due to the loss of x rays from atoms in the detector crystal. Single-energy and multiple-energy radioisotope spectra were used for input data to develop the response function. A simple parameterization for the response function was used (Seelentag and Panzer 1979). Figure 5 presents calibration data before and after the efficiency and scattering corrections. The leading edge of the Compton continuum is not fully subtracted, and remains in the corrected spectra.

Use of the simple parameterization contributed significantly to the uncertainty in the number of photons near 6 MeV versus the number at lower energies. In locations which have simple spectra dominated by 6-MeV and 511-keV photons, the undersubtraction of the leading edge of the Compton continuum added to the spectra, while the oversubtraction resulted in negative values that were set to zero. The uncertainty in the ratio of low- to high-energy photons may be as high as 50%. However, this uncertainty did not affect the results. It did not contribute significantly to uncertainties below 2 MeV.

For photon spectrometer measurements at the higher exposure rates and at locations for which directionality was considered important, a lead collimator was used. The collimator was composed of approximately 2.5 cm of lead fashioned in the shape of a cylinder with a front plate. A 3-mm-diameter hole was drilled in the center of the front plate. The collimator was mounted so that the detector could be inserted on a level surface without supporting the collimator weight. The response function of the detector with collimator was determined using isotopic sources and incorporated in the data analysis procedure. Figure 6 shows a ^{60}Co source pulse-height distribution and energy distribution following analysis with collimator corrections. The residual counts at the lower energies are insignificant compared to the ^{60}Co source photons.

The lower part of Figure 3 showed the procedure used to calculate effective exposure-to-dose correction, or C_x, factors. The corrected photon spectra represent photons entering the detector per time, or fluence. Fluence

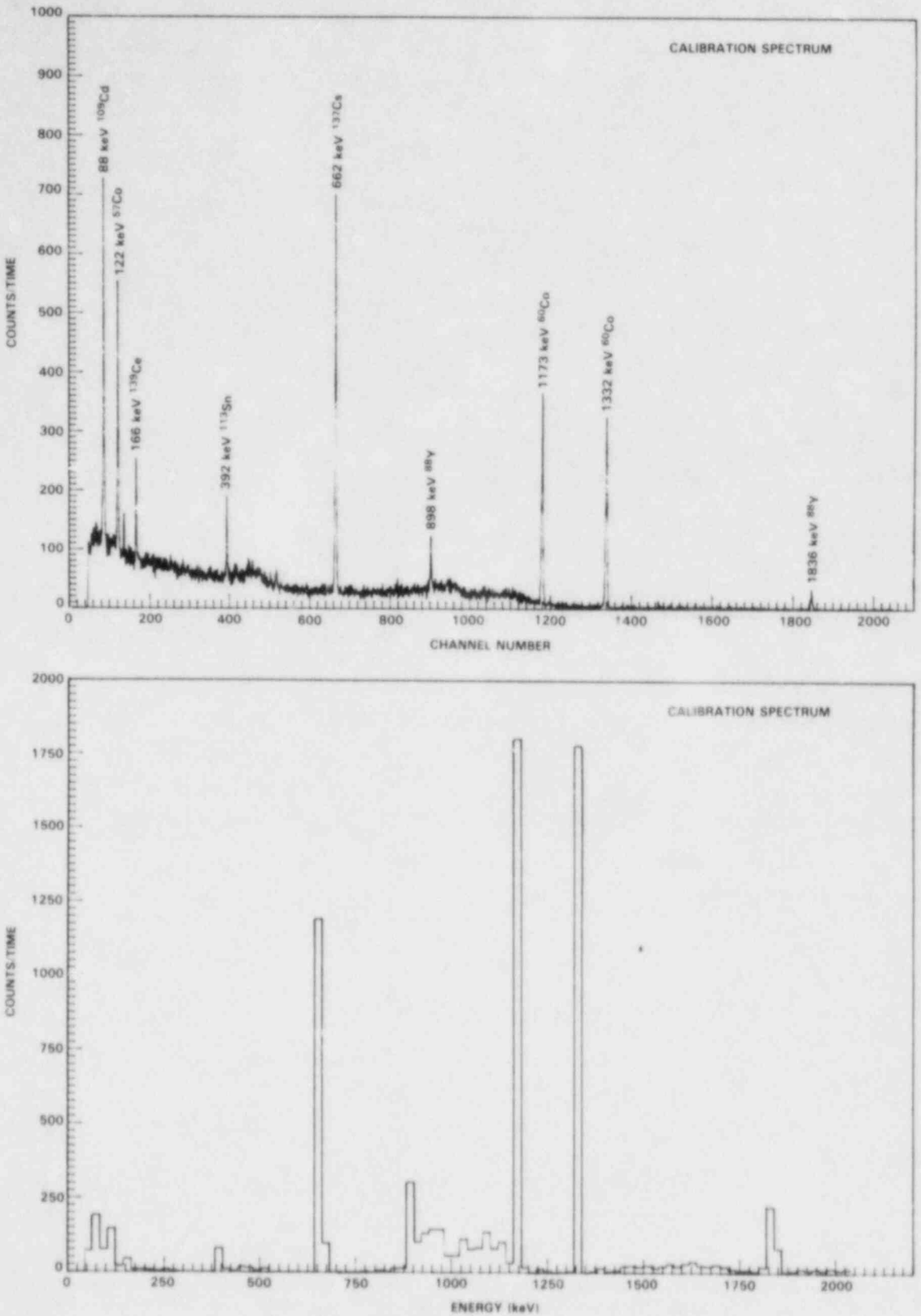

FIGURE 5. Calibration Data for the Photon Spectrometer.
Top: Before Efficiency and Scattering Corrections.
Bottom: After Efficiency and Scattering Corrections.

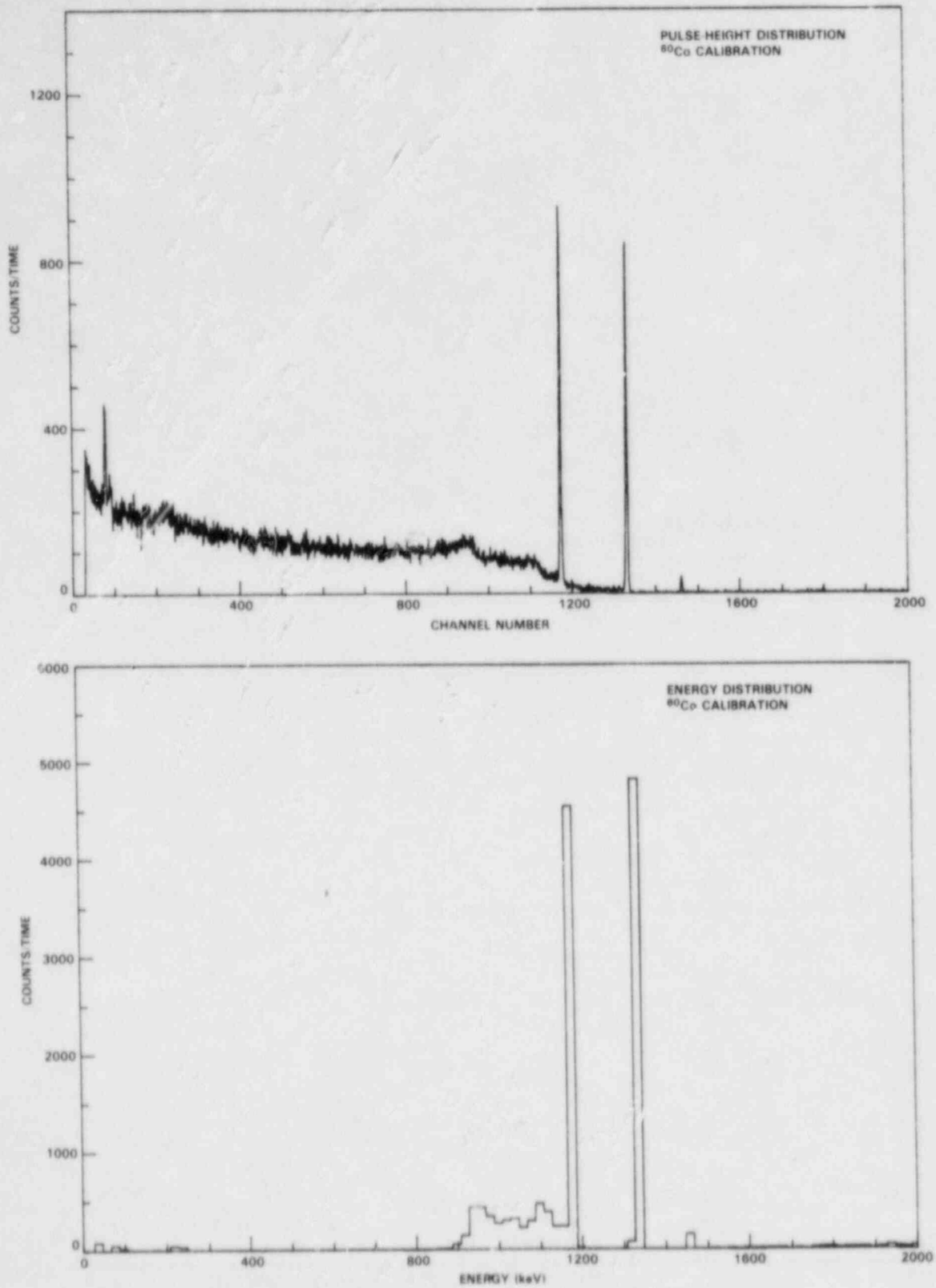

FIGURE 6. Calibration Data with Lead Collimator for the Photon Spectrometer

was converted to exposure rate for each energy interval using the curve in Figure 7 (DHEW 1970). The C_x factors taken from the calculations of Dimbylow and Francis (1979) for the ICRU sphere were weighted by the corresponding exposure rate to calculate effective C_x factors. Because factors at all energies were not available, some interpolations were required.

As indicated in Figure 3, geometry factors can significantly affect the result. Figure 8 illustrates curves for C_x factors for parallel incidence and isotropic incidence. For parallel incidence, all photons are assumed to travel parallel to each other with no intensity variations with distance. For isotropic incidence, all photons are generated in the space around the ICRU sphere, or on the inner surface of a large sphere concentric with the ICRU sphere. Photons travel in all directions. The shallow-depth C_x factors for isotropic incidence have approximately the same magnitude as the shallow and deep C_x factors for parallel incidence. However, the deep-depth C_x factors for isotropic incidence are considerably smaller than for parallel incidence. This is due to a reduction in the dose rate at 1 cm compared to the exposure rate because most of the photons have to transit a large portion of the ICRU sphere to deposit the dose.

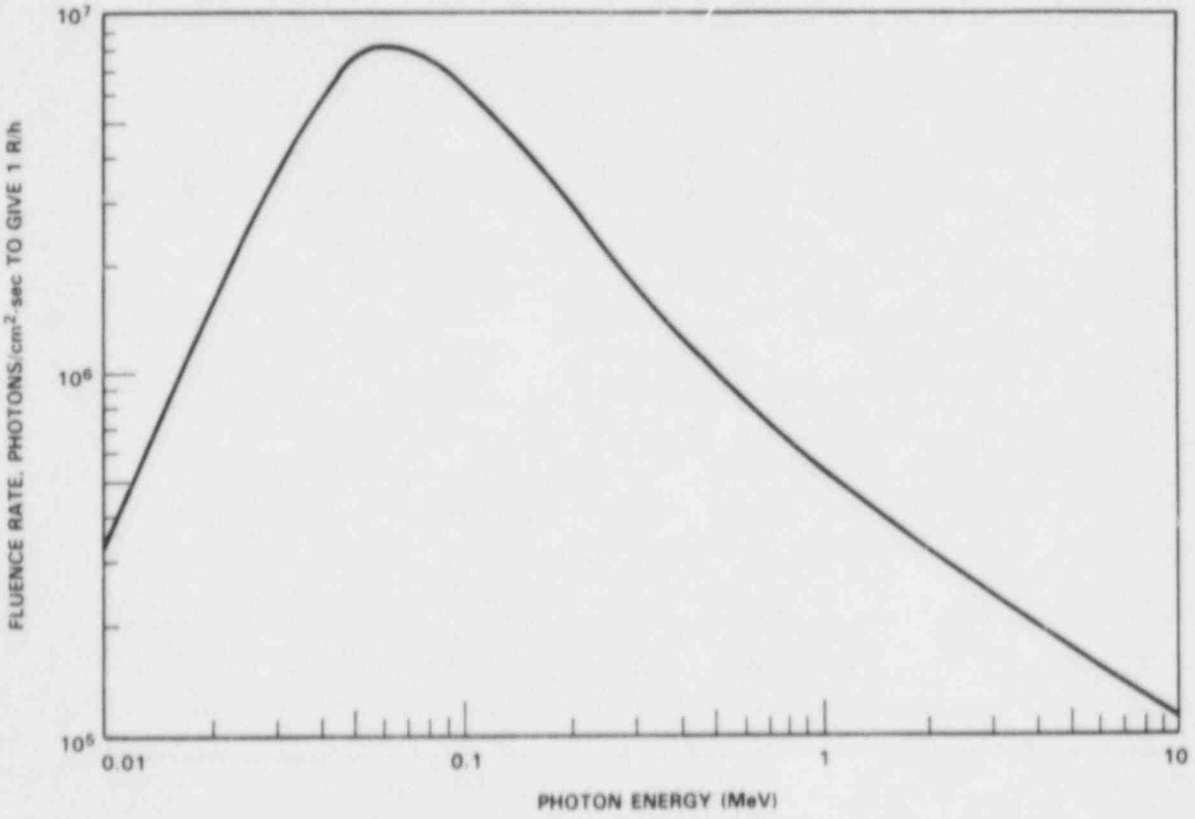

FIGURE 7. Conversion from Photon Fluence to Exposure Rate

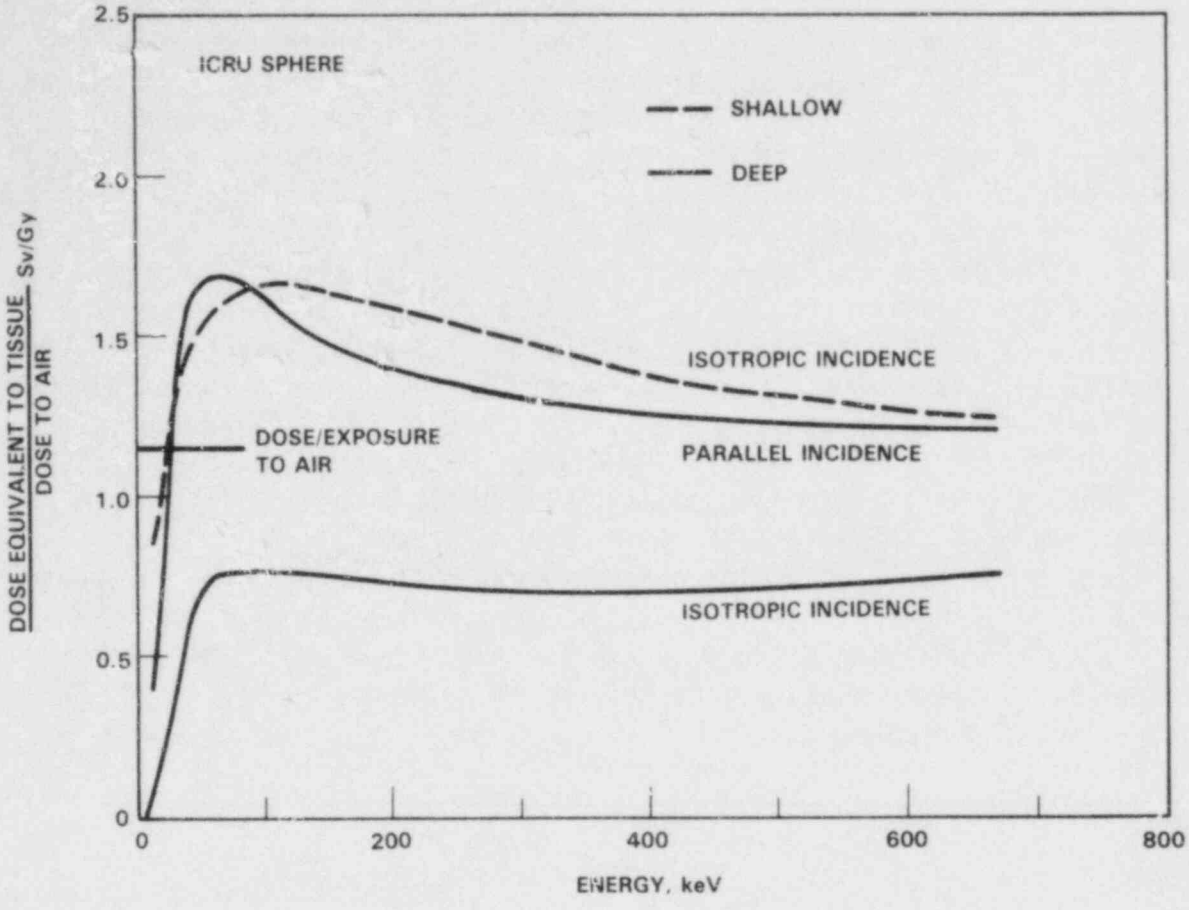

FIGURE 8. Curves for the Conversion of Exposure to Dose in the ICRU Sphere. Dose equivalent to tissue divided by dose to air is converted using dose per exposure to air.

Dimbylow and Francis calculated two C_x values: the maximum dose in the sphere at each shell depth, and the dose along the central axis of the sphere parallel to the beam direction. The central axis values approximate the worst-case example of dosimeter underresponse for high-energy photons, assuming that the dosimeter is mounted toward the source. Both quantities are listed in the data tables in Section 3 for the high-energy fields.

Correction factors other than C_x factors may be more useful for particular applications. The energy response of an instrument can be used to generate correction factors for instrument response to dose as easily as to generate conversion factors for exposure to dose.

2 2 TISSUE-EQUIVALENT EXTRAPOLATION CHAMBER AND ION CHAMBER MEASUREMENTS

Direct measurements of effective C_x factors were performed using ionization chambers to measure dose in a tissue-equivalent (TE) phantom and exposure in air at the same position. The C_x factor was obtained by calculating the ratio of dose rate to exposure rate. This technique can determine the true C_x factor for a pure photon field, including all geometry effects. For each location, the C_x factor may change with angle due to nonuniformly distributed sources. However, given the exposure rate, the dose to the ICRU sphere or a worker would change with angle in a similar manner.

The dose measurements were performed using a parallel-plate extrapolation chamber embedded inside a TE phantom. An extrapolation chamber is an ionization chamber whose volume can be varied. Data collected for many measurement volumes were used to calculate dose for the small-volume limit. A schematic diagram is shown in Figure 9. A cylindrical plug of TE plastic was moved inside a 30-cm x 30-cm x 15-cm block of the same plastic. The front surface of the plug was coated with a conducting graphite mixture and scribed into a circular collecting electrode of 27-cm^2 area and an outer guard ring. A thin (approximately 7-mg/cm^2) piece of TE plastic was stretched over the opening to provide a front window. The inner surface of the front window was coated with graphite to provide the high-voltage electrode. A stepping motor with remote

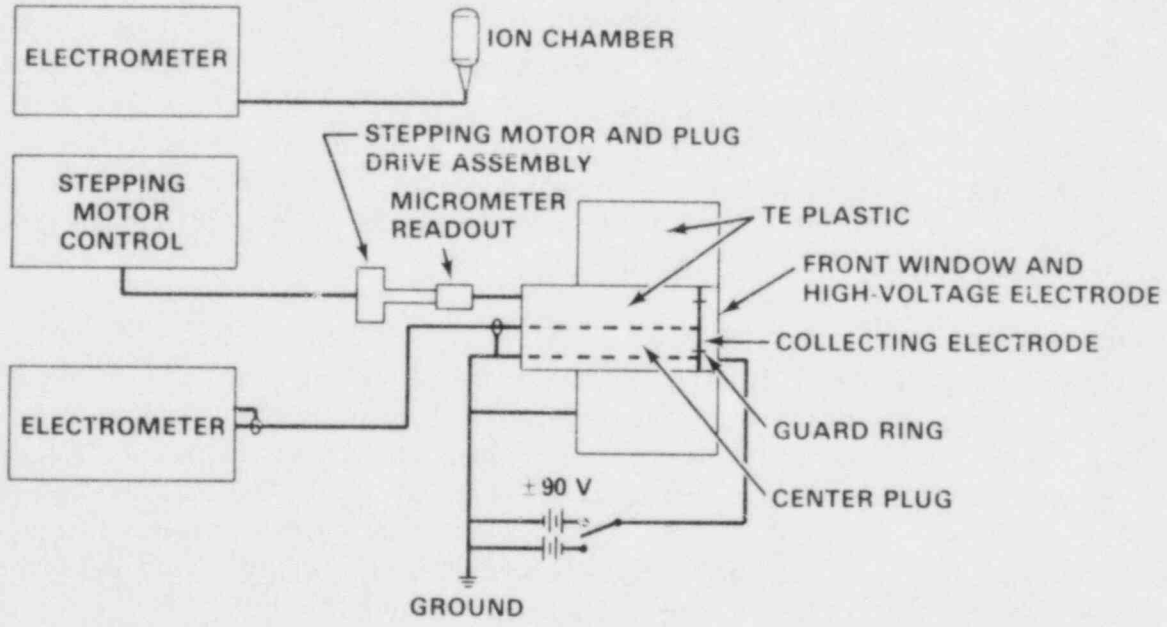

FIGURE 9. Equipment Arrangement for Tissue-Equivalent Extrapolation Chamber/Ion Chamber Combination

control was used to reduce the electrode separation in well-determined increments. The number of motor steps per millimeter was calibrated using a micrometer readout on the drive shaft. Voltage was applied to the electrodes, and the current going to ground from the collecting electrode was integrated using an electrometer. An ionization chamber and electrometer were used to measure exposure. Both the center of the front face of the extrapolation chamber and the center of the ionization chamber were reproducibly placed in a given location using a base plate and a mounting jig.

The composition of the TE plastic is described by Yoder et al. (1979). The low-energy response of the plastic is similar to that of tissue with trace elements. Nelson and Chilton (1983) performed Monte-Carlo calculations and found good agreement. Differences found between Yoder's laboratory measurements and the Monte-Carlo calculations for the TE plastic and for idealized tissue with trace elements were small compared with the uncertainties of the field measurements. Differences in response between the spherical geometry used by Dimbylow and Francis and the slab geometry of the extrapolation chamber were also small compared with the uncertainties of the field measurements. No corrections to the data were performed.

2.3 THERMOLUMINESCENCE DOSIMETRY

Thermoluminescent dosimeters were used to obtain a measurement of dose at many depths simultaneously. The distribution of dose as a function of depth changes with photon energy and beta-particle energy. The phosphors used were LiF:Mg (TLD-700) and CaF_2:Mn (TLD-400), which are sensitive to photon and beta-particle radiation. The TL material was placed inside of a 20-cm x 20-cm x 15-cm Plexiglas® (methylmethacrylate) phantom or packaged in a multielement dosimeter with varying thicknesses of aluminum filters. The multielement dosimeters were used primarily to monitor for the presence of beta particles for the extrapolation chamber measurements.

The advantages of TL dosimetry are that: 1) dose rates can vary over a wide range, overlapping both the photon spectroscopy and extrapolation chamber techniques; 2) fewer assumptions of source geometry are required compared to the photon spectroscopy techniques; 3) many depths can be monitored simultaneously; and 4) beta-particle contributions can be relatively easily identified. Disadvantages are that: 1) the data provide much less information on spectral composition, and 2) differences between the calibration and measurement geometries increase the uncertainty of the measurements.

® Plexiglas is a registered trademark of Rohm and Haas Company.

The interpretation of TLDs exposed in an unknown photon field suffers because of the non-tissue-like response of the phosphors as a function of photon energy. The response of LiF:Mg increases by almost a factor of two at x-ray energies. To improve the discrimination between energies, the CaF_2:Mn phosphor was added to three of the phantom depth positions. As shown in Figure 10, the response of CaF_2:Mn is large at x-ray energies. The ratio between phosphors was used to discriminate between energies.

The TLD were placed at eight depths, from the surface to 7 cm inside the phantom (Figure 11). They were staggered around the central axis of the phantom to reduce shielding effects by upstream dosimeters. The response of the TLD was determined for the four radiation sources listed in Table 3. The relative response per rem as a function of depth is presented in Figure 12. The estimated depth-dose response for 6-MeV photons was added for reference. The data were analyzed by performing a linear least-squares fit to the calibration data set. After the optimum combination of the calibration response

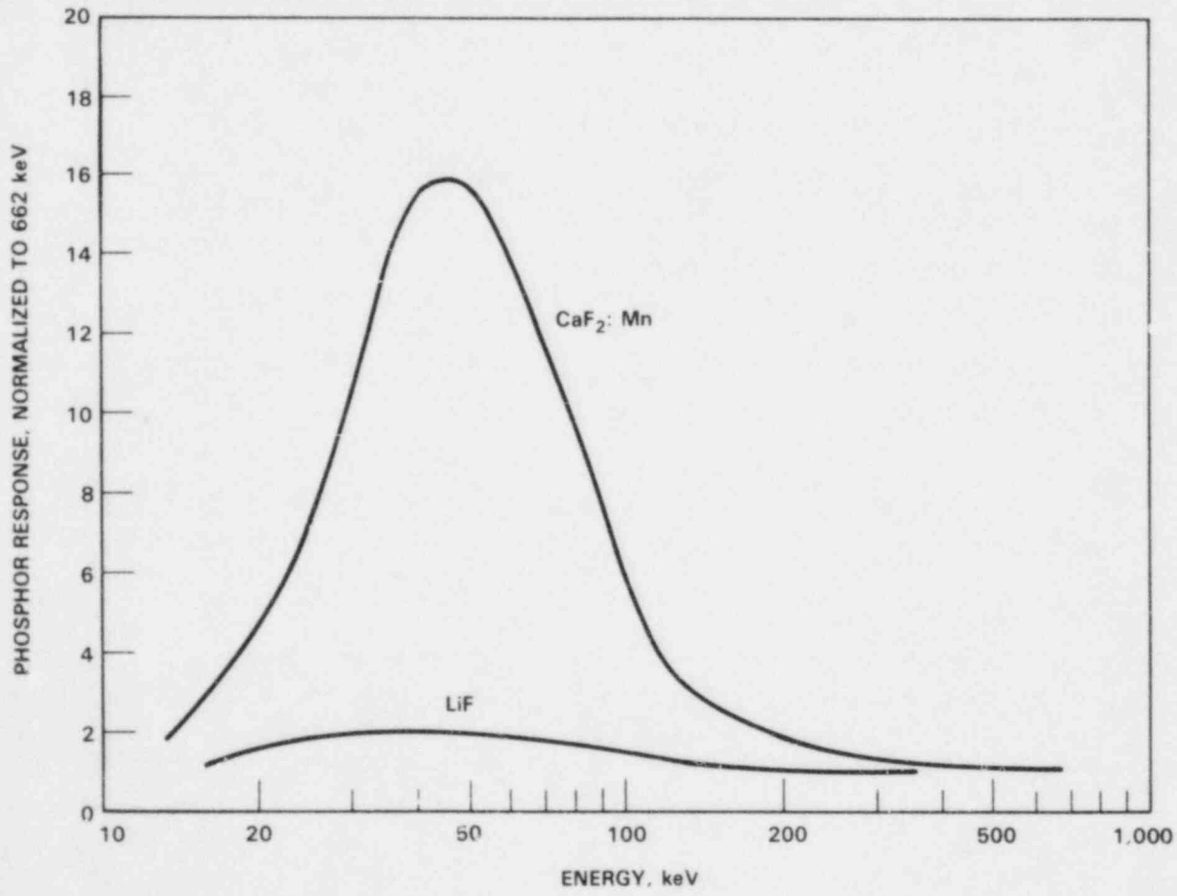

FIGURE 10. Response Comparison of CaF_2:Mn and LiF:Mg Versus Photon Energy

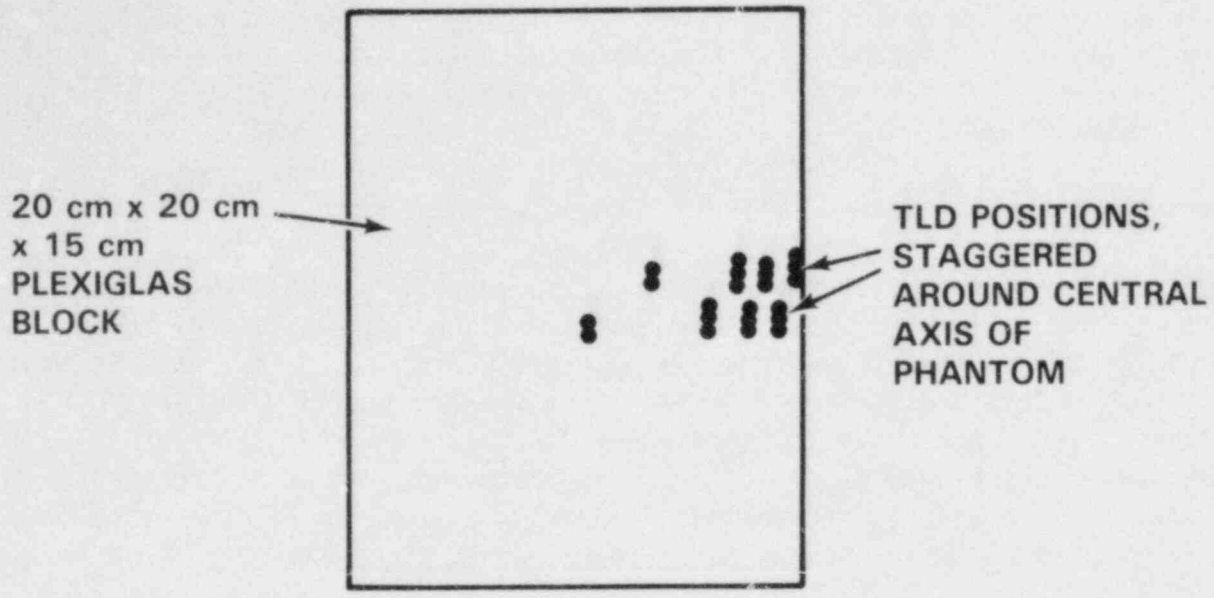

FIGURE 11. TLD-Loaded Phantom

TABLE 3. Calibration Sources for the TLD-Loaded Phantom

Source	Type	Energy	Comments
^{137}Cs	Medium-energy photon	662 keV	
MFE[a]	Low-energy photon	34 keV (effective)	NBS filter technique
H150[a]	Low-energy photon	120 keV (effective)	NBS filter technique
$^{90}Sr/^{90}Y$	Beta	2.3 MeV (maximum)	

(a) Appendix of National Bureau of Standards (NBS) Special Publication 250 (1983). Support for the MFE technique has been discontinued by NBS.

functions was determined, estimates of the effective exposure-to-dose factors were made. This technique was shown to be inappropriate for areas containing large contributions of photons above 3 MeV. Even though there is a significant difference between the response to 6-MeV photons and the response to photons of other energies, the apparent presence of very high energy electrons in plant environments did not permit a similar analysis without significant ambiguities.

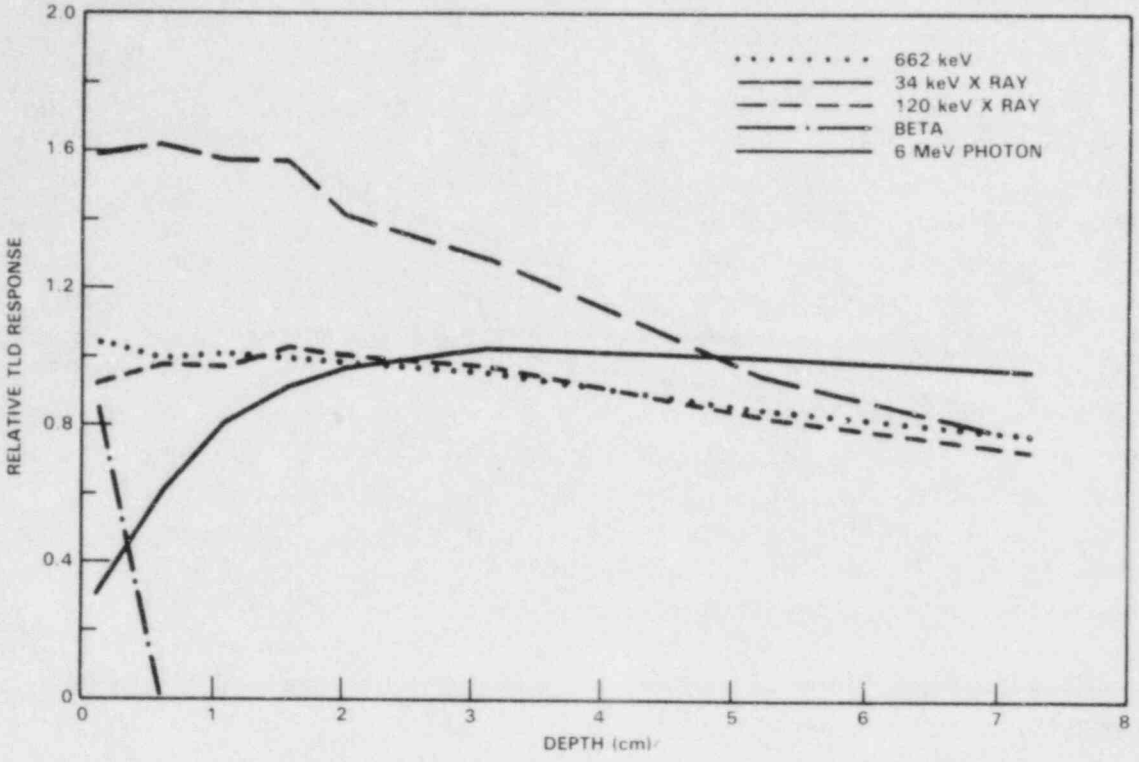

FIGURE 12. TL Response Per Rem Versus Depth

3. SITE MEASUREMENTS

Measurements were performed at seven sites. The type and amount of data collected varied due to variations in the sites' access policies, level of contamination, equipment malfunctions, and research emphasis in areas for which additional data was required.

Delays were often experienced gaining access to the plants. Training and paperwork requirements have increased over the last few years. The time delay between arrival and the initiation of measurements varied from less than 1 day to 2-1/2 days. The greatest delays occurred when formal classroom instruction was required on radiation safety, plant security, mask fitting, and the use of a self-contained breathing apparatus (SCBA). The requirements for plant access and the use of respirator protection also varied. For example, one plant required a polygraph test, another did not allow unescorted access to any plant areas, and a third required complete medical records.

Preparation time for plant access varied with the level of contamination at the measurement locations. Typically, the measurement equipment was packaged in plastic and carried or transported by cart to the site locations where it would be used. Anticontamination dress and occasionally a respirator were required. Access to PWR containment during reactor operation required full anticontamination dress and a full-face respirator or SCBA. The number of measurements were limited by the short length of stay time due to the elevated temperatures and/or dose rates.

The data collected during each site visit is described below. The letter designations for the sites were selected to correspond with neutron and beta measurement projects reported elsewhere (Endres et al. 1983; Rathbun and Roberson 1983). The sites are listed in the approximate chronological order of data collection. When a display of site layouts was considered useful, letter designations were given to each measurement location. These designations are noted on the site layouts. Spectra for all sites are compiled in Appendix A.

3.1 SITE G - OPERATING PWR

This first site visit was primarily a learning experience. The photon spectrometer measurements were not useful because dose rates exceeded maximum acceptable levels. The rates inside containment were substantially above the levels observed on previous visits. A collimator assembly for the spectrometer detector was subsequently built to allow measurements to be performed at

higher rates. The extrapolation chamber experienced almost a factor of ten increase in current not associated with radiation (leakage). This was attributed to the elevated temperatures and vibration present inside containment. The addition of an insulated mounting plate and improved electronic connectors minimized this effect during future measurement trips. A return visit to Site G was planned but was cancelled due to an extended shutdown period.

The extrapolation and ion chamber measurements performed in containment are presented in Table 4. The neutron-to-gamma dose-equivalent ratio at the measurement site was 2.5. A correction for the neutron response of the detectors shifted the dose-to-exposure ratio by less than 10%. The cause of measured values greater than unity is not understood. However, the measurements have relatively large uncertainties. The elevated surface dose indicates that current monitoring requirements are adequate.

Two TLD-loaded phantom exposures were performed, one in the auxiliary building near the primary-coolant sampling station and another in containment near the primary-side piping (hot legs) of the steam generator. These data are plotted in Figure 13. Both measurements show an enhanced TLD response at the shallow depths. The measurement performed near the sampling station was analyzed for beta and photon components (Table 5). The result was a small beta component combined with a primarily medium-energy photon component. The measurement in containment showed a large surface dose characteristic of high-energy electrons (1 to 10 MeV) with a penetrating photon component. This location was expected to contain a heavy contribution from ^{16}N or other high-energy photons. The TLD phantom measurement is consistent with the combination of high-energy photons (5 to 10 MeV) with a large number of high-energy electrons created in the surrounding building and shielding materials.

TABLE 4. Extrapolation and Ion Chamber Measurements, Site G

Location	Exposure Rate (mR/h)	Dose Rate (mrad/h)	Effective C_X Factor (rad/R)
Operating PWR			
- Containment, Facing Reactor			
- shallow	148	215	1.45 ± 0.20
- deep	103	123	1.19 ± 0.19

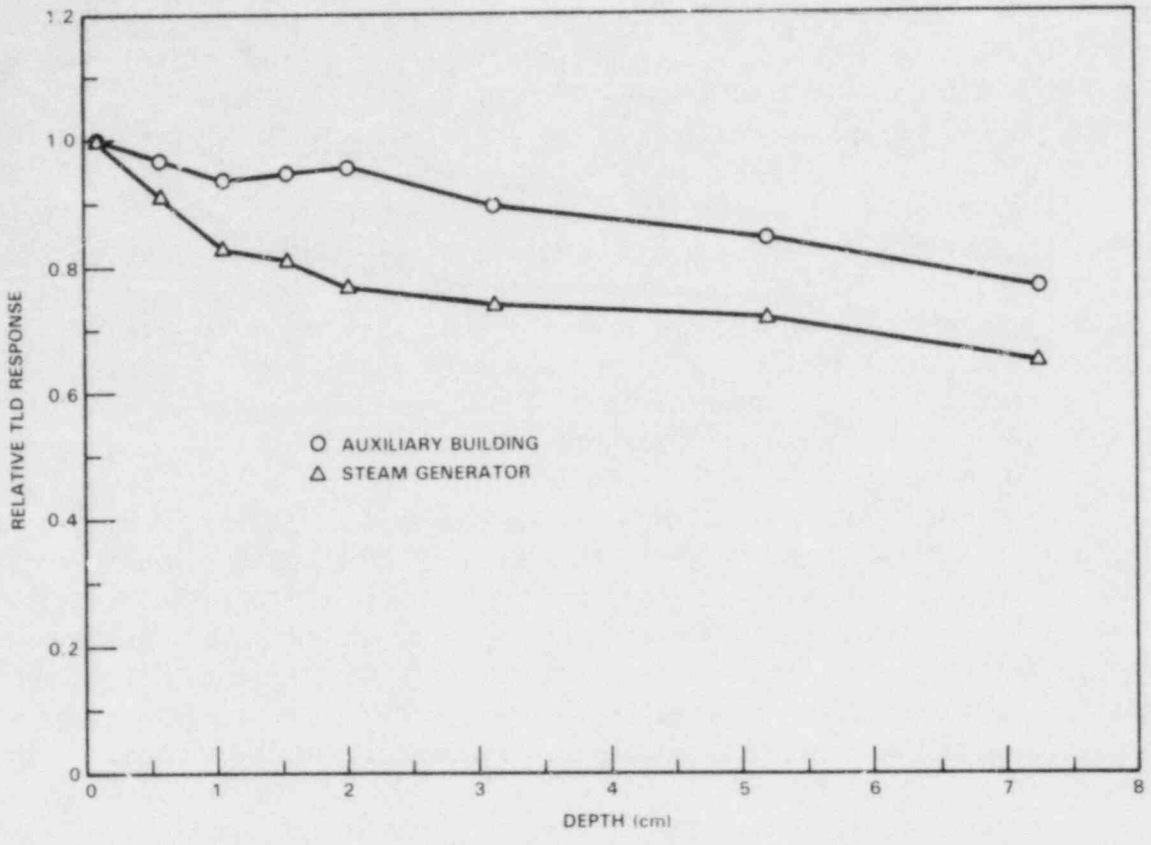

FIGURE 13. TLD-Loaded Phantom Measurements, Site G

TABLE 5. TLD-Loaded Phantom Measurements, Site G

Location	Shallow Dose Rate (mrad/h)	Field Strength (mrad/h) for Photons				Effective C_x (rad/R)
		34 keV	120 keV	662 keV	Beta	
Operating PWR						
- Auxiliary Building Sample Station	64	0	0	62	2	1.03
- Steam Generator Hot Legs	2300	(analysis inappropriate)				

The surface enhancements of the dose measured inside containment do not indicate that personnel doses are being underestimated using current monitoring requirements.

3.2 SITE K - SHUTDOWN AND OPERATING PWR

This twin-reactor site was visited while one of the reactors was shut down for maintenance and one was operating. The shutdown and operating units had equivalent full-power operating times of 5 years and 1/2 year, respectively. The measurement locations in containment are shown in Figures 14 and 15. Other areas visited included the auxiliary building and the contaminated-waste storage area. The measured exposure or dose rates for each technique can vary significantly for the same location because the rates changed dramatically over a few meters when near a large centralized source.

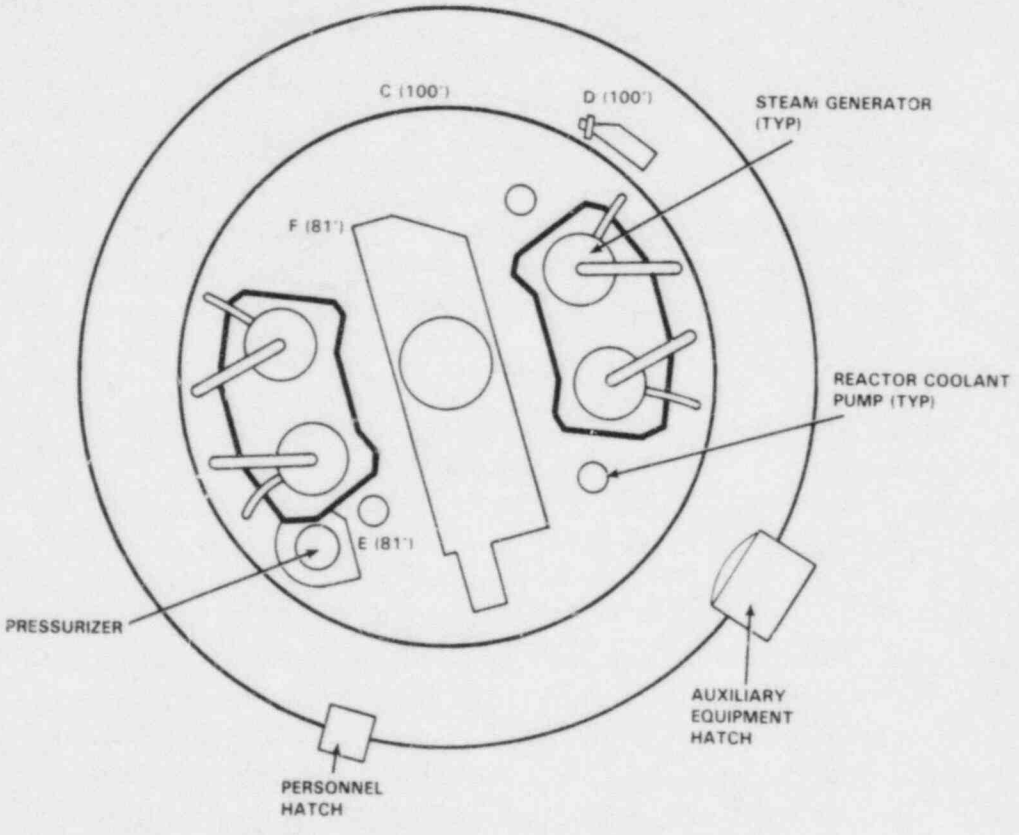

FIGURE 14. Containment Layout at the 130-ft Elevation for the Shutdown PWR, Site K. Measurements were performed at locations C through F at the elevations shown in parentheses.

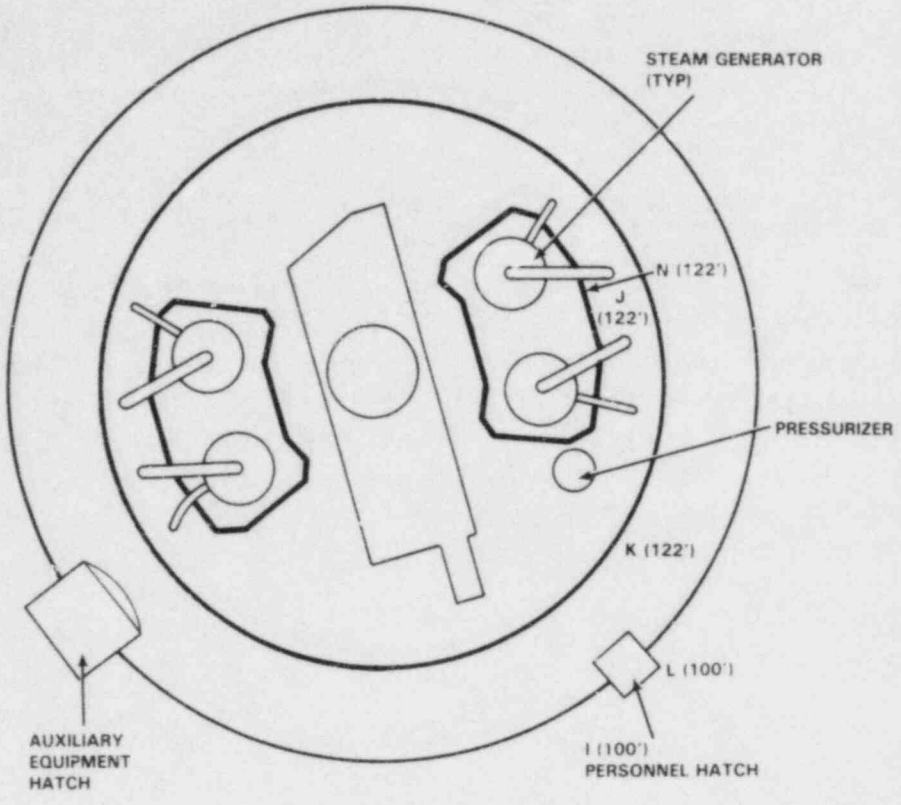

FIGURE 15. Containment Layout at the 122-ft Elevation for the Operating PWR, Site K. Measurements were performed at locations I through L and N at the elevations shown in parentheses.

Photon spectrometer measurements were performed with a 48-cm^3 Ge detector. The locations of the measurements are listed in Table 6. Six measurements were performed in the shutdown reactor, six measurements in the operating reactor, and one measurement in a drum storage area used for both units.

Measurements in the shutdown reactor were performed in the effluent sample room, the auxiliary building, and at two levels in containment. The exposure rates ranged from 0.3 to 12 mR/h. Three of the spectra taken are shown in Figures 16, 17, and 18. The effective C_x factor labelled on the figures is the greatest of the 3 maximum values calculated. The prominent characteristics are the presence of ^{60}Co (5.3-y half-life), ^{58}Co (71-d half-life), electron-positron annihilation radiation and a continuum between approximately 70 keV and 220 keV. The presence of the radioactive isotopes is probably due to "crud" buildup. The ratio of the number of continuum photons to source-decay photons changes by a factor of about 3 from location A (Figure 16) to location D (Figure 18), with a corresponding small increase in the C_x factor.

TABLE 6. Photon Spectrometer Measurements, Site K

Location	Exposure Rate (mR/h)	Effective Maximum C_x (rad/R) 0.007 cm	0.3 cm	1.0 cm	Effective Central C_x (rad/R) 0.3 cm	1.0 cm	2.5 cm
Shutdown PWR							
A-Effluent Sample Room	1	1.01	1.04	1.04			
B-Auxiliary Bldg. Demineralizer Room, Reactor Coolant Filter (100-ft elevation)	0.3	1.06	1.08	1.08			
C-Containment, Reactor Shield Vent Fan (100-ft elevation)	1	1.02	1.05	1.05			
D-Containment, Iodine Removal Fan (100-ft elevation)	1	1.04	1.07	1.07			
E-Containment, Under Reactor Coolant Pump #13 (81-ft elevation)	12	1.01	1.04	1.04			
F-Containment, Under Reactor Coolant Pump #11 (81-ft elevation)	12	1.01	1.04	1.04			
Operating PWR							
G-Effluent Sample Room	1	1.04	1.06	1.06			
H-Auxiliary Bldg. Demineralizer Room, Reactor Coolant Filter (100-ft elevation)	0.2	1.06	1.09	1.09			
I-Containment, Personnel Hatch (100-ft elevation)	0.4	1.03	1.02	1.01			
J-Containment, Near Bioshield of Steam Generator (122-ft elevation)	1.3	1.07	1.08	1.08			
K-Containment, Overlooking Reactor Cavity (122-ft elevation)	2	1.00	1.01	1.03	0.72	0.96	1.02
L-Containment, Outside Airlock (100-ft elevation)	0.9	0.93	0.97	0.95	0.70	0.98	0.99
Other							
M-Hot Drum Storage Area	50	0.99	1.02	1.02			

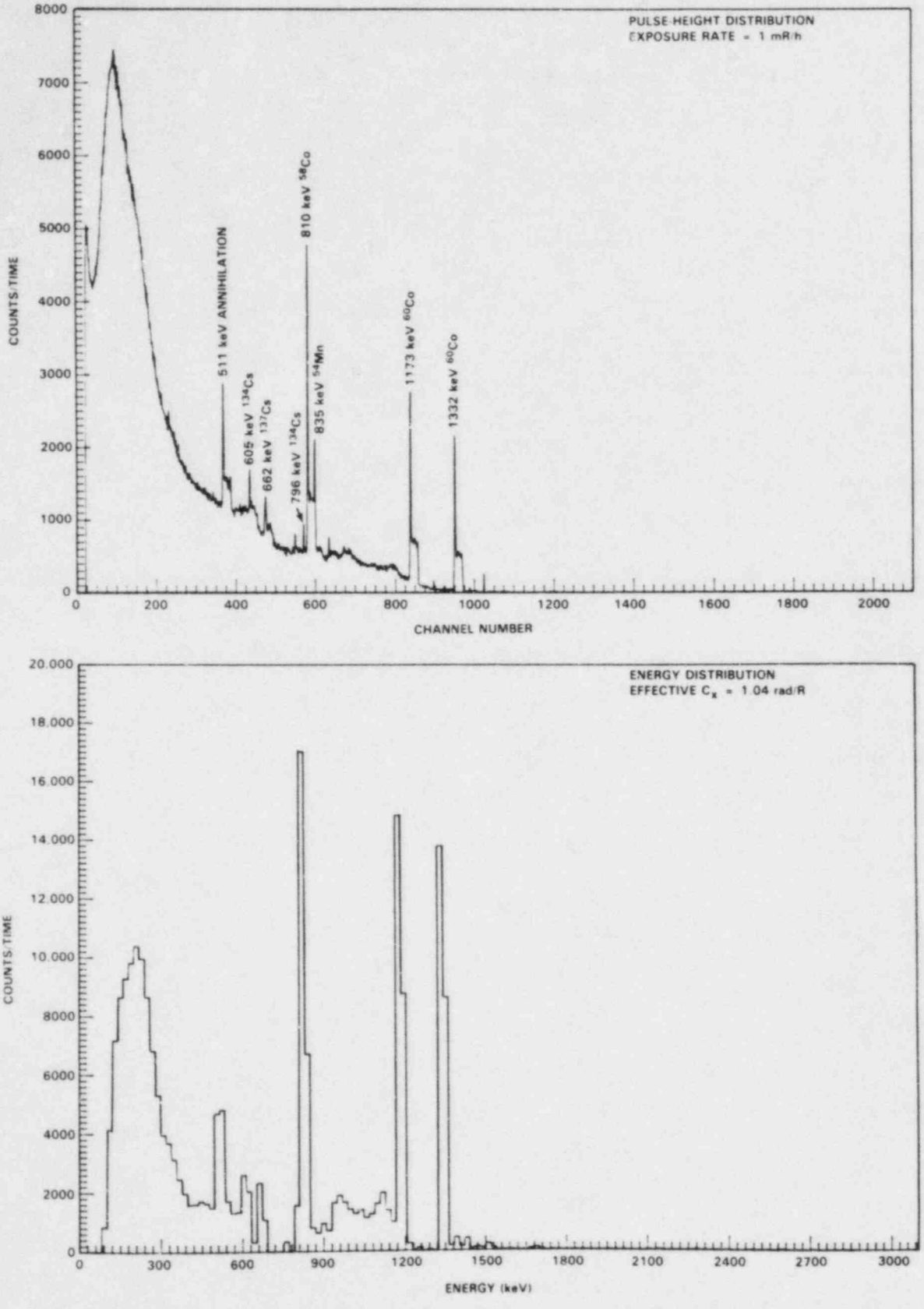

FIGURE 16. Field Data and Corrected Spectrum, Site K, Location A (Shutdown PWR, Sample Room)

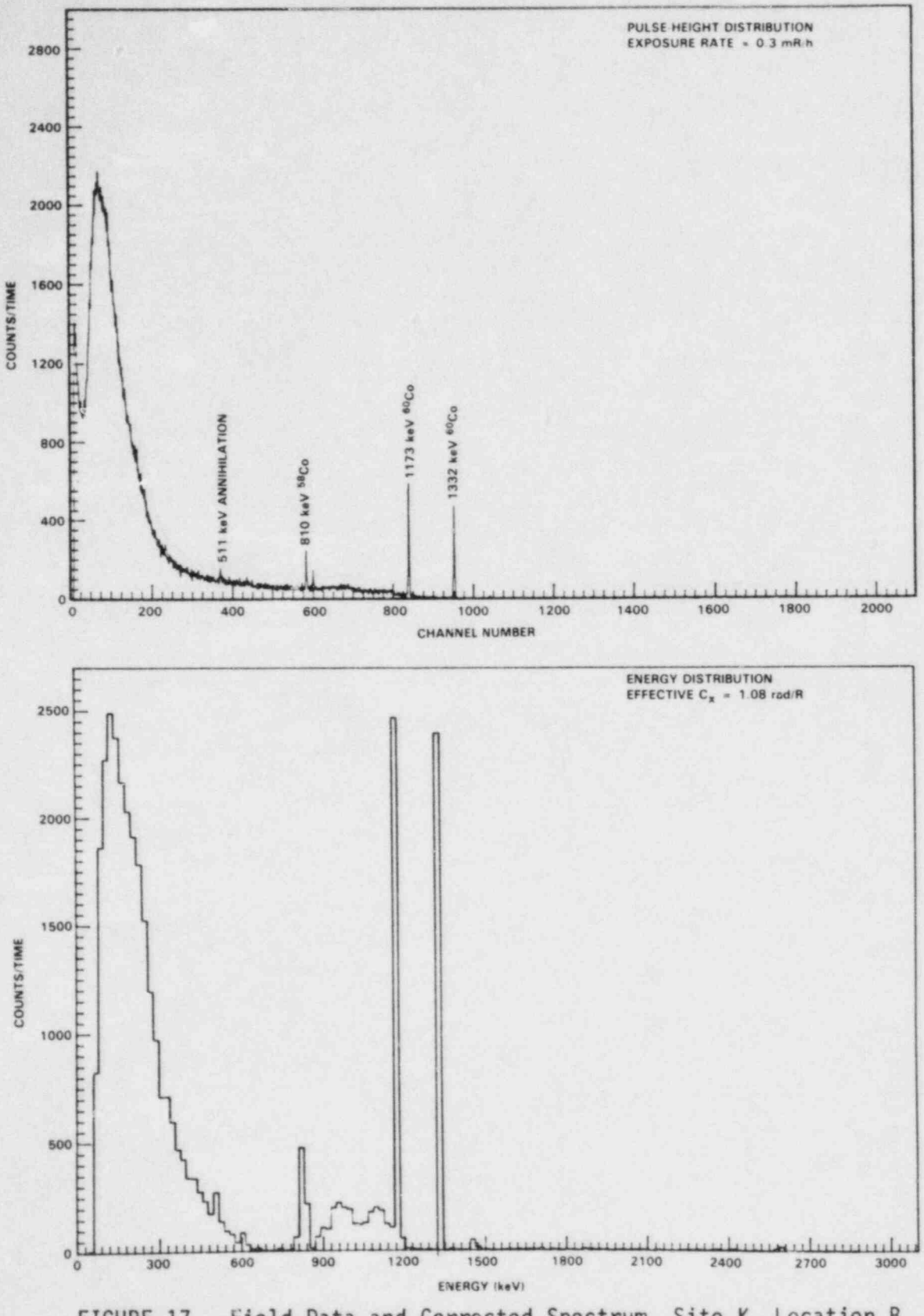

FIGURE 17. Field Data and Corrected Spectrum, Site K, Location B (Shutdown PWR, Demineralizer room)

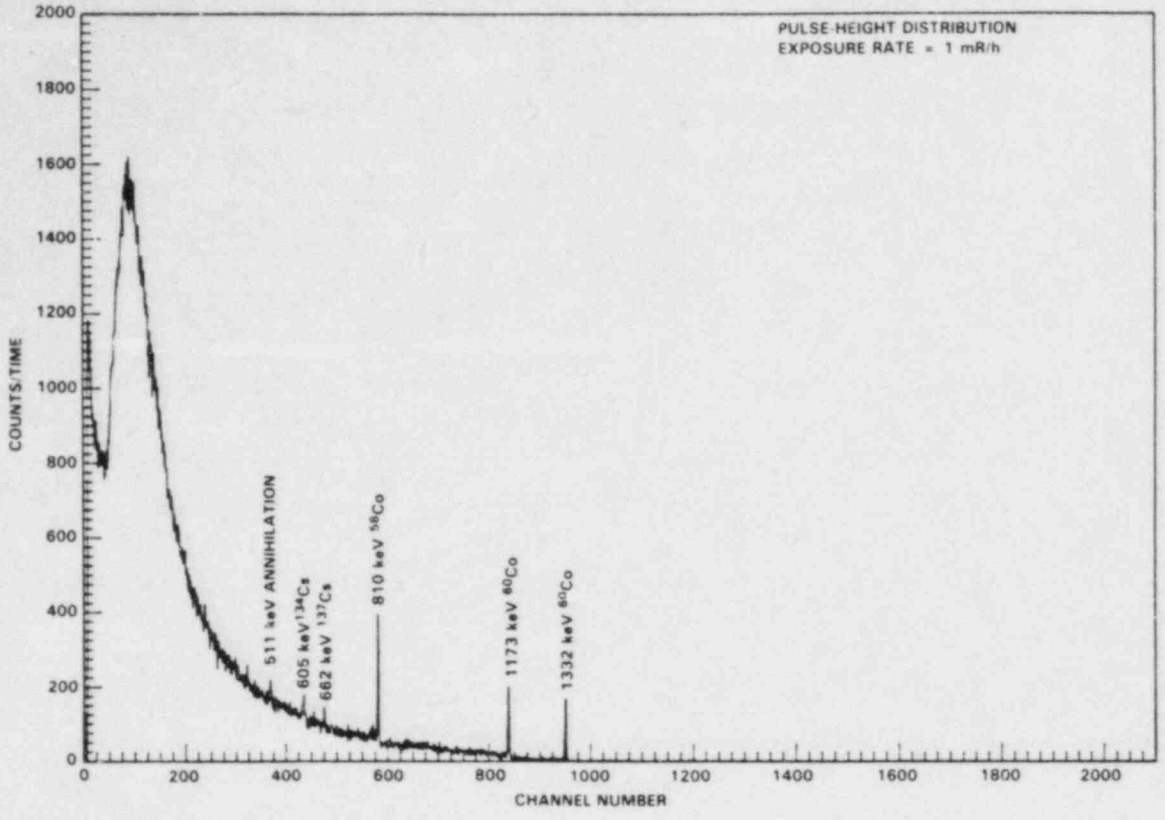

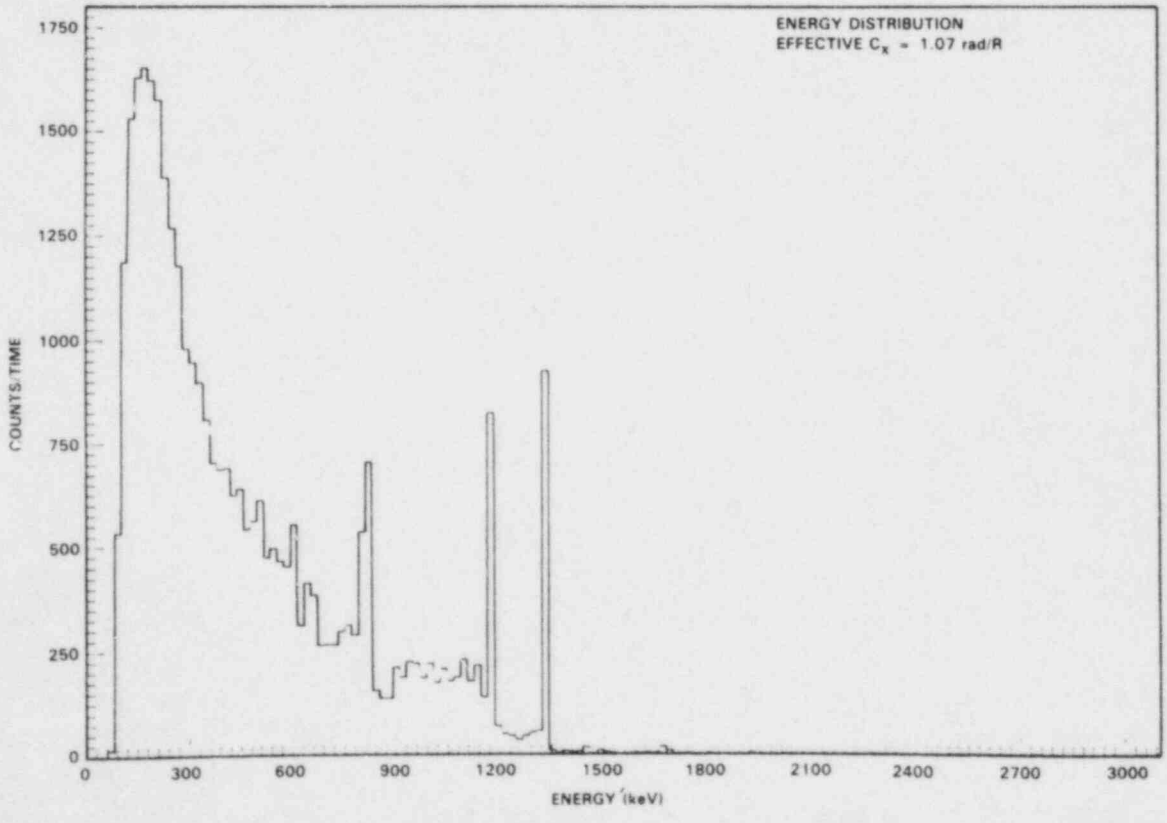

FIGURE 18. Field Data and Corrected Spectrum, Site K, Location D (Shutdown PWR, Containment, Iodine Removal Fan)

The measurement locations in the operating reactor ranged in exposure rate from 0.2 to 2 mR/h. The pulse-height distributions (Figures 19 through 21) show radioisotope spectra from short-lived isotopes in addition to the long-lived isotopes. Prominent short-lived isotopes are ^{133}Xe (5 d) and ^{135}Xe (9 h). Xenon is a fission product that easily diffuses into the coolant water and containment atmosphere. The long-lived isotopes present included ^{58}Co and ^{60}Co.

The relative compositions of the cobalt isotope annihilation radiations are similar for the spectra taken in the effluent sample rooms of the shutdown and operating reactors (Figures 16 and 19). However, an enhanced scatter component and the xenon radiations are prominent in the spectrum from the operating reactor. The net effect is an increase in the C_x factor from 1.04 to 1.06. The increase is primarily due to the increase in the scatter peak. The contribution to dose from the xenon peaks is small.

In the demineralizer rooms (Figures 17 and 20), ^{60}Co is more prominent in the shutdown reactor spectrum, while annihilation radiation is prominent in the operating reactor spectrum. The operating reactor has less equivalent full-power operation (1/2 y) than the shutdown reactor (5 y), and thus has less of the "crud" buildup that contains ^{60}Co. The prominence of annihilation radiation in the operating plant implies the production of short-lived positron emitters.

The spectrum shown in Figure 21 was taken overlooking the reactor cavity. The data extends up to 8 MeV. No ^{16}N photons were detected. The data is consistent with a general scatter contribution, with some evidence of capture gamma rays on iron (7.6 MeV), as were detected at another operating PWR. The calculated central C_x factors (Table 6) imply a reduced relative dose at 0.3 cm of 0.7 and a relative dose at 1 cm of near unity.

Three measurements were performed in the shutdown reactor using the TE extrapolation chamber and the ion chamber. The measurements were performed in approximately the same locations as for the measurements performed using both the photon spectrometer and the TLD-loaded phantom. The locations, the measured exposure and dose rates, and the derived effective C_x factors are given in Table 7. The measurements were performed in areas with exposure rates of about 100 mR/h. Because the chamber signals were small, the measured values have large uncertainties. A measurement in the operating reactor was attempted but was unsuccessful.

All of the effective C_x factors derived from the extrapolation chamber measurements were near or less than unity. The values less than unity are

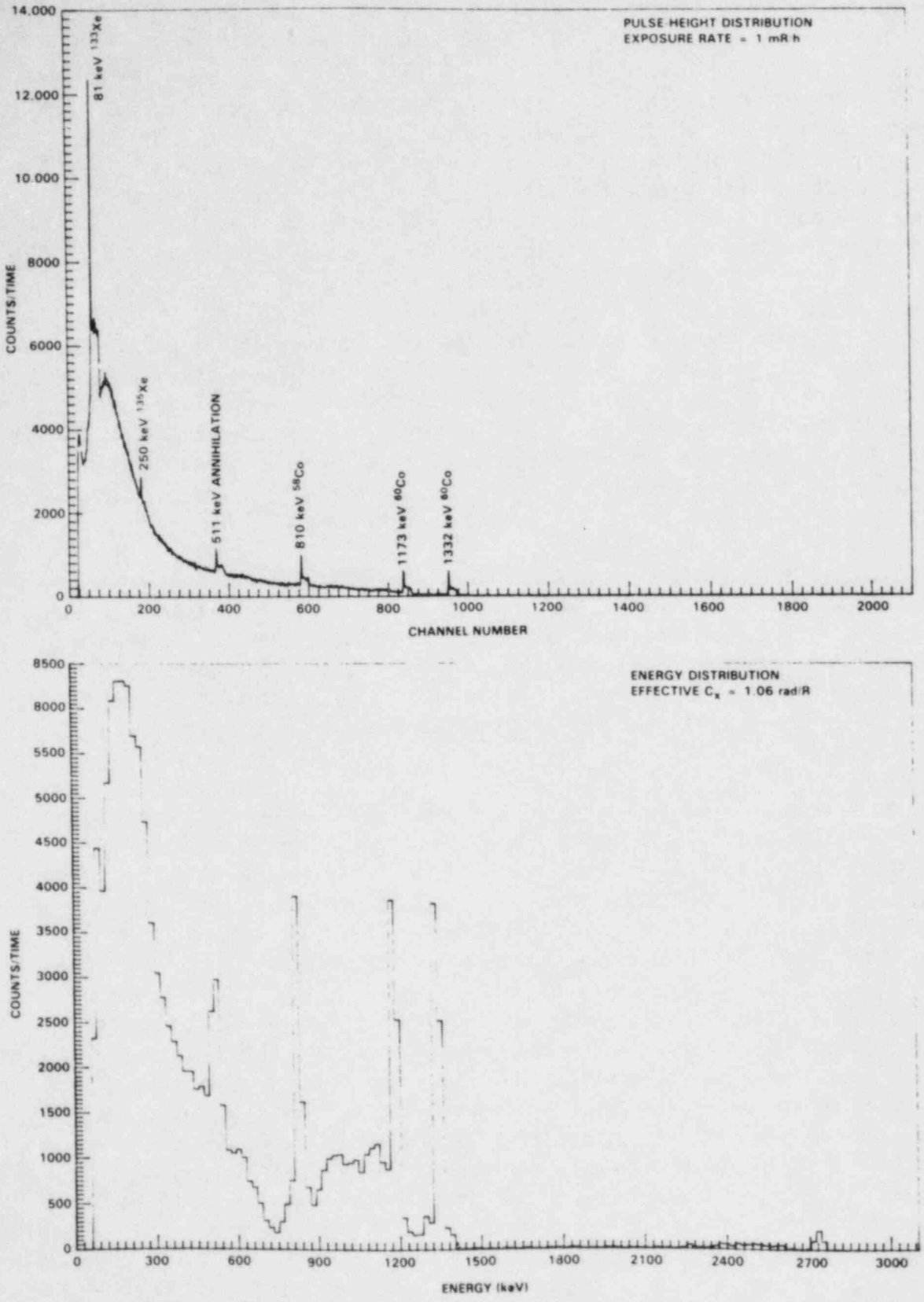

FIGURE 19. Field Data and Corrected Spectrum, Site K, Location G (Operating PWR, Sample Room)

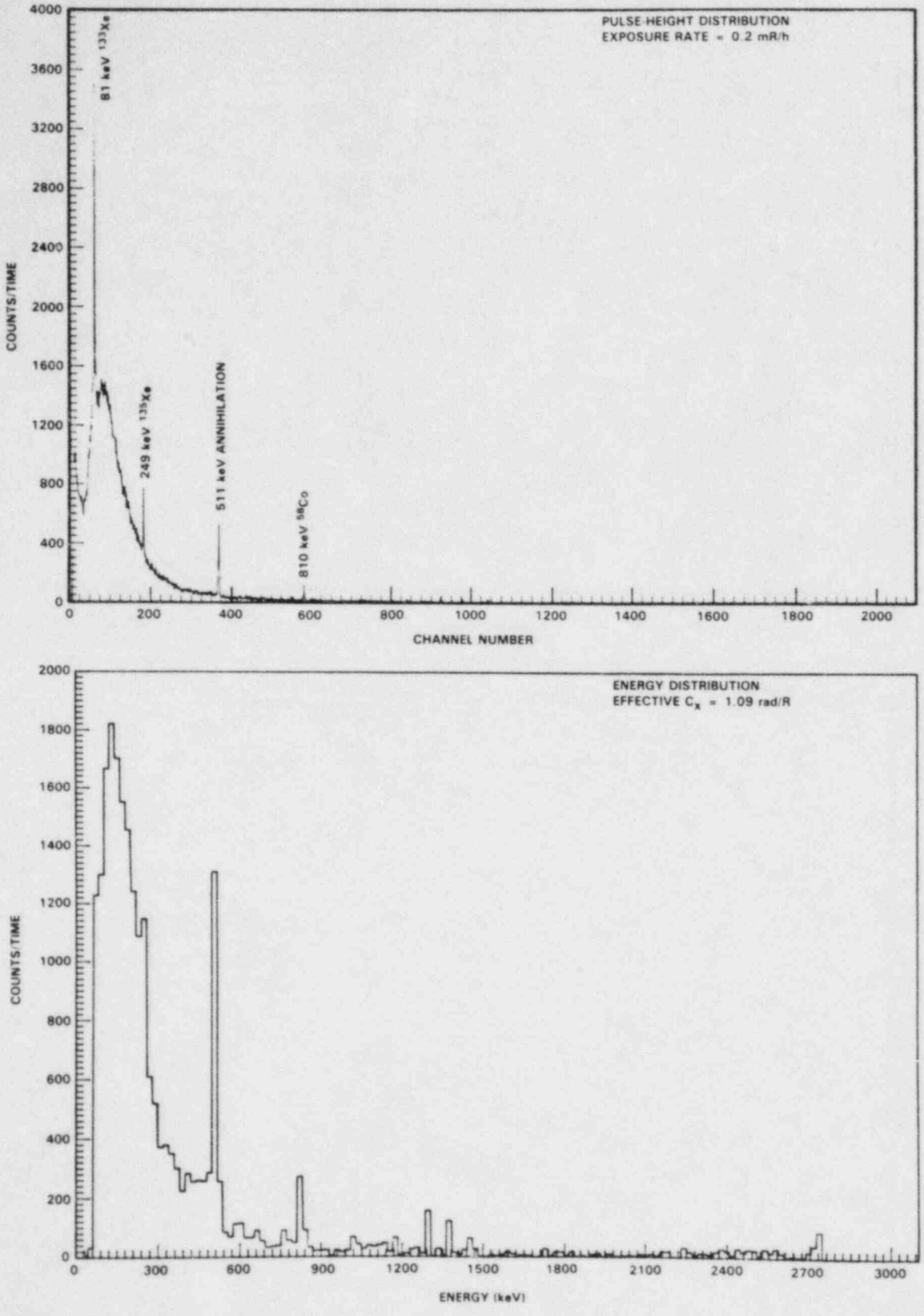

FIGURE 20. Field Data and Corrected Spectrum, Site K, Location H (Operating PWR, Demineralizer Room)

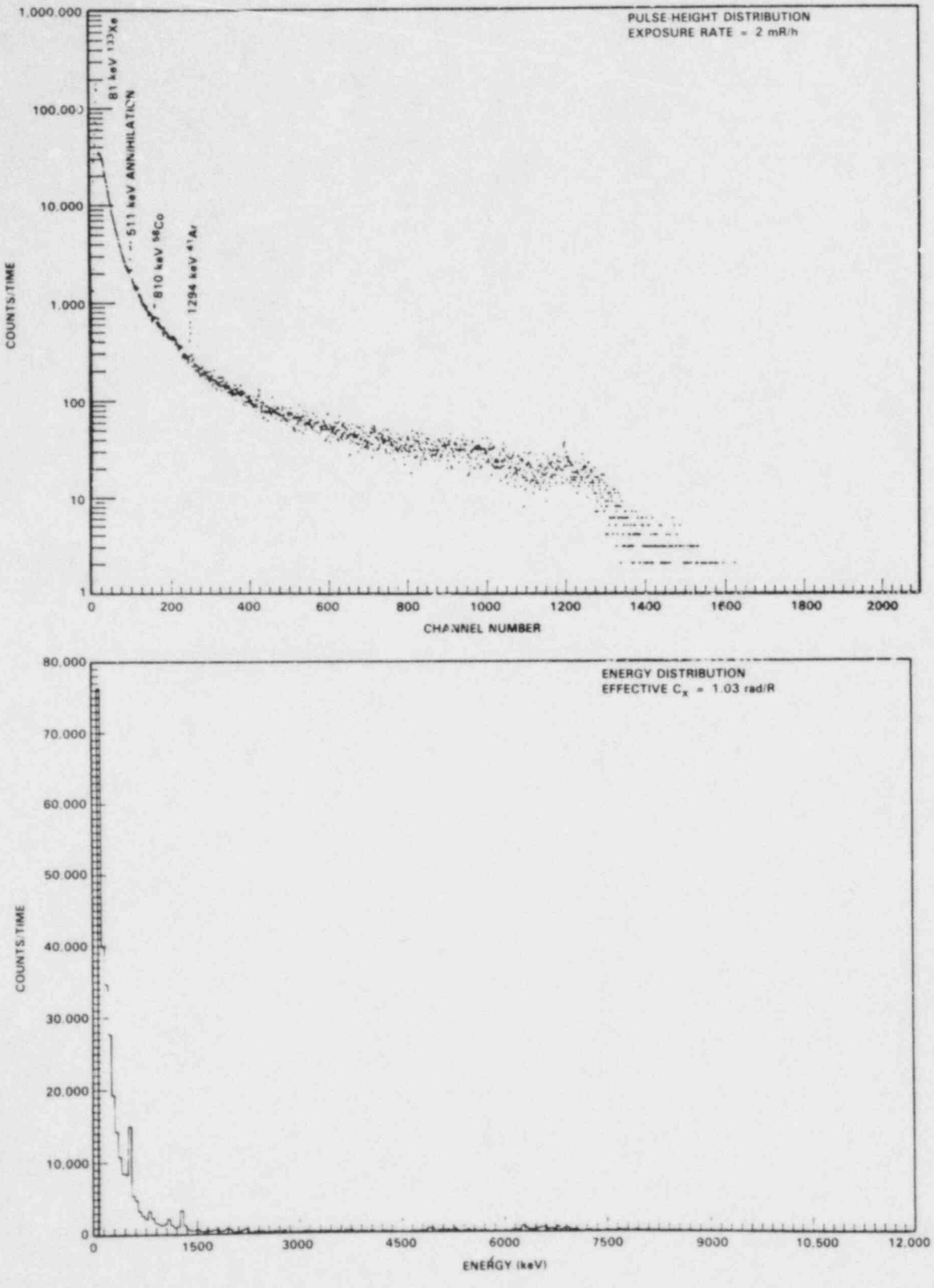

FIGURE 21. Field Data and Corrected Spectrum, Site K, Location K (Operating PWR, Containment, Overlooking Reactor Cavity)

TABLE 7. Extrapolation Chamber and Ion Chamber Measurements, Site K

Location	Exposure Rate (mR/h)	Dose Rate (mrad/h)	Effective Exposure-to-Dose Conversion Factor
Shutdown PWR			
E-Drain Valve, Reactor Coolant Pump #13			
Shallow	96	97	1.01 ± 0.09
Deep		87	0.91 ± 0.15
F-Drain Valve, Reactor Coolant Pump #11			
Shallow	87	69	0.79 ± 0.12
Deep		83	0.95 ± 0.08
Storage Area			
M-Hot Drum Storage Area			
Shallow	77	72	0.94 ± 0.20
Deep		57	0.74 ± 0.16

probably due to the presence of distributed sources. Corrections have been made for beta particles. The data does not indicate a significant component of low-energy photons at the higher dose rates.

The TLD-loaded phantom measurements were performed in four locations with exposure rates ranging from 70 to 260 mrad/h. Table 8 contains the measurement locations and the results of the fitting. Locations E, F, and M are dominated by medium-energy photons, resulting in effective C_x factors near unity. Figure 22 contains the response of the TL dosimeters versus depth. All curves are normalized to the surface reading. Locations E and F show similar depth-dose functions characteristic of penetrating radiation. Location M has a slightly less penetrating field. Location N (steam generator) has a 7% enhancement at 1 cm compared to the surface. This is possibly caused by partially shielded beta particles from ^{16}N or high-energy electrons created by the high-energy photons.

Measurements at Site K offered a direct comparison of shutdown and operating conditions and information of the effects of plant age. The presence of xenon isotopes in the operating plant did not significantly increase the dose received. In addition, a compensating effect was the increase in the 511-keV

TABLE 8. TLD-Loaded Phantom Measurements, Site K

Location	Surface Dose Rate (mrad/h)	Field Strengths (mrad/hr) for Photons 34 keV	120 keV	662 keV	Beta	Effective[a] C_x (rad/R)
Shutdown PWR						
E-Drain Valve, Reactor Coolant Pump #13	115	7	0	90	8	1.04
F-Drain Valve, Coolant Pump #11	106	0	0	97	9	1.03
Storage Area						
M-Hot Drum Area	67	8	0	59	5	1.05
Operating PWR						
N-Steam Generator	160	(analysis inappropriate)				

(a) For the shallow depth (0.007 cm).

annihilation radiation for the operating plant. Differences in dosimetry between the shutdown and operating plants were mainly due to the high-energy photon fields inside containment. The effect of plant aging was to increase the amount of radioactive cobalt, lowering the effective C_x factors a few percent. The highest calculated C_x factors (1.08/1.09) occurred in the demineralizer rooms and inside containment behind the bioshield. In both cases, the low-energy scatter continuum was a dominant part of the spectrum. Other locations with large continua also had a significant high-energy tailing. The maximum effect of low-energy photons was to increase the C_x factors by less than 10%. The effect of operating the plant and the effect of increased age totalled only a few percent difference in C_x factors. The extrapolation chamber measurements indicated that the calculated C_x factors may be overestimated due to distributed-source effects.

The spectra taken inside containment of the operating reactor contained a sufficiently large contribution from high-energy photons to deposit less dose at 0.3-cm than at 1-cm or 2.5-cm depths. However, a TL phantom measurement did not confirm the result, possibly indicating the presence of significant beta or electron fields.

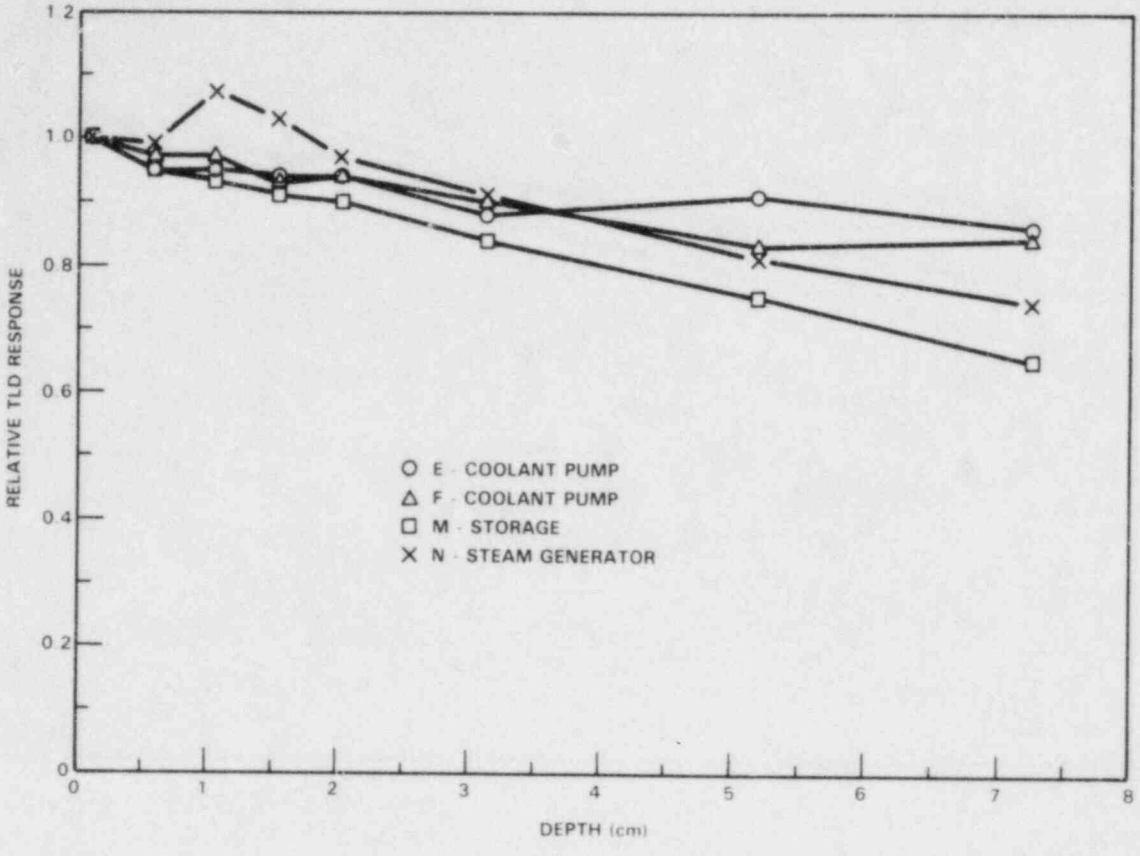

FIGURE 22. TLD-Loaded Phantom Measurements, Site K

3.3 SITE B - SHUTDOWN AND OPERATING PWR

The PWR at Site B was visited twice, with measurements taken once under shutdown and once under operating conditions (89% of full power). Measurements were performed at 19 locations ranging in exposure rate from 0.4 mR/h to 10.8 R/h. The measurement locations are identified alphabetically on schematic layouts of containment (Figures 23 and 24).

Spectra were taken with a 59-cm^3 intrinsic Ge detector (during reactor shutdown) and a 31-cm^3 intrinsic Ge detector (during reactor operation). Measurement locations and the calculated maximum C_x factors are listed in Table 9. The C_x values for the shutdown reactor vary between 1.02 and 1.07. A typical spectrum is presented in Figure 25. Radiation from cesium isotopes contributed significantly to the dose rates, resulting in C_x values near unity.

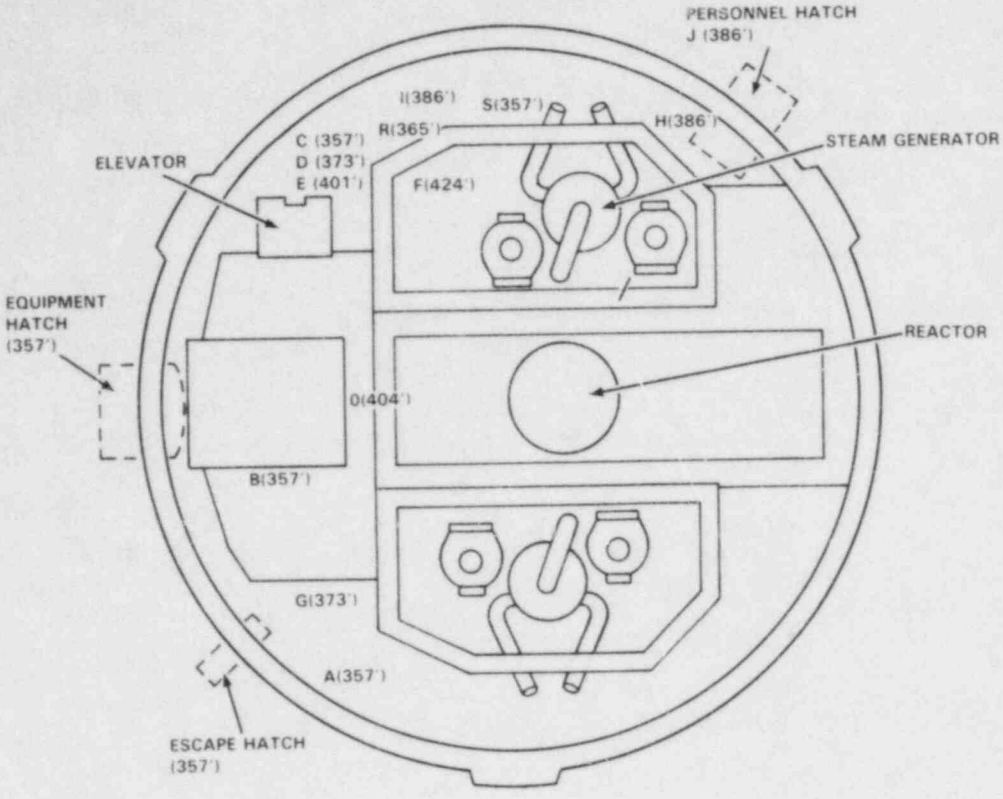

FIGURE 23. Containment Layout at the 401-ft Elevation, Site B. Measurements were performed at the locations and elevations indicated.

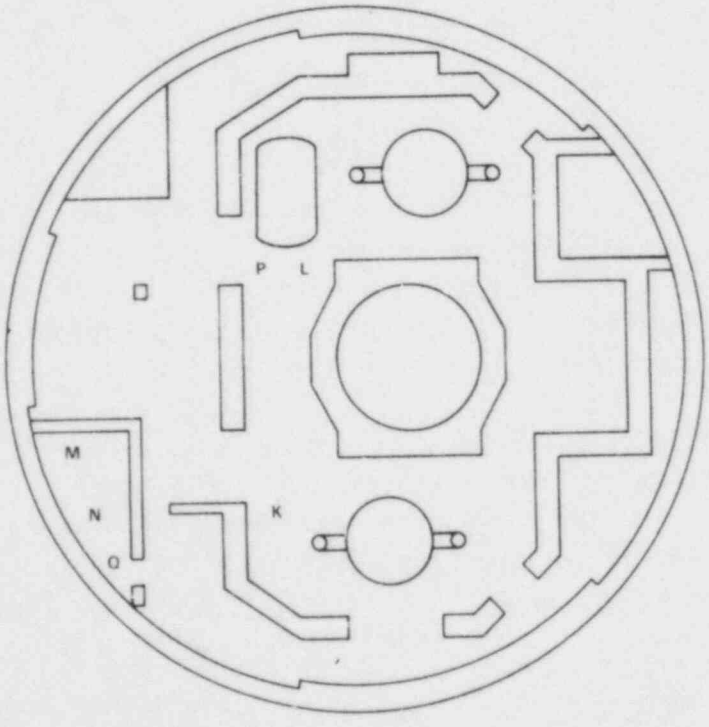

FIGURE 24. Containment Layout at the 336-ft Elevation, Site B. Measurements were performed at the locations indicated.

TABLE 9. Photon Spectrometer Measurements, Site B

Location	Exposure Rate (mR/h)	Effective Maximum C_x (rad/R) 0.007 cm	0.3 cm	1.0 cm	Effective Central C_x (rad/R) 0.3 cm	1.0 cm	2.5 cm
Reactor Containment, PWR Shutdown							
A-Near Escape Hatch (357-ft level)	8	1.02	1.03	1.03			
B-Near Equipment Hatch (357-ft level)	5	1.06	1.07	1.07			
C-Near Elevator (357-ft level)	8	1.04	1.05	1.05			
D-Near Elevator (373-ft level)	8	1.04	1.05	1.05			
E-Near Elevator (401-ft level)	4	1.05	1.06	1.06			
F-Deck (424-ft level)	2	1.06	1.07	1.07			
G-Above Escape Hatch (373-ft level)	10	1.02	1.03	1.03			
Reactor Containment, PWR Operating							
H-Near Personnel Hatch (386-ft level)	3	0.91	0.96	0.99	0.59	0.89	0.98
I-Near Stairway (386-ft level)	5	0.92	0.97	1.00	0.62	0.89	0.98
E-Near Elevator (401-ft level)	7	0.84	0.90	0.95	0.38	0.80	0.94
J-In Personnel Hatch	0.4	1.01	0.91	0.91	0.77	0.87	0.92

The spectra measured inside containment during reactor operation had contributions from high-energy photons. In addition to a general distribution of energies up to approximately 8 MeV, several capture gamma transitions were observed. Indicated on Figure 26 are capture gamma transitions for iron and hydrogen. The pulse-height distribution is plotted on a log scale to allow observation of the high-energy contributions. The cesium isotopes were again observed, along with positron-electron annihilation radiation and xenon isotopes. The high-energy photons contributed more to the dose rate than the medium- or low-energy photons. This resulted in maximum C_x factors at or below unity. Photons from ^{16}N were not observed at the locations monitored. The calculated central C_x factors indicated reduced doses at the 0.3-cm and 1-cm depths compared to the 2.5-cm depth.

Extrapolation chamber and ion chamber measurements for Site B are listed in Table 10. An effort was made to measure fields over a wide range of dose rate (106 mrad/h to 10.8 rad/h). Due to time constraints, it was sometimes more productive to measure several locations at one depth rather than one location at several depths. The 1-cm position was chosen because no corrections for beta dose were required.

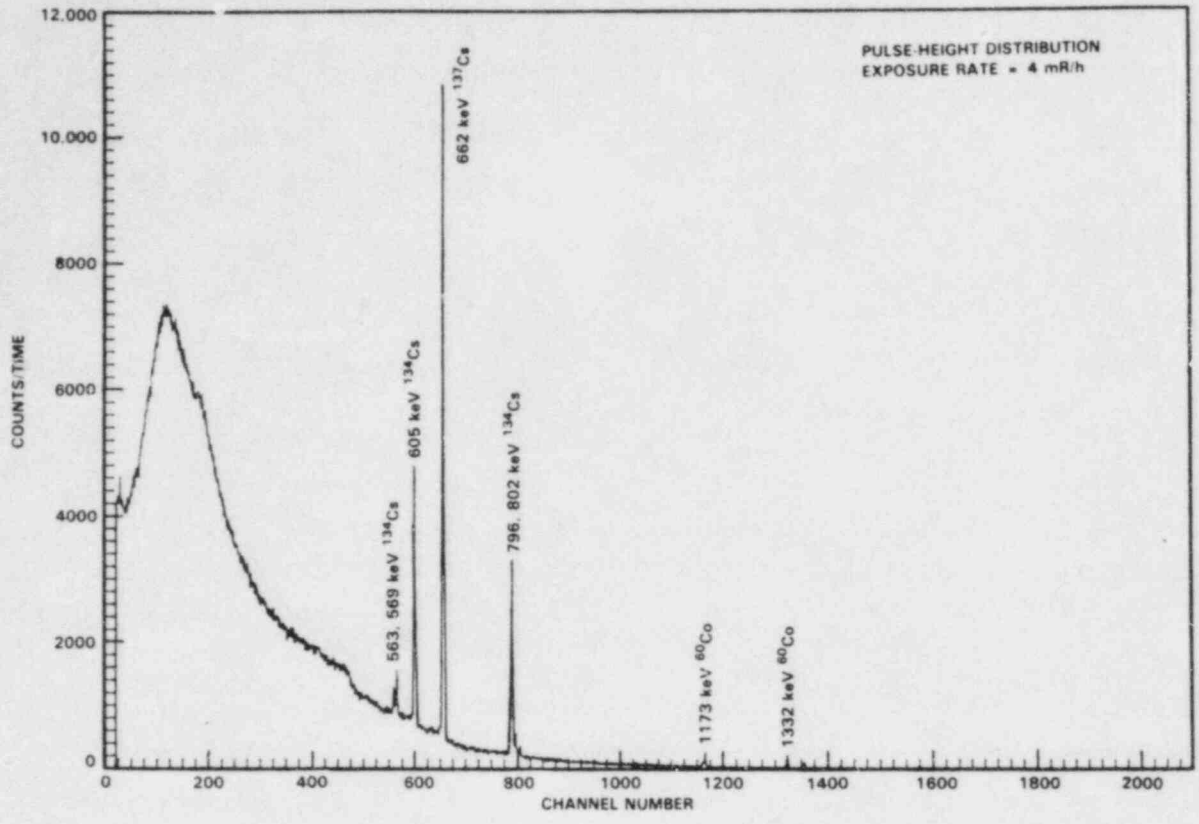

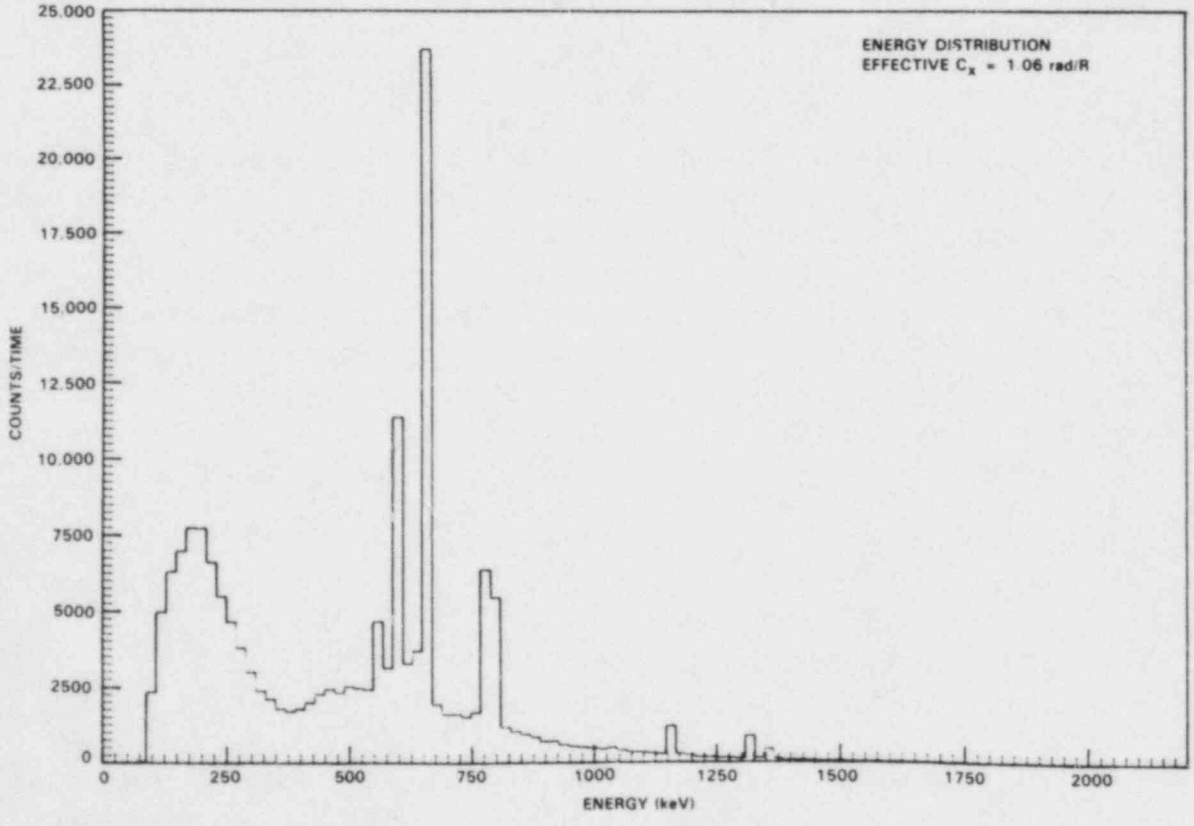

FIGURE 25. Field Data and Corrected Spectrum, Site B, Location E (Shutdown PWR, Near Elevator, 401-ft Elevation)

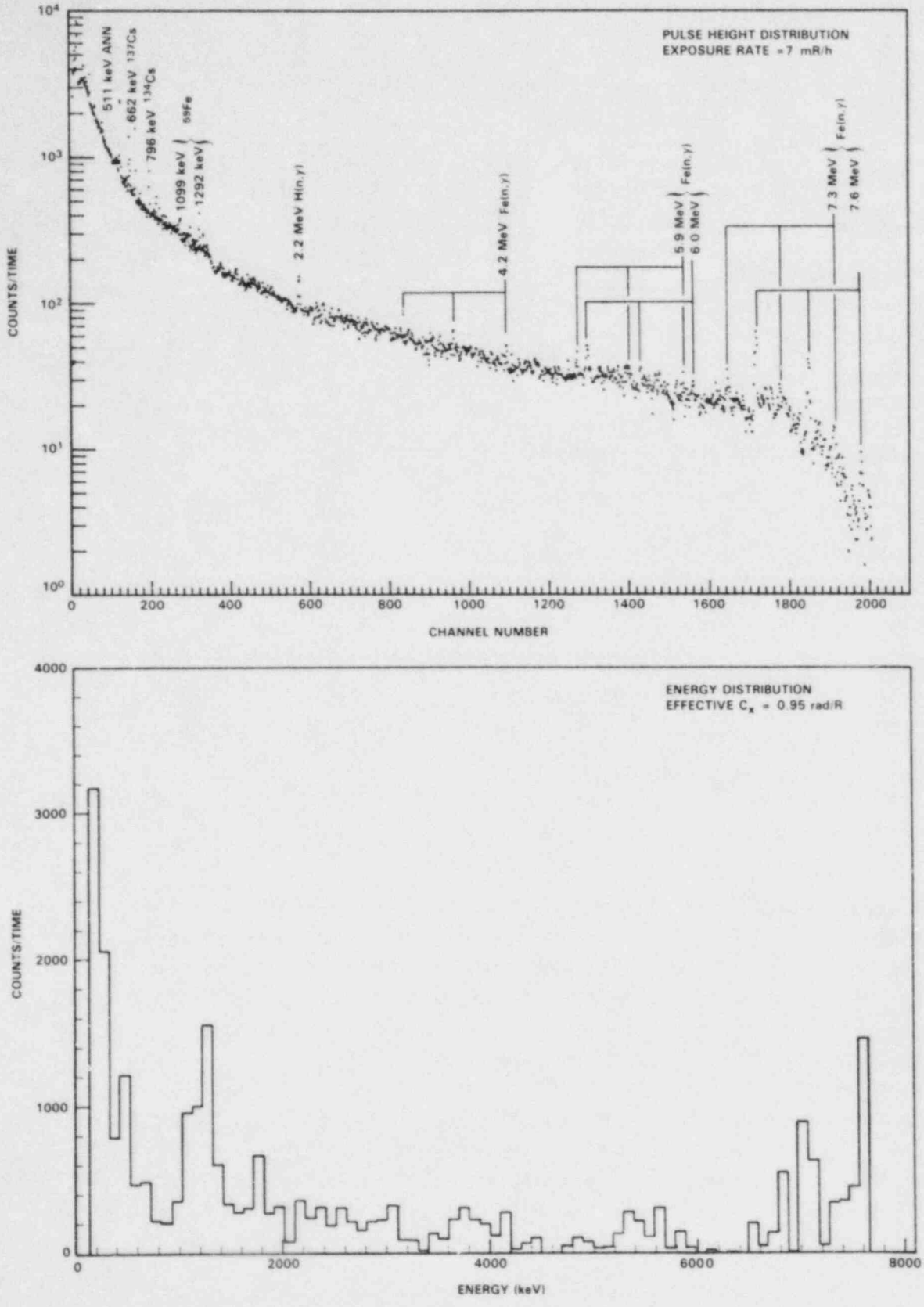

FIGURE 26. Field Data and Corrected Spectrum, Site B, Location E (Operating PWR, Near Elevator, 401-ft Elevation)

TABLE 10. Expolation Chamber and Ion Chamber Measurements, Site B

Location	Exposure Rate (mR/h)	Dose Rate (mrad/h)	Beta Dose Rate (mrad/h)	Effective Exposure-to-Dose Conversion Factor
PWR Shutdown (containment)				
K-Piping Near Steam Generator (336-ft-level basement)				
Shallow	195	196	22	0.89 ± 0.07
Deep		160	-	0.82 ± 0.04
L-Piping Near Reactor Core (336-ft-level basement)	135	106	-	0.79 ± 0.08
M-Let-Down Heat Exchanger (336-ft level)	10,800	10,800	-	1.00 ± 0.05
N-Removed Nozzles (336-ft level)	900	804	-	0.89 ± 0.05
PWR Operating (containment)				
O-Upper Deck Overlooking Reactor Cavity (404-ft level)	136	223	0	1.64 ± 0.11
		195	-	1.43 ± 0.10

All measurements for the shutdown reactor were performed at the basement level (336 ft), where sufficiently large dose rates were present. Effective C_x values were unity or less. The major contributor to dose was medium-energy photons. The values less than one were probably due to distributed sources. The source measured in the let-down heat exchanger room (10.8 R/h) was well localized, giving the C_x factor expected for a ^{60}Co and Cs source.

The extrapolation chamber measurement performed during reactor operation was taken from a location overlooking the reactor cavity. The neutron-to-photon ratio in dose equivalent was approximately 2:1. The correction to the dose and exposure was less than the uncertainty of the effective C_x measurement. The results indicate a 15% surface enhancement compared to the 1-cm

depth. There was no observed reduction of dose rate at the surface due to high-energy photons. The cause of the elevated magnitude of the measured C_x factors is not understood. The spectral measurements indicate that it cannot be explained by the presence of low-energy photons.

The TLD-loaded phantom measurements are presented in Table 11. The two measurements performed during reactor shutdown indicate a dominant contribution from medium-energy photons. Response versus depth is plotted in Figure 27. All measurements show an enhanced surface dose. The measurements performed during reactor operation are generally more penetrating.

TABLE 11. TLD-Loaded Phantom Measurements, Site B

Location	Surface Dose Rate (mrad/h)	Field Strengths (mrad/h) for Photons				Effective[a] C_x (rad/R)
		34 keV	120 keV	662 keV	Beta	
Shutdown PWR (Containment)						
P-336-ft Level, Toward Reactor Core	70	0	0	70	0	1.03
Q-336-ft Level, At Entrance to Let-Down Heat Exchanger Room	50	11	0	39	0	1.06
Operating PWR (Containment)						
R-365-ft Level, on Stairwell Toward Core	20	(analysis inappropriate)				
S-357-ft Level, Near Penetration in Bioshield	40	(analysis inappropriate)				

(a) Calculated for the shallow depth (7 mg/cm^2).

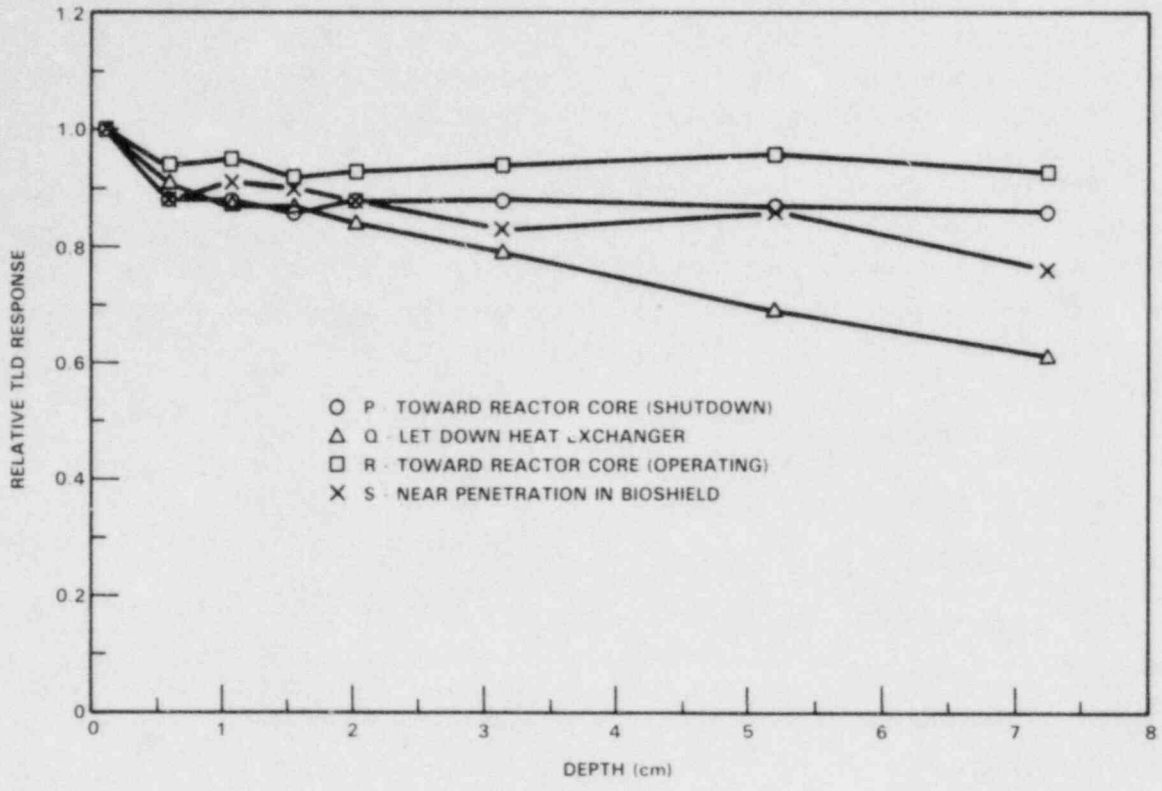

FIGURE 27. TLD-Loaded Phantom Measurements, Site B

The calculated C_x factors ranged up to 1.07. The dominant contribution to the spectra was from cesium isotopes. The extrapolation chamber measurements resulted in C_x factors less than unity for the lower dose rates. The distribution of sources may lower the C_x factor below unity for most locations.

Measurements performed inside containment indicated a dominant contribution to dose from high-energy photons. However, both the extrapolation chamber and the TLD phantom measurements resulted in higher surface doses than depth doses. No indications were found that personnel doses are being underestimated using current monitoring requirements.

3.4 SITE M - SHUTDOWN AND OPERATING BWR

The BWR at Site M was visited twice, with measurements taken under both shutdown and operating conditions (55% of full power). Measurements were performed at 29 locations ranging in exposure rate from 0.2 mR/h to 7.5 R/h.

The photon spectrometer measurements were performed with a 31-cm^3 intrinsic Ge detector. The measurement locations are listed in Table 12. All measurements performed during shutdown and all those performed during operation except in the location near the turbine did not have a significant high-energy contribution. The maximum calculated C_x factors ranged from 1.02 to 1.16. Most values were very close to unity because the contributions to exposure were dominated by medium-energy photons. Photons from ^{60}Co were the dominant contribution (Figure 28). The larger values were due to larger relative contributions from scattered photons. The data taken at the door of the cleanup phase separator room (Figure 29) shows an almost pure scatter spectrum. Photons from ^{60}Co scattered off a concrete wall before exiting through the door. While the spectrum peaks at about 120 keV, the higher-energy tail extends to above 500 keV. The relative importance of the medium-energy photons is enhanced by the flux-to-exposure conversion. The result is an effective C_x factor of 1.16.

TABLE 12. Photon Spectrometer Measurements, Site M

Location	Exposure Rate (mR/h)	Effective Maximum C_x, rad/R			Effective Central C_x, rad/R		
		0.007 cm	0.3 cm	1.0 cm	0.3 cm	1.0 cm	2.5 cm
Shutdown BWR							
Reactor Building							
Refuel Pool, HEPA Filter Hose	4	0.98	1.02	1.02			
Refuel Pool, General Area[a]	0.4	1.01	1.04	1.04			
Dry Well, Valve	2	0.99	1.02	1.02			
Turbine Building							
Turbine Blade Housing Diaphram	0.2	1.02	1.05	1.05			
Operating BWR							
Reactor Building							
First Floor, Opposite Airlock	2.5	1.01	1.04	1.04			
First Floor, Outside RHR Valve Room	0.2	1.03	1.06	1.04			

TABLE 12. (contd)

Location	Exposure Rate (mR/h)	Effective Maximum C_x, rad/R			Effective Central C_x, rad/R		
		0.007 cm	0.3 cm	1.0 cm	0.3 cm	1.0 cm	2.5 cm
Operating BWR (contd)							
Reactor Building (contd)							
First Floor, Near Scram Discharge Lines	4		1.01	1.04	1.04		
Second Floor, Outside Spent Resin Room	11		1.01	1.03	1.04		
Second Floor, Near Clean-Up Phase Separator Room Door	1		1.15	1.15	1.15		
Second Floor, Near Clean-Up Phase Separator Room Door	4		1.16	1.16	1.16		
Second Floor, Near Containment	5		1.01	1.04	1.04		
Third Floor, Near Jungle Room Door	4.5		1.02	1.05	1.05		
Fourth Floor, Laundry Area	1		1.02	1.05	1.05		
Fifth Floor, 0.6 m from Cavity	4		1.00	1.03	1.03		
Fifth Floor, 1 m from New Fuel Storage	1.5		1.02	1.05	1.05		
Turbine Building							
Behind Shield Wall	2		0.83	0.88	0.94	0.38	0.82	0.99
Near Turbine	14		0.81	0.86	0.93	0.32	0.79	0.92
SE Corner of CO_2 Unit	0.3		0.96	1.01	1.01			
Off-Gas Building								
Near Charcoal Absorbers	2		1.00	1.03	1.03			

(a) NaI(Tl) data also taken at this location.

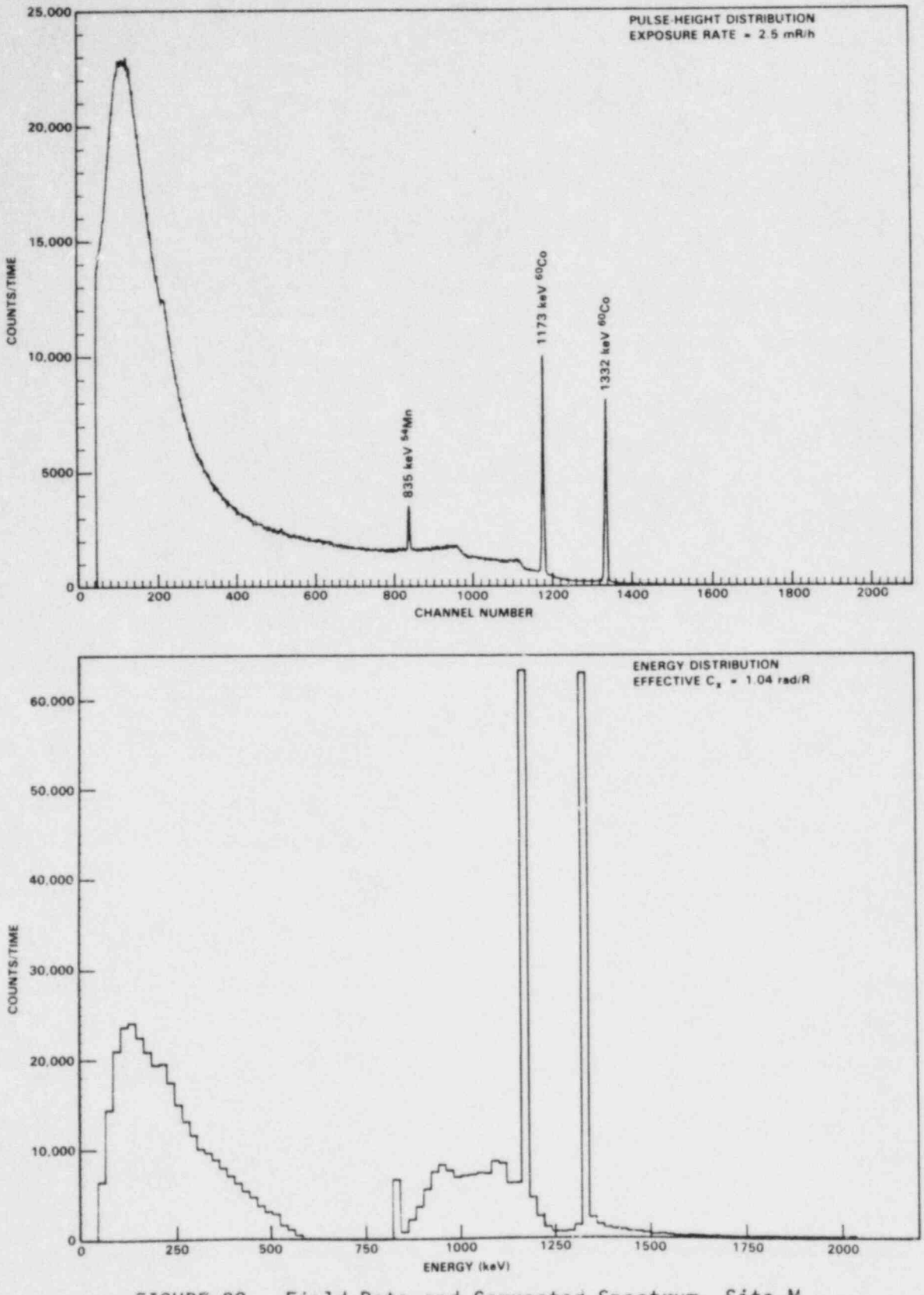

FIGURE 28. Field Data and Corrected Spectrum, Site M (Operating BWR, Reactor Building, First Floor, Opposite Airlock)

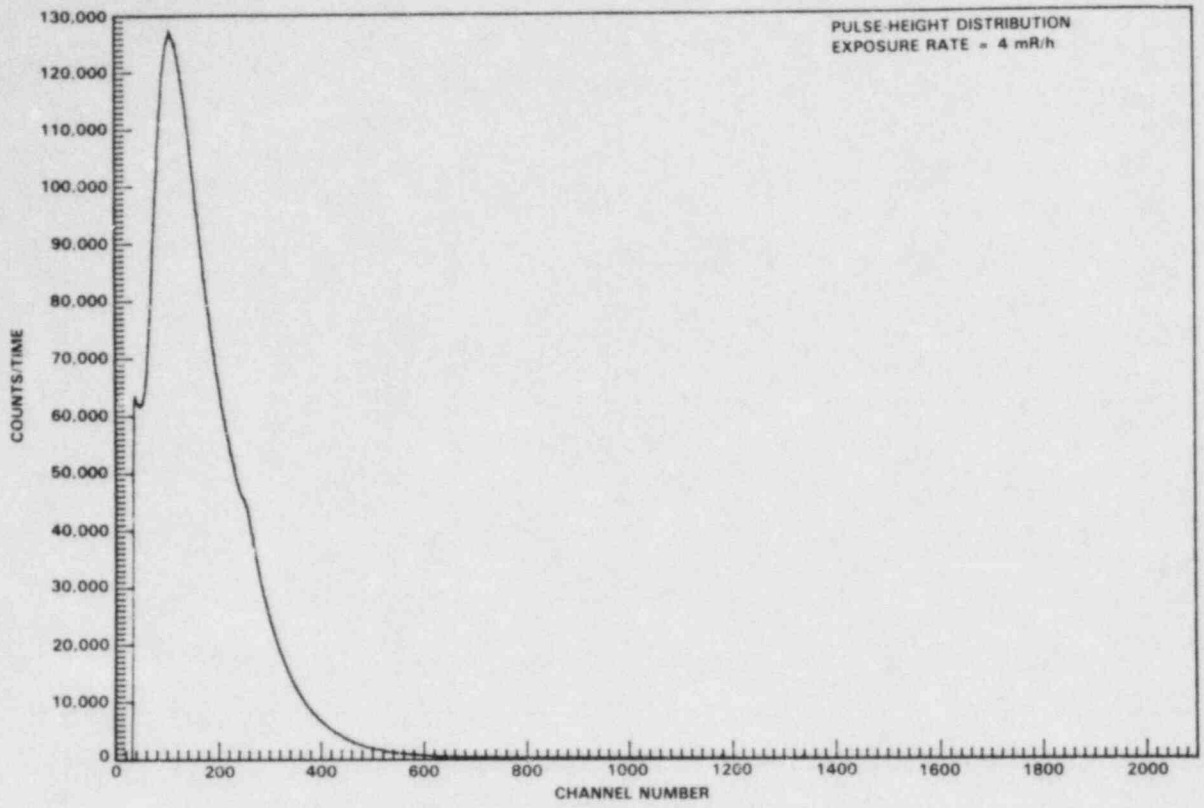

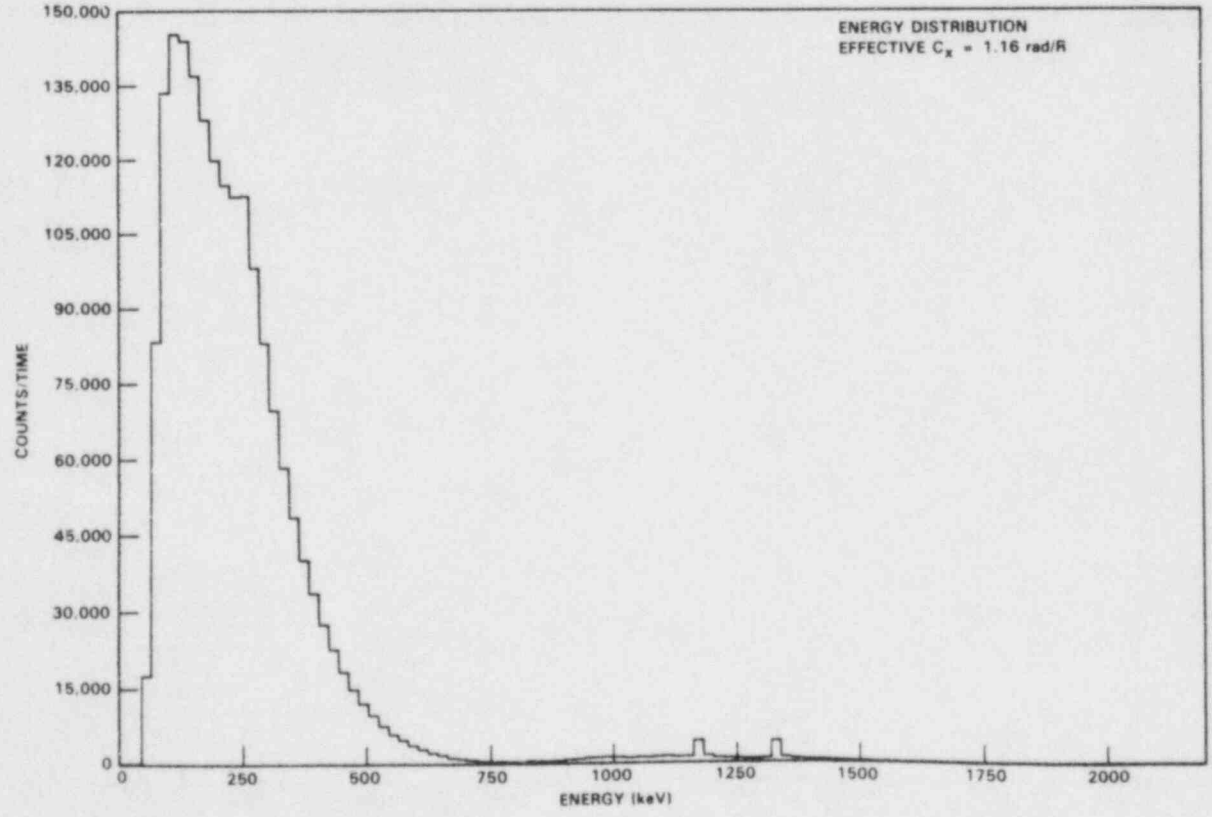

FIGURE 29. Field Data and Corrected Spectrum, Site M (Operating BWR, Reactor Building, Second Floor, Near Clean-Up Phase Separator Room Door)

Spectra taken in the turbine room during operation show a dominant ^{16}N peak at 6.1 MeV and the 511-keV annihilation photons. The presence of annihilation photons is expected because a major mechanism of energy loss at high energies is pair production. The ^{16}N photons are approximately seven times more efficient in depositing dose than the 511-keV photons, and are therefore the major contributor to dose.

The effect of using the lead collimator was investigated by performing several measurements with and without the collimator. In general, the use of the collimator generated additional background counts at the low energies, which decreased the quality of the data. However, it was noted that the appearance of the spectra also changed. Figures 30 and 31 present data collected at the same location with and without using the lead collimator. The proportion of scattered photons is decreased compared to the ^{60}Co decay photons. Because the collimator allows photons to enter unattenuated only through a small opening, the conclusion is that the scatter is coming from a different direction than the ^{60}Co decay photons. The calculated C_x factor decreased from 1.04 to 1.02 without the scattered photons. If the scattered photons coming from different directions were added properly, the calculated C_x factor would probably be even lower. It has been observed using the extrapolation chamber that source geometry effects lower the C_x values in most locations.

The effect of the collimator in areas containing ^{16}N-decay photons was to almost eliminate the 511-keV photons from the spectrum. This effect is in agreement with the interpretation that the 511-keV photons originate from all directions, dependent on the intensity of high-energy photons interacting in matter. The effect of this on the high-energy results is minimal, since the ^{16}N photons are the dominant component and the dosimetric measurements automatically account for geometry effects.

The results of measurements performed with the extrapolation and ion chambers are given in Table 13. Measurements performed in the high-pressure steam injection room (HPSI) and at the fuel pool heat exchanger resulted in effective C_x values at or below unity. The shallow-depth values were less than the 0.3-cm and the deep-depth values, indicating a nearly pure photon field consistent with the ^{60}Co energies. The deep-depth values less than unity are attributed to geometry effects. The measurement at the clean-up phase separator tank was taken with the chambers in direct view of the radiation source. The results are consistent with a dominant ^{60}Co photon field. An appropriate measurement location for the extrapolation chamber with a sufficiently large dose rate of high-energy photons was not found. The humidity and temperature were too high in the heater bay, and the dose rates were too low in the turbine room.

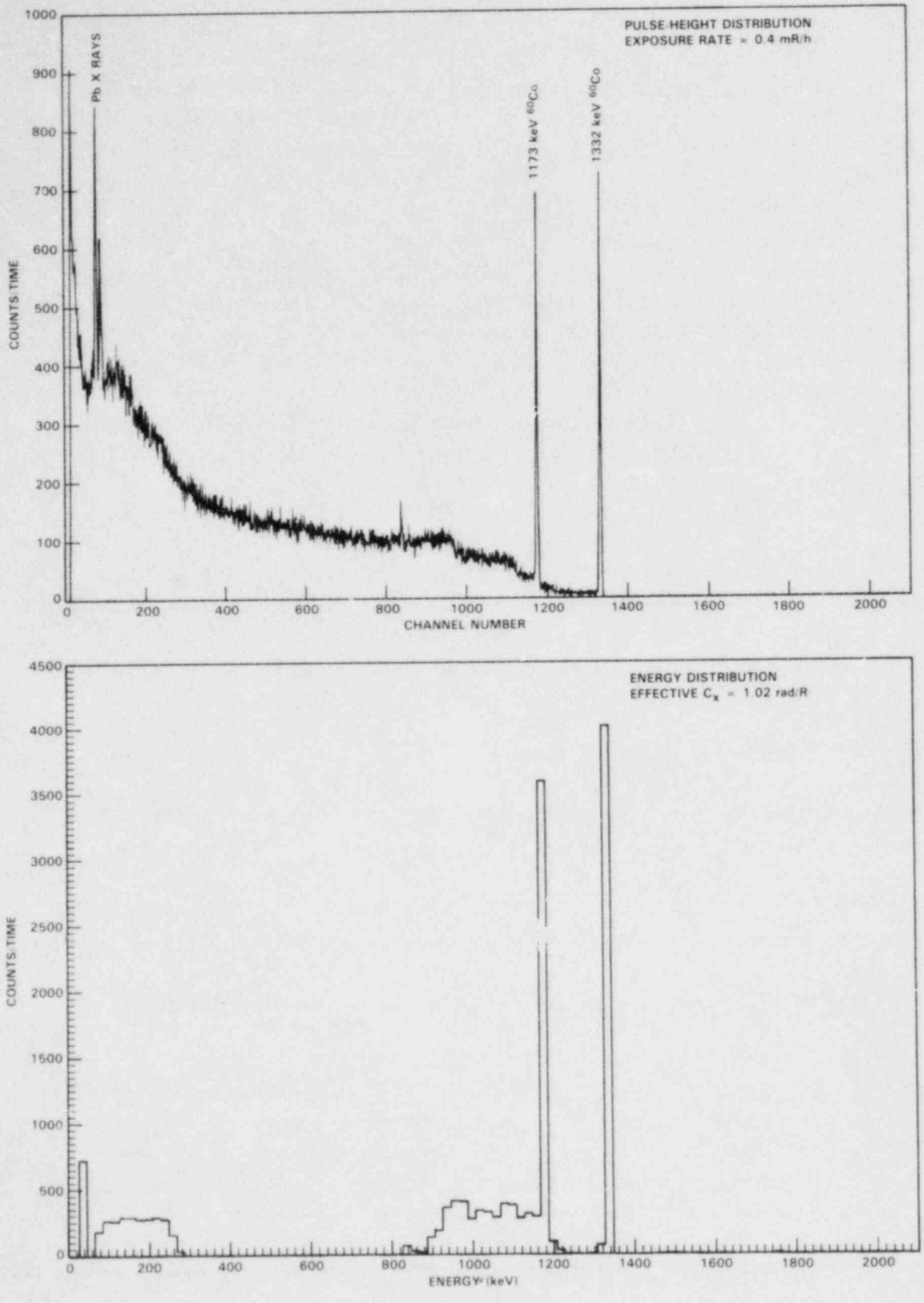

FIGURE 30. Field Data and Corrected Spectrum, Site M (Shutdown BWR, Refuel Pool General Area, Collimated)

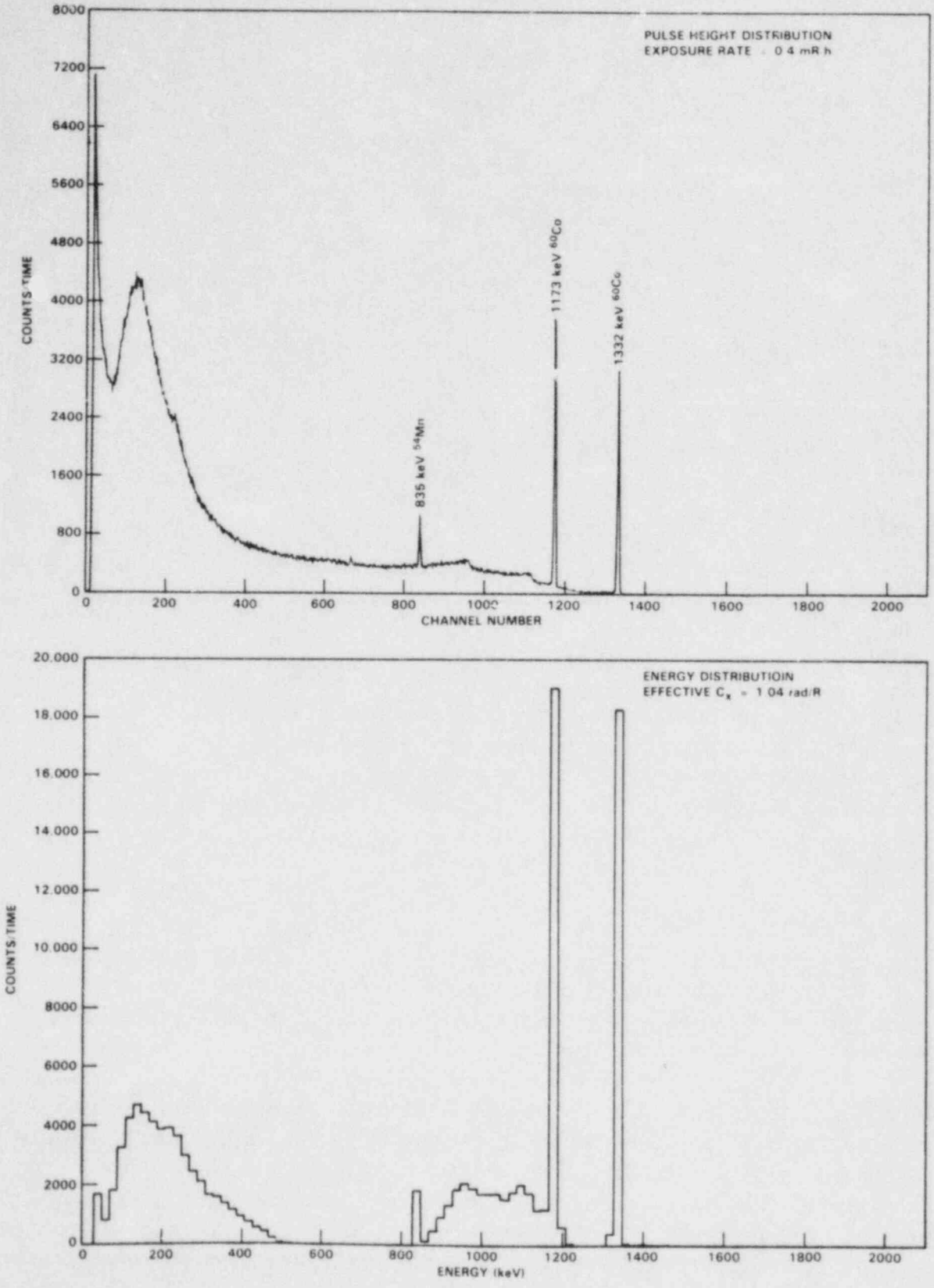

FIGURE 31. Field Data and Corrected Spectrum, Site M (Shutdown BWR, Refuel Pool General Area, Uncollimated)

TABLE 13. Extrapolation Chamber and Ion Chamber Measurements, Site M

Location	Exposure Rate (mR/h)	Dose Rate (mrad/h)	Effective C_x Factor (rad/R)
Shutdown BWR			
HPSI	2030		
Shallow		1770	0.87 ± 0.04
0.3 cm		2000	0.98 ± 0.04
Deep		1940	0.96 ± 0.04
Operating BWR			
Fuel Pool Heat Exchanger	178		
Shallow		149	0.84 ± 0.08
0.3 cm		180	1.01 ± 0.07
Deep		163	0.92 ± 0.04
Clean-Up Phase Separator Tank	7350		
Deep		7540	1.03 ± 0.03

The TLD-loaded phantom measurements are described in Table 14. Effective C_x factors for locations not containing high-energy photons ranged from 1.03 to 1.15. The measurement at the clean-up phase separator door was made at the highest dose rate without opening the door and entering the room. The results are consistent with the photon spectrometer measurements. The measurement performed at the turbine blade housing diaphragm showed primarily a beta field and was not analyzed for C_x factor. The TLD response versus depth is presented in Figure 32 for the shutdown reactor measurements and Figure 33 for the operating reactor measurements.

The TLD phantom placed in the heater bay was directed up toward the pipes near the ceiling that carry steam to the turbine. This field was expected to contain a large contribution of ^{16}N photons. A reduction in dose at the surface compared to the 2.5-cm depth was not observed. The depth-response curve has a surface enhancement of 30%.

The most significant effects of the presence of low-energy photons at Site M were found at the door to the clean-up phase separator room. The cause of the low energies was scatter from a suspected large concentration of ^{60}Co in the clean-up phase separator tank. Due to the polyenergetic distribution of the scattered photons, the calculated maximum C_x factor calculated from the photon spectrum was 1.16. All other locations not containing energies above

TABLE 14. TLD-Loaded Phantom Measurements, Site M

Location	Surface Dose Rate (mrad/h)	Field Strengths (mrad/h) for Photons				Effective C_x (rad/R)[a]
		34 keV	120 keV	662 keV	Beta	
Shutdown BWR						
Torus Drainline, HPSI	44	0	13	28	3	1.12
Turbine Blade Housing Diaphragm	162	0	0	8	154	-
Dry Well, Valve	183	0	13	162	8	1.05
Operating BWR						
Reactor Building Containment Equipment Storage Cage	20	0	1	18	1	1.05
Clean-Up Phase Separator Door	15	1	5	7	2	1.15
Skimmer Surge Task Room	43	0	0	38	5	1.03
Heater Bay	150	-				

(a) Shallow depth (7 mg/cm^2).

3 MeV had a large contribution from medium energy photons, primarily ^{60}Co, which reduced the calculated C_x values. Large contributions to dose from high-energy photons were found. However, no surface reduction in dose was observed. Current monitoring requirements appear adequate for the high-energy photon fields encountered.

A spectrum was taken using a 2-in. x 2-in. NaI(Tl) detector at the same location as one of the Ge spectra. The purpose was to demonstrate the utility of using the less-expensive detector for plant monitoring. Figure 34 presents a calibration and field measurement using a NaI(Tl) detector. The resolution is poor, but the peaks are recognizable. Figure 31 showed the Ge spectrum in the same location. All of the peaks present in the Ge spectrum are present in the NaI(Tl) spectrum. For spectral monitoring, the data analysis procedure would be the same for both detectors. The calibration spectrum provides efficiency and scatter signal versus energy.

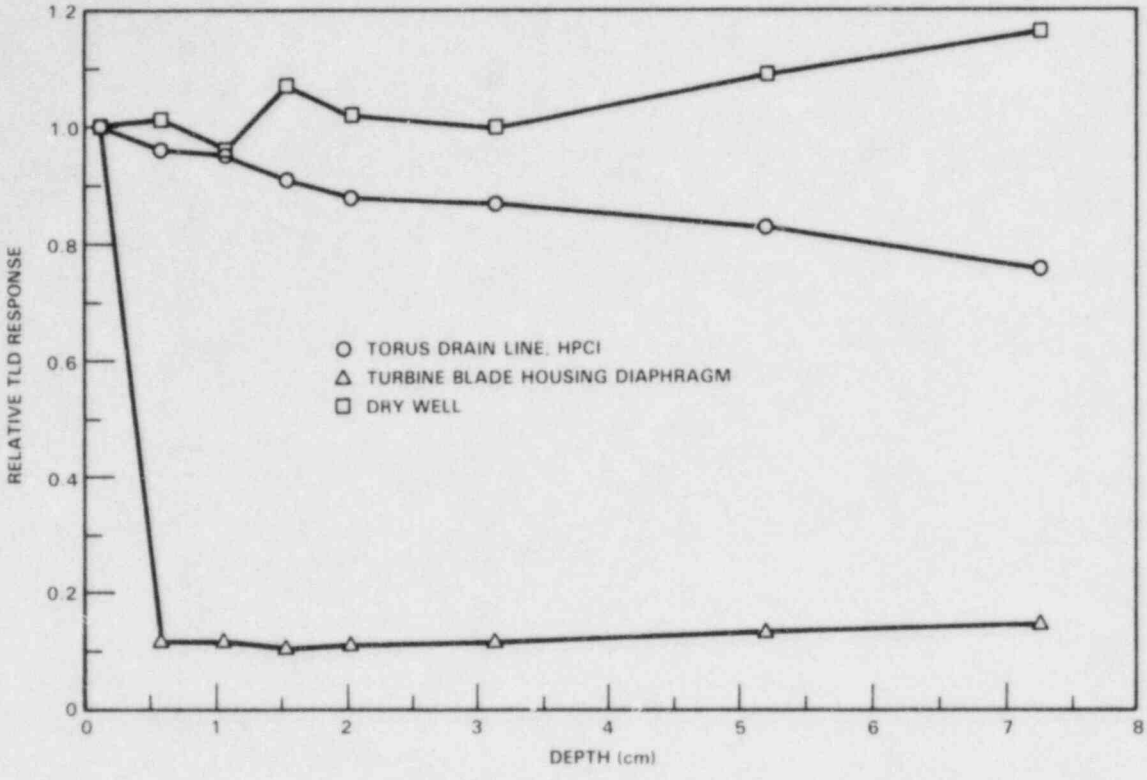

FIGURE 32. TLD-Loaded Phantom Measurements, Site M (Shutdown BWR)

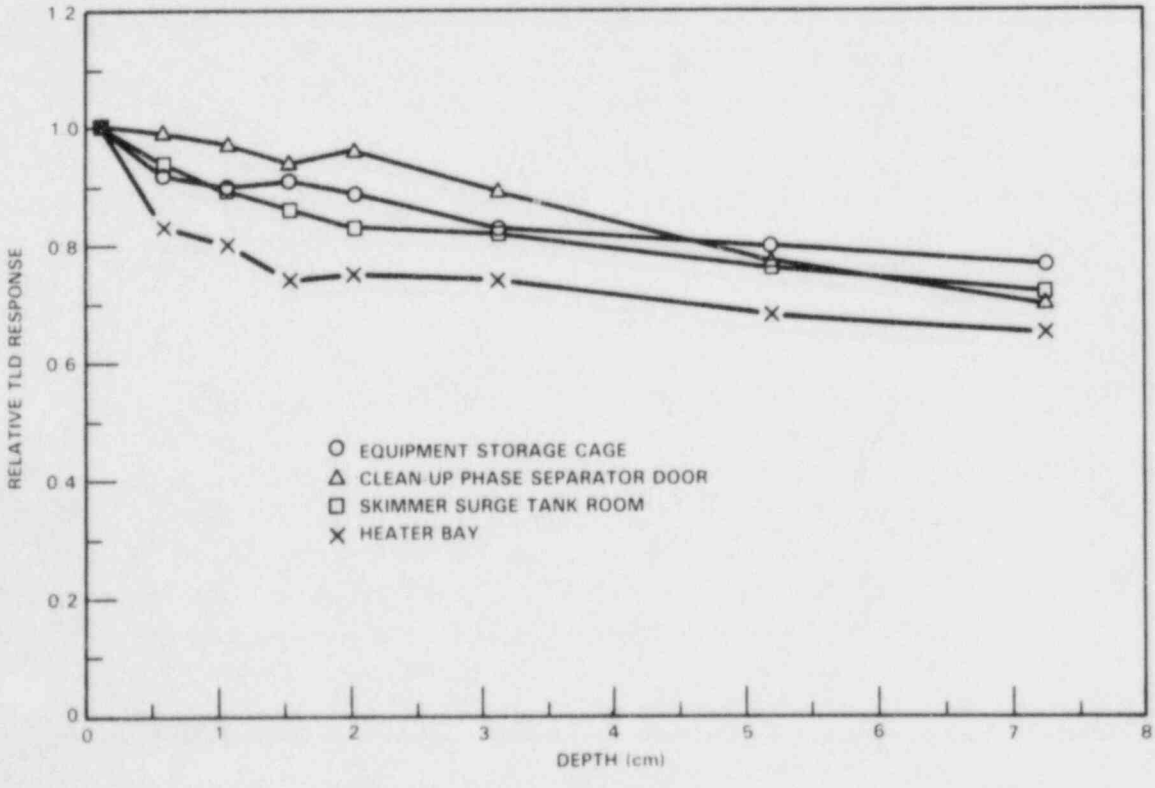

FIGURE 33. TLD-Loaded Phantom Measurements, Site M (Operating BWR)

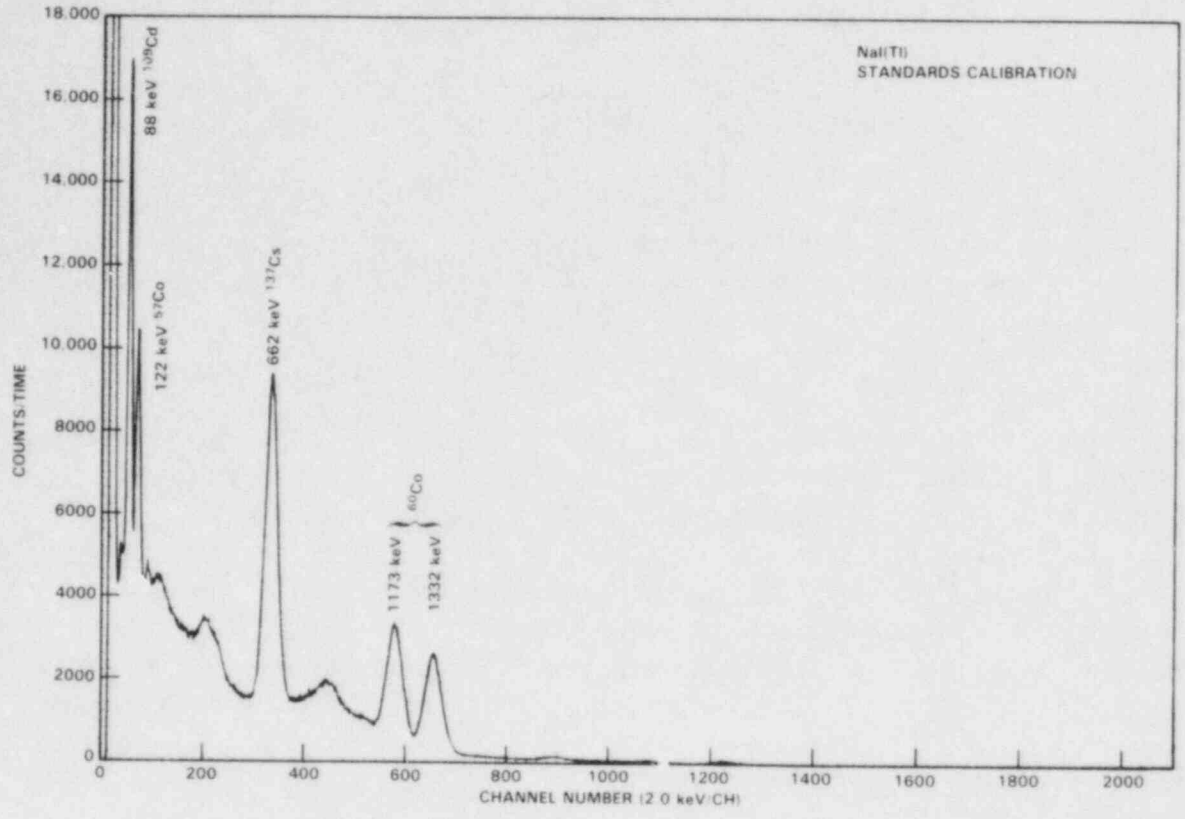

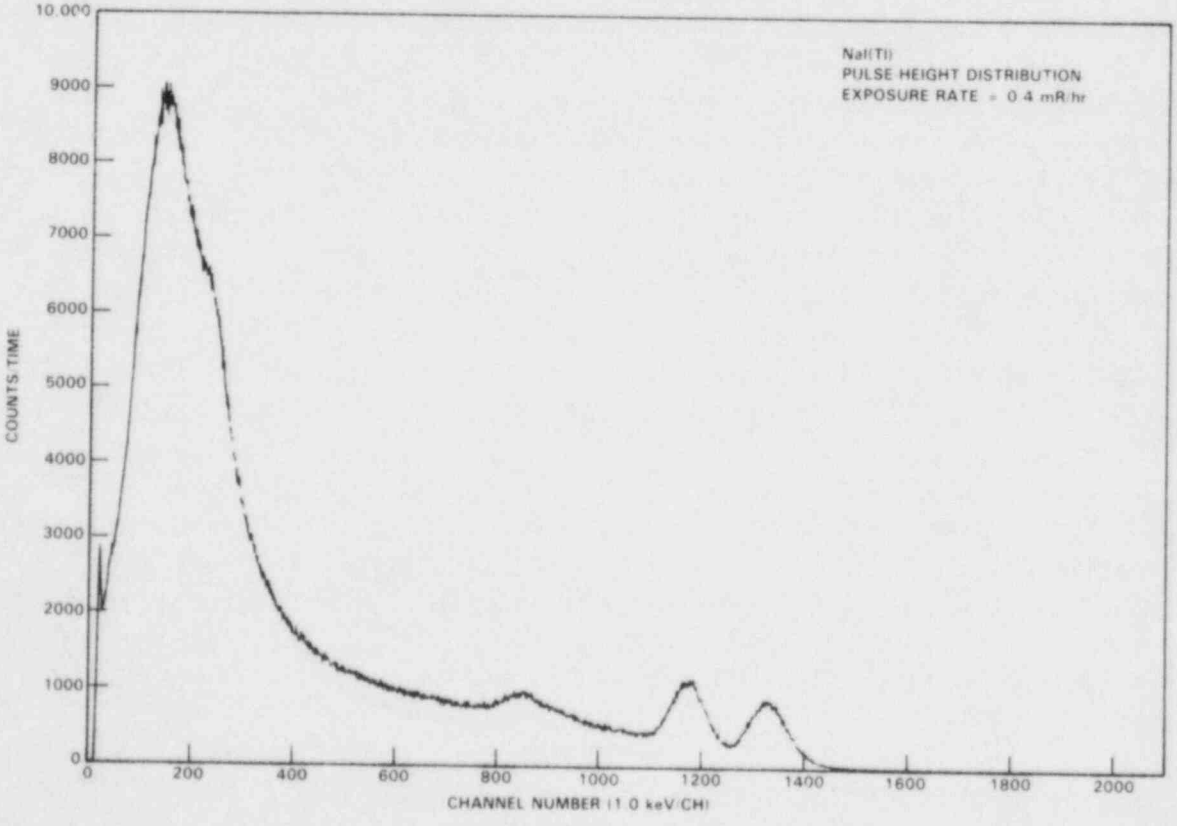

FIGURE 34. Calibration and Field Data, NaI(Tl) Detector

3.5 SITE Q - OPERATING BWR

Measurements were performed at 12 locations including areas in the turbine building, the reactor vessel sampling station, the spent-fuel room, and the waste storage facility. Emphasis was placed on monitoring areas with dominant high-energy photon contributions. A 31-cm^3 intrinsic Ge detector was used to measure spectra at the locations given in Table 15. The locations of the TLD phantom measurements are listed in Table 16. Extrapolation chamber measurements were not performed because the equipment was inoperable due to damage during shipment.

Measurement locations on the turbine floor of the turbine building are indicated in Figure 35. Locations included a high-rate area near the turbine (location E, approximately 900 mR/h), an area behind the bioshield (location D, 4 mR/h), and an area far from the turbine (location A, 4 mR/h). The photon spectra are dominated by high-energy photons, primarily 6.1-MeV photons from ^{16}N (Figure 36). The analysis of the spectral data summarized in Table 15 includes the calculated maximum C_x factors and the calculated central C_x factors. Calculations for all turbine building locations except the laundry/turbine loading area (location F) indicate approximately 40% and 90% of the maximum dose at 0.3 cm and 1 cm depths, respectively, for a pure photon field.

The underresponses predicted from the spectral data from the turbine building were not observed with the TLDs. The TLD phantom measurements were performed at locations C and E. The TLD phantom analysis using the linear least-squares technique was not reported because the set of basis energies were not representative of the radiations present. Figure 37 shows the depth-dose curves for these measurements. The data for both location C and location E show a surface enhancement rather than a surface underresponse. Additional measurements were made with multielement dosimeters to help characterize the surface response with location. These data, presented in Table 17, showed a surface enhancement, in approximate agreement with the TLD phantom results. Locations C and D have the greatest enhancement compared to locations E and B.

The enhancement shown in locations C and D extends to a tissue depth of approximately 1 cm. It could be the result of a range of electrons with an approximate maximum energy of 3 MeV or photons with an approximate energy of 15 keV. The observed response at depths greater than 1 cm implies penetrating photon energies, consistent with the presence of ^{16}N.

TABLE 15. Measurement Locations for Photon Spectrometer, Site Q

Location	Exposure Rate (mR/h)	Effective Maximum C_x, rad/R			Effective Central C_x, rad/R		
		0.007 cm	0.3 cm	1.0 cm	0.3 cm	1.0 cm	2.5 cm
Turbine Building							
A-Floor 272 Near Viewing Gallery	4	0.81	0.87	0.93	0.35	0.80	0.93
B-Floor 272 Behind Stairwell	10	0.82	0.88	0.94	0.38	0.82	0.94
C-Floor 272 NW Corner of Turbine	24	0.81	0.87	0.93	0.34	0.80	0.93
D-Floor 272 SW Corner Behind Shield Wall	4	0.81	0.87	0.93	0.35	0.81	0.93
F-Floor 248, Laundry/Turbine Loading Area	0.5	1.01	1.03	1.03			
G-Floor 248, Entrance #1 to Turbine Bldg.	1.5	0.82	0.88	0.94	0.38	0.81	0.93
H-Floor 248, Entrance #2 to Turbine Bldg.	5	0.81	0.87	0.94	0.37	0.81	0.93
I-Floor 248, General Area	0.7	0.82	0.88	0.94	0.39	0.86	0.93
Other							
J-Reactor Vessel Sampling Station	4.5	1.05	1.06	1.05			
K-Spent-Fuel Room	3.3	0.83	0.88	0.94	0.36	0.84	0.93
L-Waste Storage Area	3.0	1.04	1.05	1.05			

TABLE 16. TLD-Loaded Phantom Measurements, Site Q

Location	Shallow Dose Rate (mrad/h)	Field Strength[a] (mrad/h) for Photons 34 keV	117 keV	662 keV	Beta	Effective C_x[b] $(rad/R)^x$
C-Turbine Bldg., Floor 272	35	(analysis not appropriate)				
E-Turbine Bldg., Floor 272	910	(analysis not appropriate)				
J-Reactor Vessel Sampling Station	16	0	2	14	0	1.07

(a) Maximum dose at the shallow tissue depth.

(b) Shallow depth (7 mg/cm^2).

The photon spectra show that the dominant dose contributor is photons from ^{16}N. Only a relatively small contribution from medium-energy photons was observed (primarily 511-keV annihilation radiation). The surface enhancement could be due to one or a combination of several mechanisms. Possibilities are: 1) very low energy photons, 2) beta particles or electrons, and 3) the geometry of incident photons or electrons. These possibilities will be discussed in order.

Photons at energies below 20 keV are present, but not in the intensities required to produce a surface enhancement. Spectral data were taken for energies down to 15 keV for several locations. The large enhancement required to input the measured surface dose was not observed.

Nitrogen-16 emits beta particles at 4 MeV to 10 MeV, along with the photons. If ^{16}N atoms were being released into the atmosphere around the turbine, the associated beta particles would give a surface enhancement. An enhancement of about a factor of two would be present without shielding. However, this cannot be the only explanation for the enhancement seen, because location D, which is behind a shielding wall and should be preferentially protected from the beta particles, also has a surface dose enhancement.

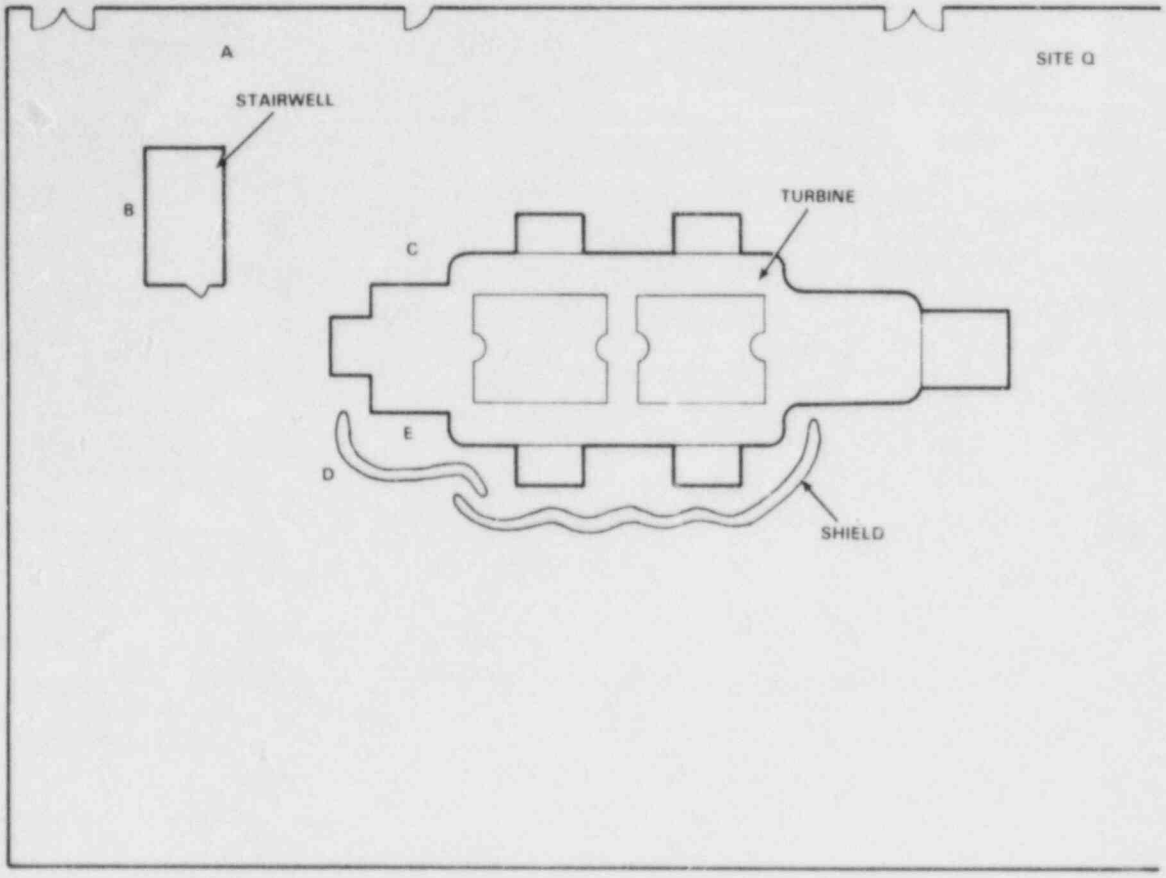

FIGURE 35. Schematic Diagram of the Turbine Floor, Site Q

Knock-on electrons exit all material through which photons pass. In the turbine room, this material includes both the generating equipment and shielding. The maximum electron energy is the same as the energy of the photons (approximately 6 MeV in the turbine room). The mean electron energy is much lower, about one-third of the photon energy. These electrons deposit 30 to 100 times more dose per particle than do photons of the same energy. Because the pair-production reaction for photons is dominant at 6 MeV, more electrons are generated in higher-atomic-number materials. The mass attenuation coefficient is 70% higher for lead than for tissue. Rogers (1983) investigated the effects of knock-on electrons in an accelerator-produced 6- to 7-MeV beam. Measurements performed with an ion chamber with Bakelite® walls resulted in surface enhancements from +33% for a lead filter to +15% for an aluminum filter. While the differences between the geometry of an open room and that of a collimated beam could affect results significantly, the values are the right order of magnitude to explain the observed surface enhancements.

® Bakelite is a registered trademark of Union Carbide Corp., Plastics Division.

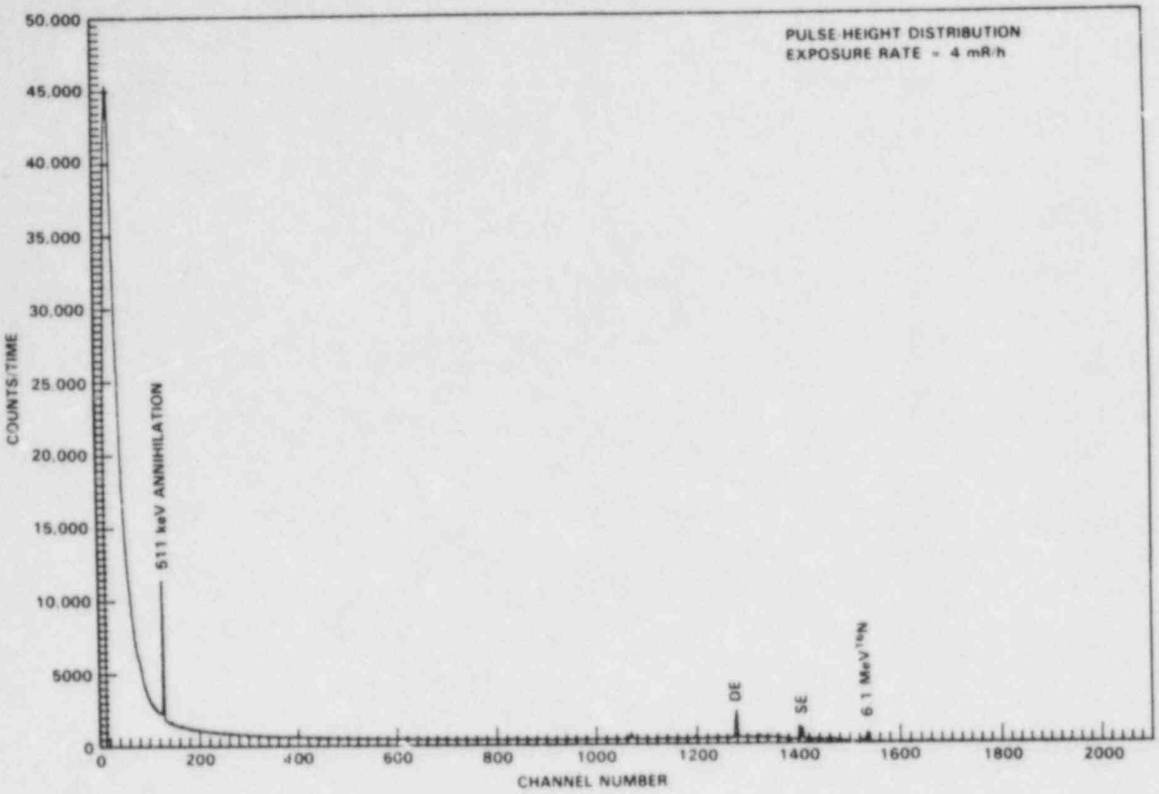

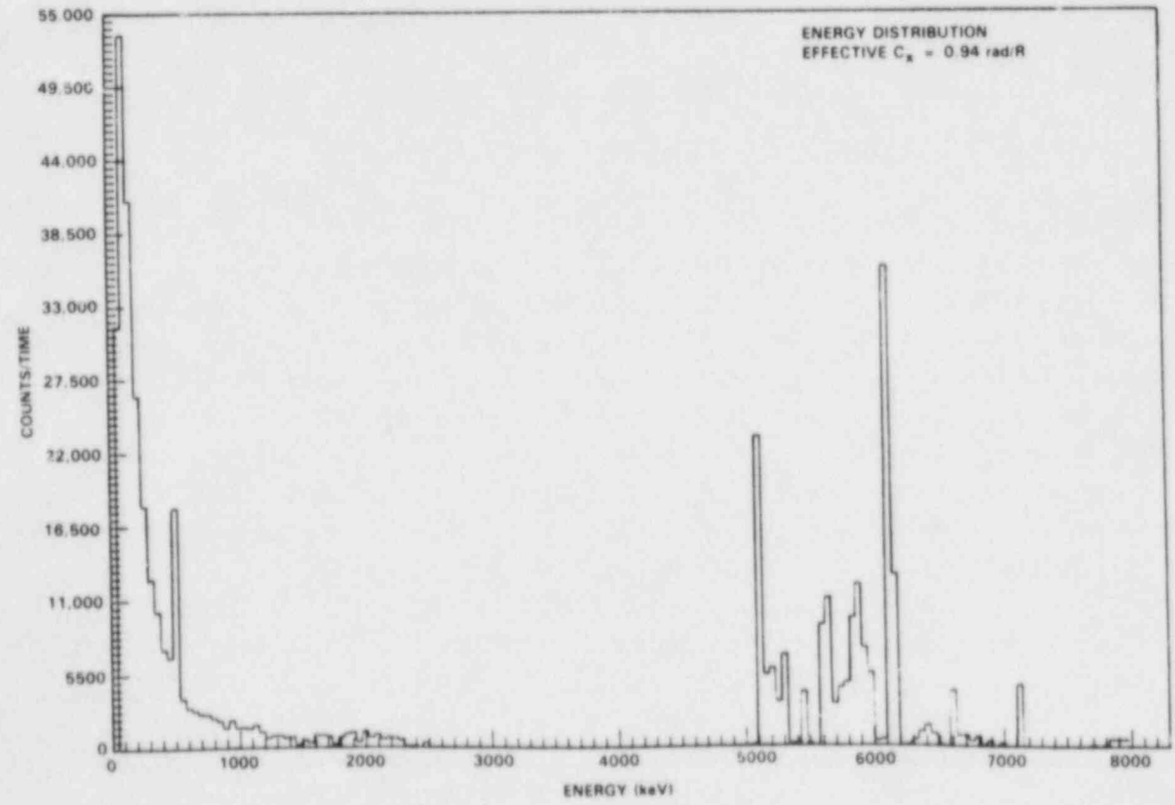

FIGURE 36. Field Data and Corrected Spectrum, Site Q, Location D (Turbine Floor 272, Behind Shield Wall)

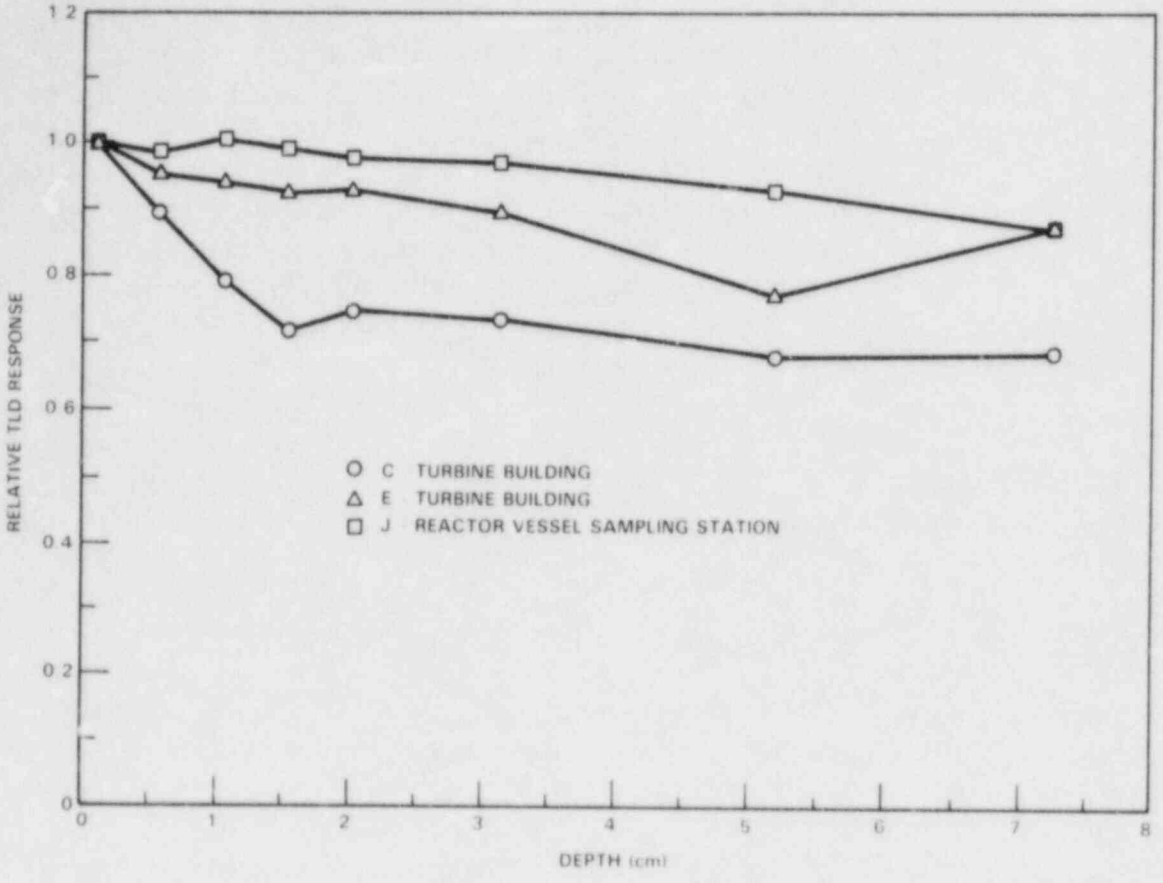

FIGURE 37. TLD-Loaded Phantom Measurements, Site Q

TABLE 17. Relative Response for Multielement Dosimeters, Site Q

Location	Exposure Rate (mR/h)	Relative TLD Response Versus Effective Filtration (mg/cm²)				
		0.12	0.26	0.34	0.98	1.12
B-Turbine Bldg., Floor 272	10	1.00	0.97	0.96	1.03	0.93
D-Turbine Bldg., Floor 272	4	1.00	0.96	0.90	0.82	0.78
E-Turbine Bldg., Floor 272	900	1.00	1.00	0.99	0.93	0.90

The direction of the incident photons or electrons affects the depth-dose distribution by depositing dose with depth along a path oblique to the front surface of the phantom or dosimeter. This effect would probably be greatest for locations C and D (close to the scatter source, but shielded from the primary source) and least for location B (far from the primary and scatter sources) and location E (close to the primary source). This effect agrees with the observations of greater enhancements at locations C and D. However, because dose deposited by the scattered continuum and the 511-keV photons is small compared to the ^{16}N photons, the knock-on electrons exiting all surface are probably the greatest contributors to this effect.

Locations F, J, and L had a negligible contribution from high-energy photons. These locations had a dominant contribution from ^{60}Co, resulting in effective C_x factors near unity. The TLD data for location J agreed with the spectrometer data.

3.6 SITE P - SHUTDOWN PWR

Measurements were performed at 10 locations, including areas in the waste storage facility, the spent-fuel pit, the auxiliary building, and containment. The locations of measurements performed with the photon spectrometer (31-cm^3 intrinsic Ge detector) are listed in Table 18 along with the exposure rates and calculated effective C_x factors. The TLD phantom measurements are summarized in Table 19 and Figure 38. The exposure rates in all areas monitored were relatively small (<20 mR/h). No higher rates were located in accessible areas.

The spectra show the dominance of ^{60}Co and the presence of several other radionuclides emitting primarily medium-energy photons. No areas were found with dominant contributions from low-energy photons. The calculated effective C_x factors range from 1.04 to 1.06.

The TLD phantom data also indicated that the primary spectral components are medium-energy photons, represented by the 662-keV component. The effective C_x values are higher for this anlaysis than for the analysis of the photon spectral data, but they are also less precise. Only a relatively small beta-field component was observed. The depth-response curves show somewhat erratic behavior, but are consistent with the above interpretation.

The data indicate that the effective C_x values are not significantly enhanced for Site P. No locations with unusual photon spectra were found.

TABLE 18. Measurement Locations for Photon Spectrometer, Site P

Location	Exposure Rate (mR/h)	Effective Maximum C_x (rad/R) 0.007 cm	0.3 cm	1.0 cm
Waste Storage Area				
A-Barrell Storage (outside Waste Disposal Bldg.)	3.0	1.05	1.05	1.05
B-Compactor Area (outside Waste Disposal Bldg.)	2.0	1.06	1.05	1.05
C-Waste Disposal Bldg.	2.7	1.06	1.06	1.06
Spent-Fuel Pit				
D-Heat Exchanger, Spent Fuel Pit	4.4	1.05	1.05	1.05
E-Ion Exchange Pit	2.4	1.05	1.05	1.05
F-Fuel Transfer Shoot	3.9	1.06	1.06	1.06
G-Spent-Fuel Pit	2.2	1.06	1.06	1.06
Auxiliary Building				
H-Primary Auxiliary Bldg., General Area	0.7	1.05	1.05	1.05
I-Open Surge Line	2.5	1.06	1.06	1.06
Containment				
J-Above Reactor Head Area (Flooded)	2.0	1.04	1.04	1.04

3.7 SITE N - OPERATING BWR

Measurements were performed at 13 locations during operation (78% of capacity). Emphasis was placed on the presence of high-energy photons, particularly due to ^{16}N. Areas monitored included the heater bay, the main steam isolation valve room (MSIV), the turbine area, and the clean-up phase separator area.

TABLE 19. TLD-Loaded Phantom Measurements, Site P

Location	Shallow Dose Rate (mrad/h)	Field Strength[a] (mrad/h) for Photon				Effective C_x[b] $(rad/R)^x$
		34 keV	117 keV	662 keV	Beta	
C-Waste Disposal Building	2.8	0	0.7	1.7	0.4	1.13
F-Fuel Transfer Shoot	16	0	6	10	0	1.16

(a) Maximum dose at the shallow tissue depth.
(b) Shallow depth (0.007 cm).

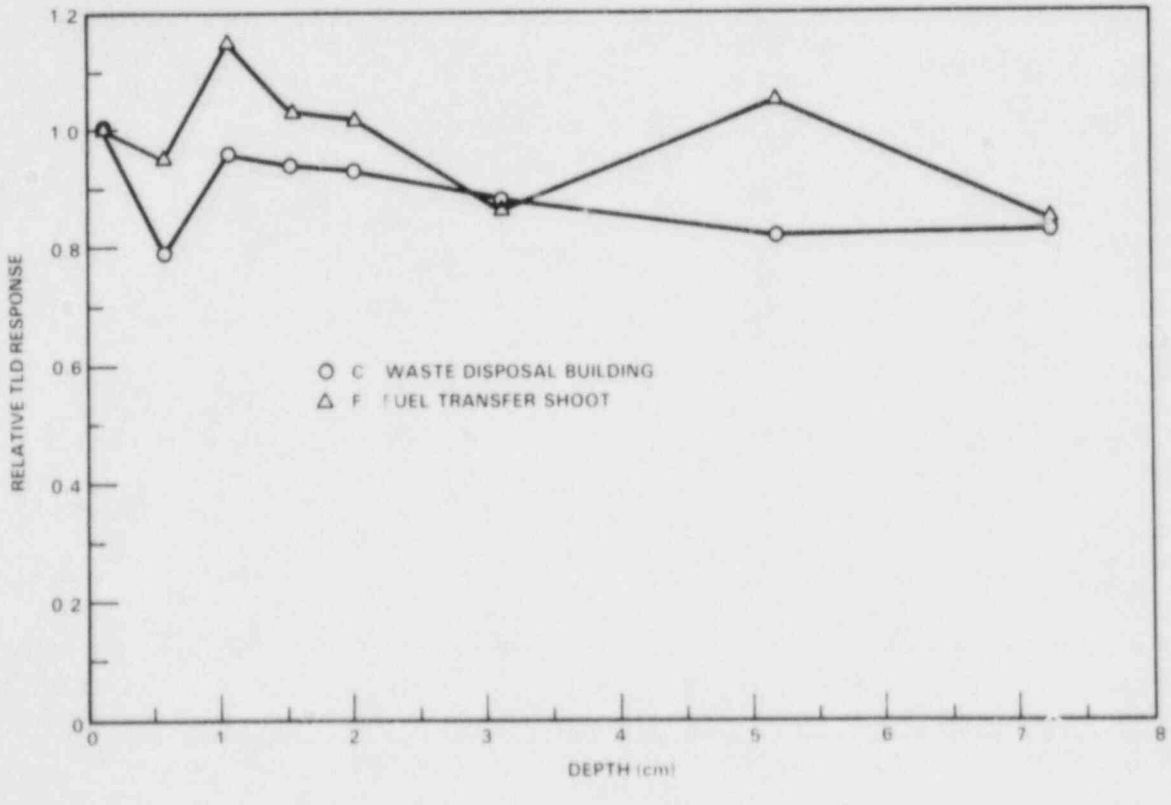

FIGURE 38. TLD-Loaded Phantom Measurements, Site P

Significant contributions to dose due to ^{16}N photons were found in the heater bay, the MSIV, and near the turbine (Figure 39). The calculated central C_x^* factors predict surface underresponses based on the photon field only (Table 20). Dosimetric data were taken in these areas to measure dose at the surface compared to dose at other depths. The results of the extrapolation and ion chamber measurements made in the MSIV are contained in Table 21. The dose measured at the surface was greater than the dose at other depths. The results for the depths 0.3 cm, 1.0 cm, and 2.5 cm were essentially the same.

The TLD-loaded phantom measurements were performed in the heater bay, the MSIV, and at two locations in the turbine room (Table 22). All locations showed an enhanced dose rate at the surface (Figure 40). The measurement for the MSIV was performed in approximately the same location as the extrapolation and ion chamber measurements, with consistent results.

The TLD phantom measurements were compared to the results of the dosimetry methods used at the plant (Table 22). The exposure rate at the phantom position was checked with a survey meter. Pocket ionization chambers and personnel dosimeters (film badges) were mounted on the front face of the phantom for timed exposures. The measured surface dose rates were higher than the survey meter readings, which is consistent with enhanced surface doses. The pocket ionization chamber and the Site N personnel dosimeter overresponded by 12% and 49%, respectively. The overresponse of the film badges was probably due to the increased response at 6 MeV for the high-atomic-number material in the film emulsion and the filter packet.

These measurements do not indicate an inadequacy in the current personnel monitoring requirements. The performance of personnel dosimeters manufactured with high-atomic-number material may be poor, but they will most likely overrespond to the high-energy photon fields.

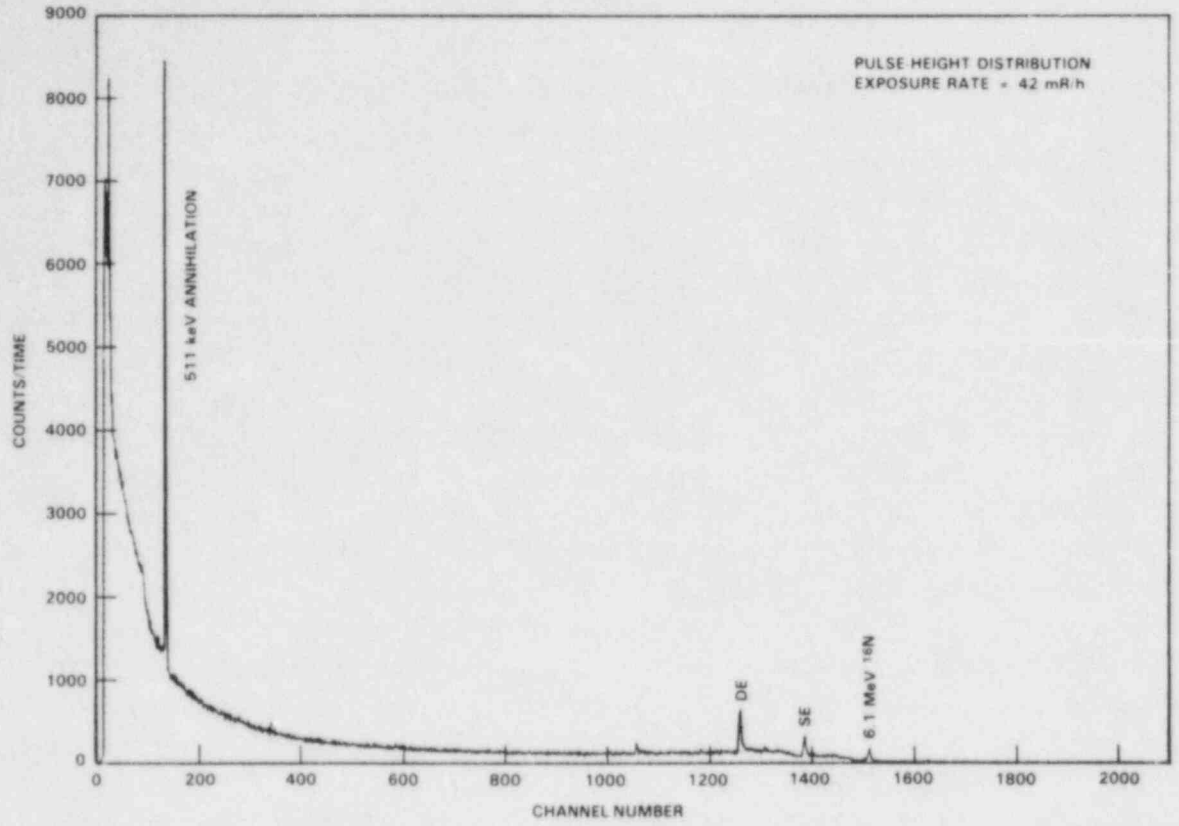

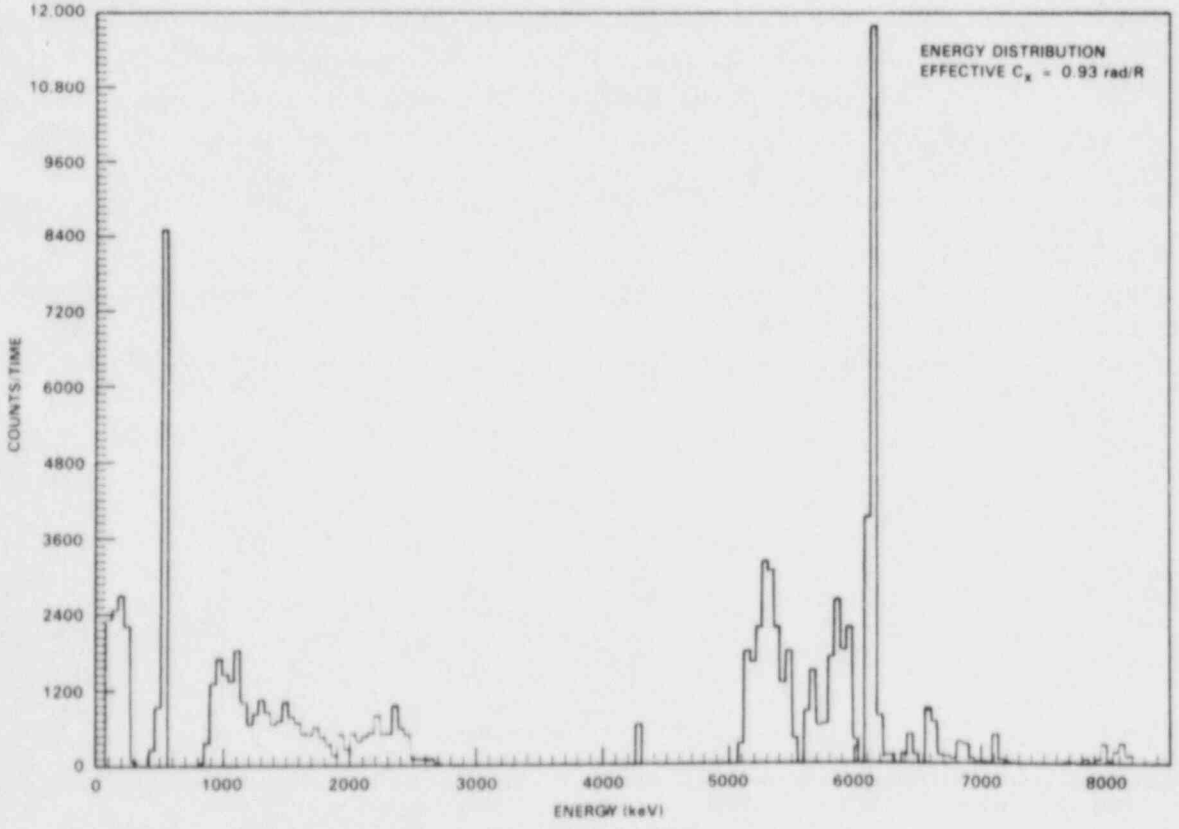

FIGURE 39. Field Data and Corrected Spectrum, Site N, Location H (Operating BWR, Turbine Room, with Collimator)

TABLE 20. Photon Spectrometer Measurements, Site N

Location	Exposure Rate (mR/h)	Maximum Effective C_x (rad/R)			Central Effective C_x (rad/R)		
		0.007 cm	0.3 cm	1.0 cm	0.3 cm	1.0 cm	2.5 cm
Operating BWR							
A-Heater Bay, Entrance	20	0.89	0.93	0.97	0.53	0.88	0.97
B-Heater Bay, Near Steam Lines	30	0.83	0.88	0.94	0.38	0.84	0.94
C-MSIV, Entrance Hallway	23	0.82	0.87	0.94	0.35	0.81	0.93
D-CRD Room	48	0.98	1.01	1.02			
E-Storage Room, Contaminated Pipe	60	0.99	1.02	1.02			
F-Turbine Floor, Outside Shield Wall	0.6	1.01	1.04	1.06	0.79	1.01	1.06
G-Turbine Floor, Maze Entrance to Turbine Room	6	0.81	0.87	0.93	0.33	0.79	0.93
H-Turbine Floor, Inside Turbine Room	42	0.81	0.87	0.93	0.33	0.80	0.93
I-Clean-Up Phase Separator Room Door	7	1.07	1.08	1.08			

TABLE 21. Extrapolation Chamber and Ion Chamber Measurements, Site N

Location	Exposure Rate (mR/h)	Dose Rate (mrad/h)	Effective C_x Factor (rad/R)
J-MSIV	338		
Shallow		372	1.10 ± 0.04
0.3 cm		270	0.80 ± 0.15
Deep		277	0.82 ± 0.06
2.5 cm		264	0.78 ± 0.04

TABLE 22. TLD-Loaded Phantom Measurements, Site N

Location	Surface Dose Rate (mrad/h)	Survey Meter (mR/h)	Pocket Ionization Chamber (mR/h)	Site N Personnel Dosimeter (mrem/h)
K-Heater Bay	106	80	130	152
J-MSIV	395	330	450	508
L-Turbine Room	84	70	83	123
M-Turbine Room	246	220	280	434

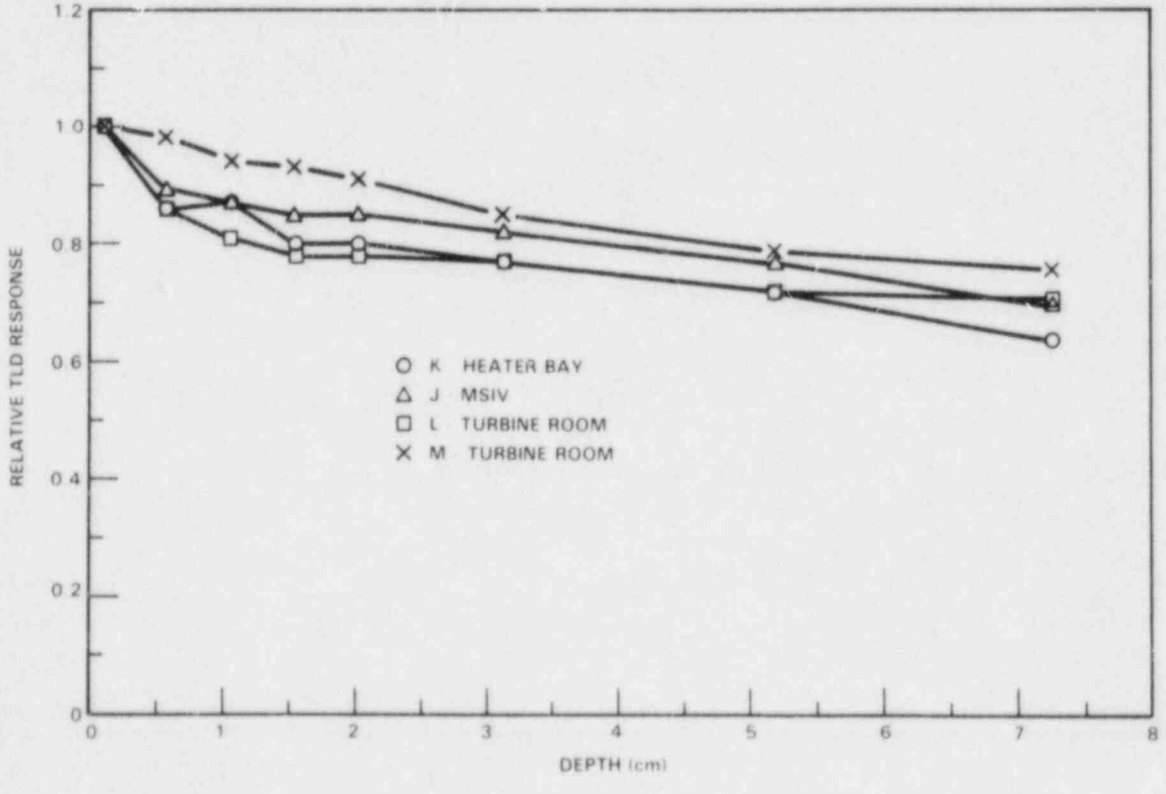

FIGURE 40. TLD-Loaded Phantom Measurements, Site N

4. DISCUSSION

The discussion section has three parts covering the impact of improved C_x factors, high-energy photon dosimetry, and recommendations for plant monitoring procedures.

4.1 IMPACT OF IMPROVED C_x FACTORS

The areas monitored can be approximately classified into four categories: 1) radiation fields dominated by decay photons from radioactive atoms in neutron-activated or fission-product deposits; 2) radiation fields dominated by a scattered-photon continuum; 3) radiation fields containing short-lived radioactive noble gases; and 4) radiation fields dominated by high-energy photons. High-energy photons have C_x factors less than unity and will be discussed in section 4.2. The remaining three categories will be discussed here in turn.

Dose rates in most plant areas are dominated by lightly shielded radioactive sources in neutron-activated or fission-product deposits. The published C_x values for the decay photons from these sources range from 1.00 rad/R to 1.04 rad/R (parallel geometry). Calculated C_x factors for these areas are, at most, a few percent higher after the addition of contributions from the scatter continuum.

The energies comprising the scatter continuum vary with location. The maximum photon flux is at approximately 120 keV, with a half-maximum range between about 70 keV and 250 keV. A higher-energy tailing to above 500 keV skews the distribution, lowering the cumulative C_x factor, for most locations. The average C_x factor for the scatter continuum is no more than 1.2. Averaging the decay photons from long-half-life sources with the scatter continuum yields calculated C_x values between 1.00 and 1.10.

Only one location, near the clean-up phase separator door at Site M (BWR), was identified as being dominated by low-energy photons. The dominance of low-energy photons is present whether the plant is operating or shutdown. A similar location was monitored at Site N. However, sufficient radioactive cesium and cobalt were in the immediate vicinity to reduce the calculated C_x value to below 1.10.

The areas with significant radioactive ("crud") buildup will not have elevated C_x factors. Clean well-shielded areas are more likely to have both elevated C_x factors and low dose rates. Two locations that were monitored had

exposure rates less than 0.1 mR/h: the worker locker room at Site M and the gatehouse at Site Q. The resulting C_x factors for these locations were 1.17 rad/R and 1.11 rad/R, respectively. While these areas will never contribute a significant amount to occupational exposure, they do illustrate the effect for uncontaminated, highly shielded areas.

Radioactive noble gases were detected inside of containment at operating PWRs. The noble gases permeate the atmosphere, giving isotropic incidence of decay photons. For isotropic incidence, only the shallow-depth C_x factors are significantly greater than unity for low-energy photons. Most photons are attenuated by the ICRU sphere (or the worker) before reaching greater depths. Because the efficiency of flux-to-dose conversion favors the higher-energy photons, the presence of photons near or greater than 1 MeV overshadows the effects of the 81-keV and 249-keV photons from the xenon isotopes. Even spectra taken in personnel hatches had sufficient higher-energy contributions to keep the calculated C_x values near unity.

As was noted several times during the description of the site measurements, at many locations the source-decay photons and the scatter continuum originate from different locations. If the locations were all in one general direction, the shallow-dose C_x factors would be little affected. However, if they were coming from opposite directions, the C_x factors would be below unity. The extrapolation chamber measurements indicated that the most likely case is for distributed sources and for C_x factors less than unity.

Average reported doses will not be substantially affected by the use of improved C_x factors. The majority of worker exposures result from the higher-exposure-rate locations. These locations are more likely to have dominant localized sources or distributed sources. The impact of changing the effective C_x values from a defined value of 1 to the actual values would not be detected among larger dosimetric uncertainties, such as changes in the response of personnel dosimeters to meet requirements in ANSI N13.11. Even dosimeters with dramatic improvements in low-energy response would not noticeably alter reported doses (<5% change). The exception would be deliberately altering the response to ^{137}Cs to achieve an overall acceptable response at low energies. This change would shift the reported doses almost in direct proportion to the response shift. Such a change is potentially serious because the response of a dosimeter to ^{137}Cs can be lowered by as much as 40% and still meet ANSI N13.11 criteria.

The desired accuracy of the reported dose for each worker may require special plant monitoring to be performed. The guidance provided by the International Commission on Radiation Units and Measurements (ICRU) Report 20

(ICRU 1971) and the National Council on Radiation Protection and Measurements (NCRP) Report No. 57 (NCRP 1978) is that reported doses be accurate to within 30% near maximum permissible levels. While the effects of C_x factors are less than 30%, it is desirable to keep each contributory effect much less than the maximum. If we chose to correct the dose if the difference were greater than one-third of the recommendation, or 10%, only one of the measurement locations investigated during this study would be identified as definitely requiring a correction. Seven other locations at four sites would be classified as marginal (calculated $C_x > 1.08$ or TLD-measured $C_x > 1.10$).

4.2 HIGH-ENERGY PHOTON DOSIMETRY

Site measurements of high-energy (>3-MeV) radiation fields were performed to help determine the adequacy of current personnel monitoring requirements. The greatest depth required for monitoring is 1 cm of tissue. Because pure high-energy photon fields (3 to 10 MeV) deposit the maximum dose at depths between 2 and 4 cm of tissue, current practices could be underestimating the maximum dose received.

Measurements were performed at three operating PWRs and three operating BWRs. Both reactor types had locations with dominant high-energy photon contributions. Inside containment at operating PWRs, there were significant high-energy photons up to 8 MeV along with contributions from low- and medium-energy photons. The predicted reduction in the measured dose at 1 cm compared to the actual maximum dose was small (approximately 10%). In turbine rooms at the BWRs approximately 80% of the dose deposited was due to high-energy photons from ^{16}N. The other major contributor was 511-keV annihilation radiation. Predicted maximum reductions in dose at 1 cm were as high as 20%.

Dosimetric measurements were peformed at all operating reactor sites. In no location was the predicted reduction in dose at depths of 1 cm and less observed. Either no enhancement or else a large (approximately 40%) enhancement of the surface dose was measured.

Measurements performed at Site Q were designed to investigate the origin of the enhanced surface dose. The only plausible explanation was the presence of knock-on electrons created by the high-energy photons interacting with all matter in the vicinity of the measurement. Electrons generated in a tissue-like material (low atomic number) would have an intensity similar to those generated inside of the phantoms. Electrons generated by material with a higher atomic number would have a greater intensity because of the atomic-number dependence of the pair production interaction. The observed surface enhancements were probably created by the presence of iron in the turbine

areas or high-atomic-number shielding components (e.g., lead). Oblique incidence of the electrons and the 511-keV photons also increased the surface dose.

Many personnel dosimeters are designed with high-atomic-number filters to achieve responses like the 1-cm depth in tissue in a compact space. These filters are typically designed and calibrated to meet the dosimetry requirements of ^{60}Co and ^{137}Cs sources. However, because pair production is the dominant interaction at high energies, these personnel dosimeters would overrespond to 6-MeV photons. Film emulsion manufactured with high-atomic-number materials would also overrespond. This effect was observed at Site Q.

4.3 RECOMMENDATIONS FOR PLANT MONITORING PROCEDURES

The greatest contribution to the difference between exposure in air and dose in phantom (or worker) is the photon backscatter created in the phantom. If a perfectly calibrated personnel dosimeter were placed on a phantom (or worker) in a low-energy photon field, it would provide an accurate dose estimate. Correction factors would only be required to compensate for a poor energy response. Both the proposed modifications to 10 CFR 20 and ANSI N13.11 (1983) encourage the use of personnel dosimeters with improved low-energy response. Exposure-rate measurements performed with ion chamber instruments require C_x factors to convert to dose rates.

Correction factors other than C_x factors may be more useful for particular applications. The energy response of an instrument or dosimeter can be used to generate correction factors for response to dose as easily as to generate factors for exposure to dose.

Quick plant surveys can be performed using photon spectrometers. A Ge, Ge(Li), or NaI(Tl) detector is adequate provided that the efficiency and response function are determined. The use of a collimator will increase the measurement range. Dosimetric measurements should be performed in areas with unusual spectra or with high dose rates. The response of personnel monitoring instruments and dosimeters should be determined by direct measurement in these locations. Correction factors may be required for jobs performed in only a few locations (if any).

The potential for inaccurate dosimetry is greater for high-energy fields than for low-energy fields. Dosimeters manufactured with high-atomic-number material for element filters and film dosimeters may overrespond by as much as 60% due to differences in the cross sections for pair production. However, these dosimeters always provide conservative dose estimates.

5. CONCLUSIONS

No locations containing primarily low-energy photons with large C_x factors (approximately 1.5 rad/R) were found during measurements at seven operating and shutdown reactors. The most significant production of low-energy photons at commercial nuclear reactors is due to scattering in shielding material. The effective C_x factor for the scattered-photon continuum is no more than 1.2 rad/R. Most locations have radiation fields of nearly all medium-energy photons due to radioactive decay of cobalt and/or cesium isotopes or a combination of medium-energy photons with a scatter continuum. The estimated C_x factors for these locations, assuming parallel incidence of the photons, ranged between 1.00 rad/R and 1.10 rad/R. Directionality measurements (made using a collimator) and dosimetric measurements indicated that most locations have distributed sources, implying effective C_x factors less than unity. Only one location was found with a spectrum composed almost entirely of scattered photons and a C_x factor of 1.16 rad/R.

Monitoring requirements at 0.007-cm and 1.0-cm depths in tissue were found to be adequate for estimating the dose received in radiation fields at commercial nuclear reactors containing high energy photons. High-energy fields were found to dominate dose received in containment of operating PWRs and in the turbine areas and heater bays of BWRs. Surface doses probably due to accompanying high-energy electrons were measured in all locations monitored. The presence of the electrons was attributed to production processes associated with the high-energy photon field interacting with all material in the vicinity. The excess surface dose observed in several locations was attributed to the interaction of the high-energy photons in atoms with high atomic numbers and to oblique incidence of the electrons. Personnel dosimeters using high-atomic-number filters and film dosimeters are predicted to overrespond in areas dominated by high-energy photons.

We recommend that the response of current personnel dosimeters to high-energy photon fields be investigated. Due to the widespread use of high-atomic-number materials for penetrating-radiation filters in personnel dosimeters, the overresponse problem is potentially significant. High-energy photon fields (>3 MeV) were not included in ANSI N13.11, yet are a major contributor to dose received at many locations in operating plants. Current and new dosimeter designs which meet specifications in ANSI N13.11 may respond poorly to high-energy fields.

The analysis of photon spectra performed here had considerable uncertainty for high-energy fields. The causes were the large efficiency corrections

required for the Ge detectors and the approximate scatter corrections applied. We recommend that further attention be given to data collection and analysis techniques for the high-energy fields. Improvements in the accuracy of reported doses will probably require accurate dosimetric measurements along with dosimeter redesign or the development of correction factors through accurate plant surveys.

6. REFERENCES

American National Standards Institute (ANSI). 1983. American National Standard Criteria for Testing Personnel Dosimetry Performance. ANSI N13.11-1983, New York, New York.

Code of Federal Regulations. Title 10, Part 20, "Standards for Protection Against Radiation." U.S. Government Printing Office, Washington, D.C.

Dimbylow, P. J., and T. M. Francis. 1979. A Calculation of the Photon Depth-Dose Distributions in the ICRU Sphere for a Broad Parallel Beam, A Point Source and an Isotropic Field. NRPB 92, National Radiological Protection Board, Harwell, England.

Endres, G. W. R., et al. 1983. Neutron Dosimetry at Commercial Nuclear Plants. Final Report of Subtask A: Reactor Containment Measurements. NUREG/CR-1769, PNL-3585, Pacific Northwest Laboratory, Richland, Washington.

Fenyves, E., and Q. Haiman. 1969. The Physical Principles of Nuclear Radiation Measurements. Academic Press, New York.

Hajnal, F., and C. Klusek. 1974. "Semi-Empirical Efficiency Equations for Ge(Li) Detectors." NIM 122:559-565.

International Commission on Radiation Units and Measurements (ICRU). 1971. Radiation Protection Instrumentation and Its Application. ICRU Report 20. ICRU Publications, Washington, D.C.

Johns, H. E., and J. R. Cunningham. 1978. The Physics of Radiology. 3rd ed. Charles C. Thomas Publisher, Springfield, Illinois.

National Council on Radiation Protection and Measurements (NCRP). 1978. Instrumentation and Monitoring Methods for Radiation Protection. NCRP Report No. 57, Washington, D.C.

Nelson, R. F., and A. B. Chilton. 1983. Low-Energy Photon Dose Deposition in Tissue Slab and Spherical Phantoms. NUREG/CR-3425, University of Illinois.

Rathbun, L. A., and P. L. Roberson. 1983. Beta Particle Measurement and Dosimetry Requirements at NRC-Licensed Facilities. NUREG/CR-3544, PNL-4886, Pacific Northwest Laboratory, Richland, Washington.

Rogers, D. W. O. 1983. "A Nearly Monoenergetic 6-7 MeV Photon Calibration Source." Health Phys. 45(1):127-137.

Seelentag, W. W., and W. Panzer. 1979. "Stripping of X-Ray Bremsstrahlung Spectra Up to 300 kVp on a Desk Type Computer." Phys. Med. Biol. 24(4):767-780.

Seltzer, S. M. 1981. "Calculated Response of Intrinsic Germanium Detectors to Narrow Beams of Photons with Energies up to ~300 keV." NIM 188:133-151.

U.S. Department of Health, Education, and Welfare (DHEW). 1970. Radiological Health Handbook. U.S. Government Printing Office, Washington, D.C.

U.S. National Bureau of Standards (NBS). 1983. Calibration and Related Measurement Services at the National Bureau of Standards. NBS Special Publication 250, Appendix.

Yoder, R. C., et al. 1979. Confirmation of Conversion Factors Relating Exposure and Dose-Equivalent Index Presented in ANSI N13.11. NUREG/CR-1057, PNL-3219, Pacific Northwest Laboratory, Richland, Washington.

APPENDIX A

PHOTON SPECTRA

APPENDIX A

PHOTON SPECTRA

The spectra collected during the site visits are presented here. Indexes showing the figure numbers and measurement locations for each site are given in Tables A.1 through A.6. The probable identification of radioactive-isotope photon lines are labelled on the pulse-height distributions, which were collected using germanium detectors. Photon lines not labelled were not identified. Corrected spectra are presented below the pulse-height distributions. The effective C_γ factors labelled on the energy spectra are the maximum calculated values assuming parallel incidence for all photons except photons from radioactive noble gases, for which isotropic incidence was assumed.

TABLE A.1. Site K - Shutdown and Operating PWR

TABLE A.2. Site B - Shutdown and Operating PWR

TABLE A.3. Site M - Shutdown and Operating BWR

TABLE A.4. Site Q - Operating BWR

TABLE A.5. Site P - Shutdown PWR

TABLE A.6. Site N - Operating BWR

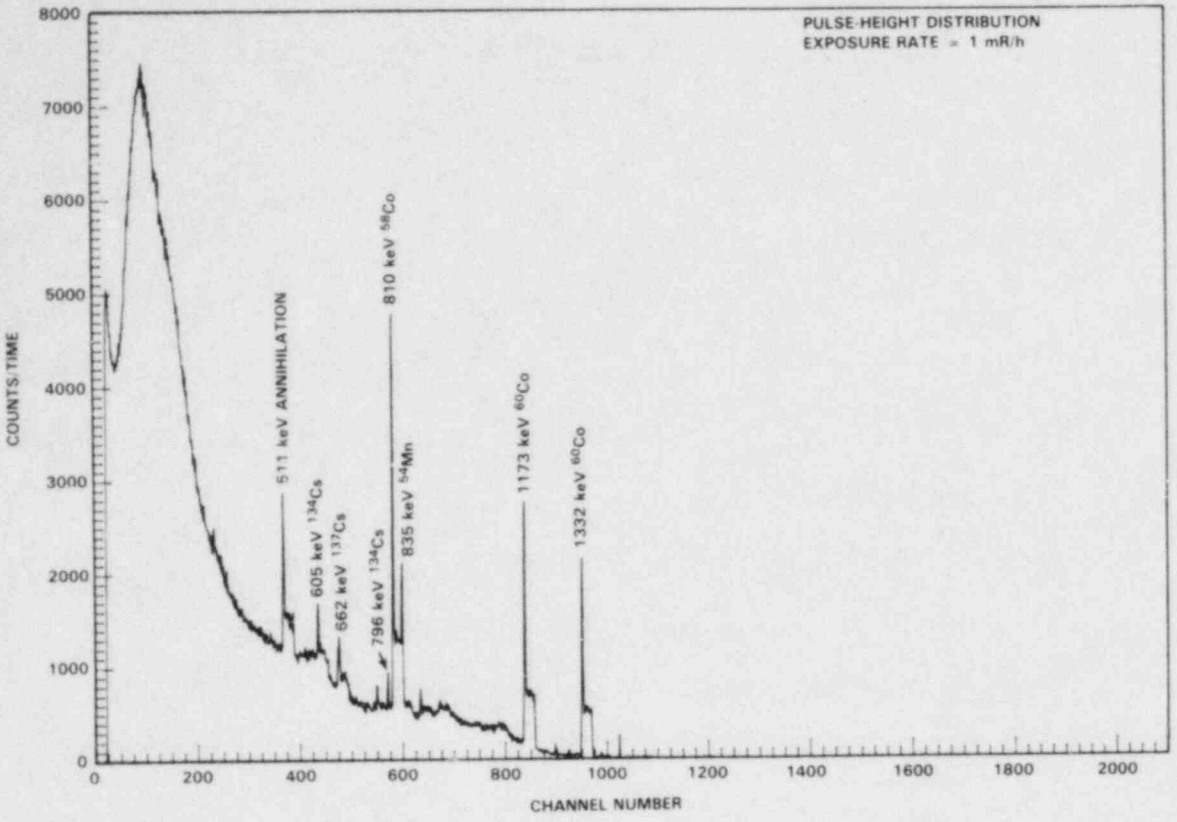

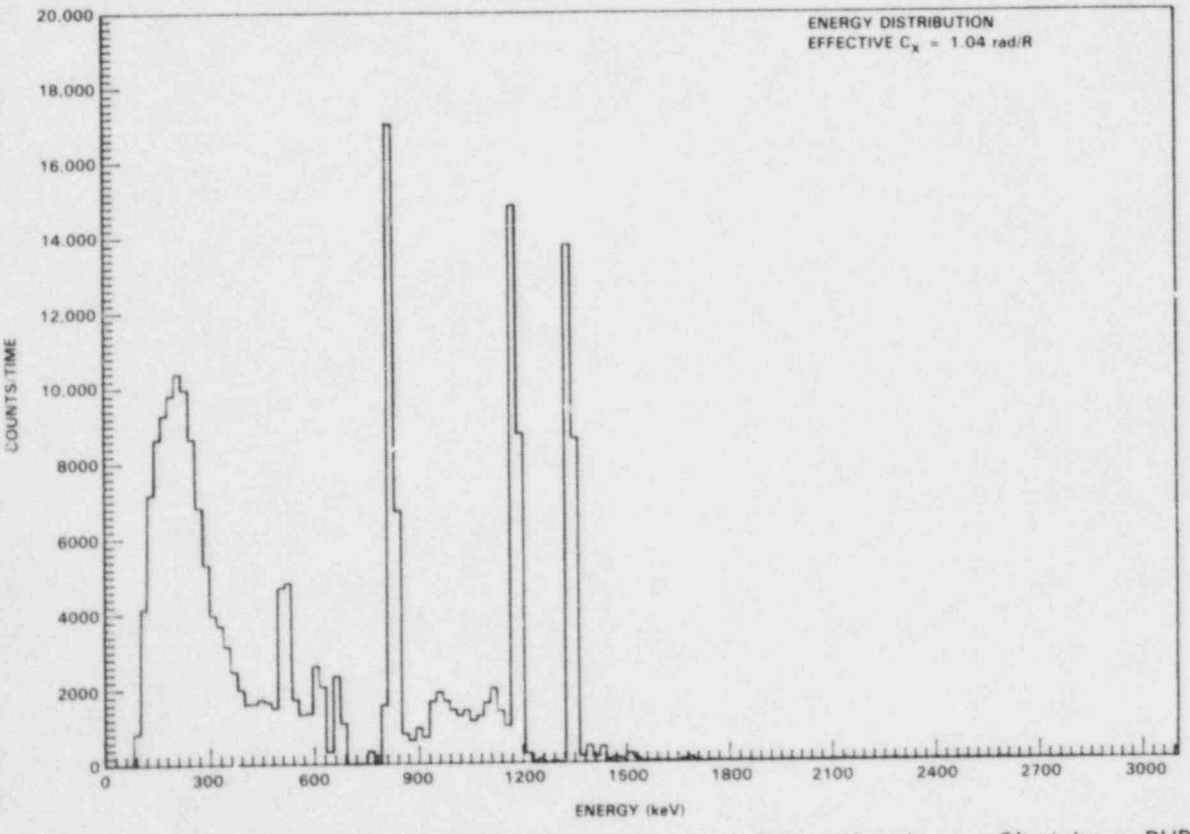

FIGURE A.1.1. Pulse-Height and Photon Energy Distributions, Shutdown PWR, Site K, Location A-Effluent Sample Room

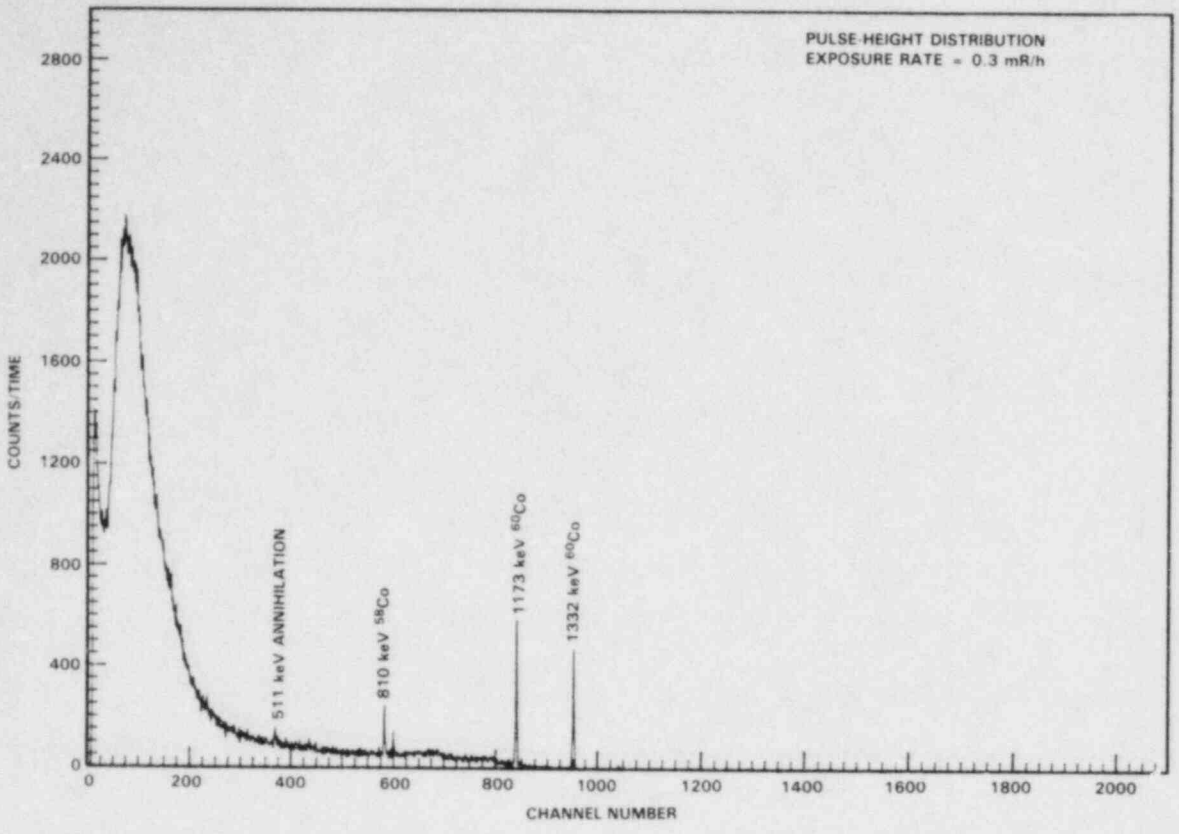

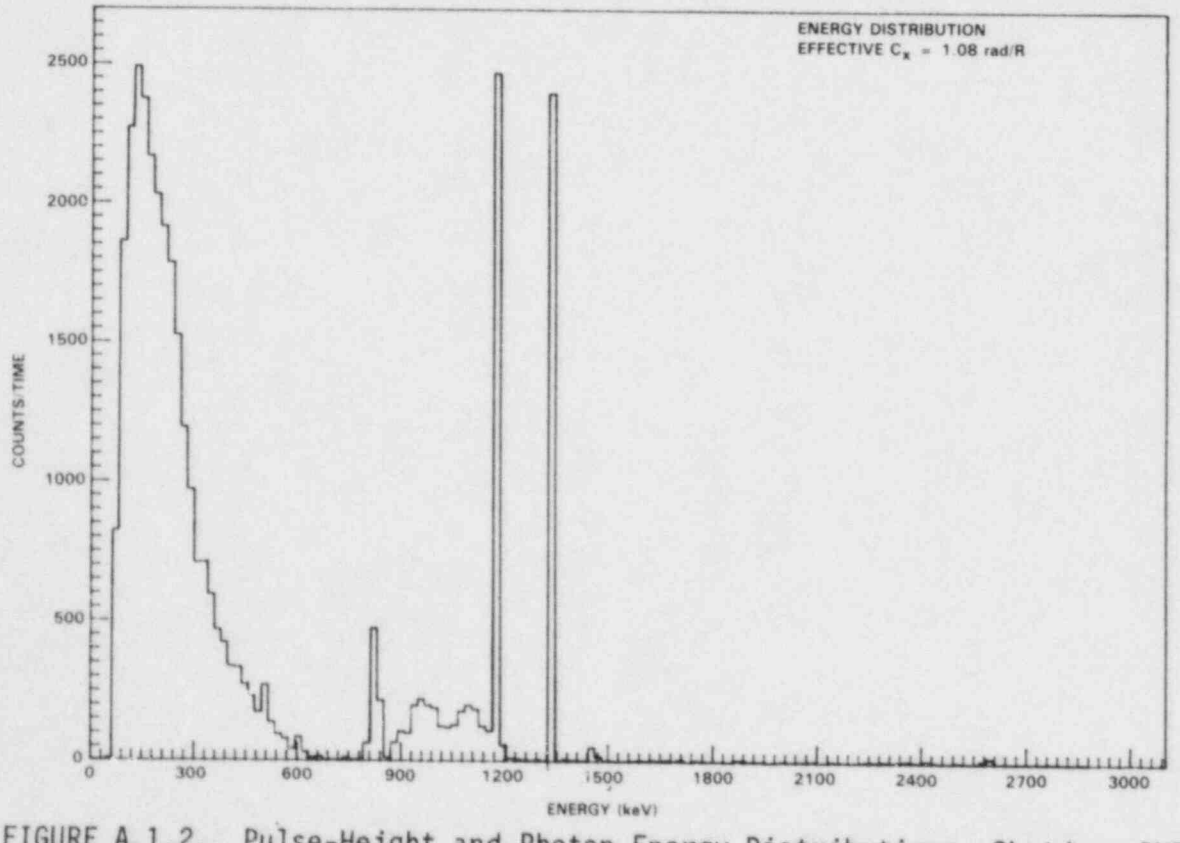

FIGURE A.1.2. Pulse-Height and Photon Energy Distributions, Shutdown PWR, Site K, Location B-Auxiliary Building Demineralizer Room, Reactor Coolant Filter

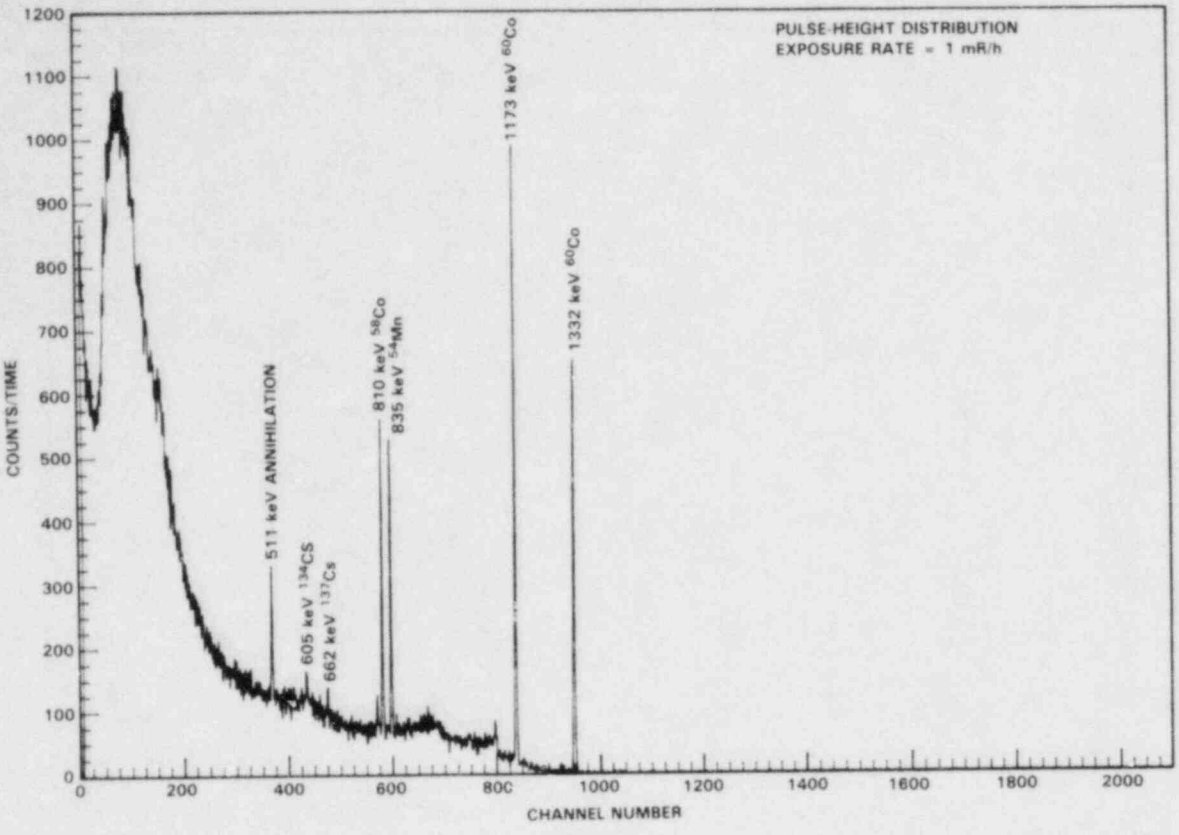

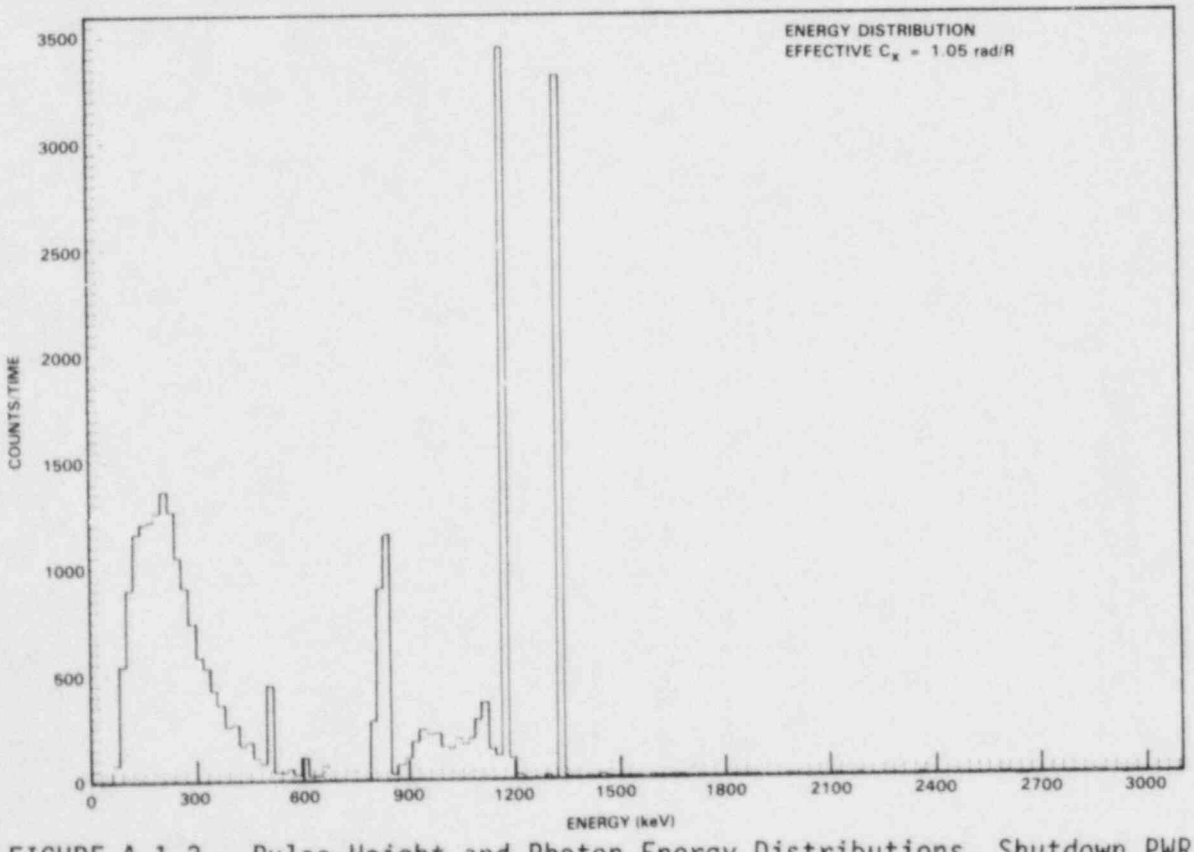

FIGURE A.1.3. Pulse-Height and Photon Energy Distributions, Shutdown PWR, Site K, Location C-Containment, Reactor Shield Vent Fan

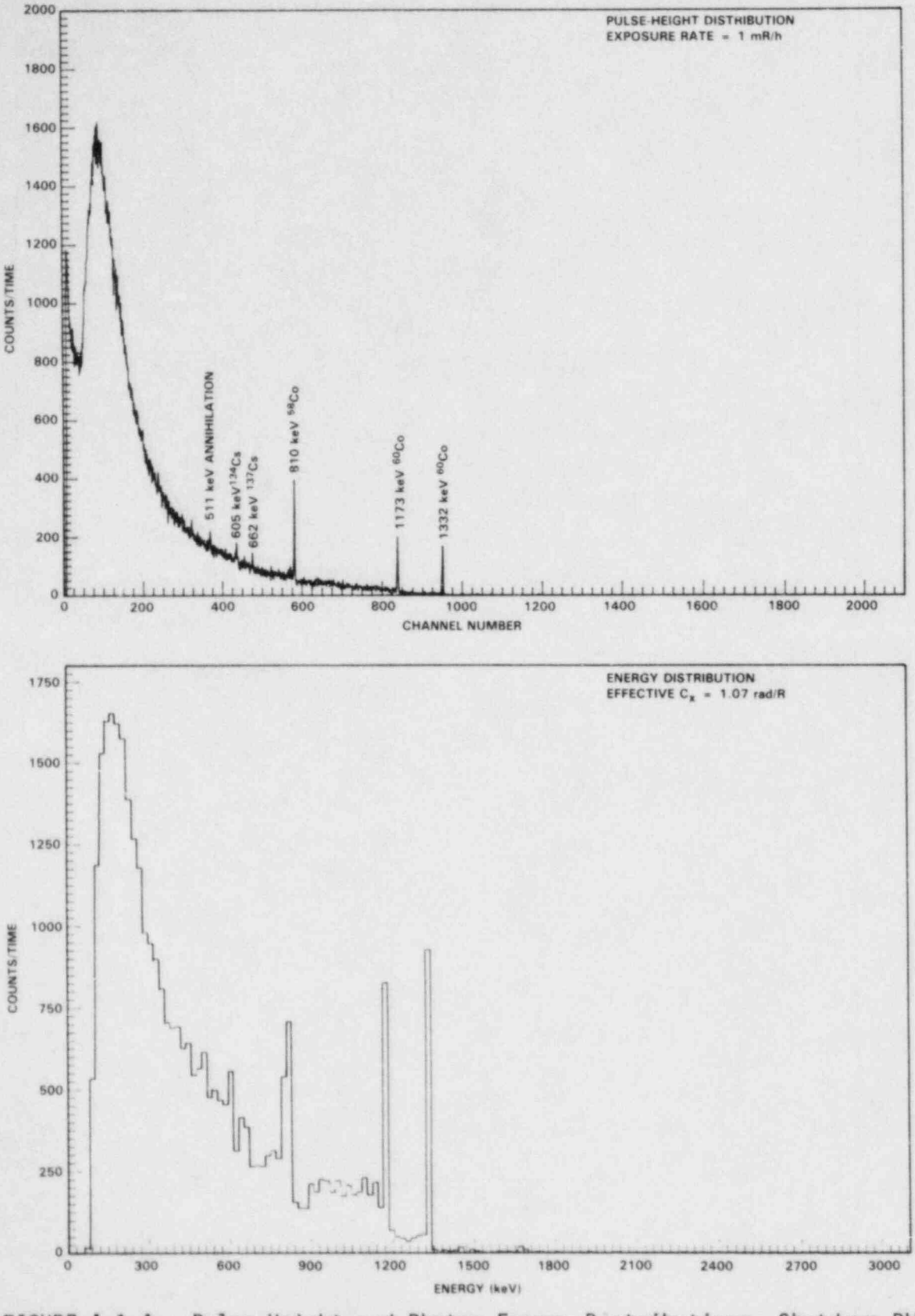

FIGURE A.1.4. Pulse-Height and Photon Energy Distributions, Shutdown PWR, Site K, Location D-Containment, Iodine Removal Fan

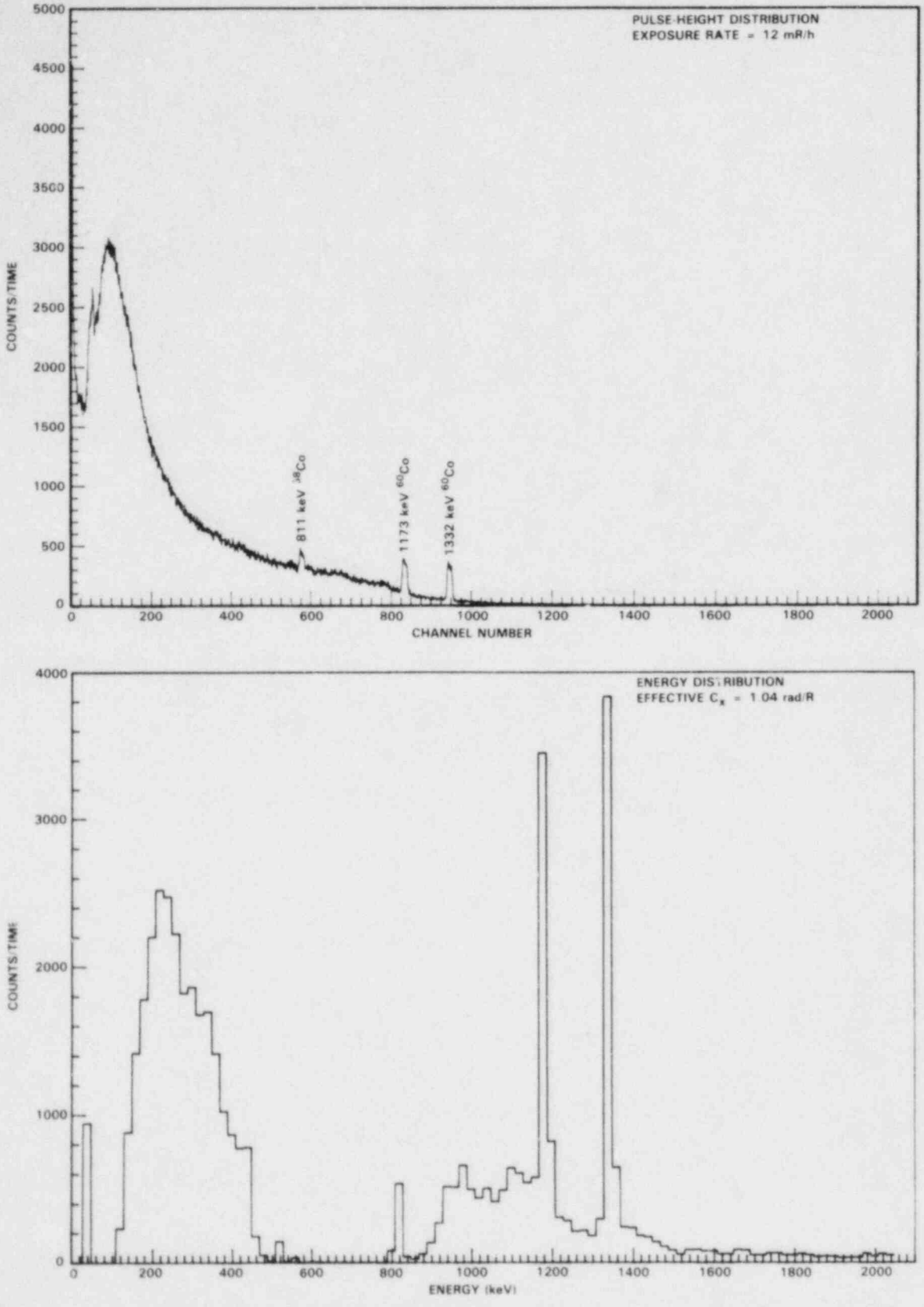

FIGURE A.1.5. Pulse-Height and Photon Energy Distributions, Shutdown PWR, Site K, Location E-Containment, Under Reactor Coolant Pump #13 (collimated)

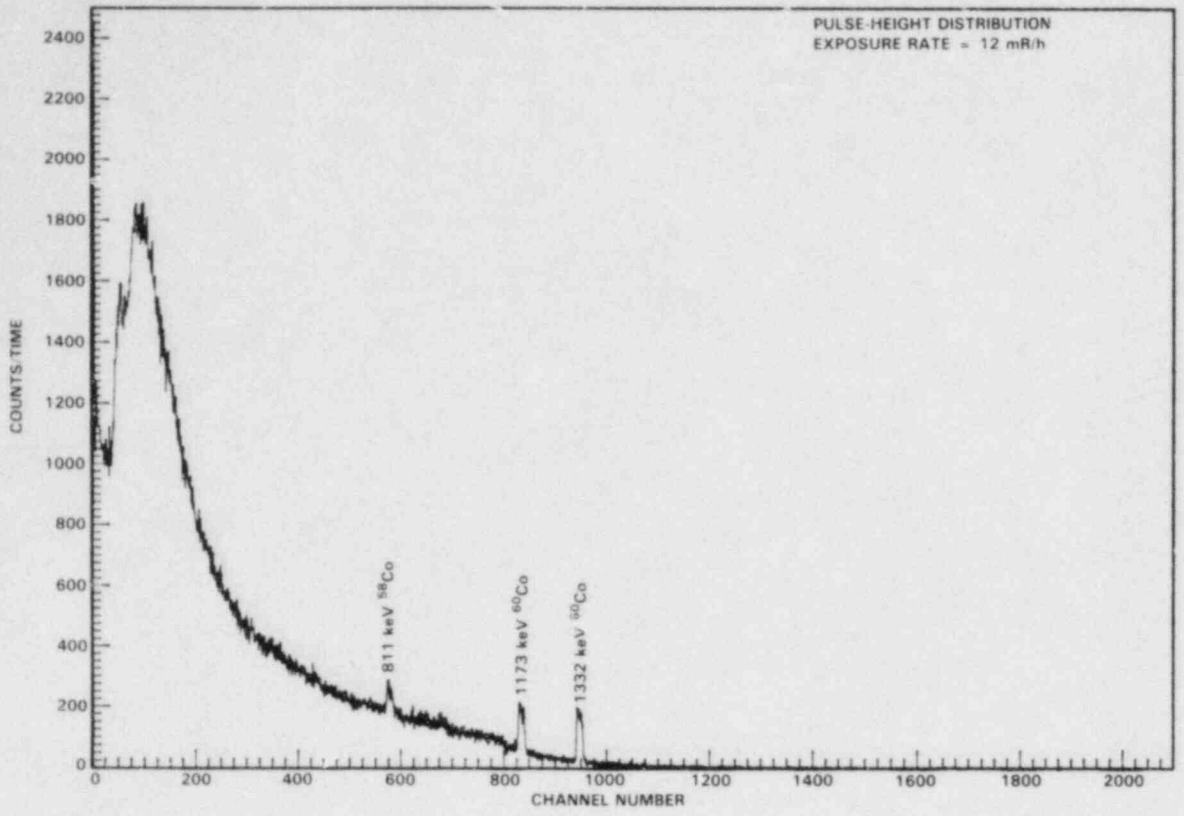

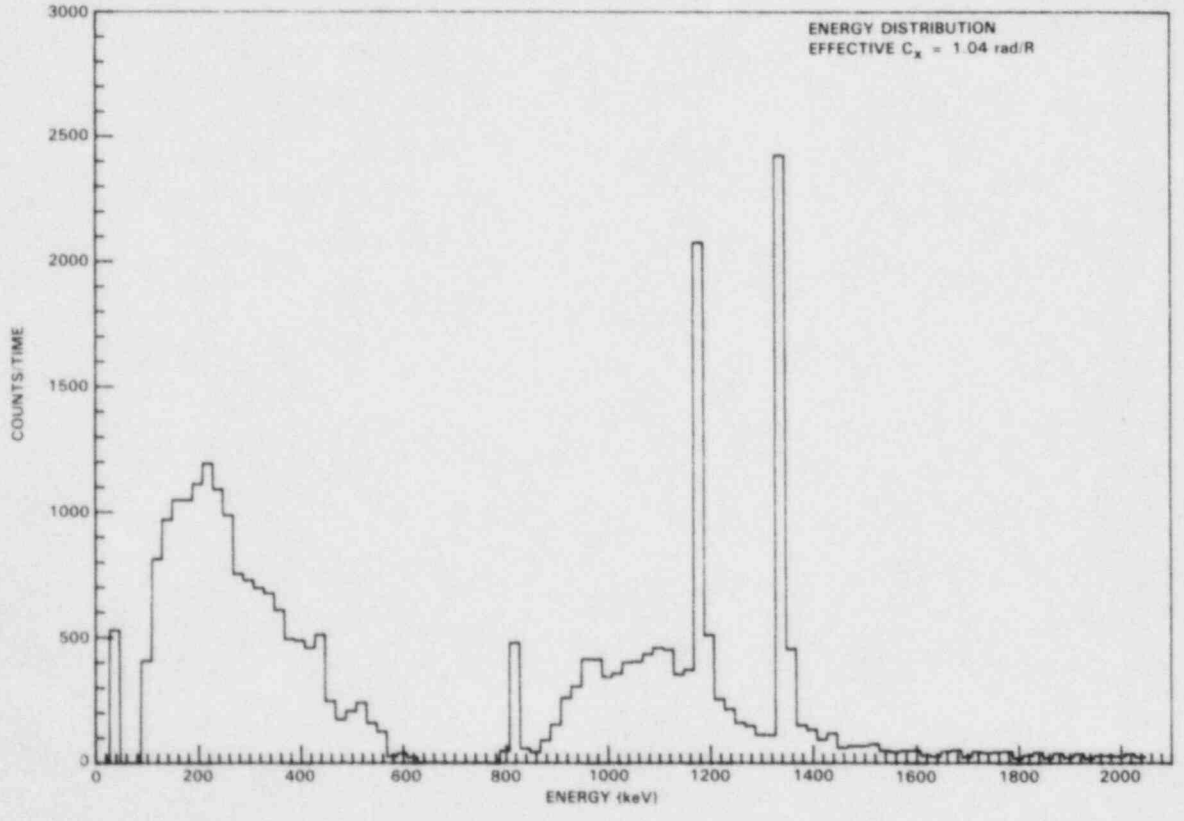

FIGURE A.1.6. Pulse-Height and Photon Energy Distributions, Shutdown PWR, Site K, Location F-Containment, Under Reactor Coolant Pump #11 (collimated)

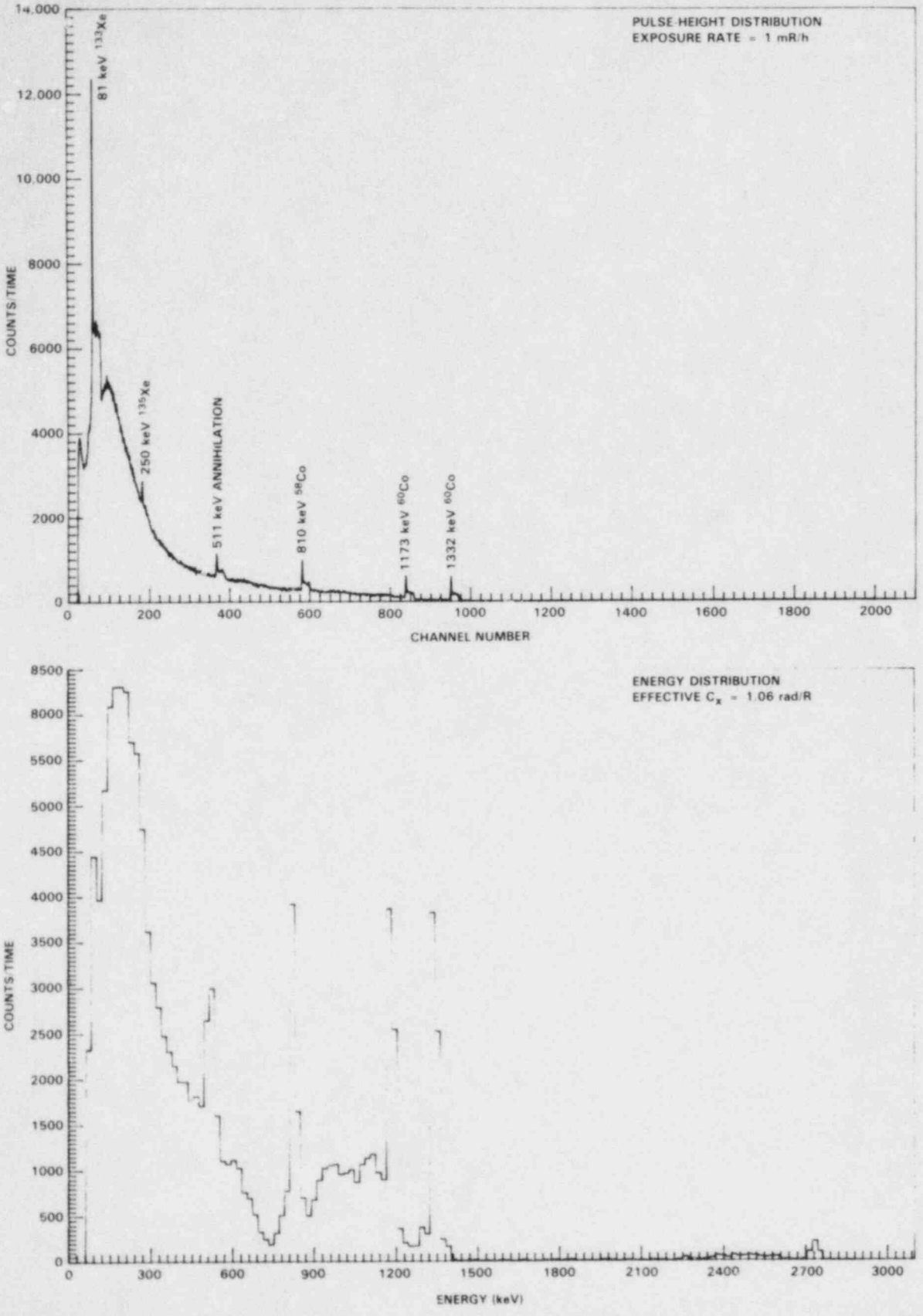

FIGURE A.1.7. Pulse-Height and Photon Energy Distributions, Operating PWR, Site K, Location G-Effluent Sample Room

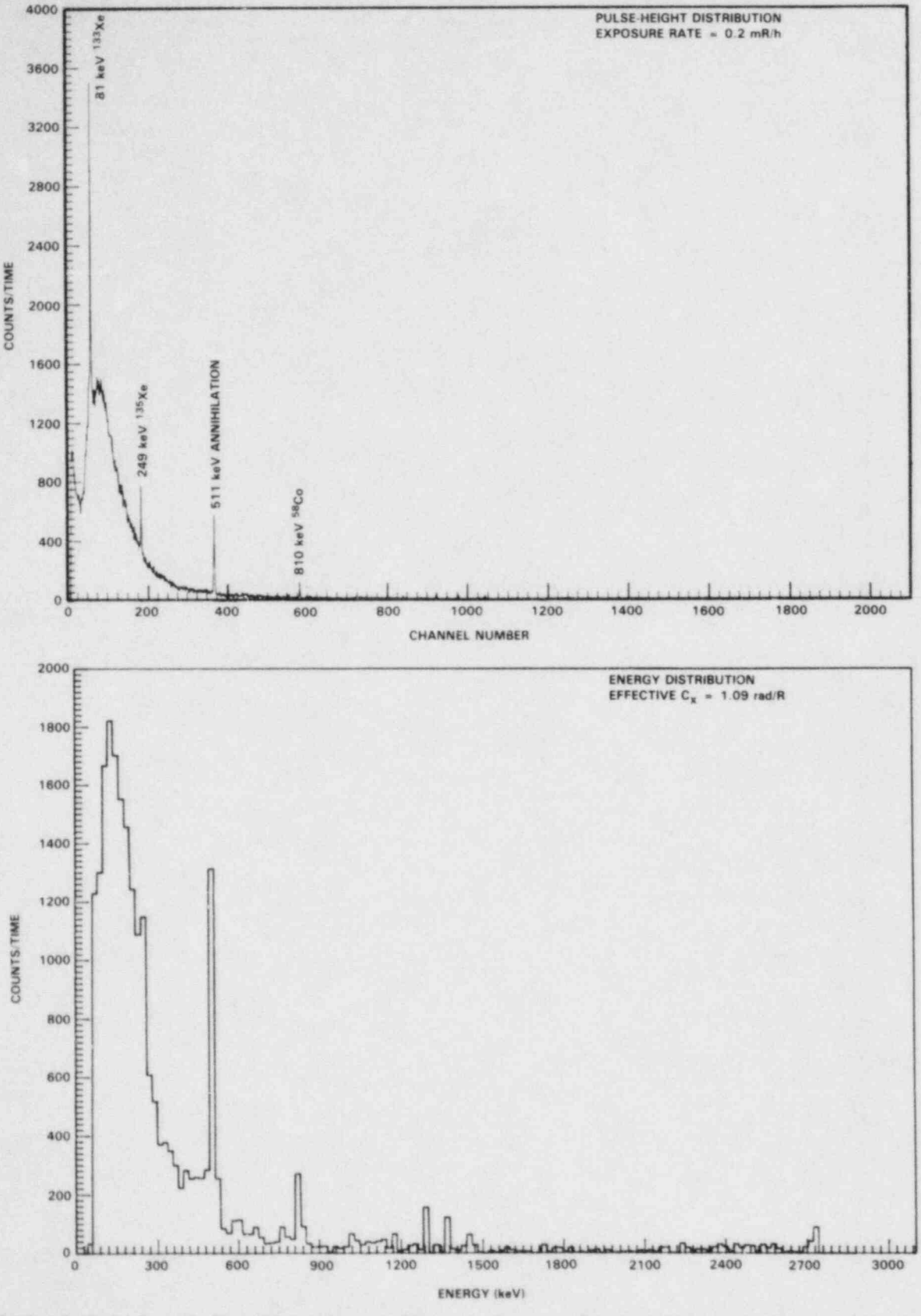

FIGURE A.1.8. Pulse-Height and Photon Energy Distributions, Operating PWR, Site K, Location H-Auxiliary Building Demineralizer Room, Reactor Coolant Filter

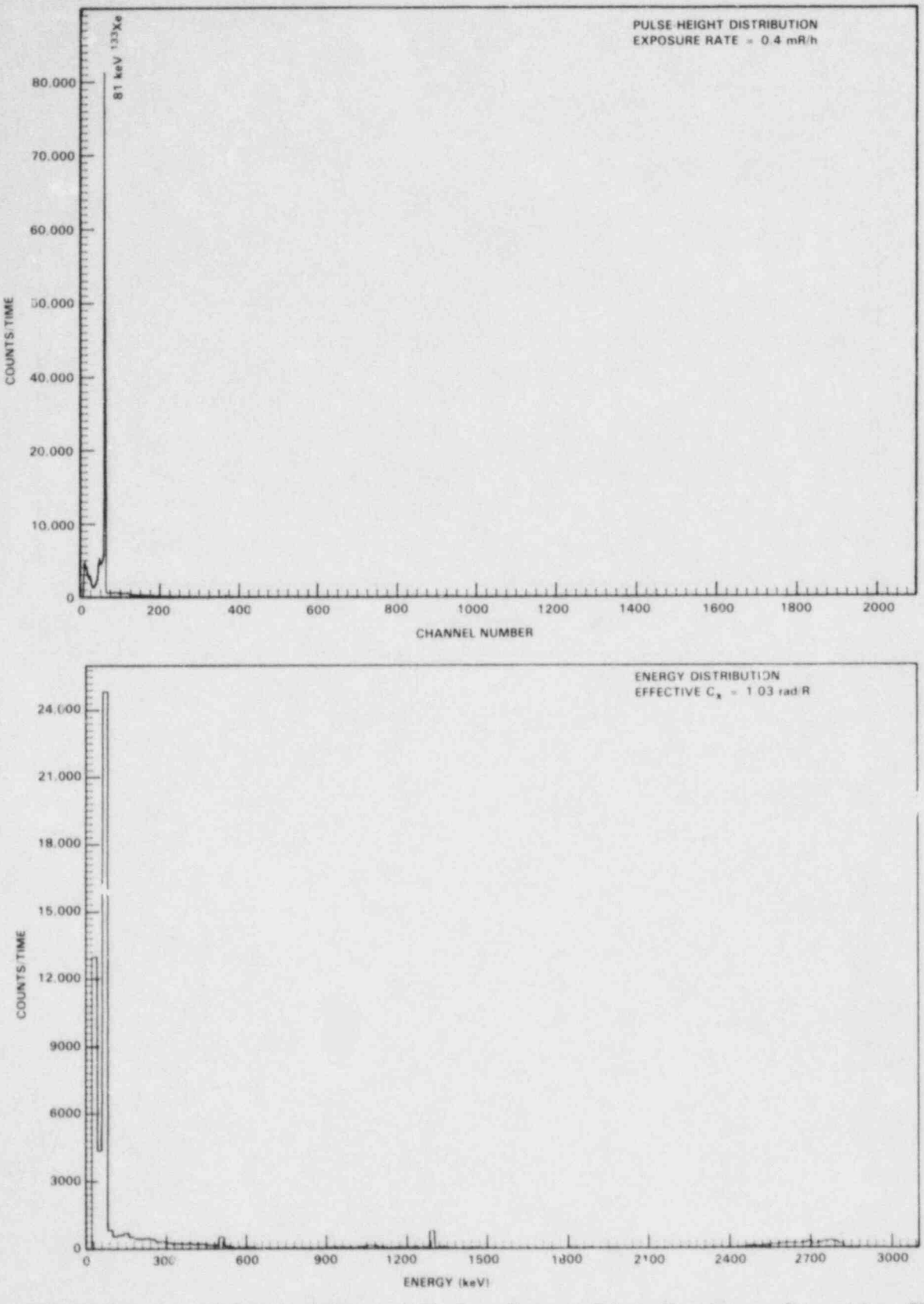

FIGURE A.1.9. Pulse-Height and Photon Energy Distributions, Operating PWR, Site K, Location I-Containment, Personnel Hatch

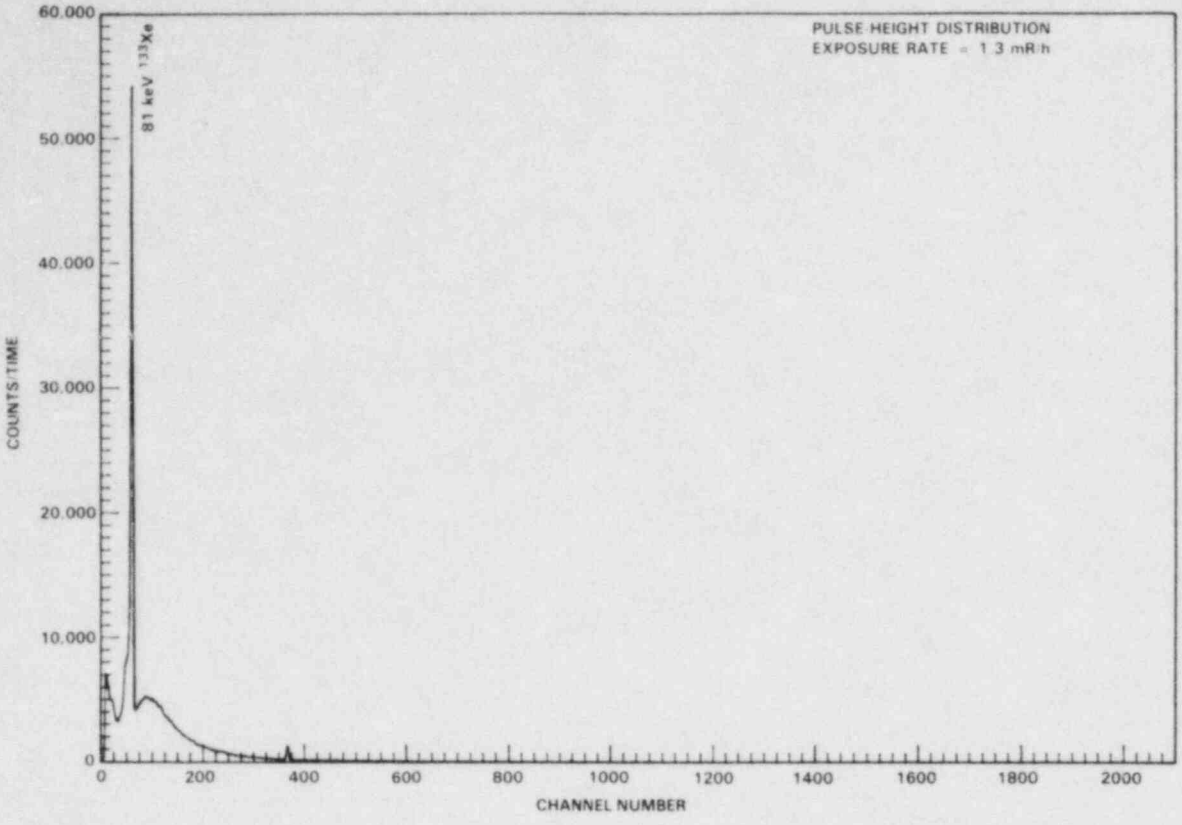

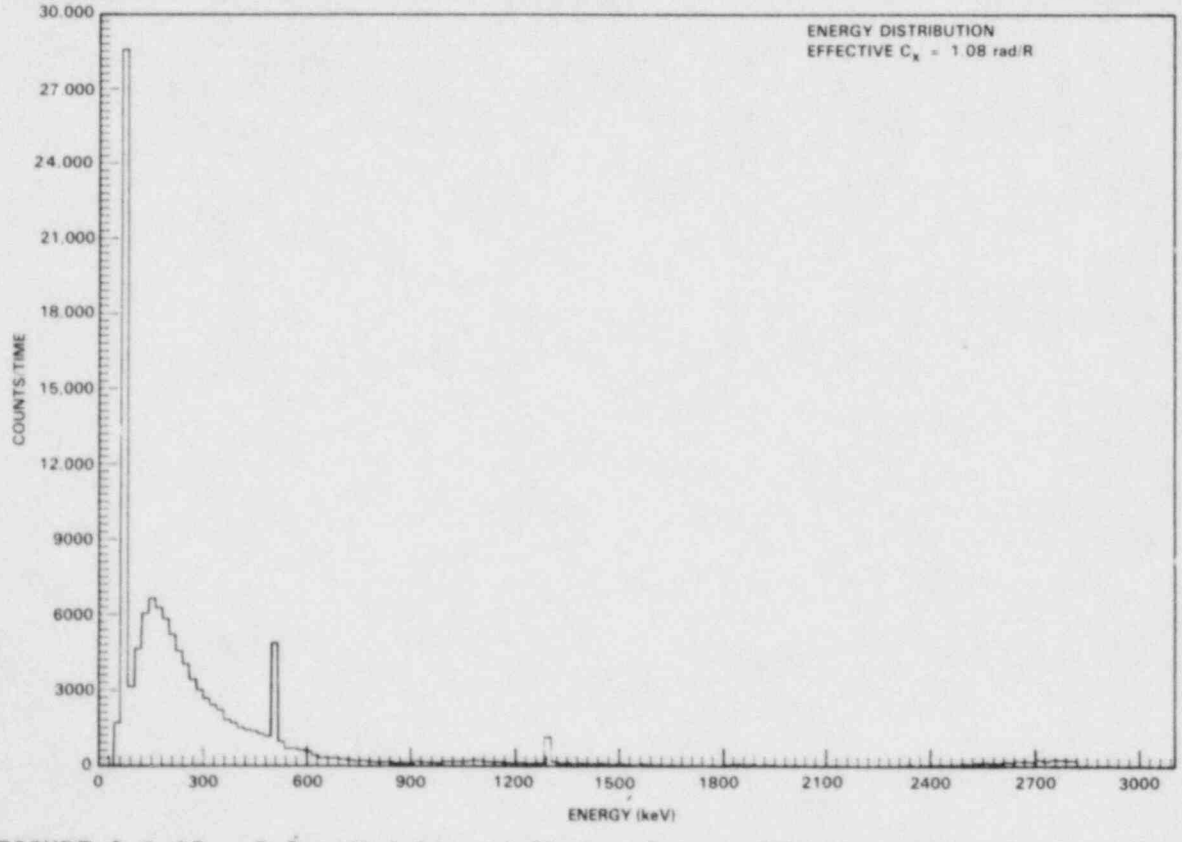

FIGURE A.1.10. Pulse-Height and Photon Energy Distributions, Operating PWR, Site K, Location J-Containment, Near Bioshield of Steam Generator

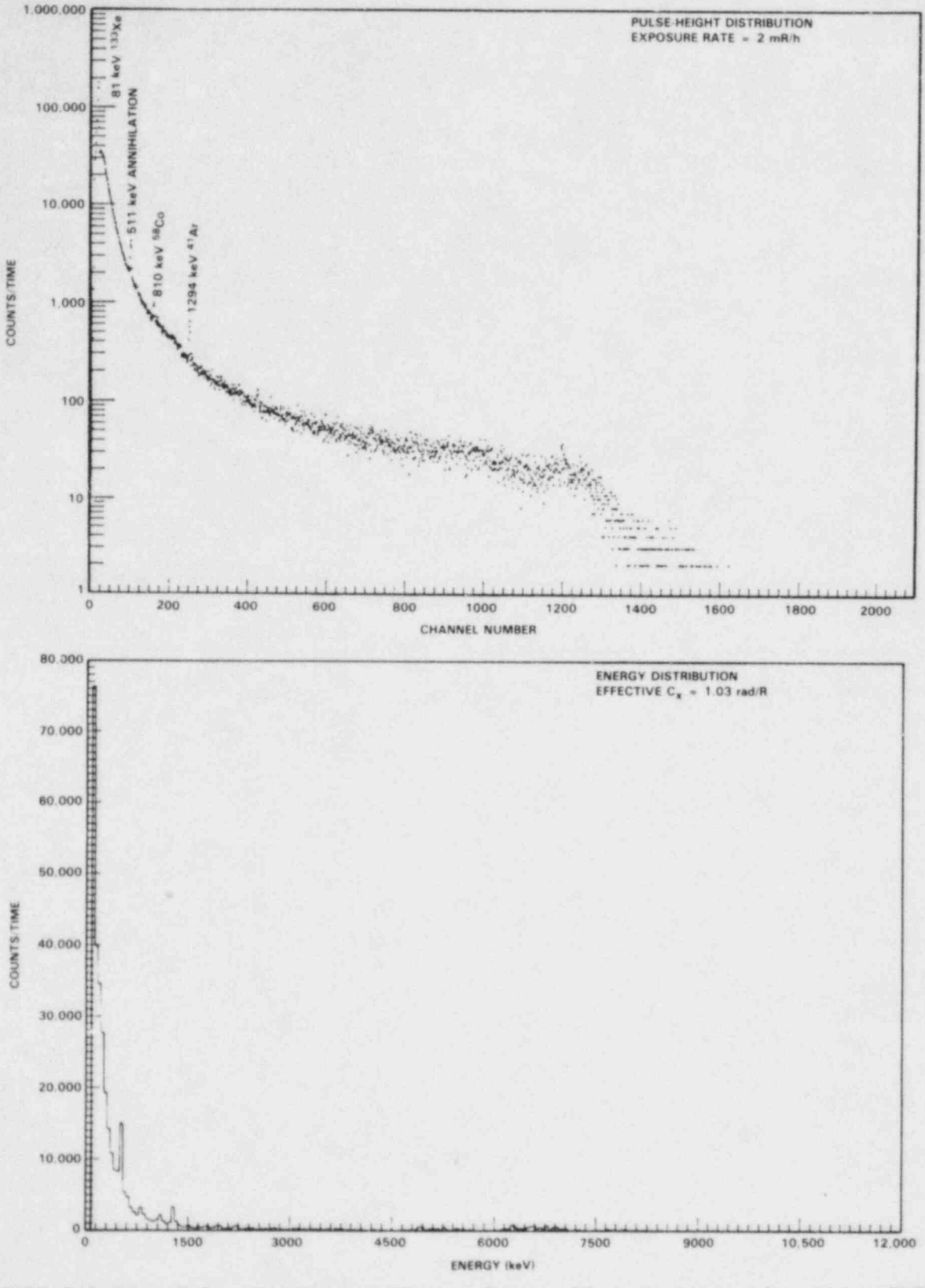

FIGURE A.1.11. Pulse-Height and Photon Energy Distributions, Operating PWR, Site K, Location K-Containment, Overlooking Reactor Cavity

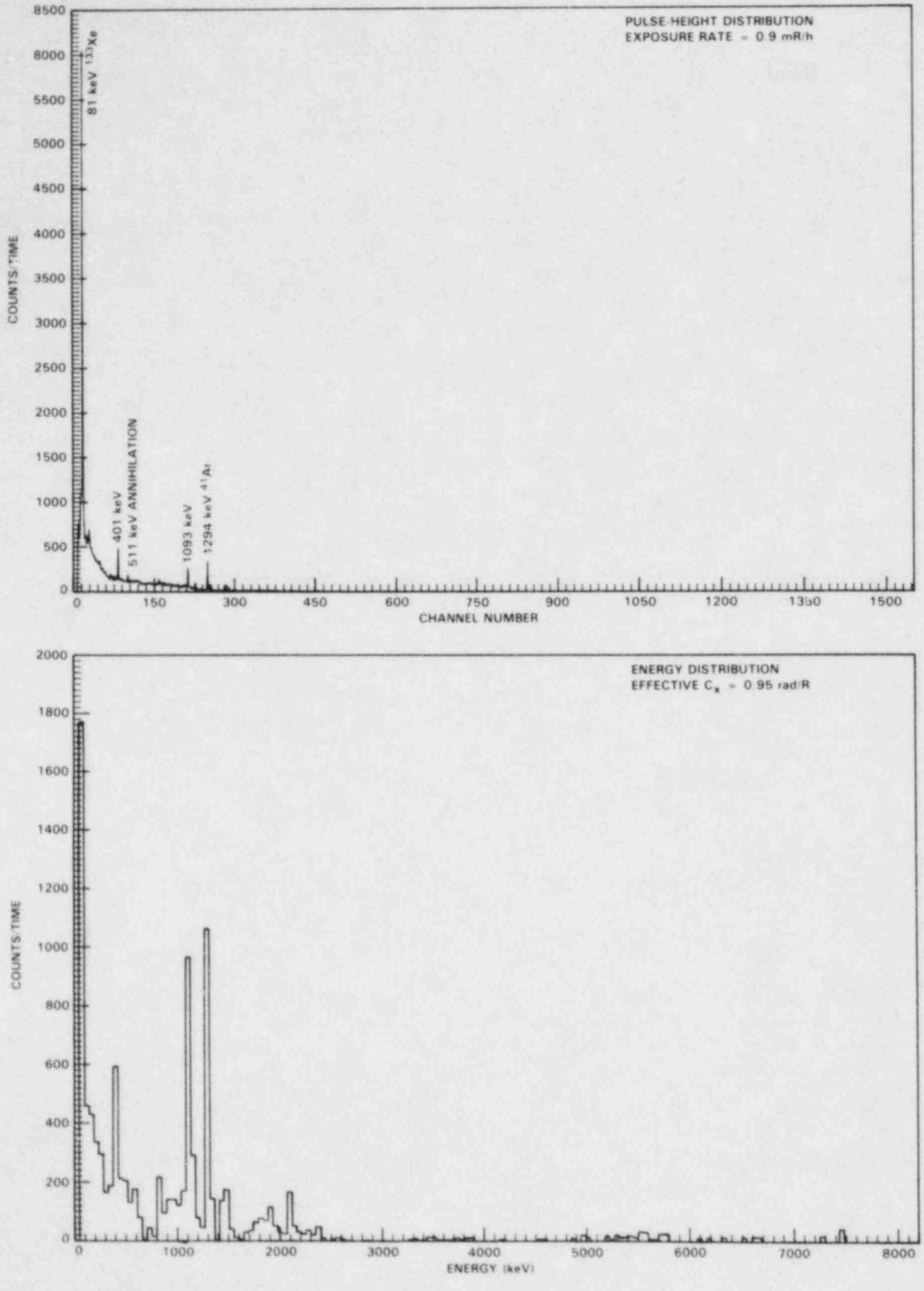

FIGURE A.1.12. Pulse-Height and Photon Energy Distributions, Operating PWR, Site K, Location L-Containment, Outside Airlock

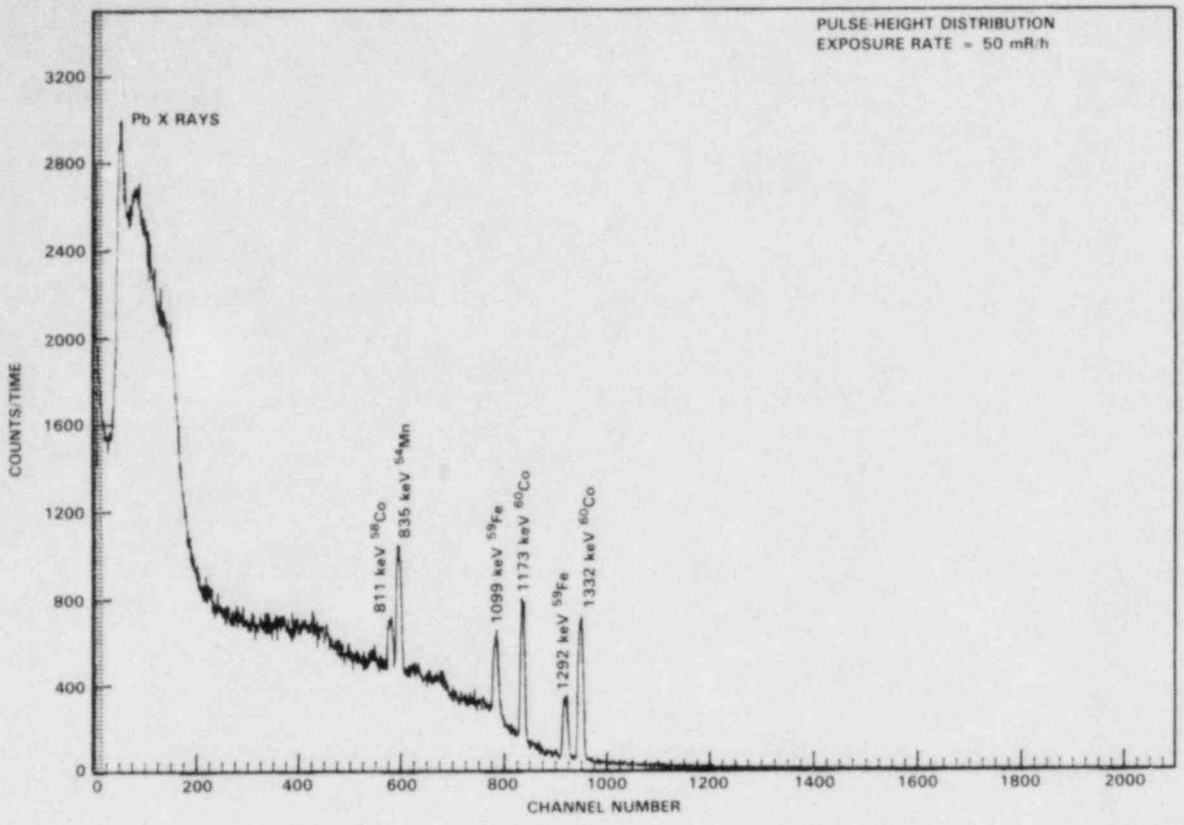

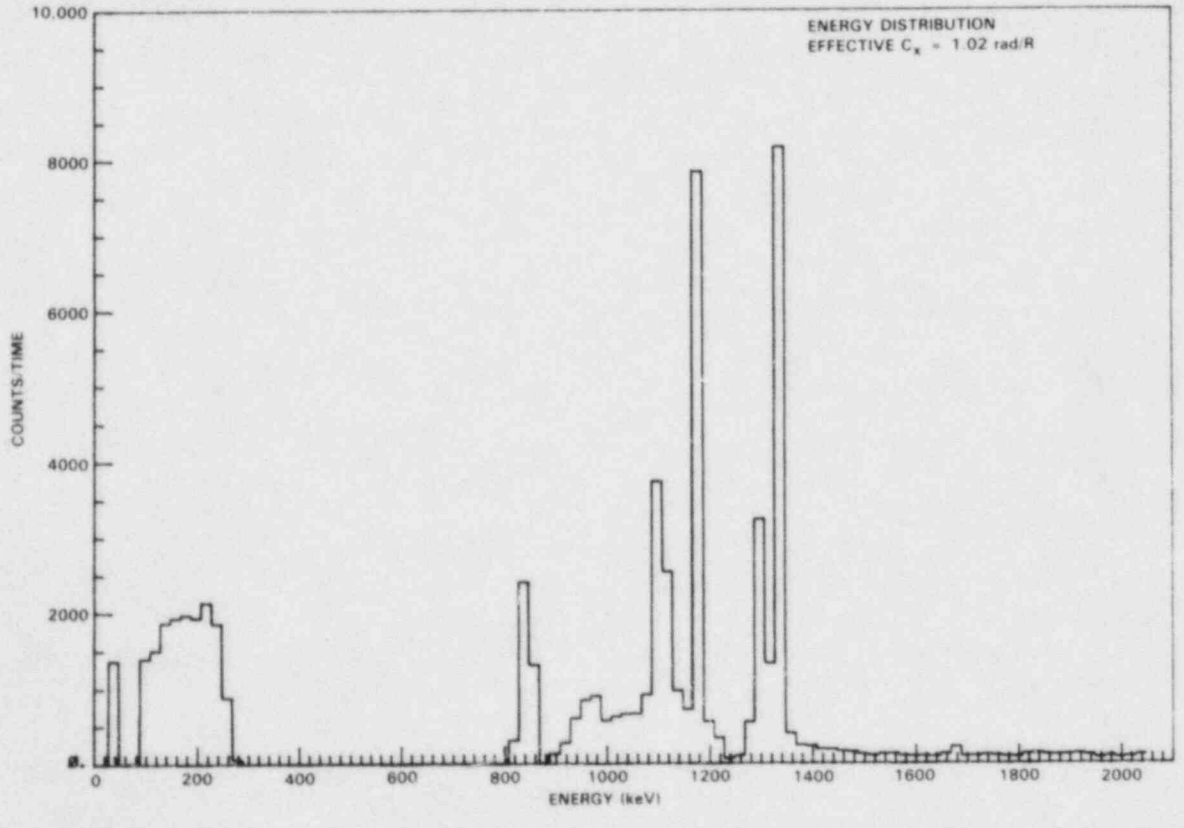

FIGURE A.1.13. Pulse-Height and Photon Energy Distributions, Site K, Operating PWR, Location M-Hot Drum Storage Area (collimated)

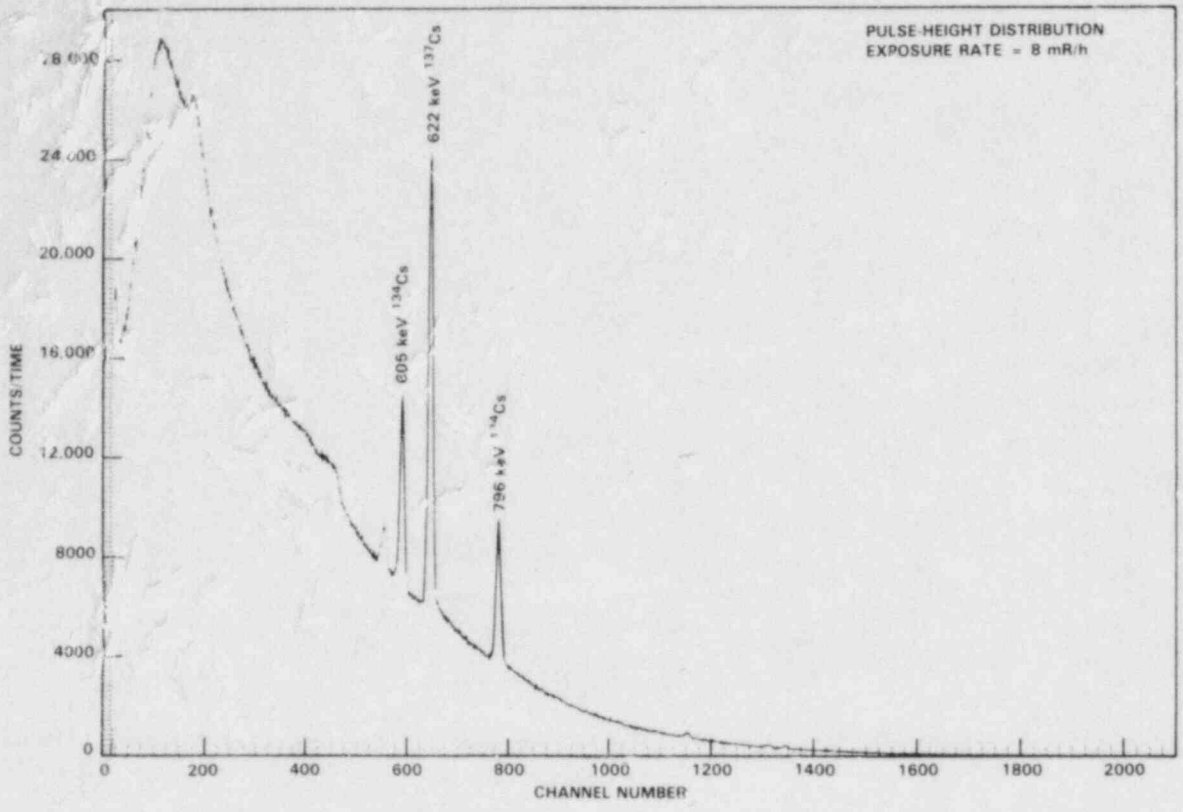

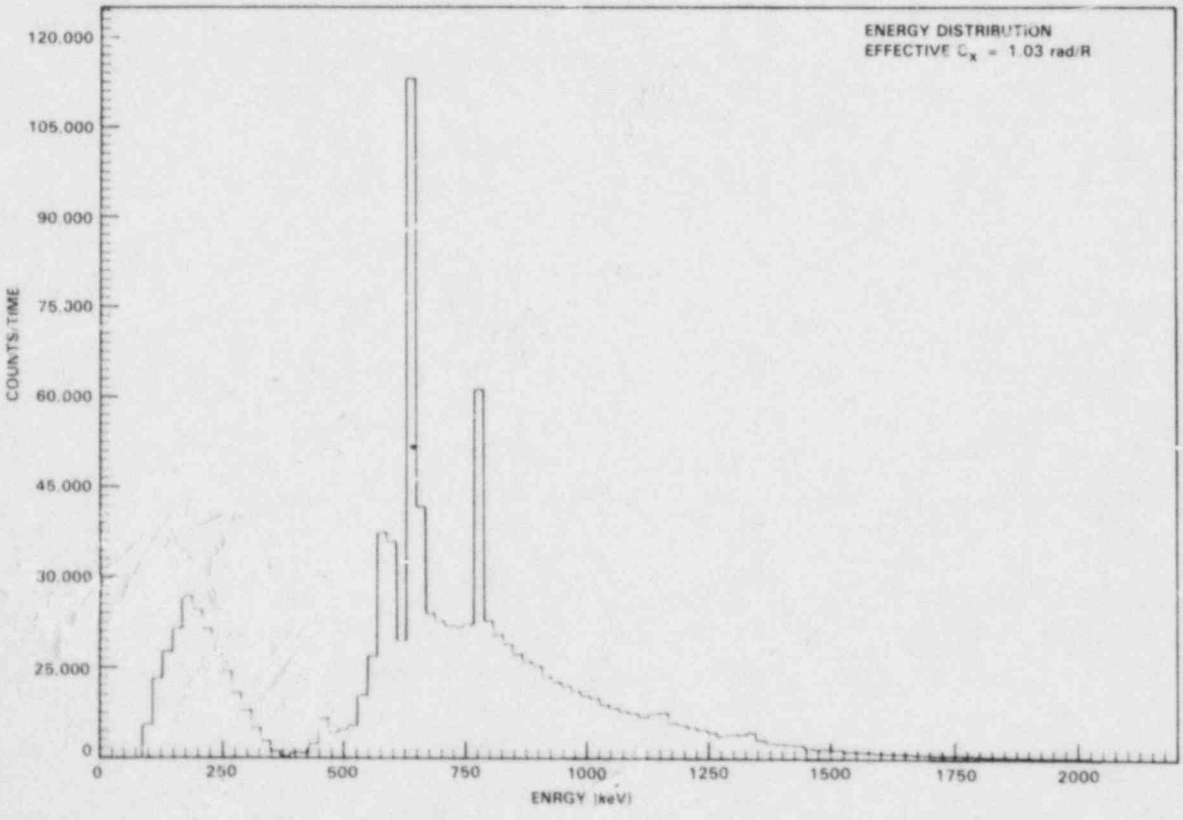

FIGURE A.2.1. Pulse-Height and Photon Energy Distributions, Shutdown PWR, Site B, Location A-Near Escape Hatch, 357-ft Level

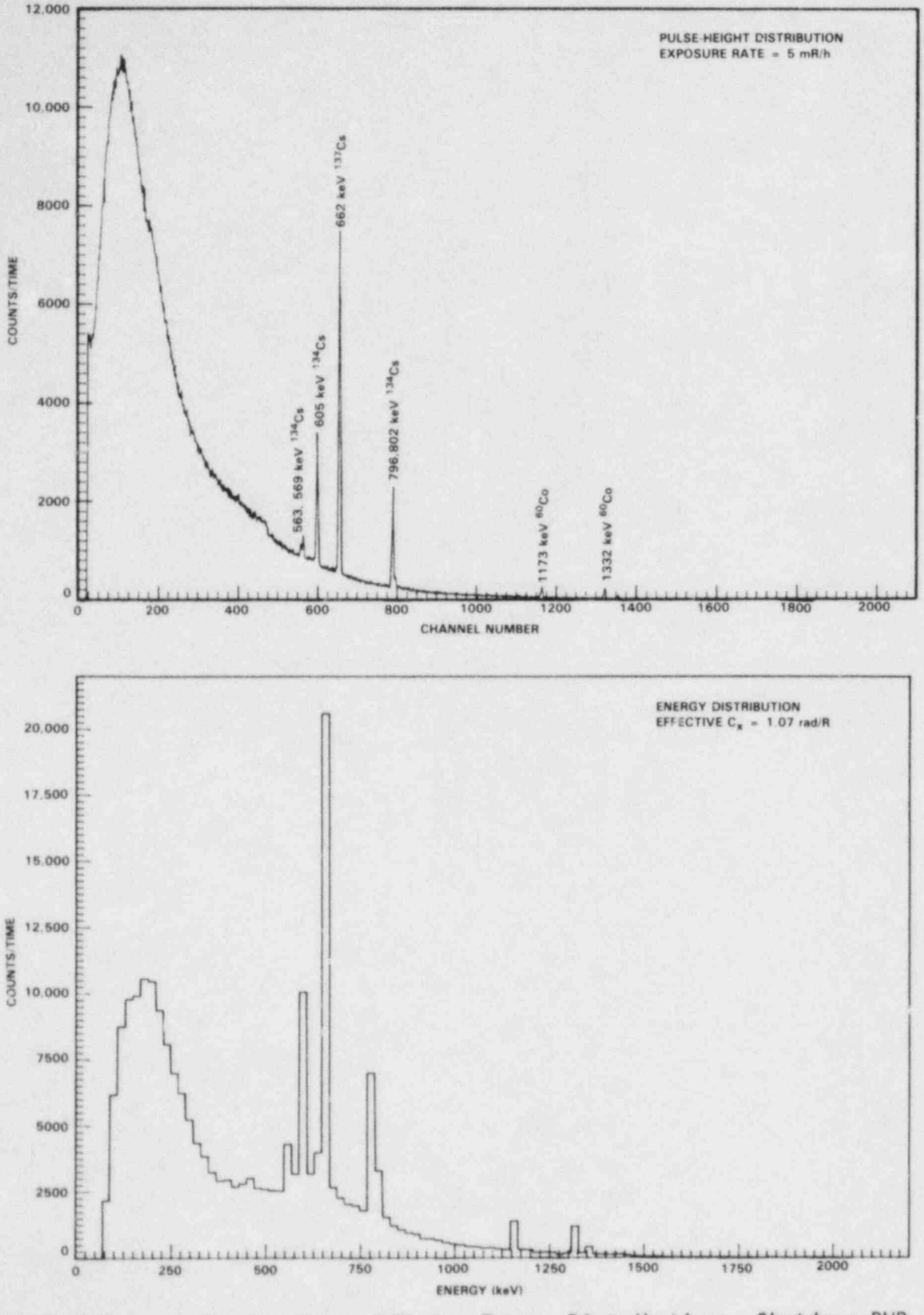

FIGURE A.2.2. Pulse-Height and Photon Energy Distributions, Shutdown PWR, Site B, Location B-Near Equipment Hatch, 357-ft Level

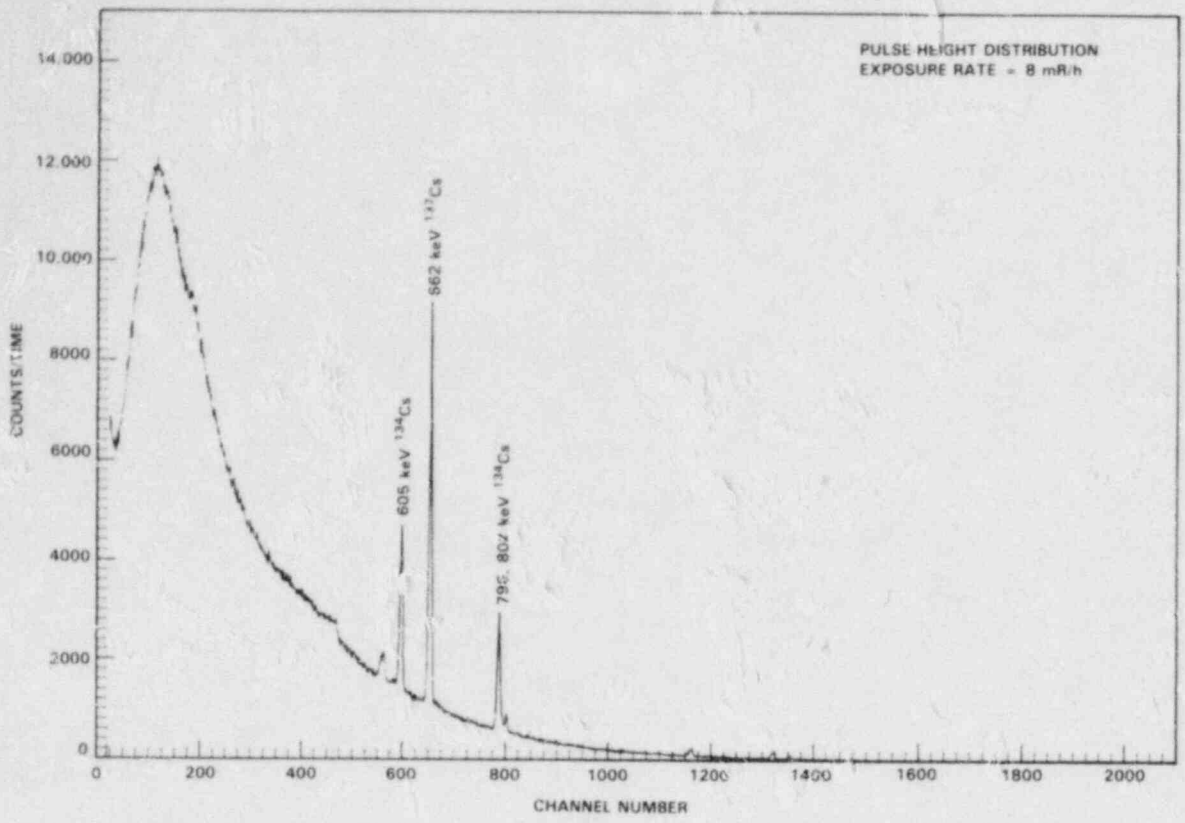

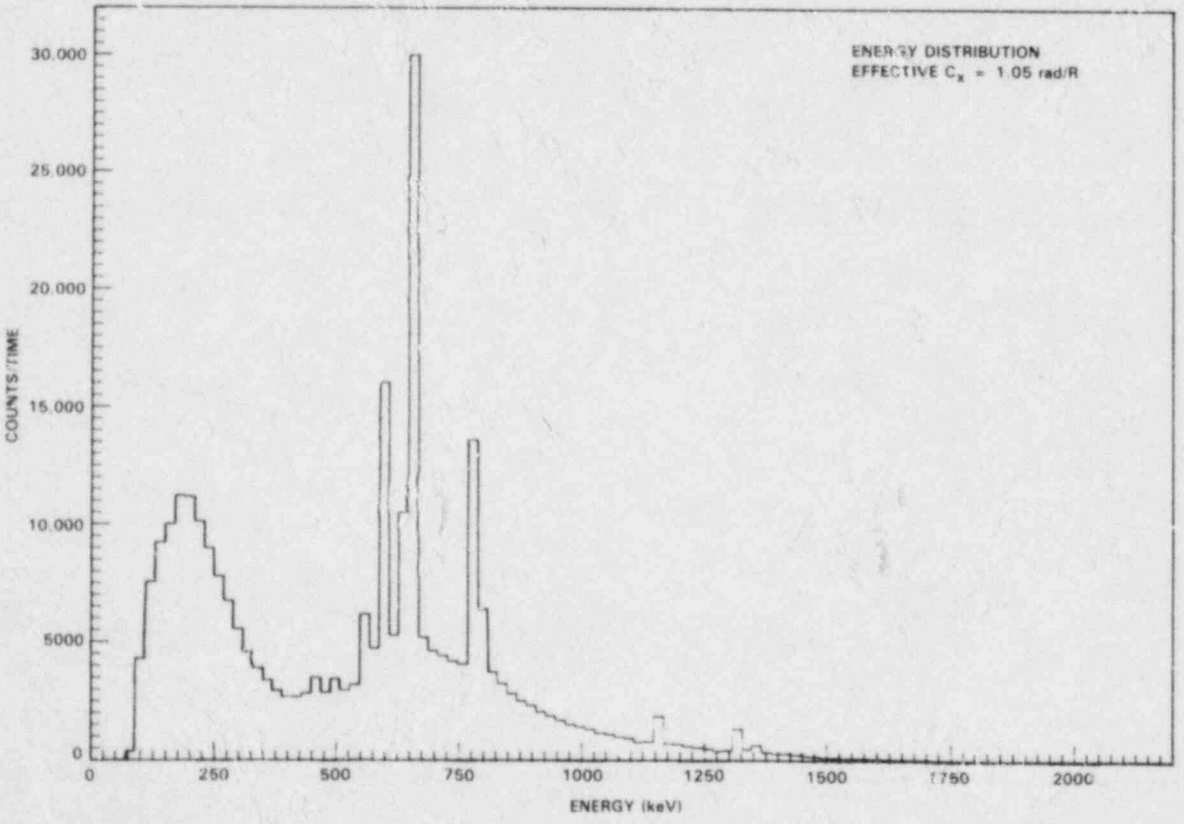

FIGURE A.2.3. Pulse-Height and Photon Energy Distributions, Shutdown PWR. Site B, Location C-Near Elevator, 357-ft Level

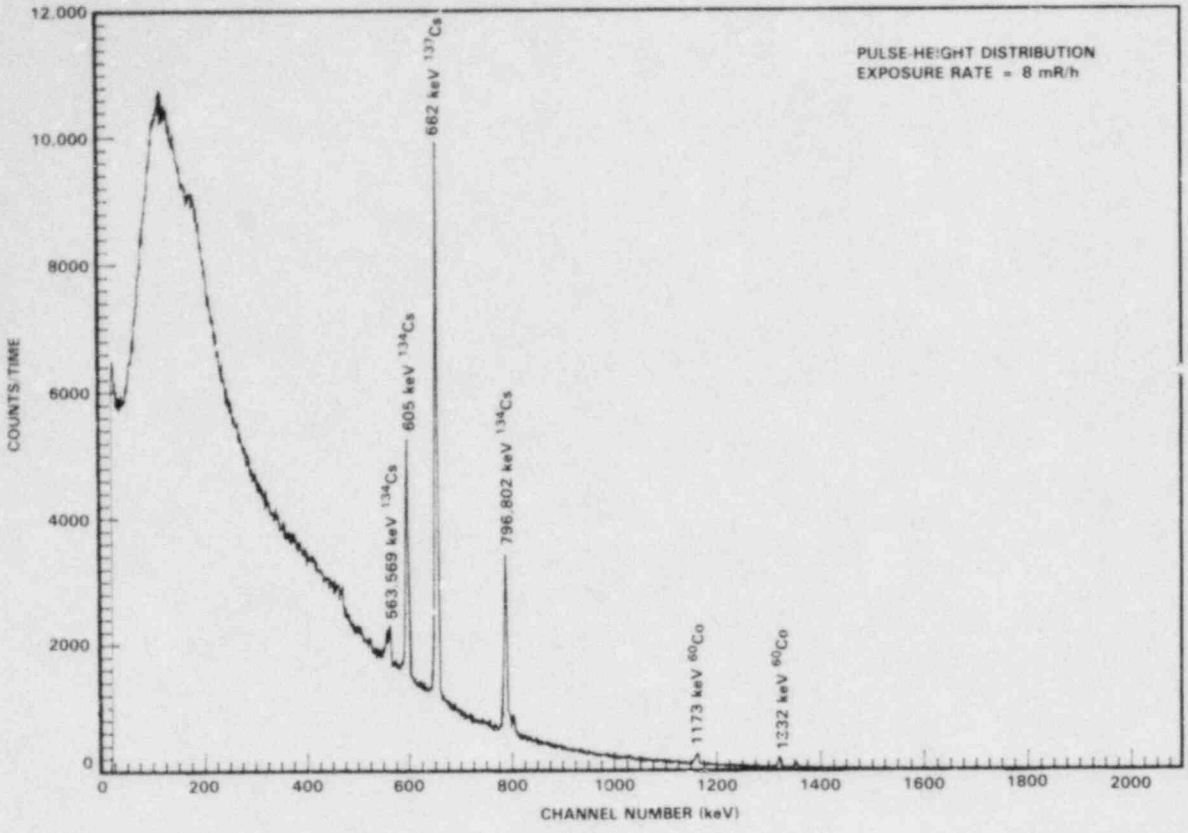

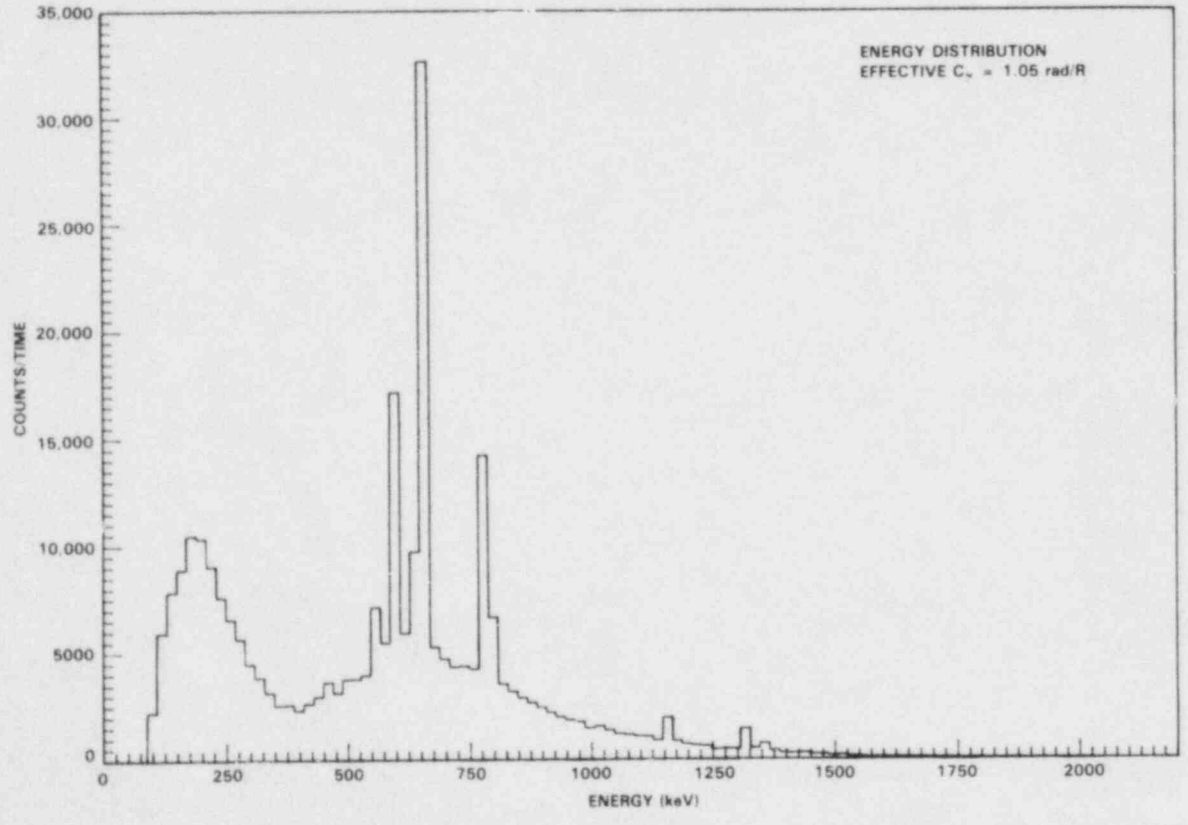

FIGURE A.2.4. Pulse-Height and Photon Energy Distributions, Shutdown PWR, Site B, Location D-Near Elevator, 373-ft Level

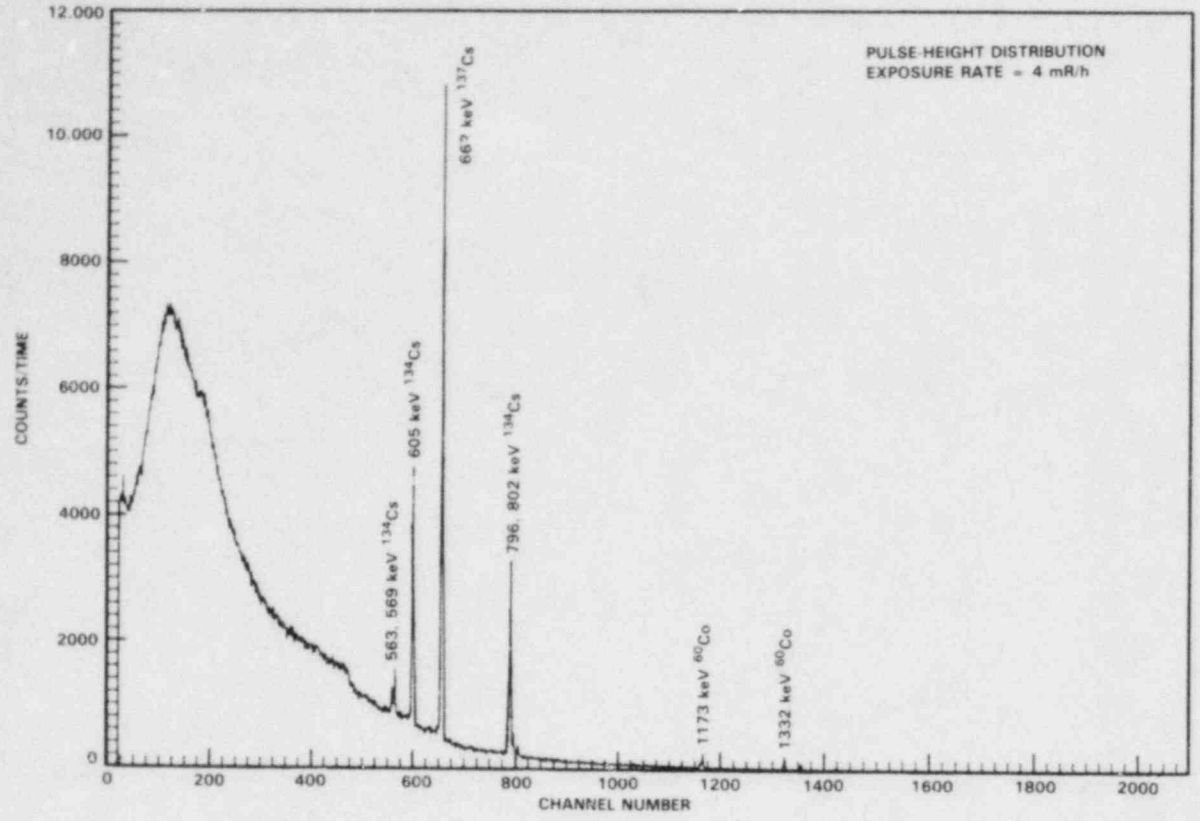

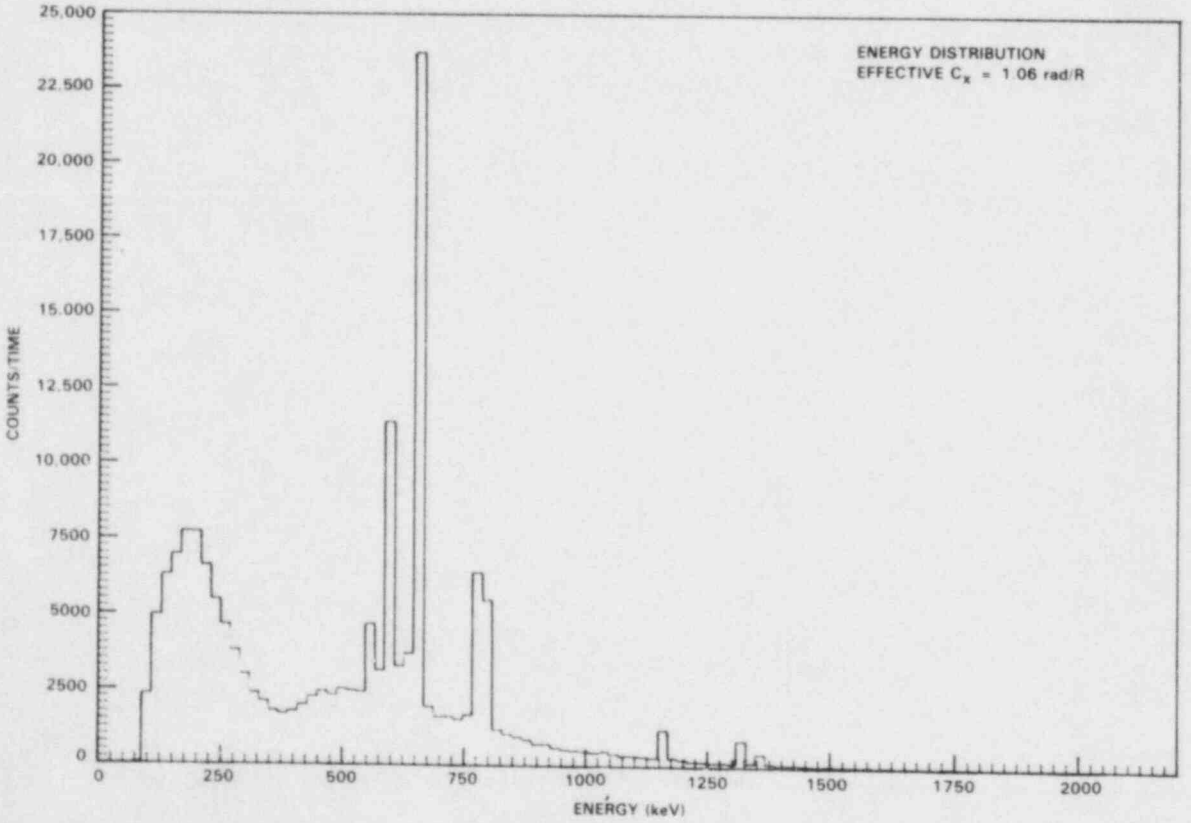

FIGURE A.2.5. Pulse-Height and Photon Energy Distributions, Shutdown PWR, Site B, Location E-Near Elevator, 401-ft Level

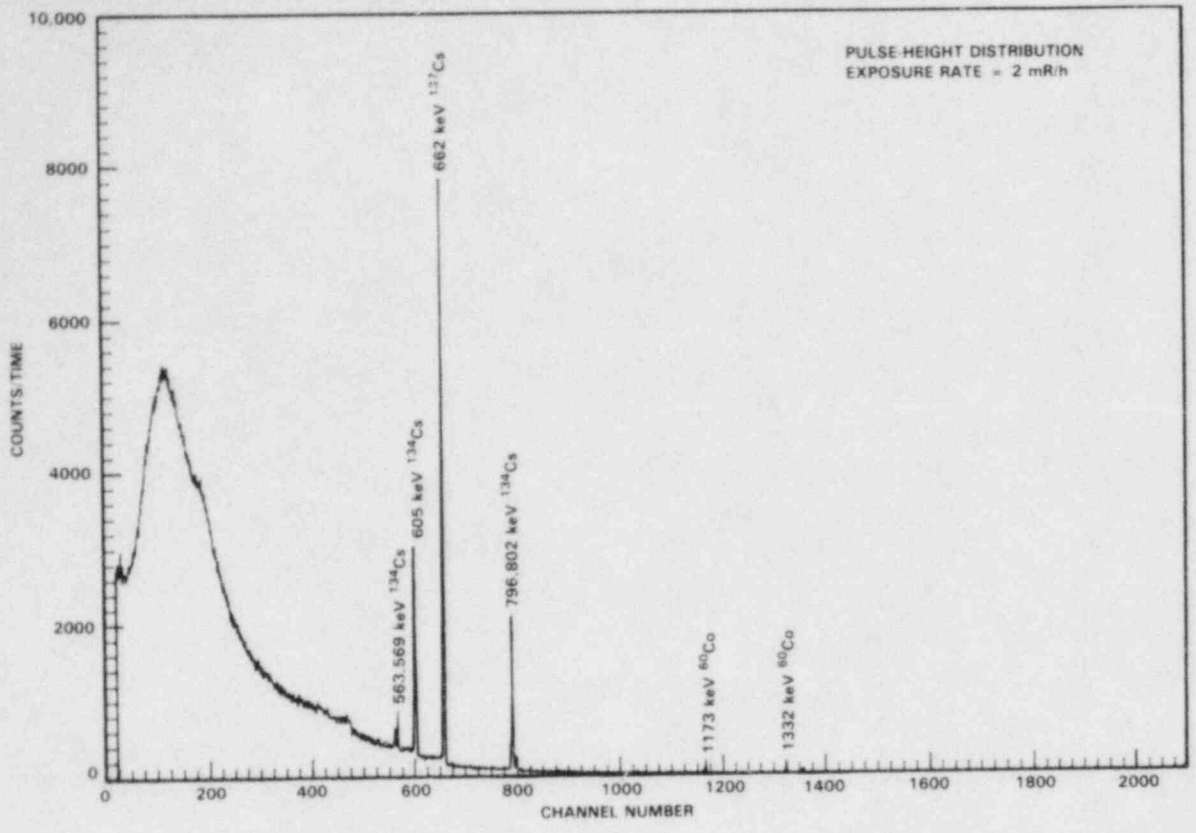

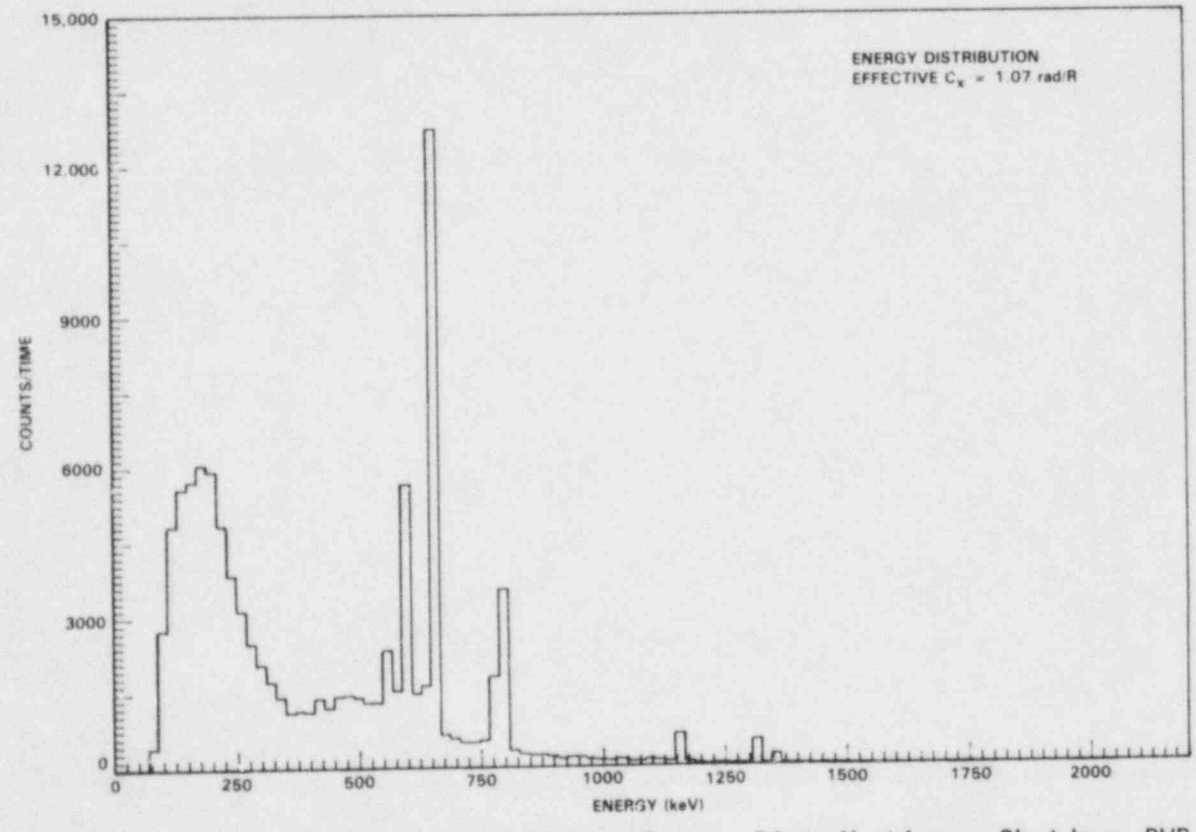

FIGURE A.2.6. Pulse-Height and Photon Energy Distributions, Shutdown PWR, Site B, Location F-Deck, 424-ft Level

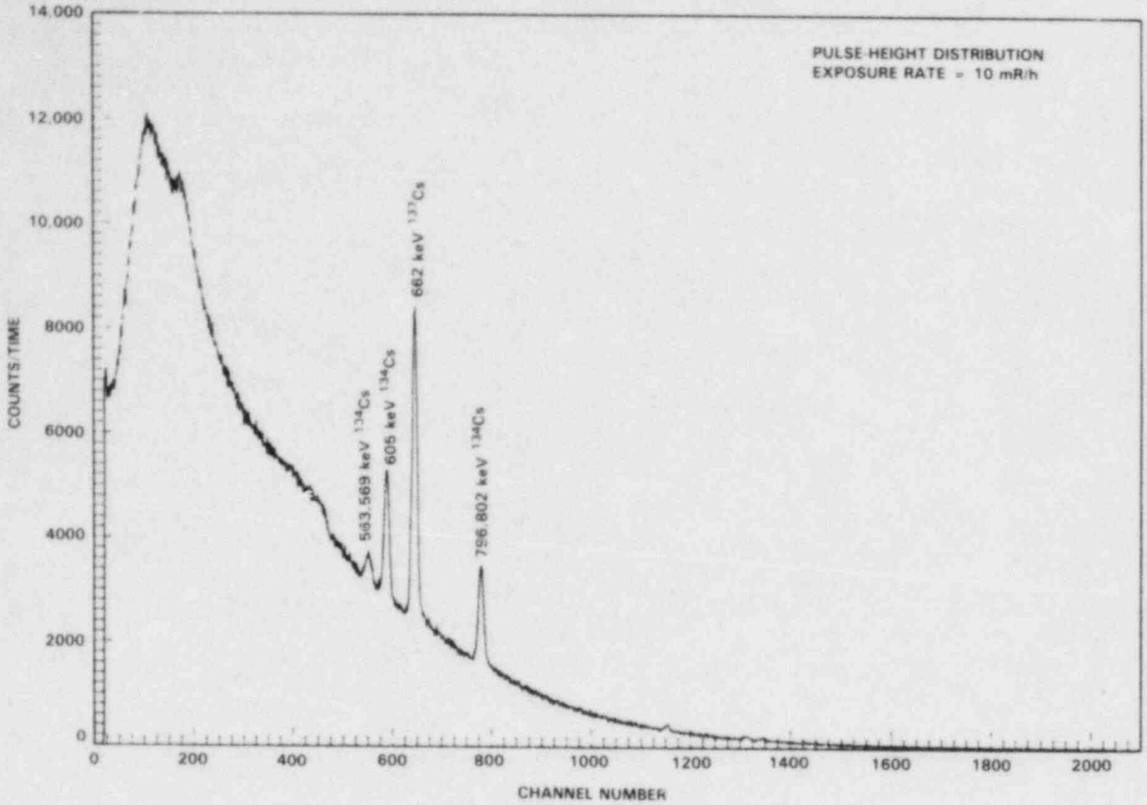

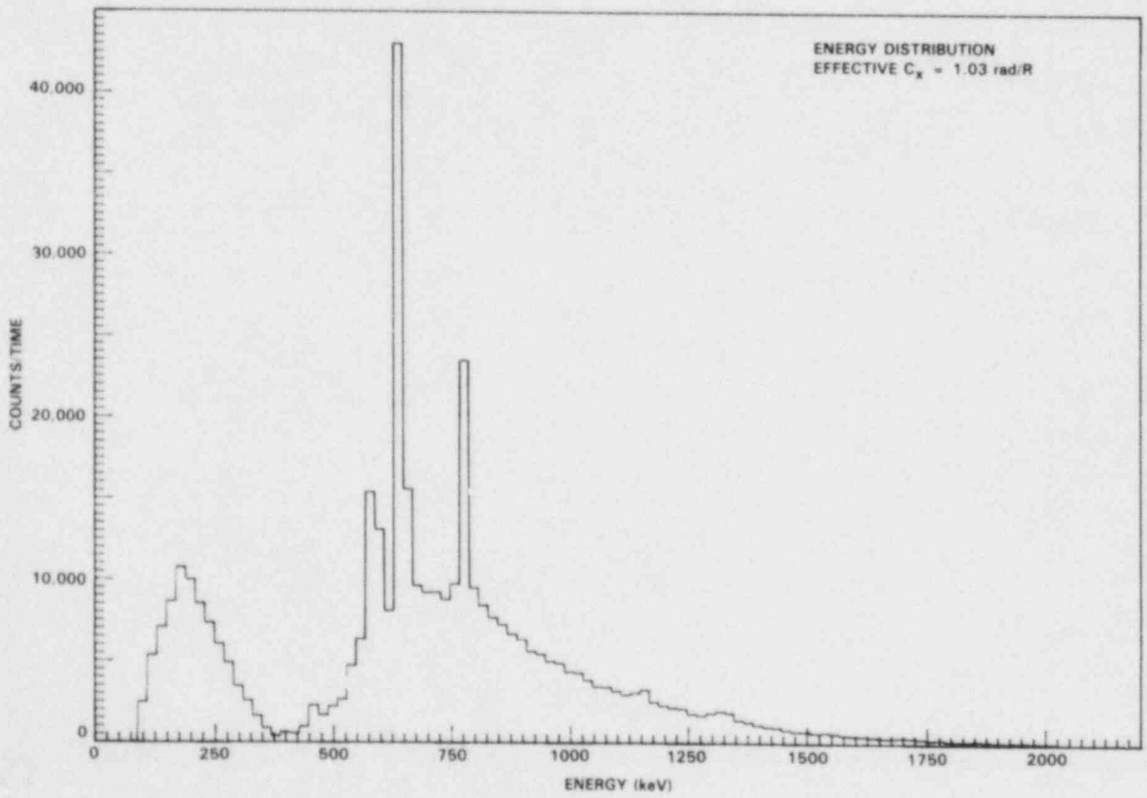

FIGURE A.2.7. Pulse-Height and Photon Energy Distributions, Shutdown PWR, Site B, Location G-Above Escape Hatch, 373-ft Level

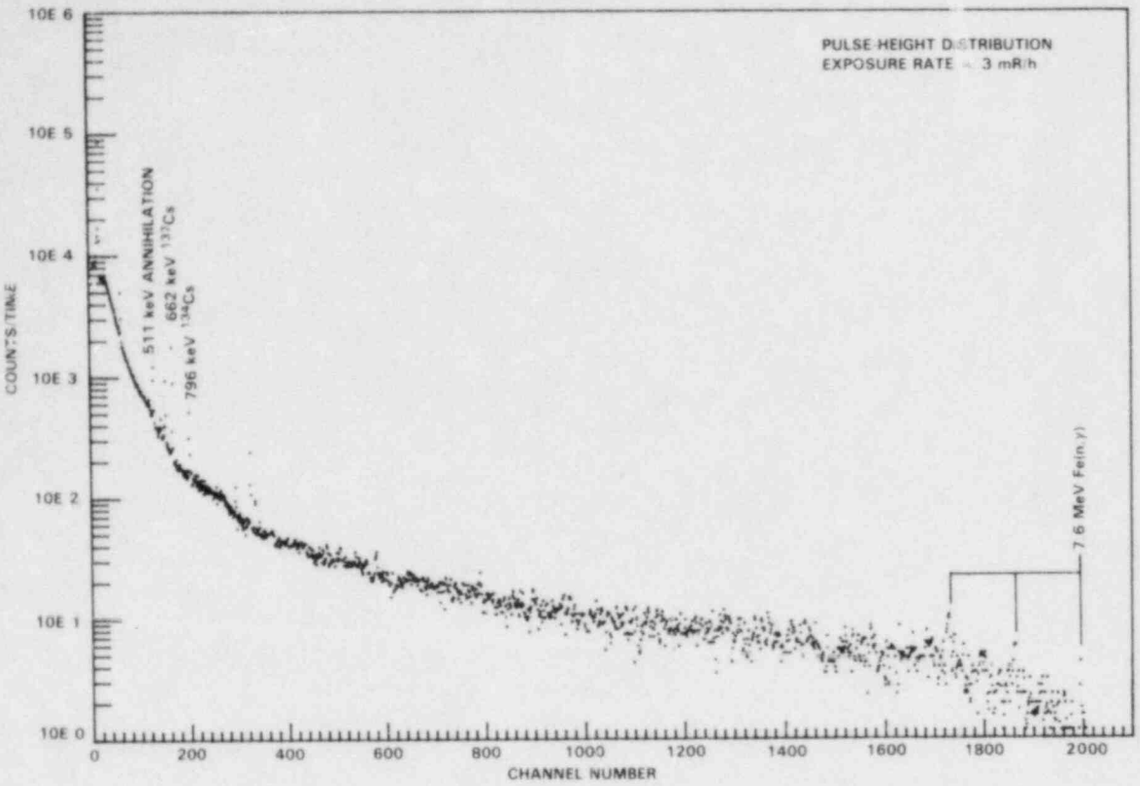

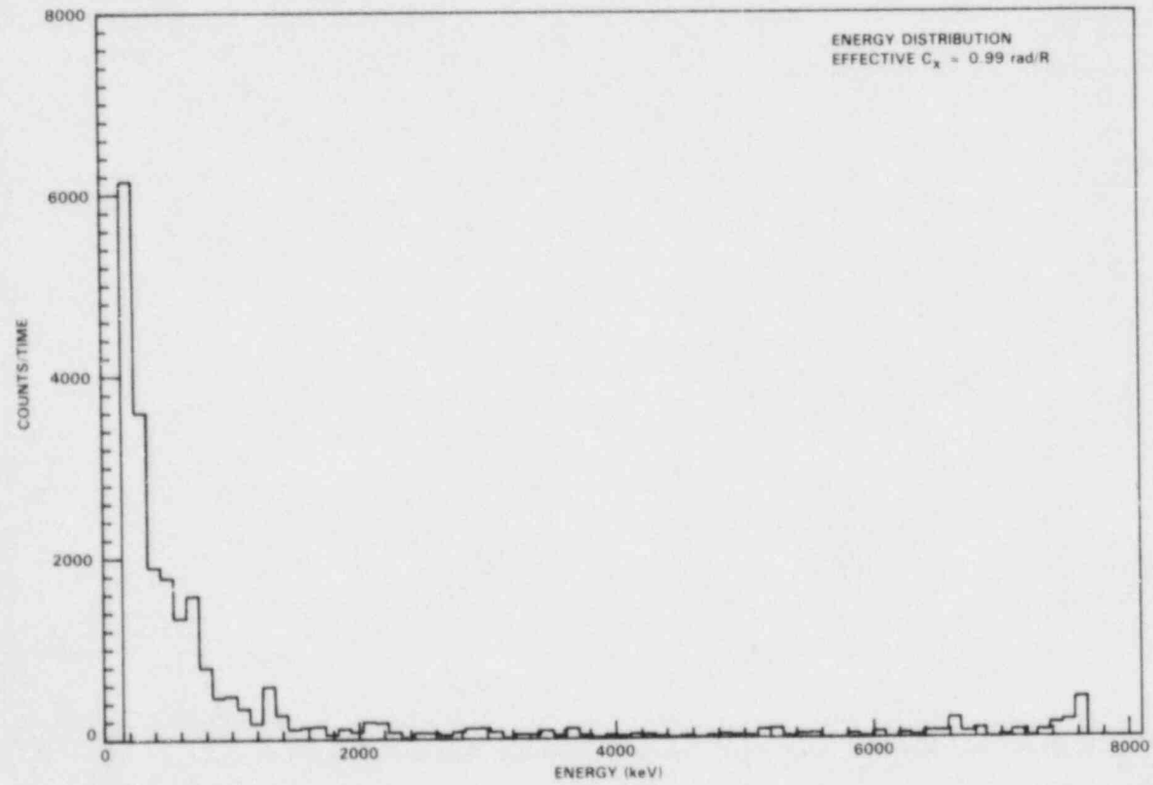

FIGURE A.2.8. Pulse-Height and Photon Energy Distributions, Operating PWR, Site B, Location H-Near Personnel Hatch, 386-ft Level

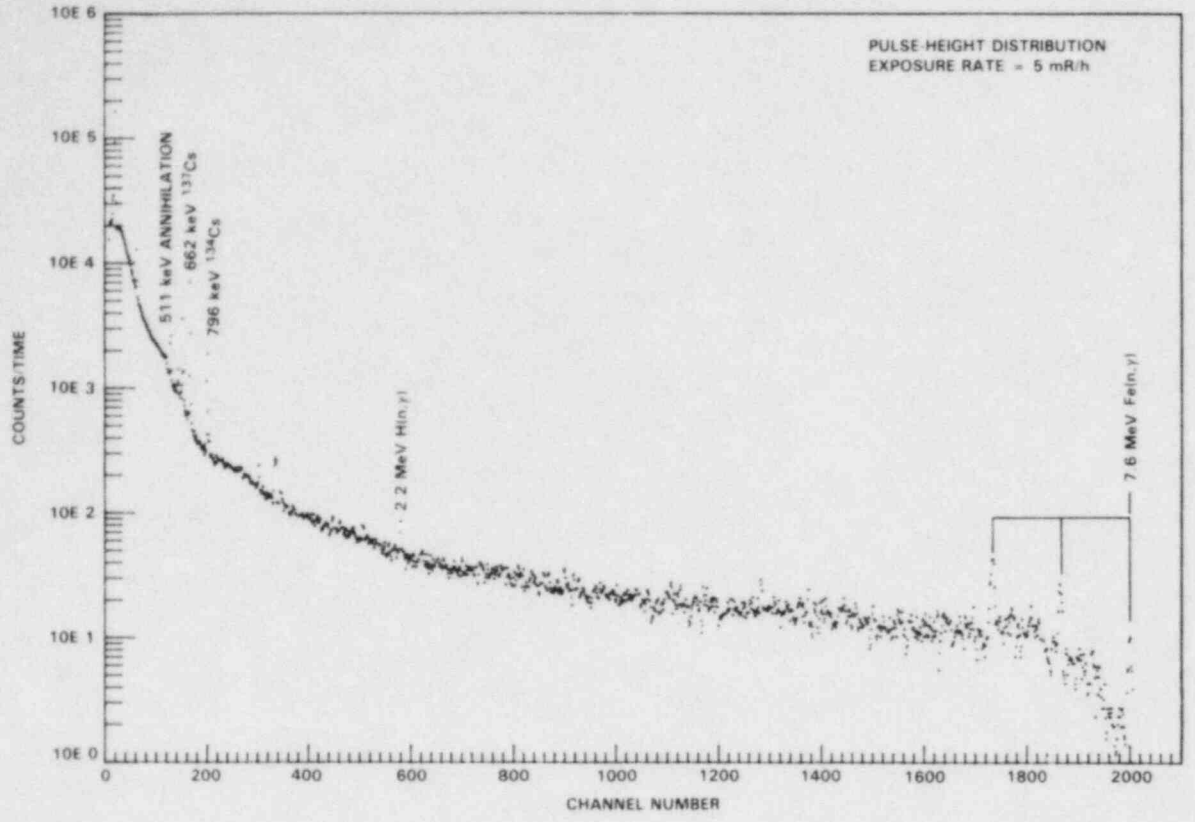

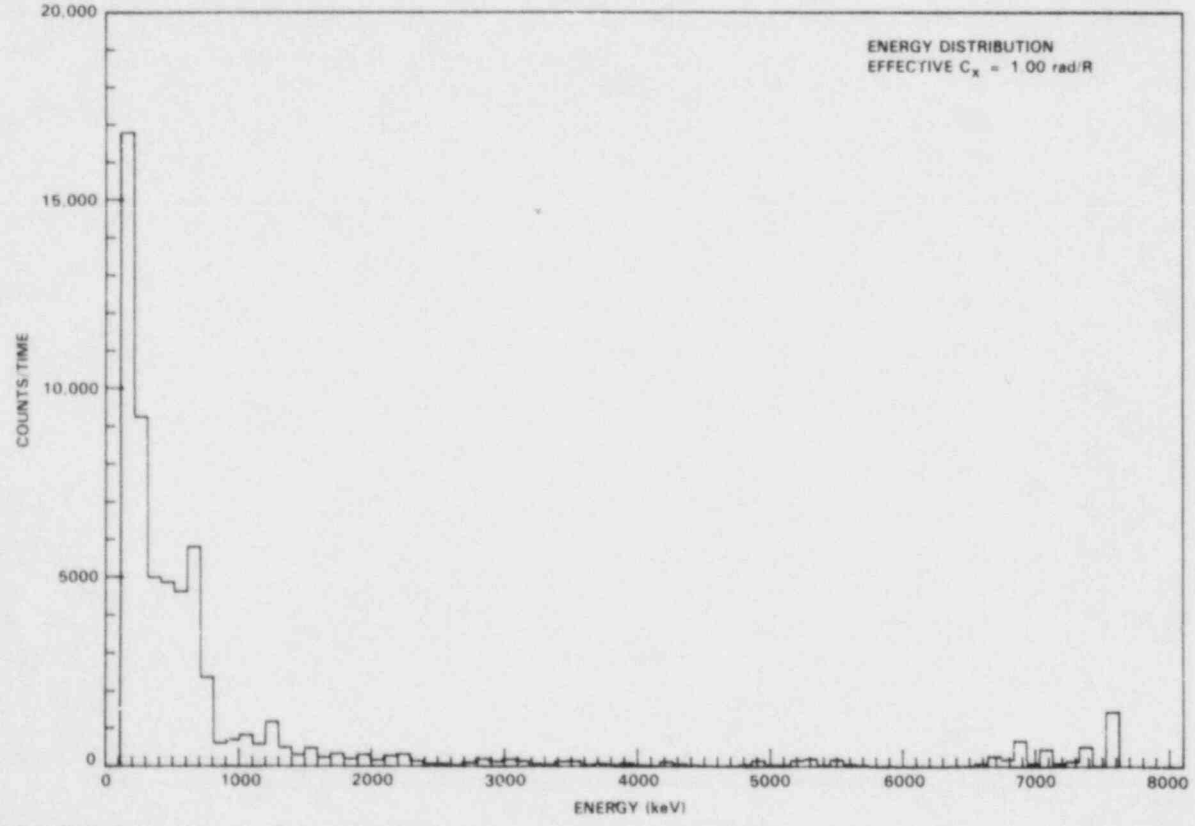

FIGURE A.2.9. Pulse-Height and Photon Energy Distributions, Operating PWR, Site B, Location I-Near Stairway, 386-ft Level

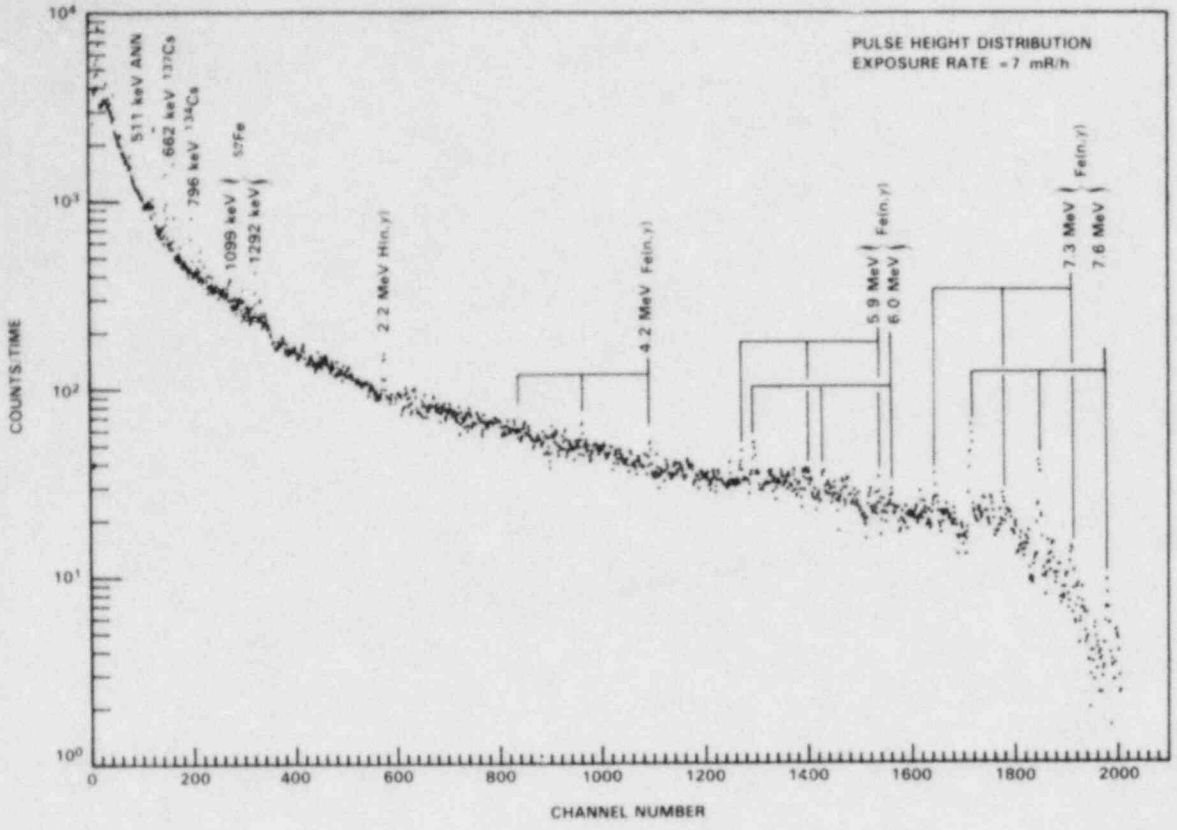

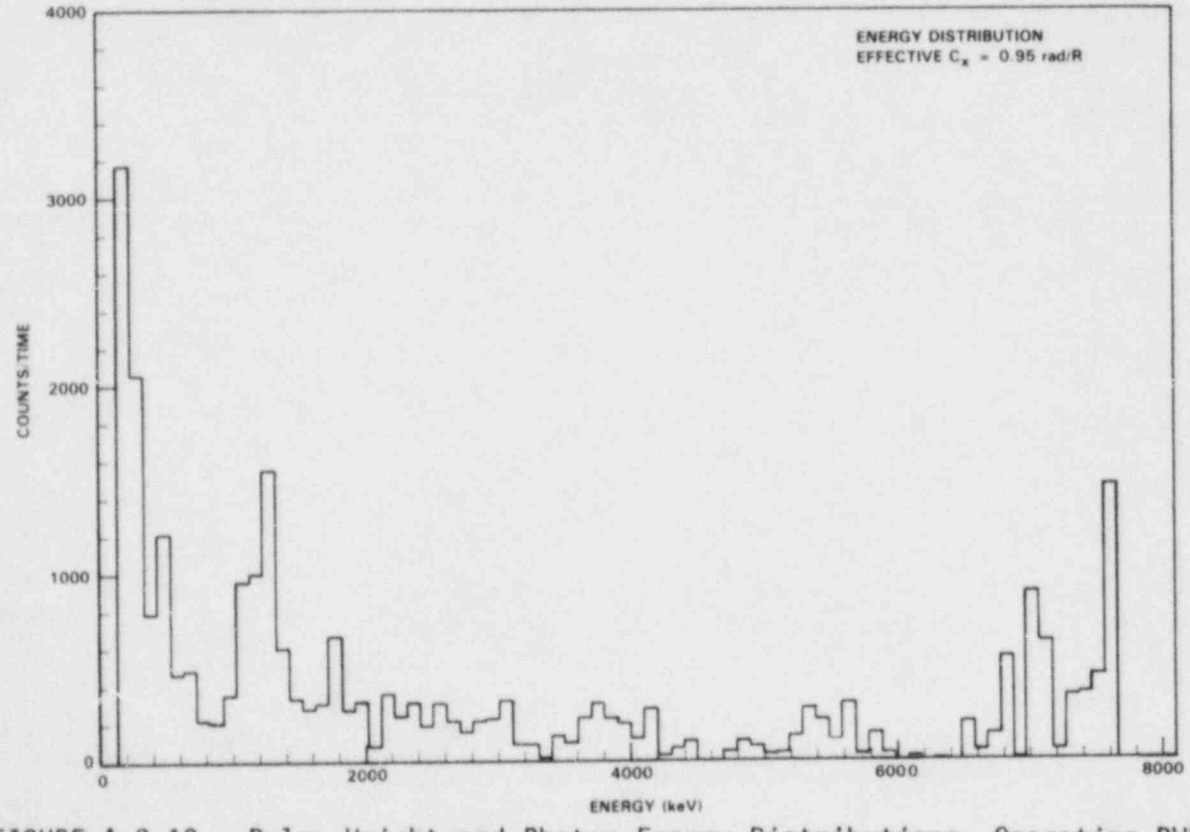

FIGURE A.2.10. Pulse-Height and Photon Energy Distributions, Operating PWR, Site B, Location E-Near Elevator, 401-ft Level (collimated)

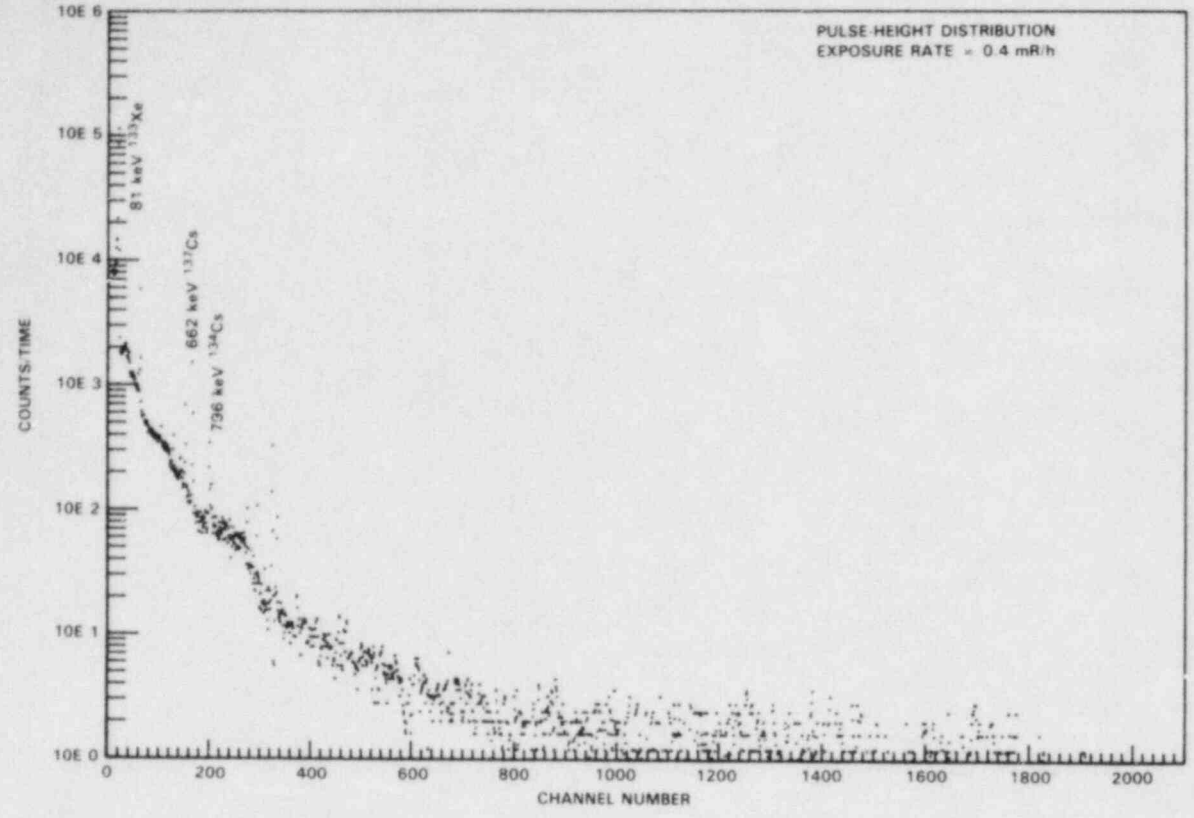

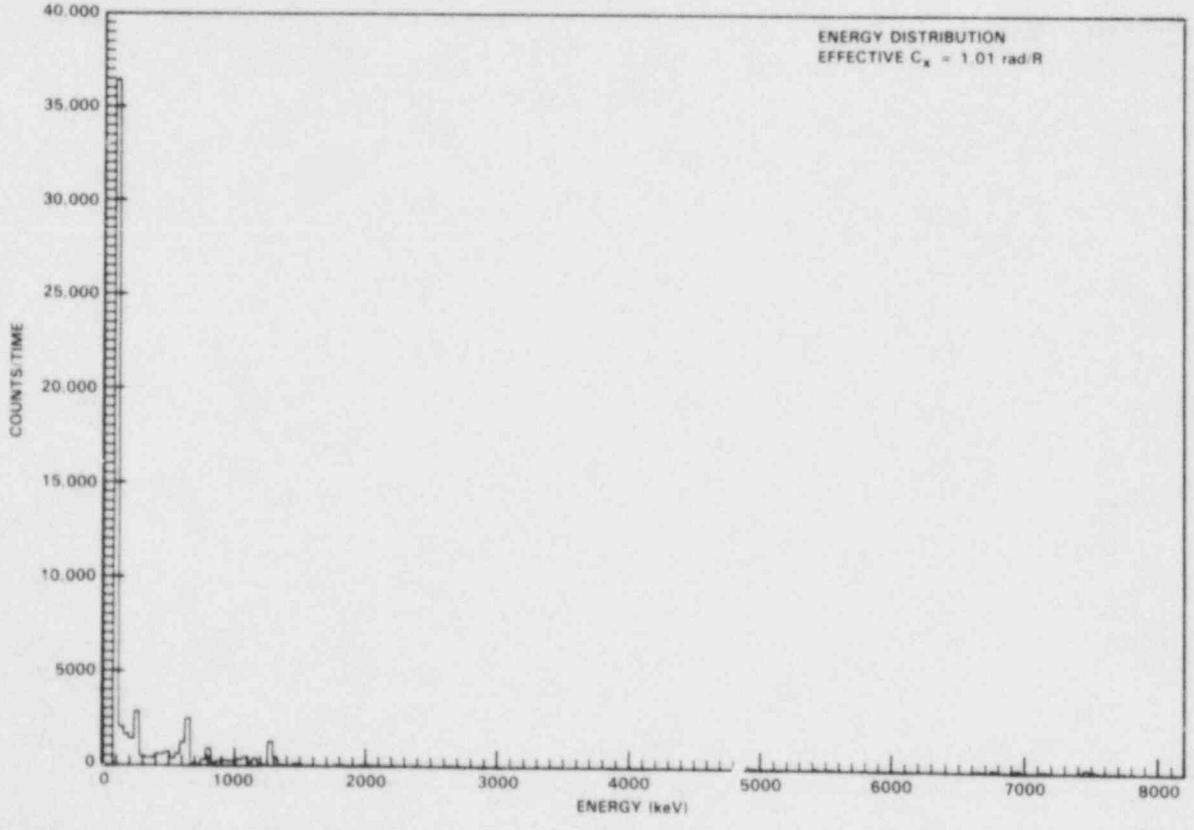

FIGURE A.2.11. Pulse-Height and Photon Energy Distributions, Operating PWR, Site B, Location J-In Personnel Hatch

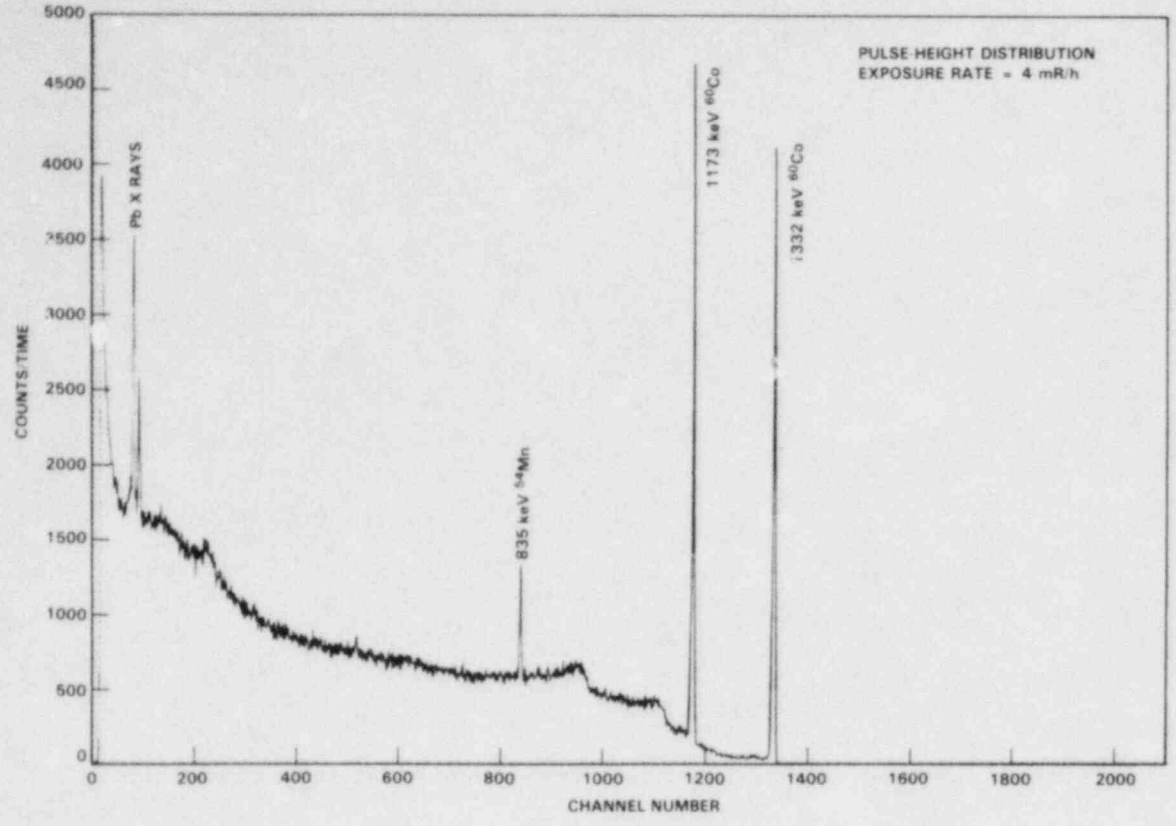

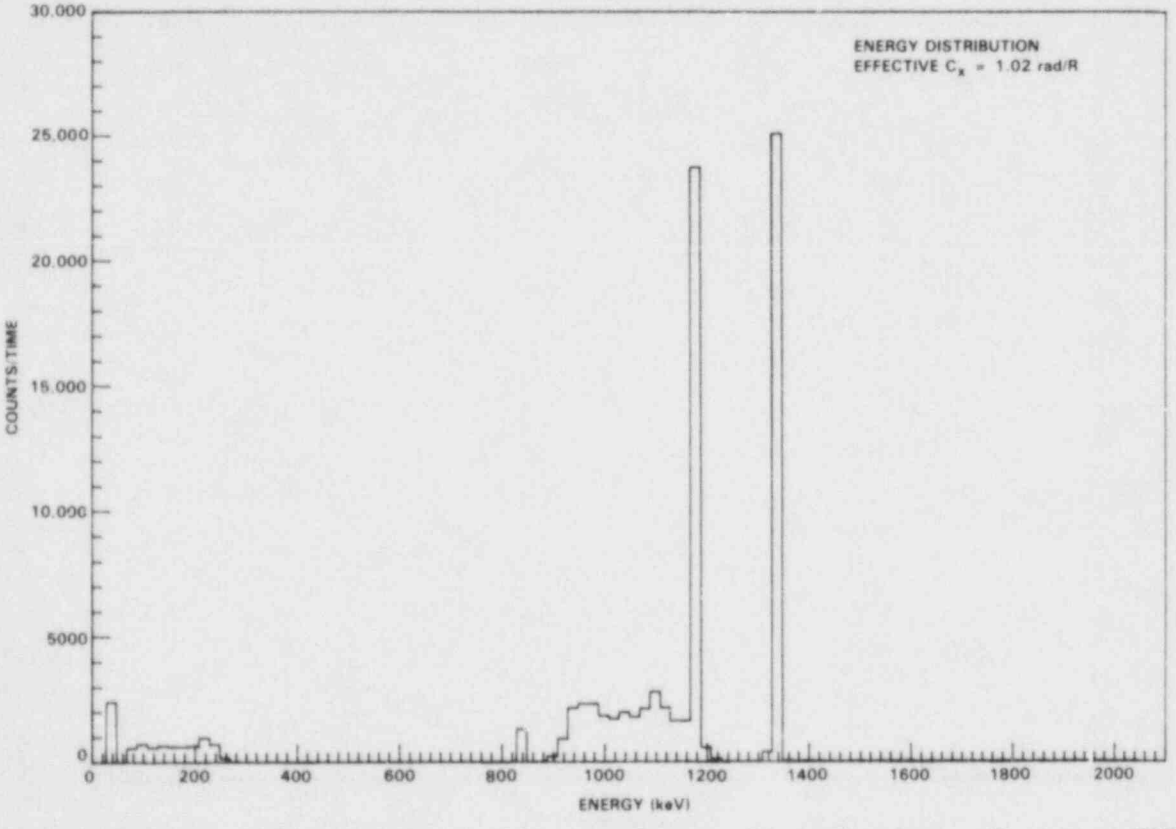

FIGURE A.3.1. Pulse-Height and Photon Energy Distributions, Shutdown BWR, Site M, Refuel Pool, HEPA Filter Hose (collimated)

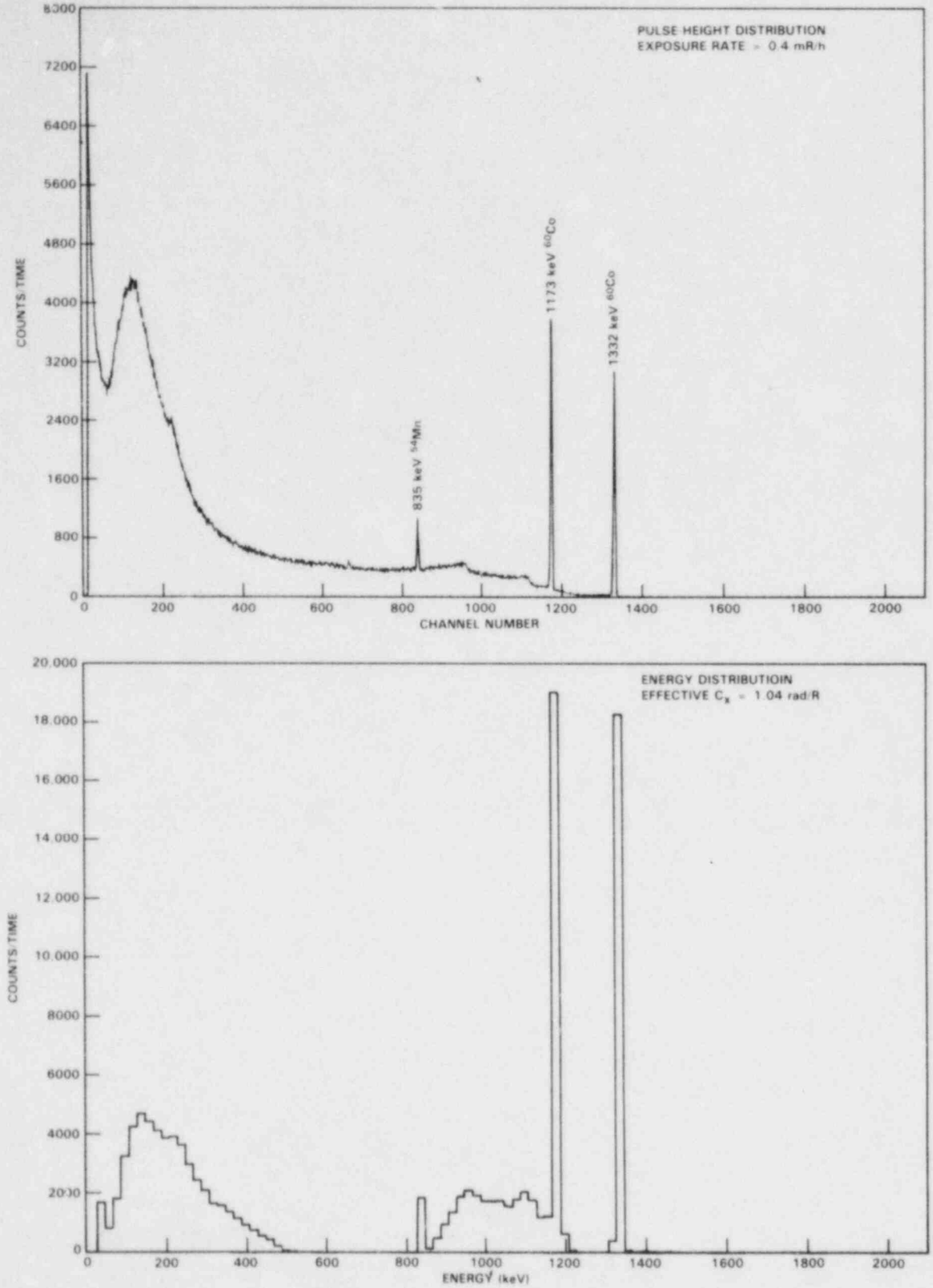

FIGURE A.3.2. Pulse-Height and Photon Energy Distributions, Shutdown BWR, Site M, Refuel Pool, General Area

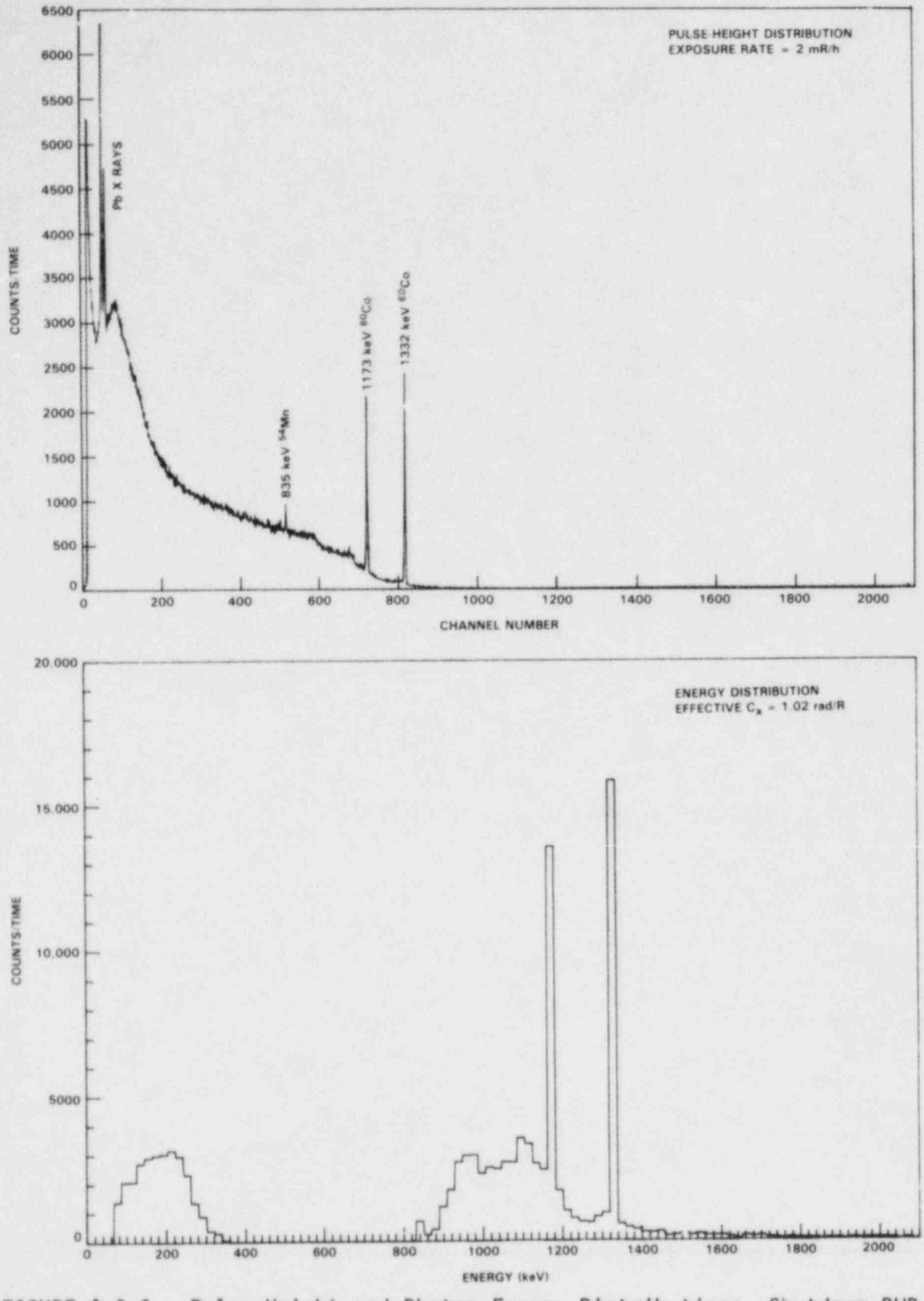

FIGURE A.3.3. Pulse-Height and Photon Energy Distributions, Shutdown BWR, Site M, Dry Well, Valve (collimated)

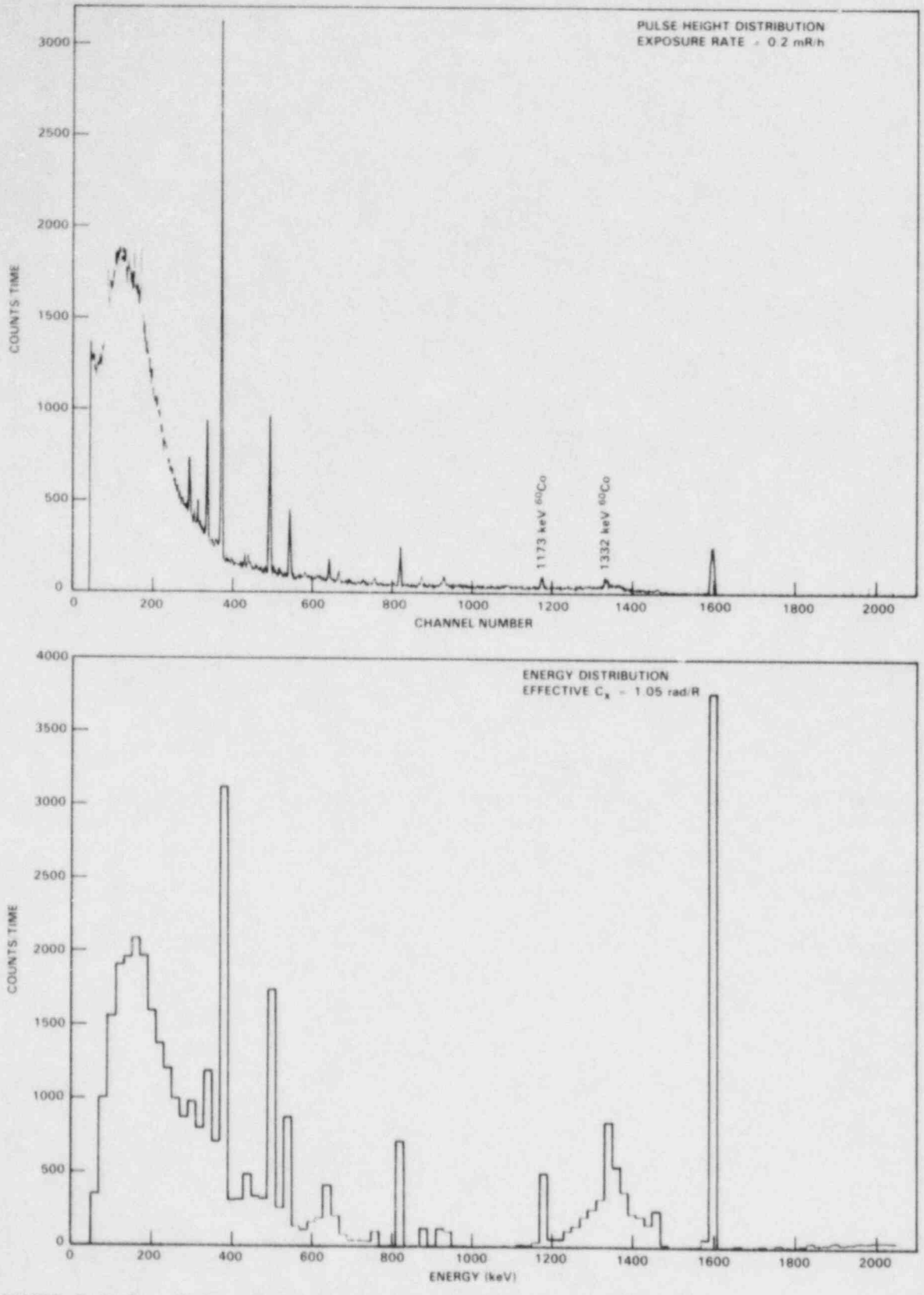

FIGURE A.3.4. Pulse-Height and Photon Energy Distributions, Shutdown BWR, Site M, Turbine Blade Housing Diaphragm

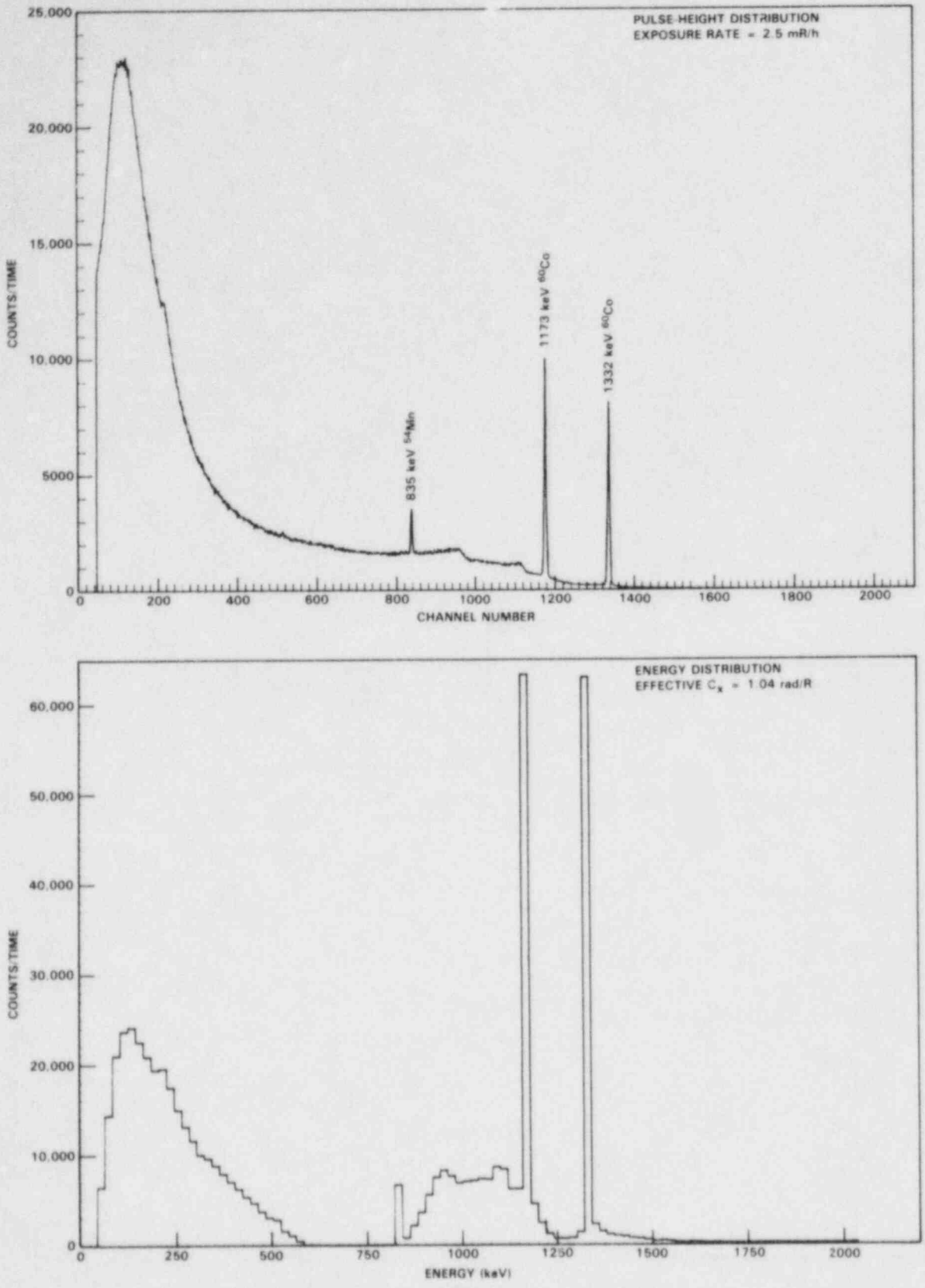

FIGURE A.3.5. Pulse-Height and Photon Energy Distributions, Operating BWR, Site M, Reactor Building, First Floor, Opposite Airlock

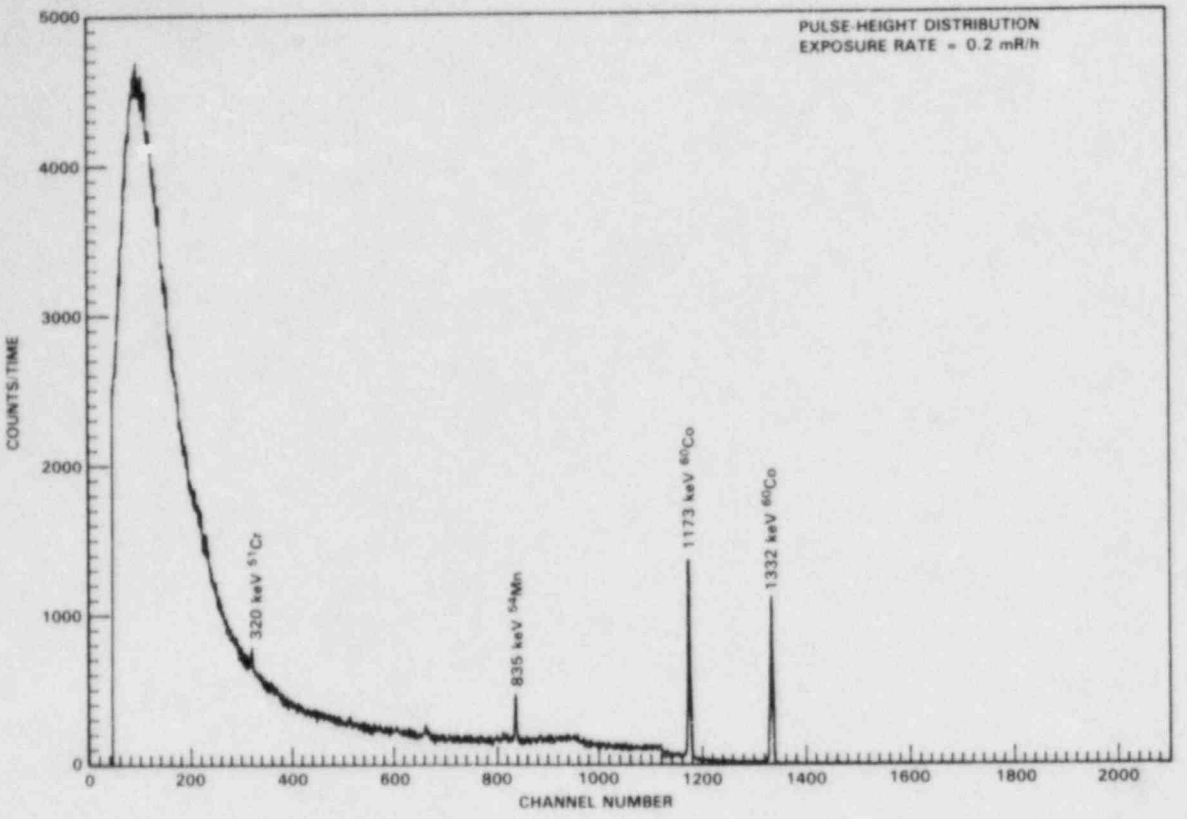

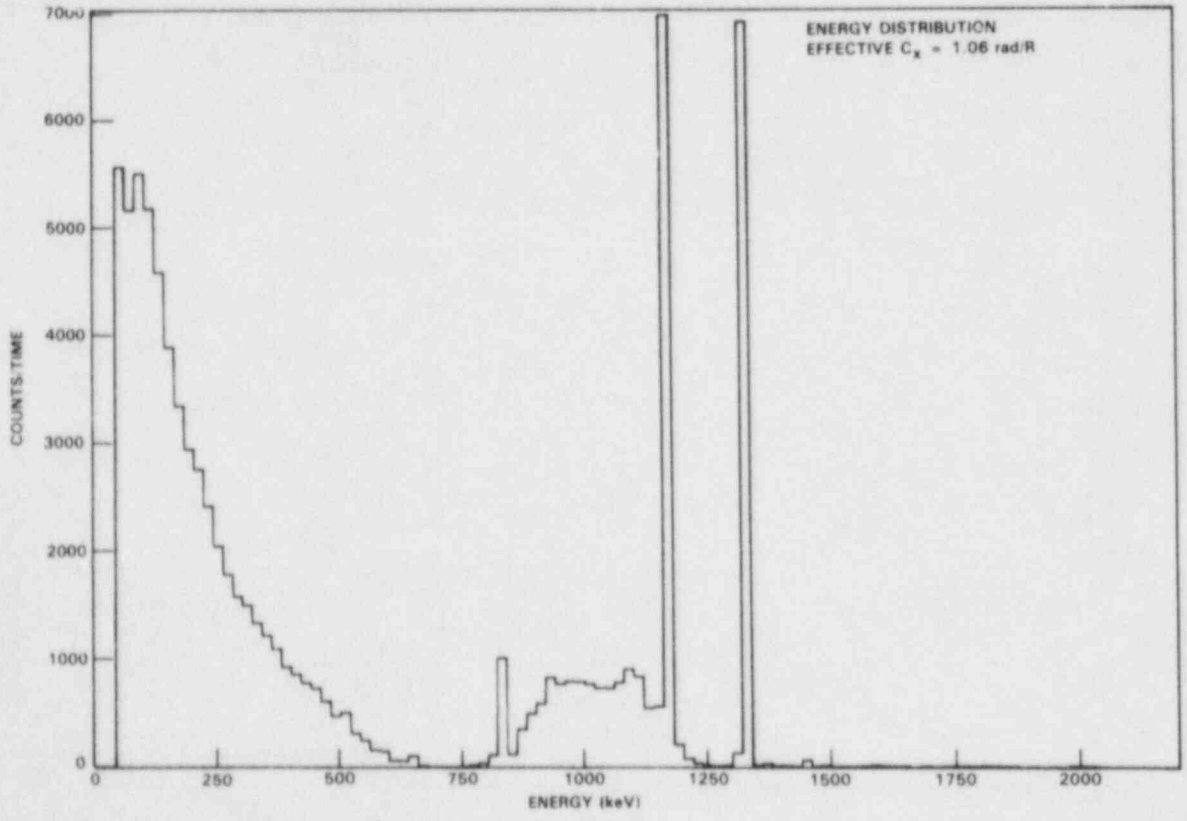

FIGURE A.3.6. Pulse-Height and Photon Energy Distributions, Operating BWR, Site M, Reactor Building, First Floor, Outside RHR Valve Room

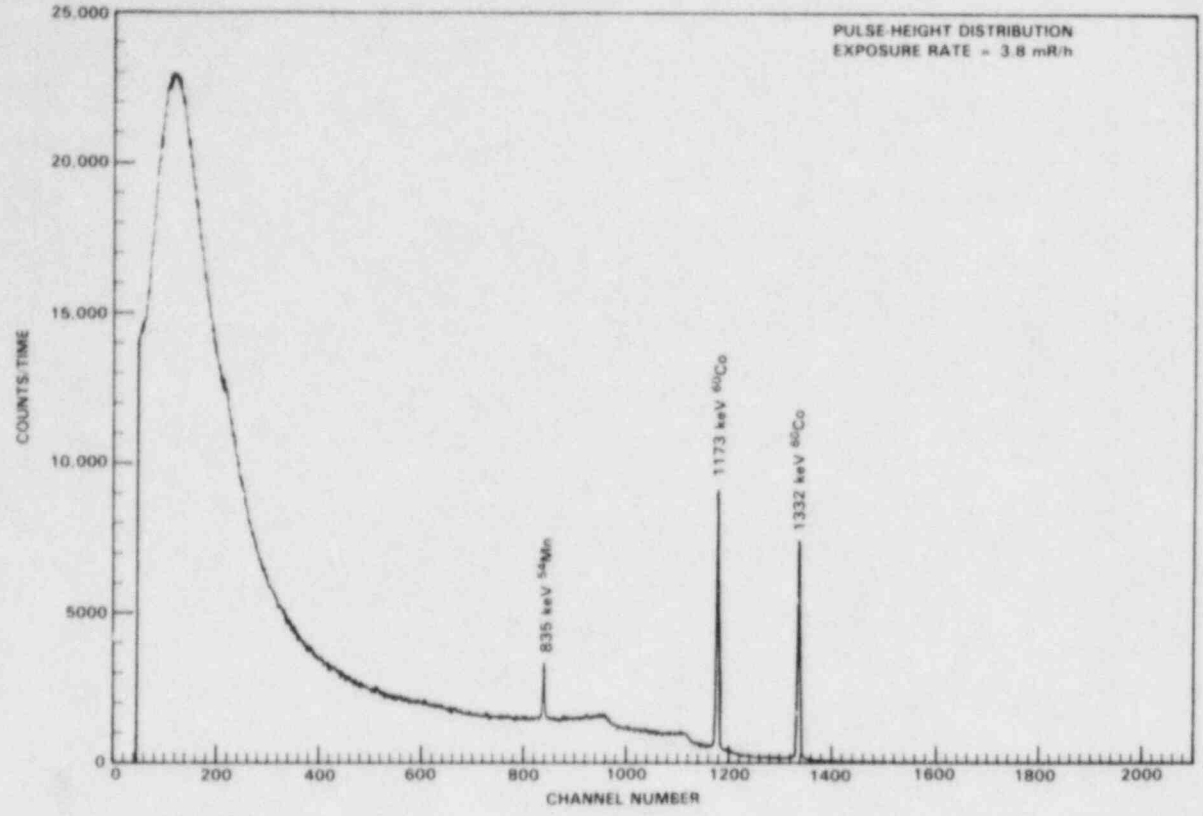

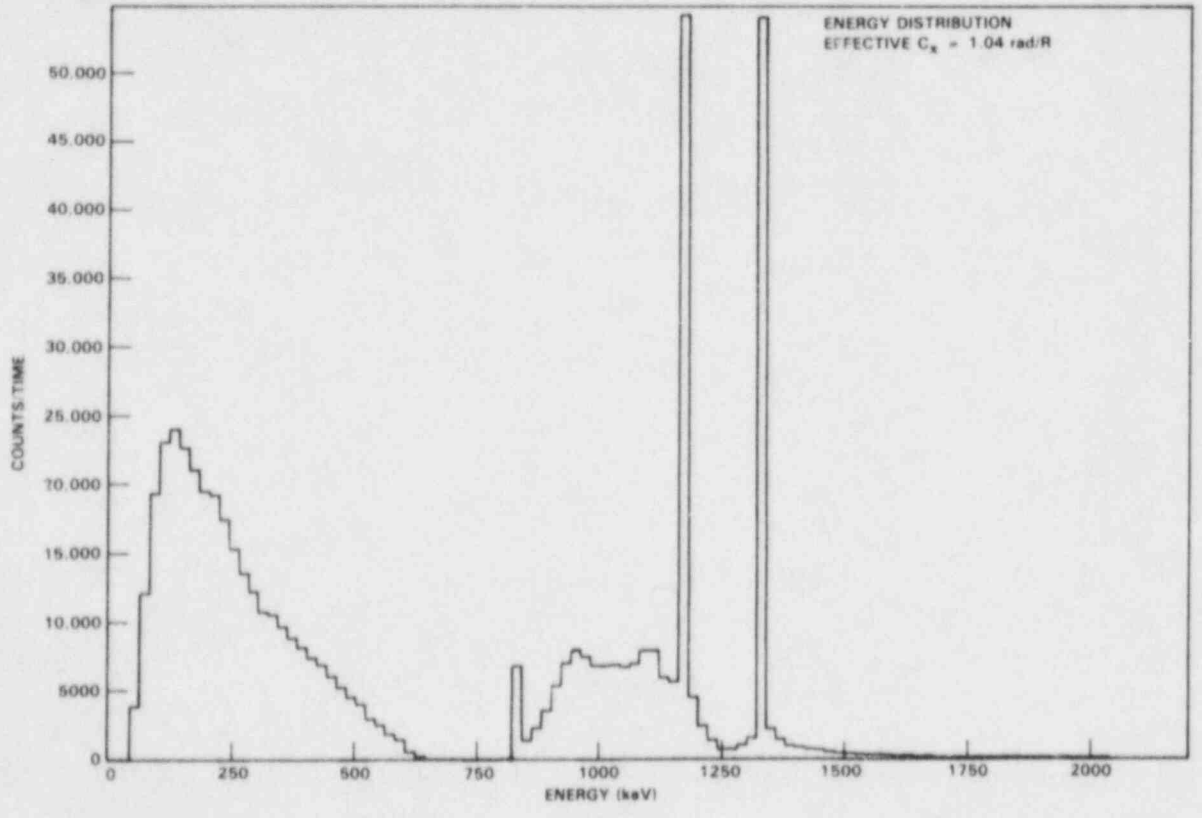

FIGURE A.3.7. Pulse-Height and Photon Energy Distributions, Operating BWR, Site M, Reactor Building, Near Scram Discharge Lines

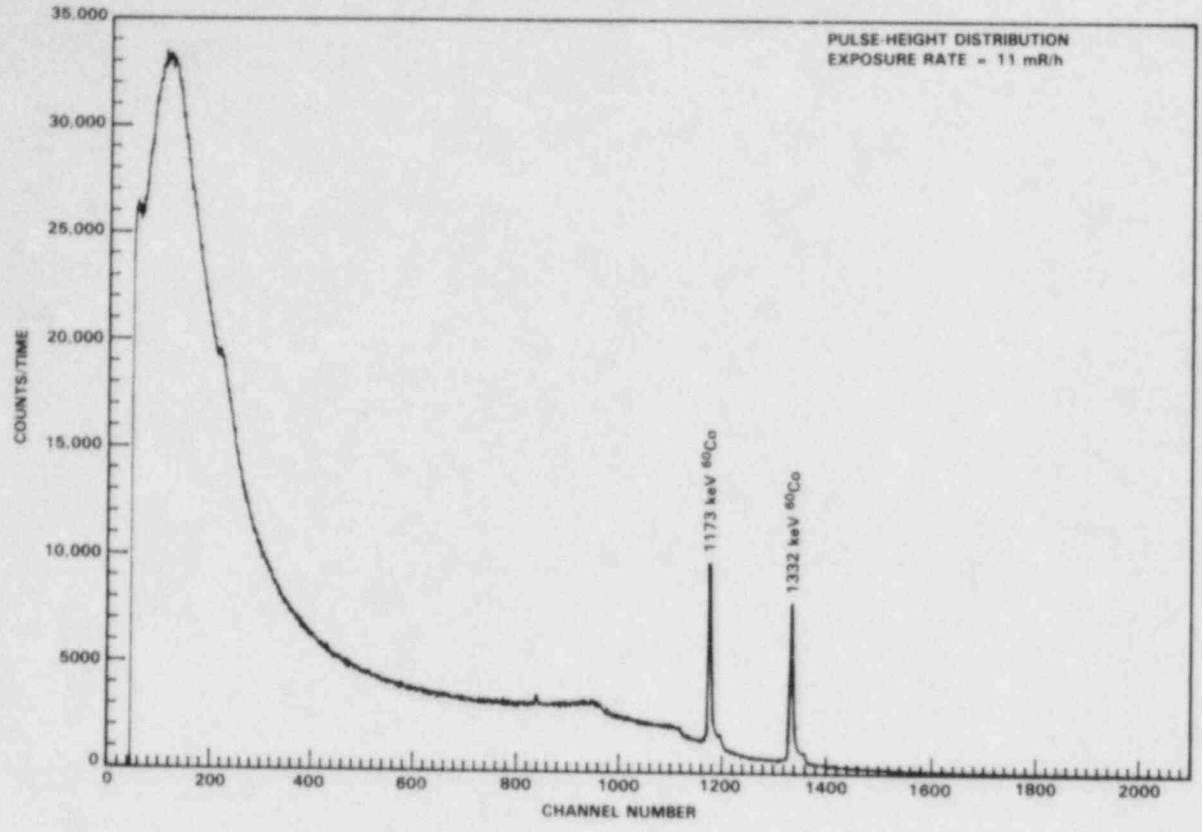

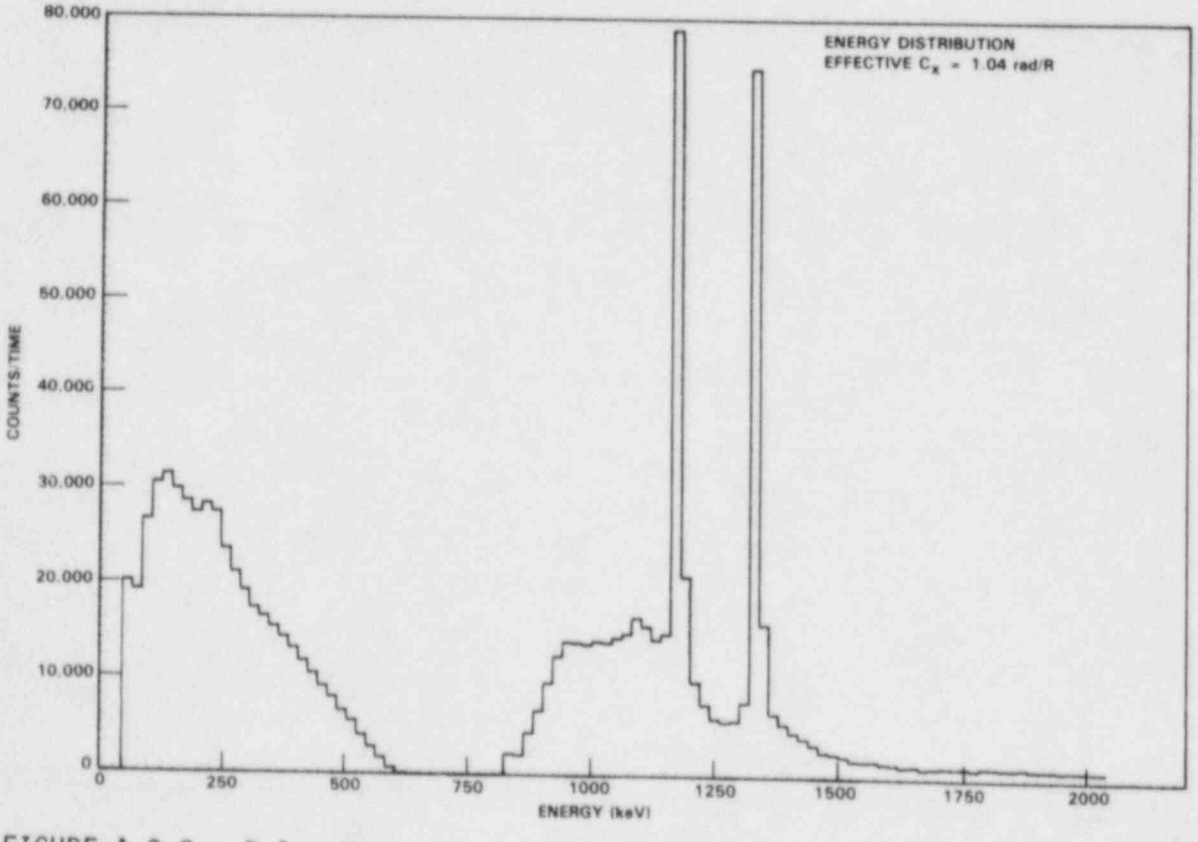

FIGURE A.3.8. Pulse-Height and Photon Energy Distributions, Operating BWR, Site M, Reactor Building, Second Floor, Outside Spent Resin Room

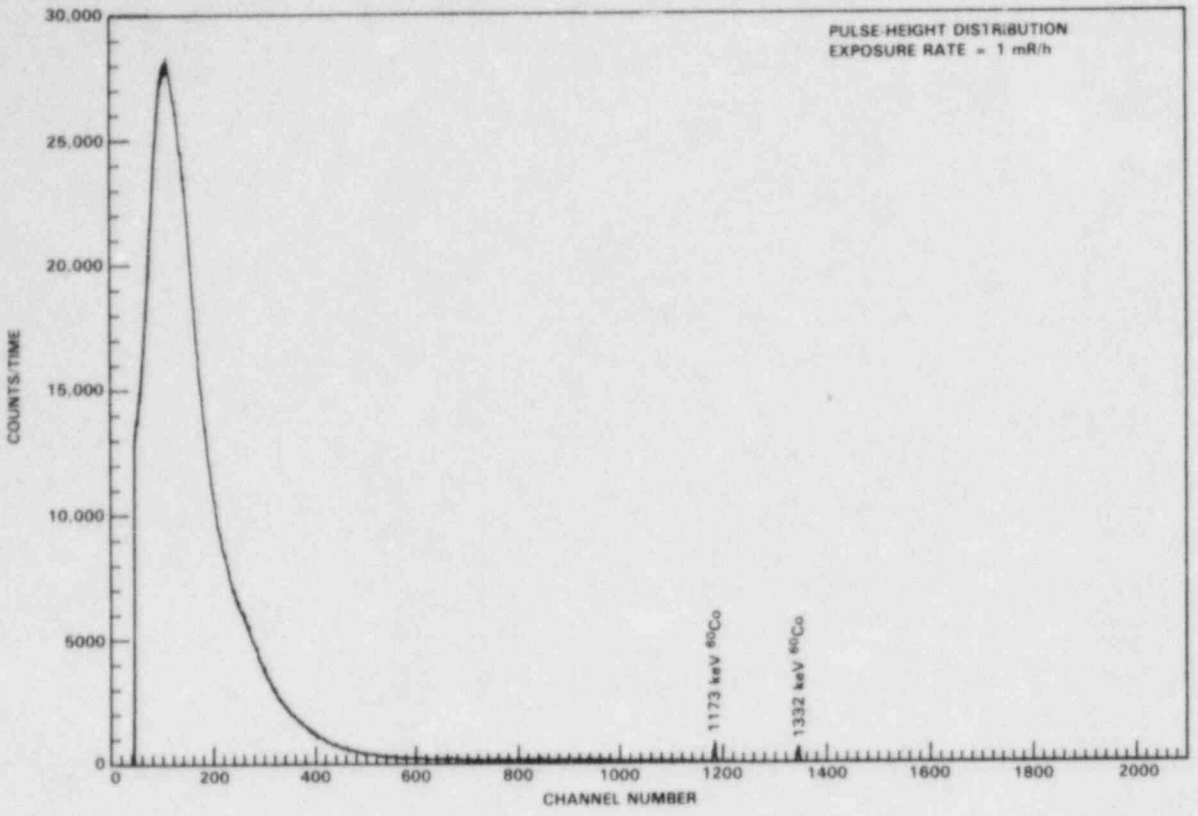

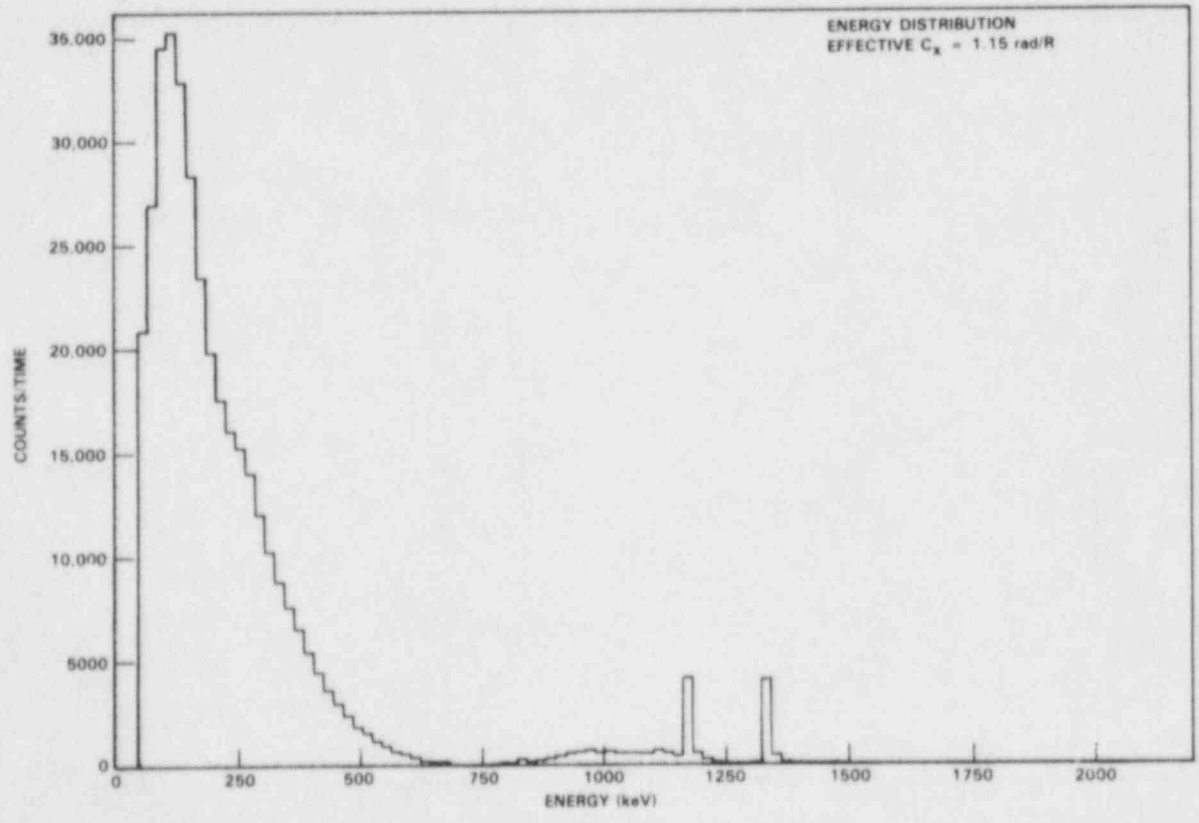

FIGURE A.3.9. Pulse-Height and Photon Energy Distributions, Operating BWR, Site M, Reactor Building, Second Floor, Near Clean-Up Phase Separator Room Door

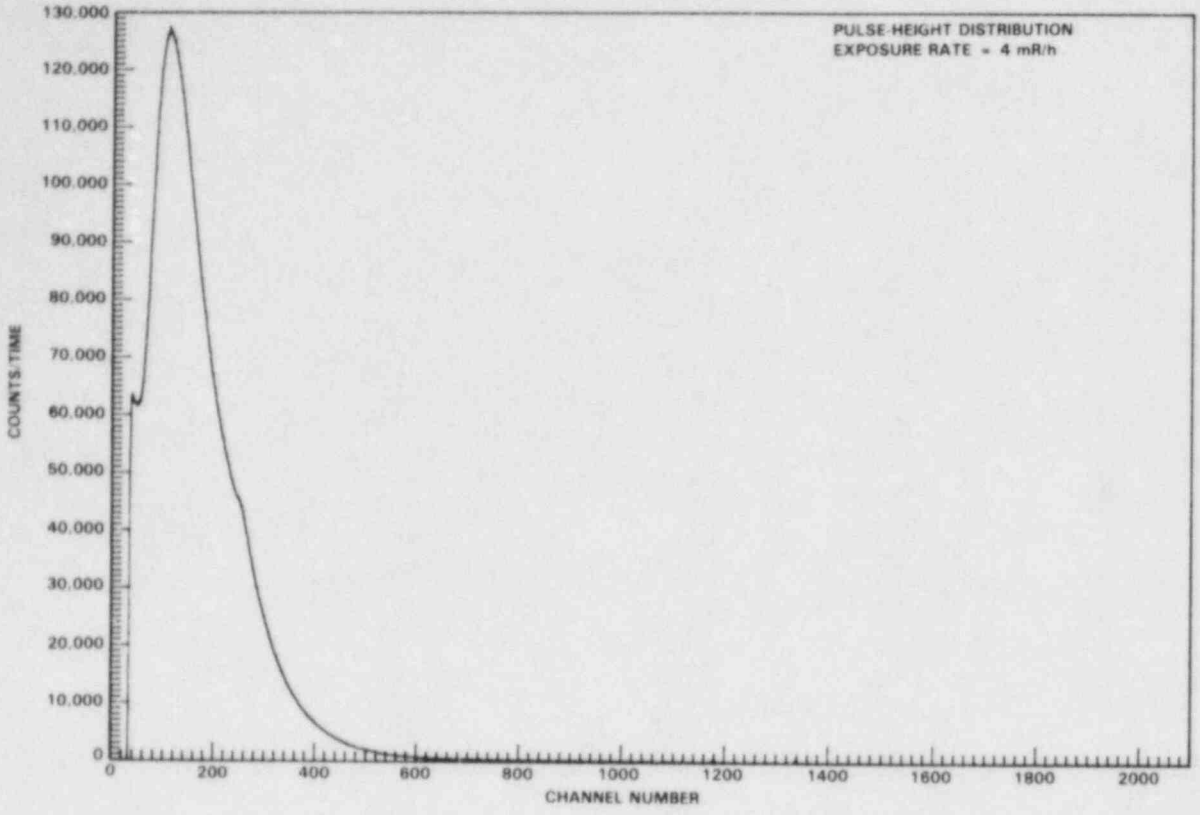

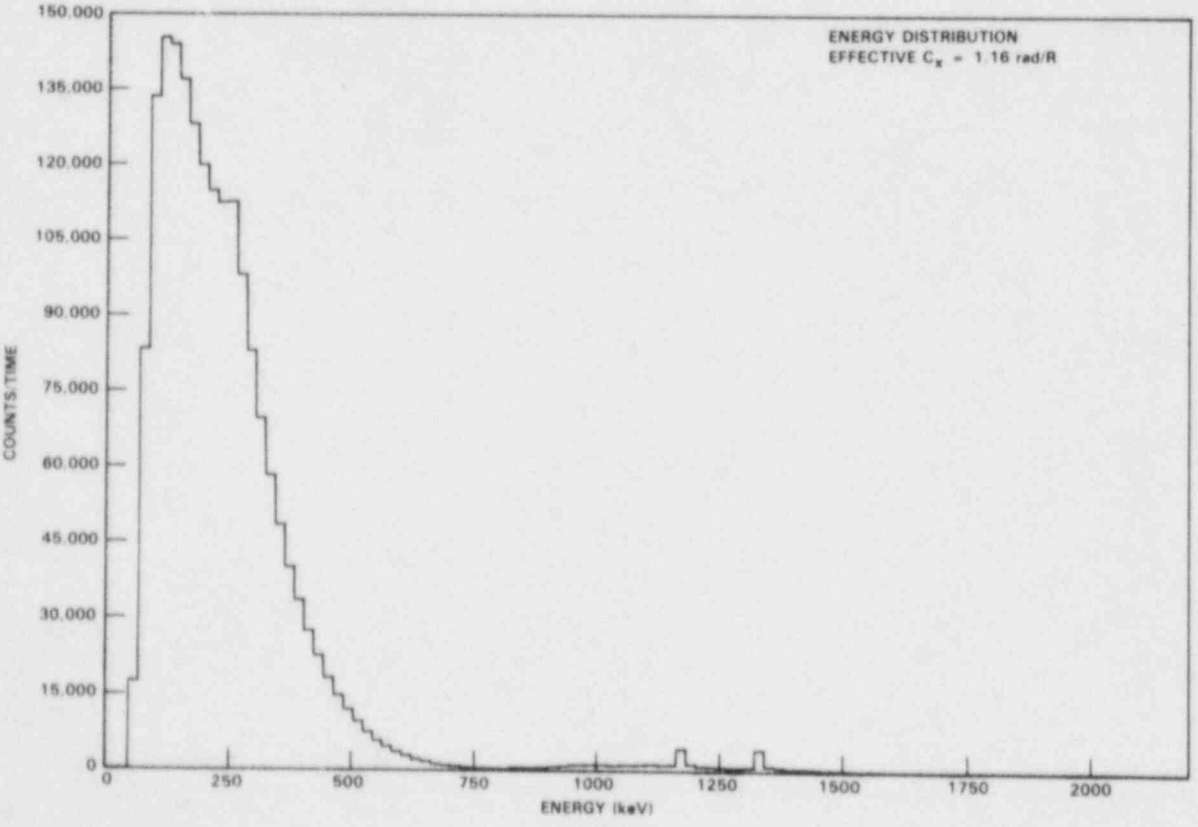

FIGURE A.3.10. Pulse-Height and Photon Energy Distributions, Operating BWR, Site M, Reactor Building, Second Floor, Near Clean-Up Phase Separator Room Door

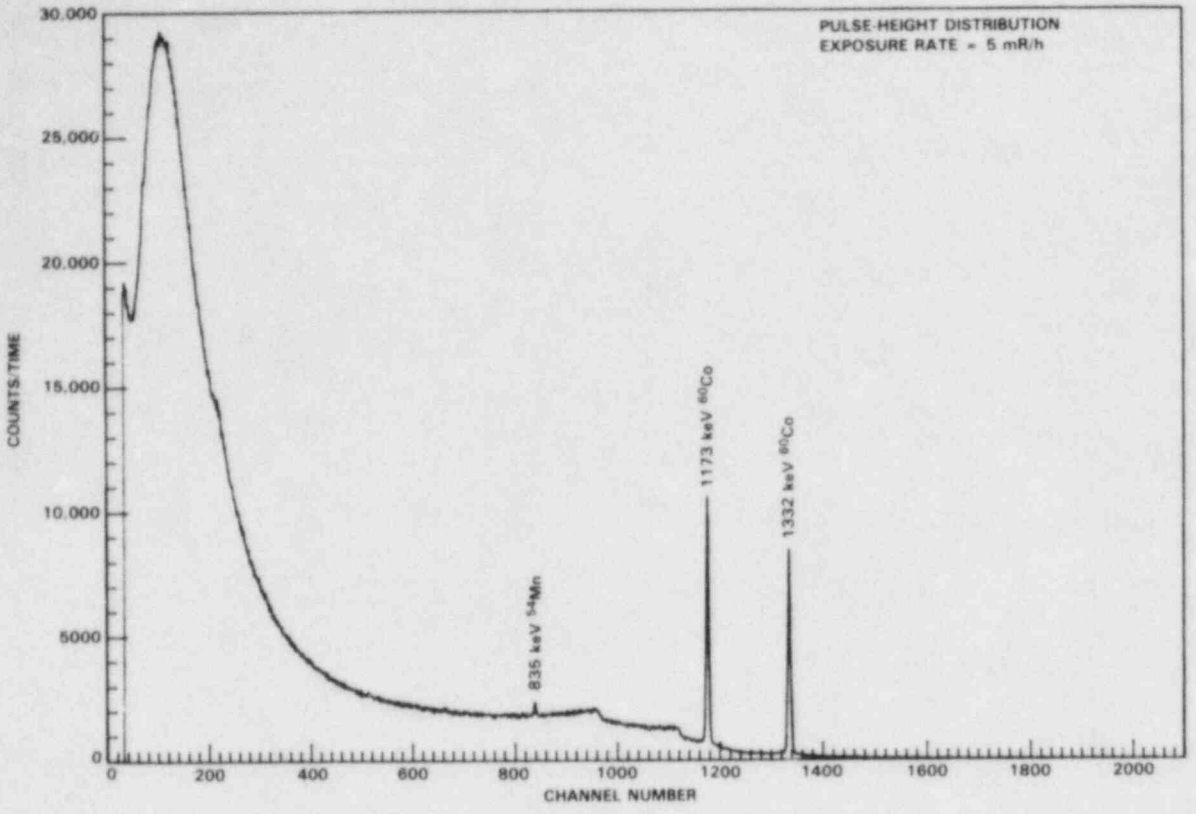

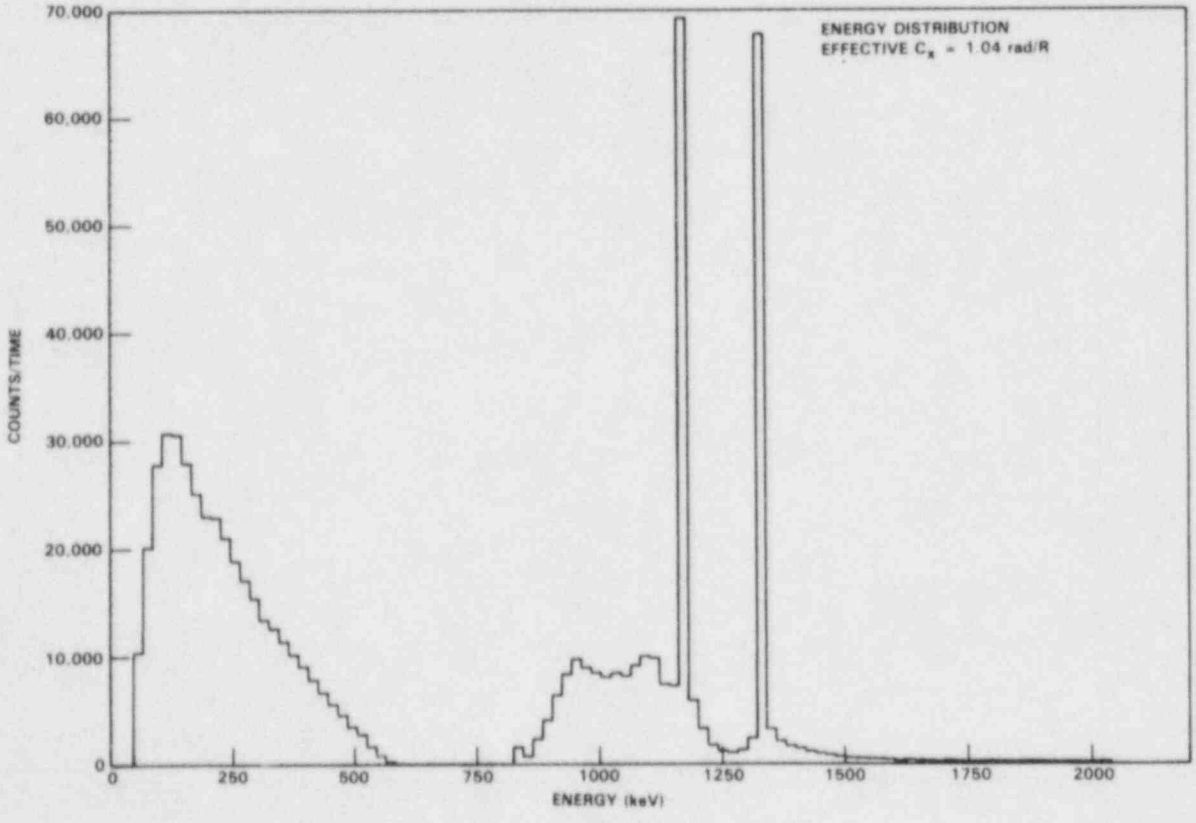

FIGURE A.3.11. Pulse-Height and Photon Energy Distributions, Operating BWR, Site M, Reactor Building, Second Floor, Near Containment

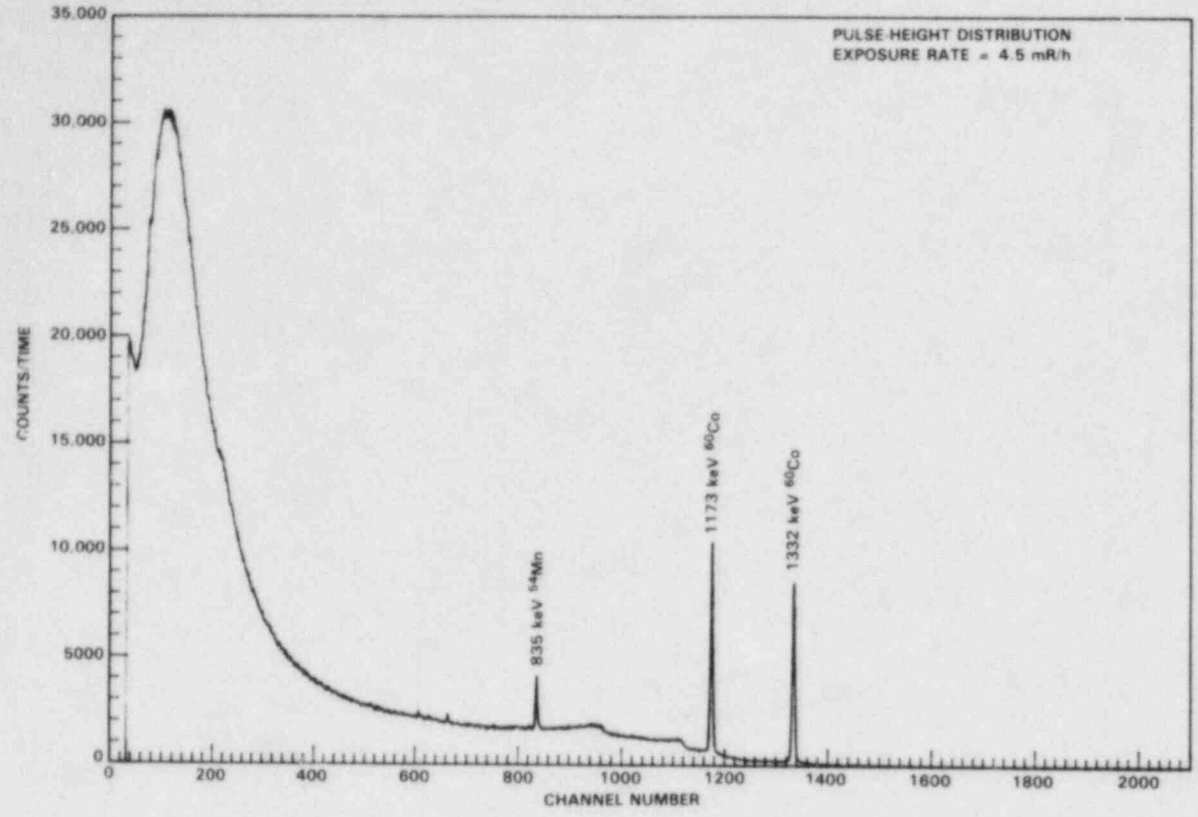

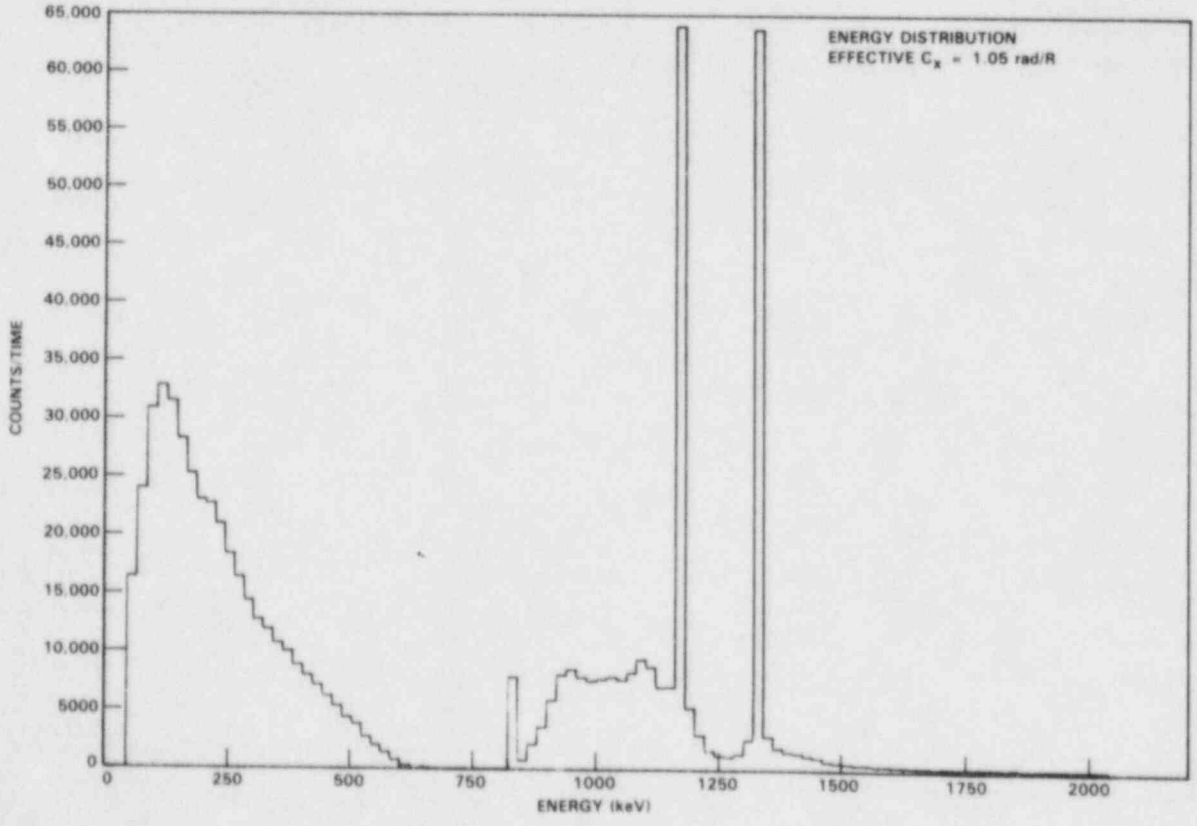

FIGURE A.3.12. Pulse-Height and Photon Energy Distributions, Operating BWR, Site M, Reactor Building, Third Floor, Near Jungle Room Door

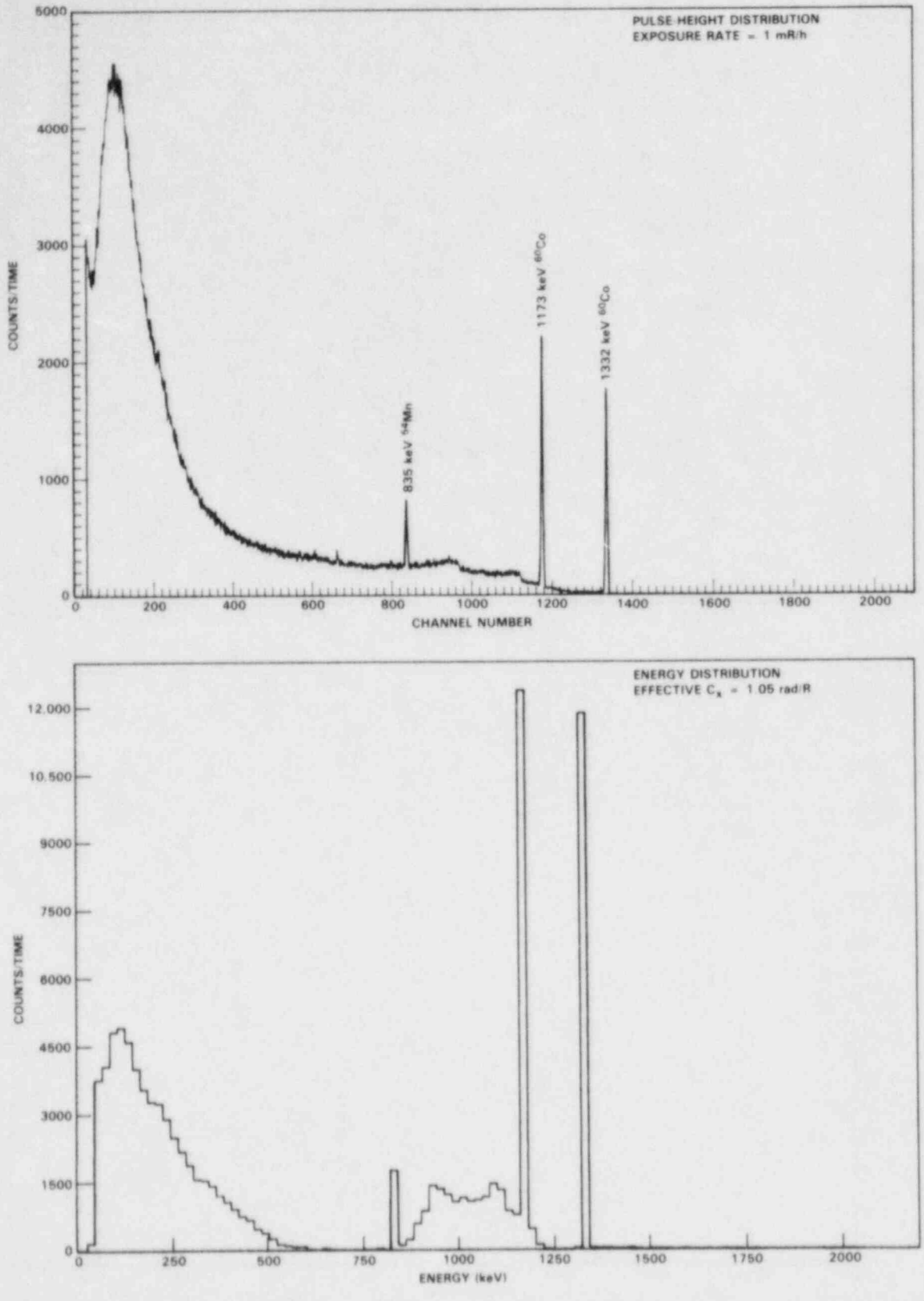

FIGURE A.3.13. Pulse-Height and Photon Energy Distributions, Operating BWR, Site M, Reactor Building, Fourth Floor, Laundry Area

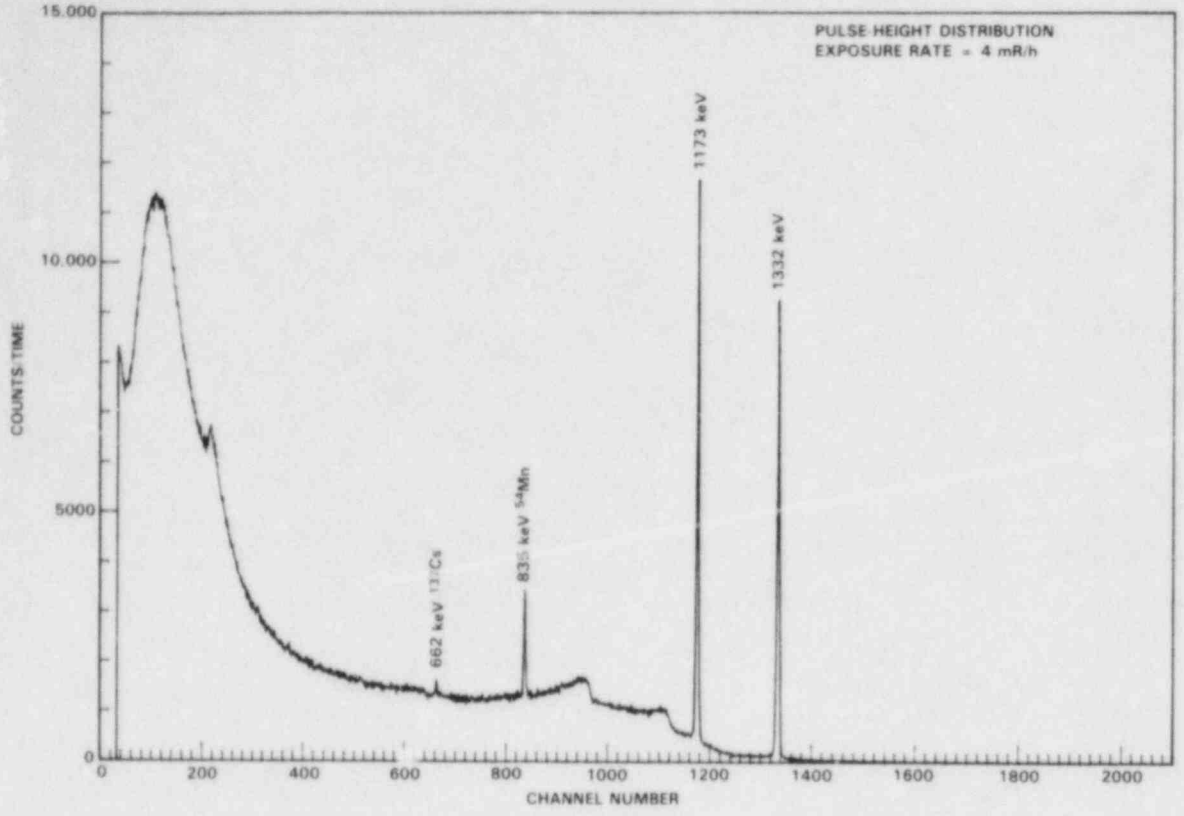

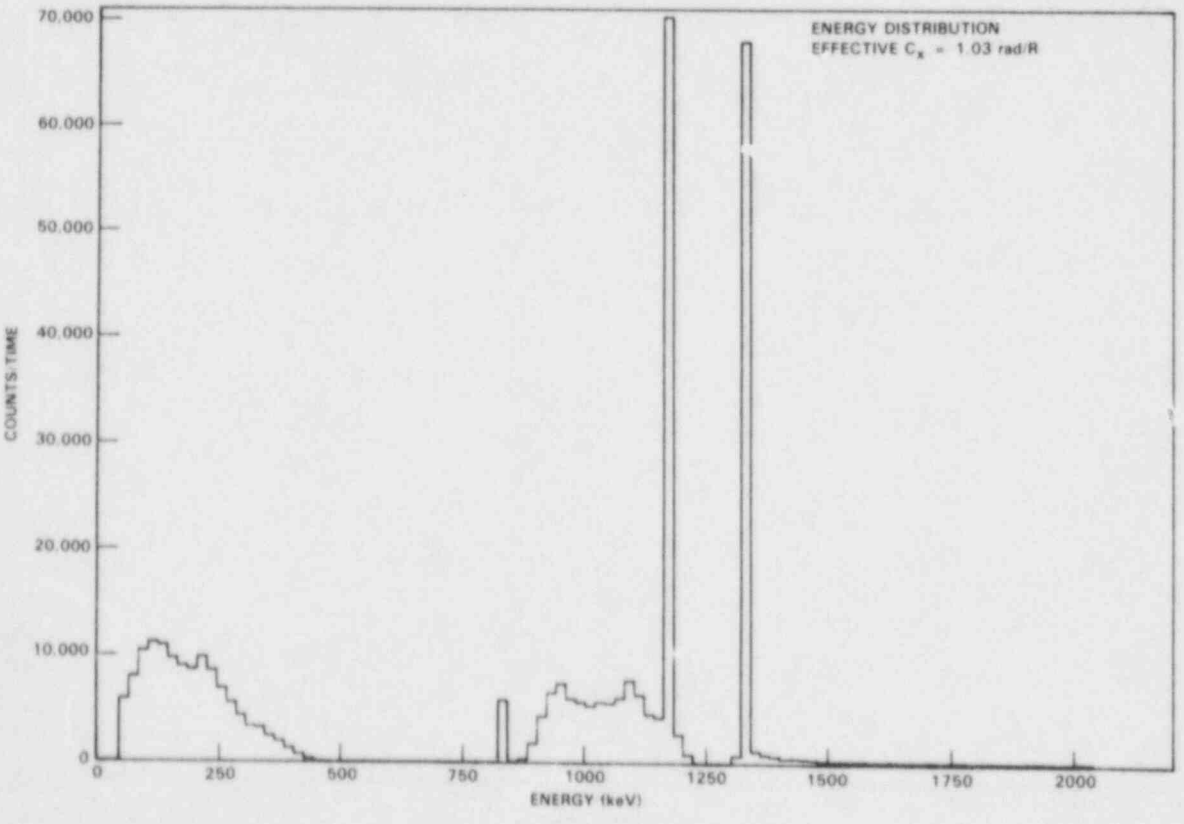

FIGURE A.3.14. Pulse-Height and Photon Energy Distributions, Operating BWR, Site M, Reactor Building, Fifth Floor, 0.6 m from Cavity

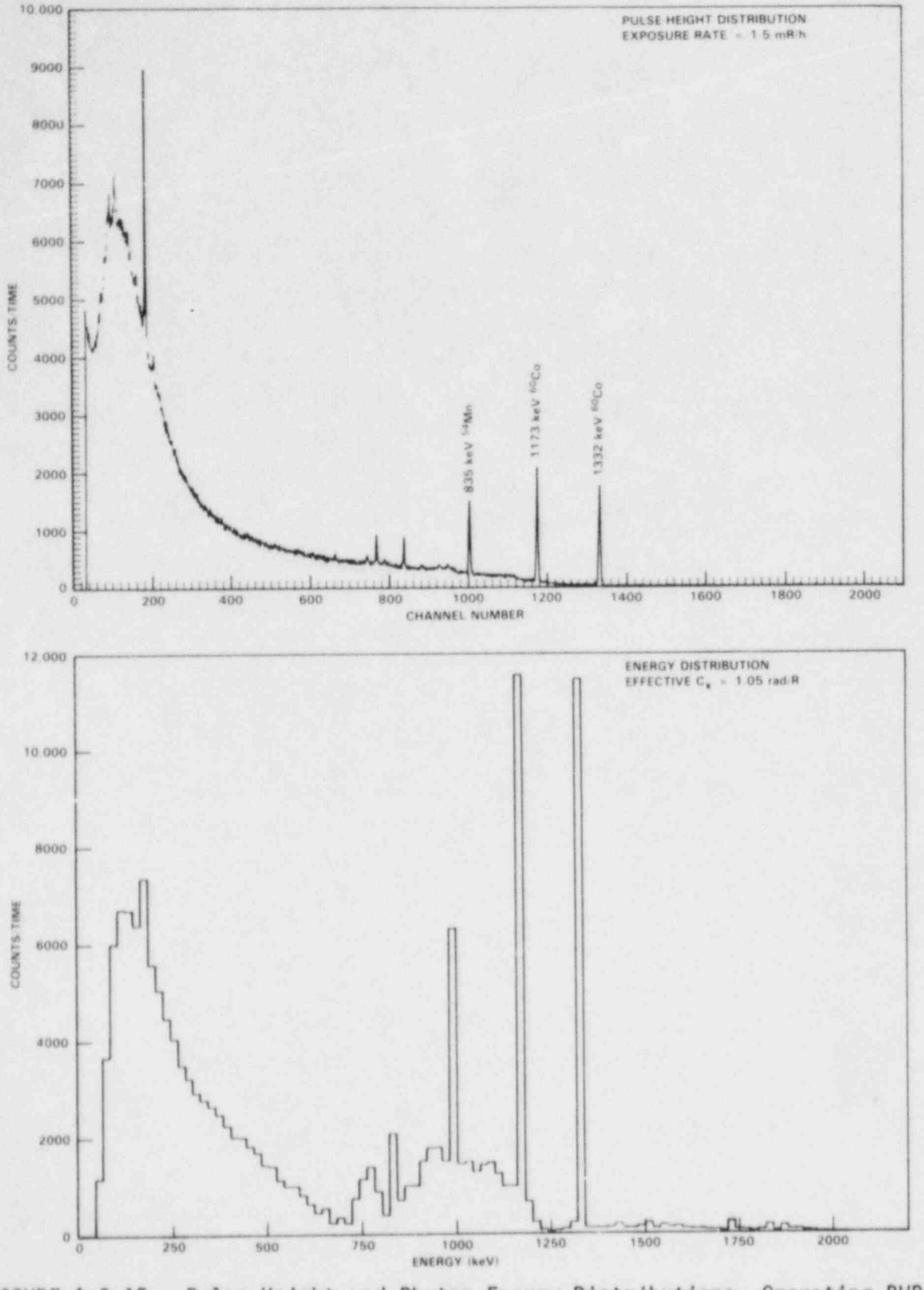

FIGURE A.3.15. Pulse-Height and Photon Energy Distributions, Operating BWR, Site M, Reactor Building, Fifth Floor, 1 m from New Fuel Storage

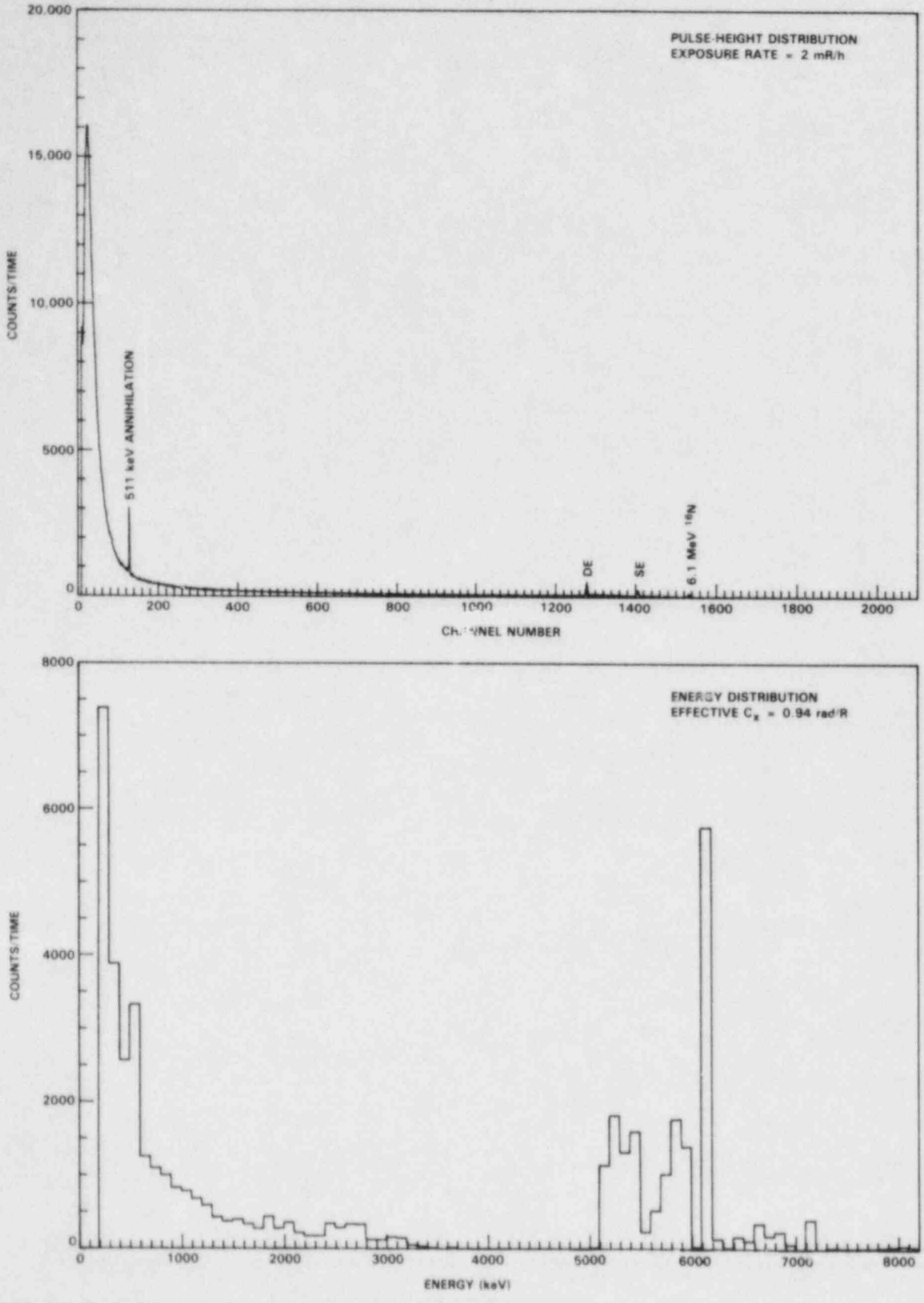

FIGURE A.3.16. Pulse-Height and Photon Energy Distributions, Operating BWR, Site M, Turbine Building, Behind Shield Wall

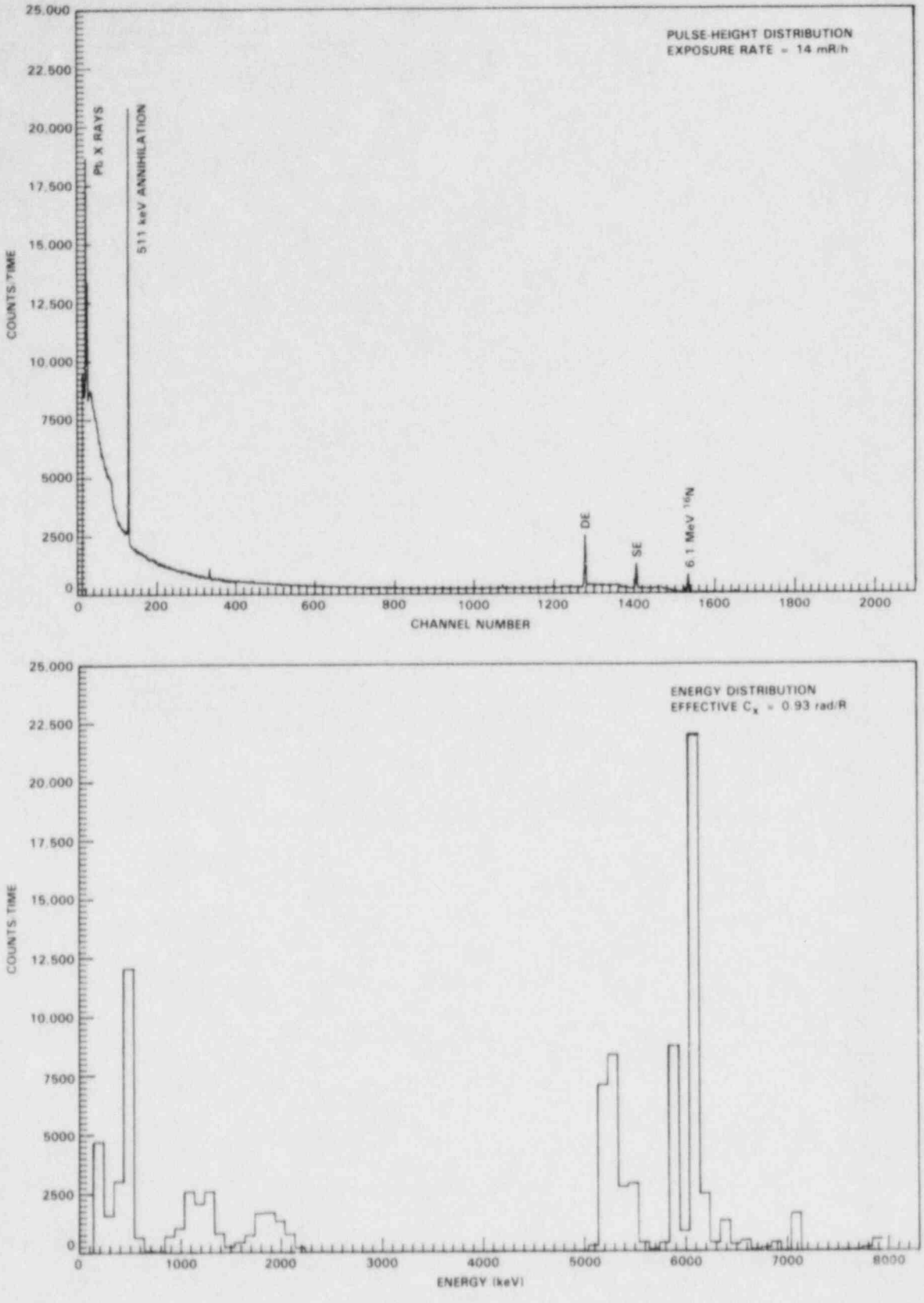

FIGURE A.3.17. Pulse-Height and Photon Energy Distributions, Operating BWR, Site M, Turbine Building, Near Turbine (collimated)

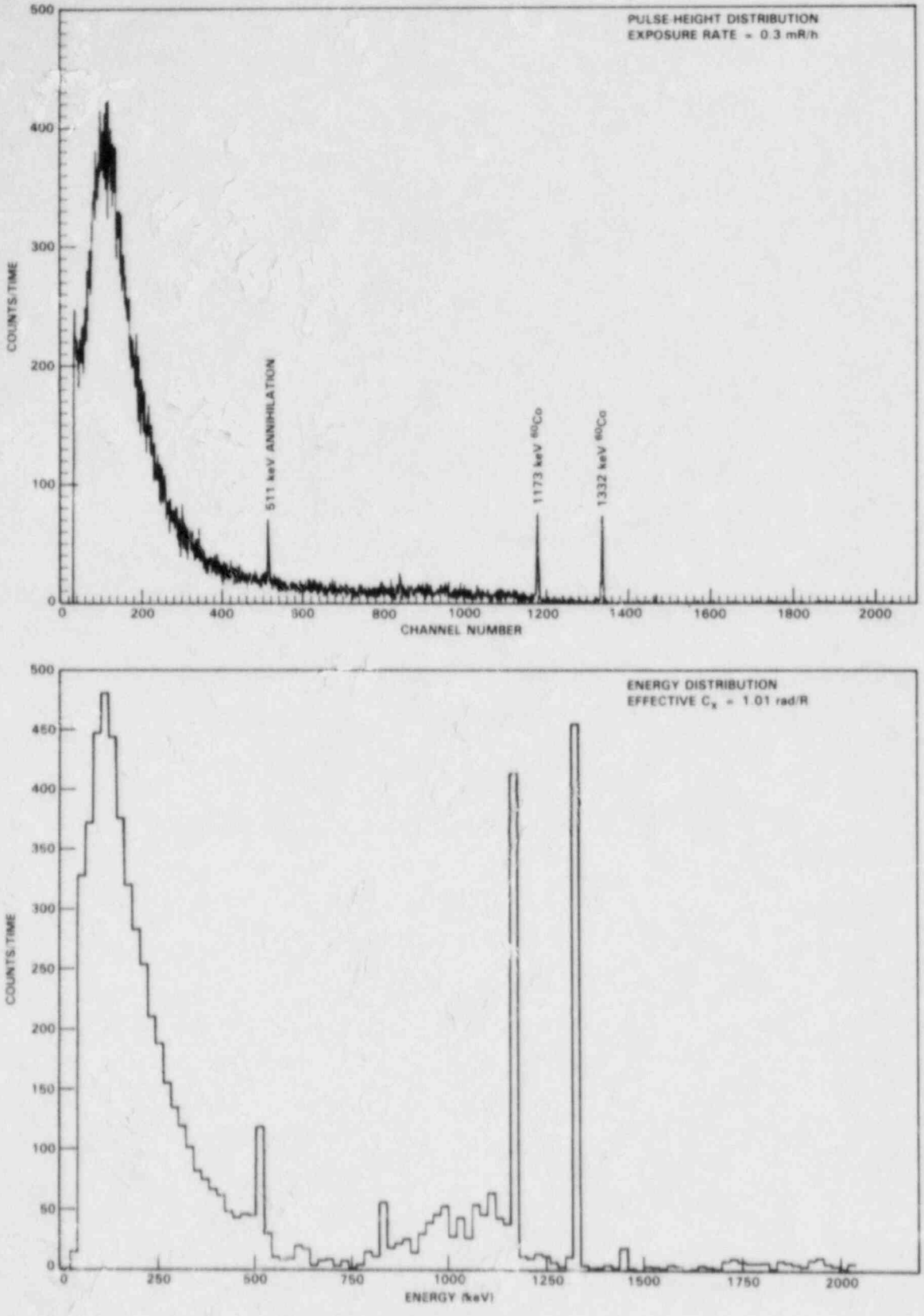

FIGURE A.3.18. Pulse-Height and Photon Energy Distributions, Operating BWR, Site M, Turbine Building, SE Corner of CO_2 Unit

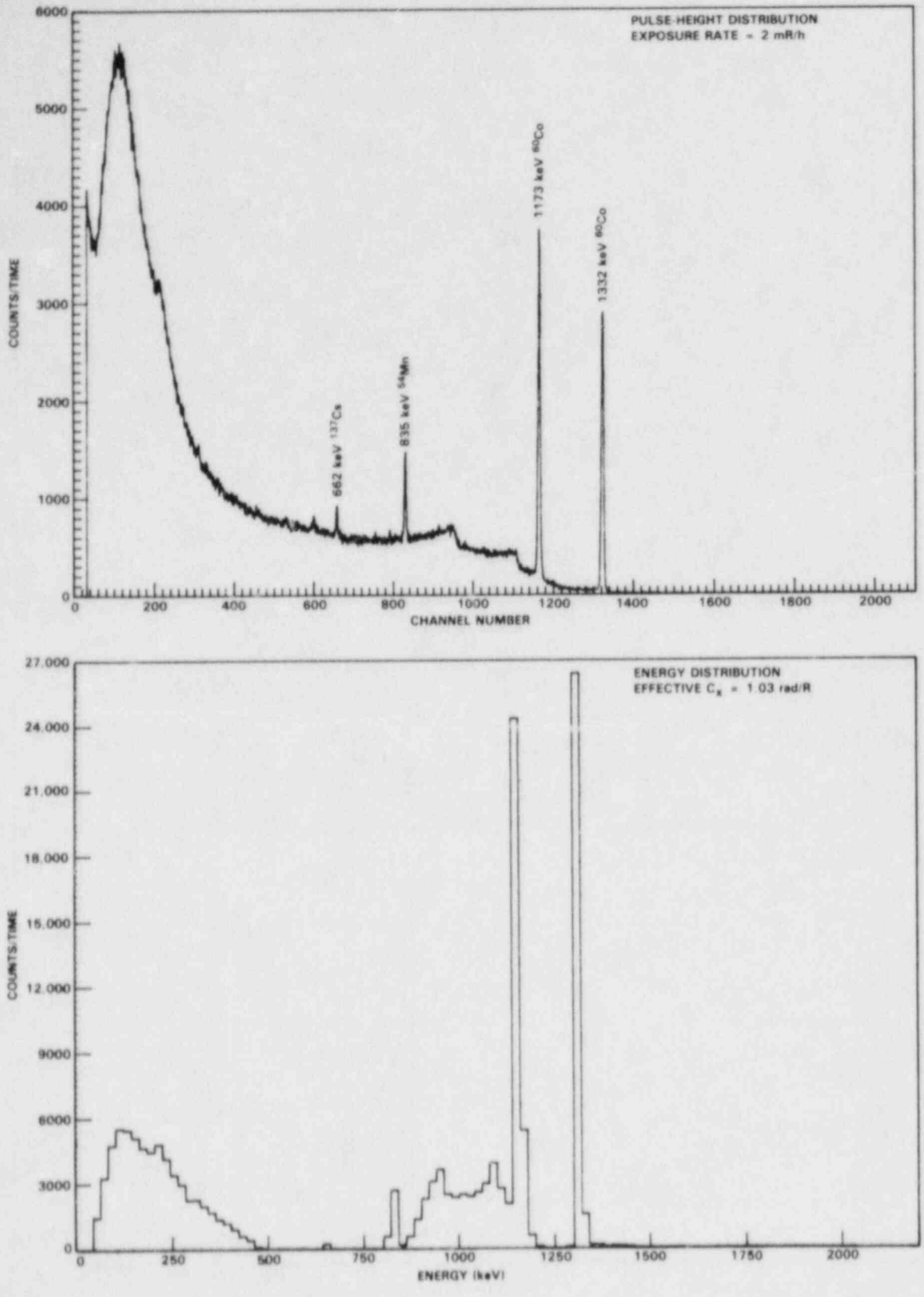

FIGURE A.3.19. Pulse-Height and Photon Energy Distributions, Operating BWR, Site M, Off-Gas Building, Near Charcoal Absorbers

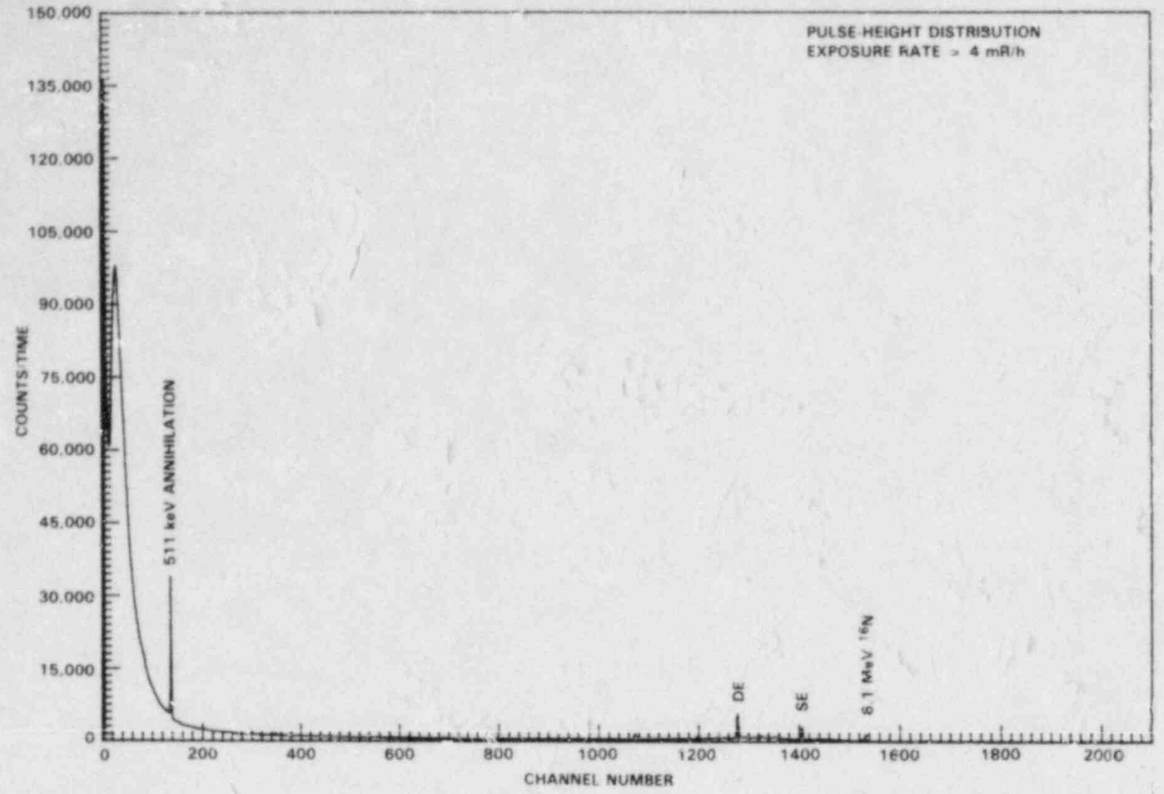

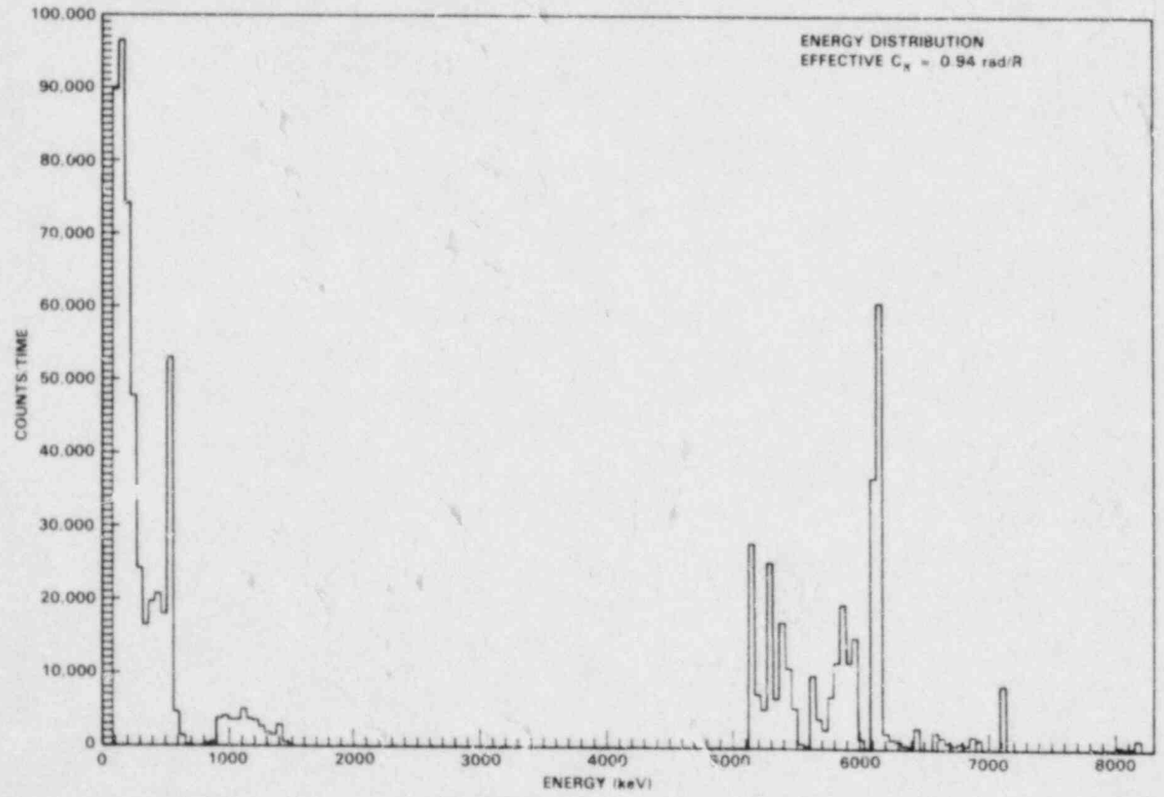

FIGURE A.4.1. Pulse-Height and Photon Energy Distributions, Operating BWR, Turbine Building, Site Q, Location A-Floor 272, Near Viewing Gallery

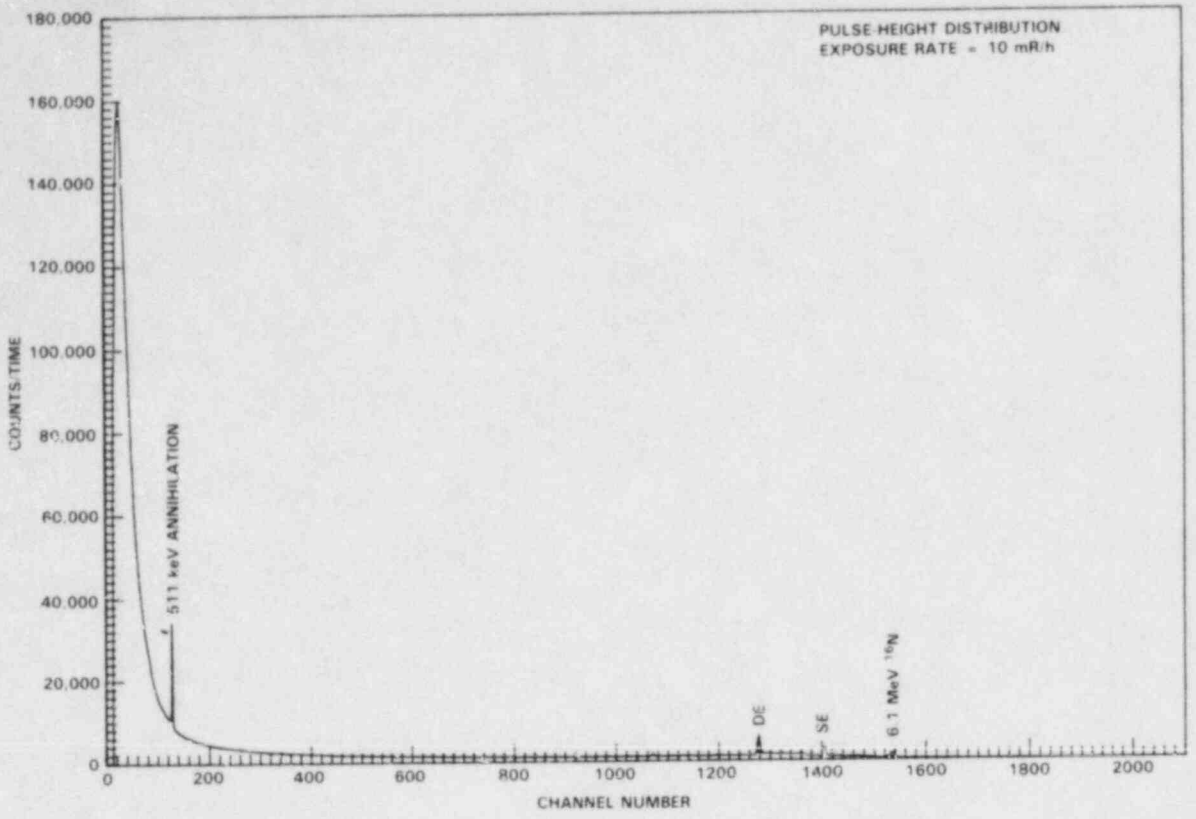

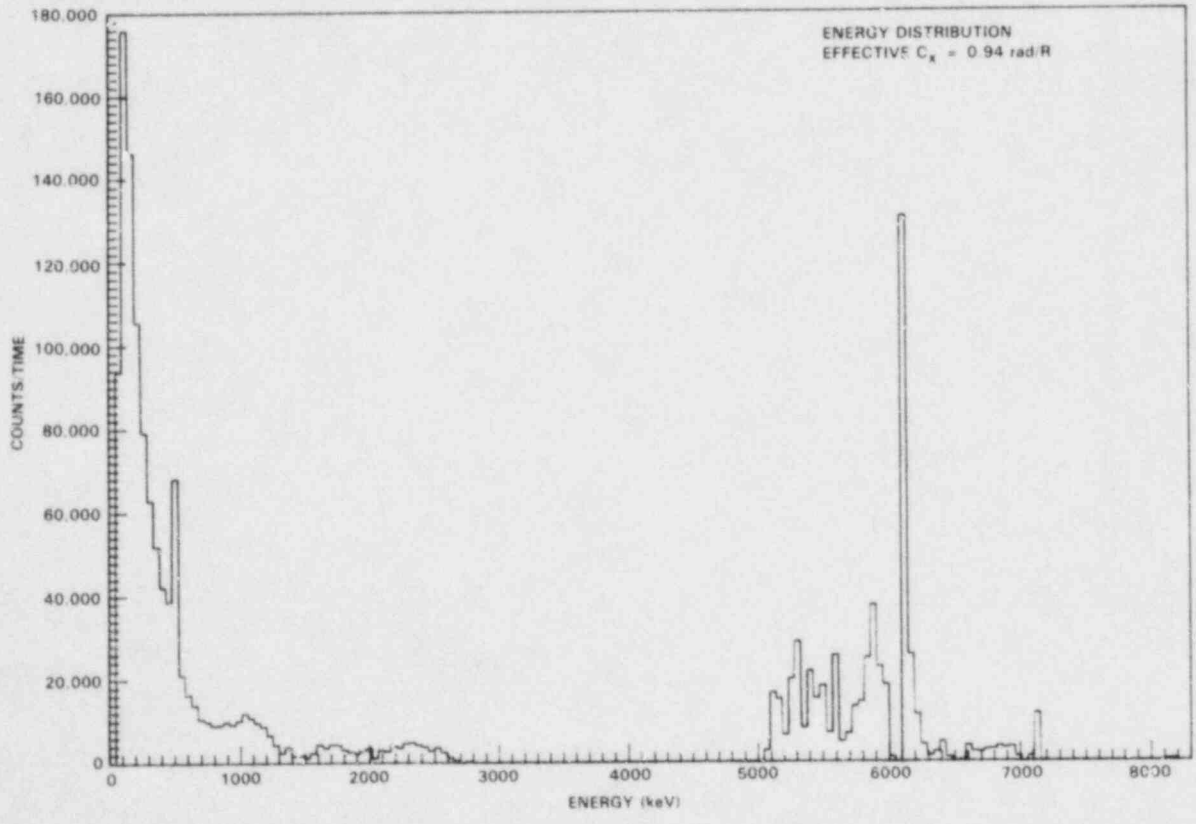

FIGURE A.4.2. Pulse-Height and Photon Energy Distributions, Operating BWR, Turbine Building, Site Q, Location B-Floor 272, Behind Stairwell

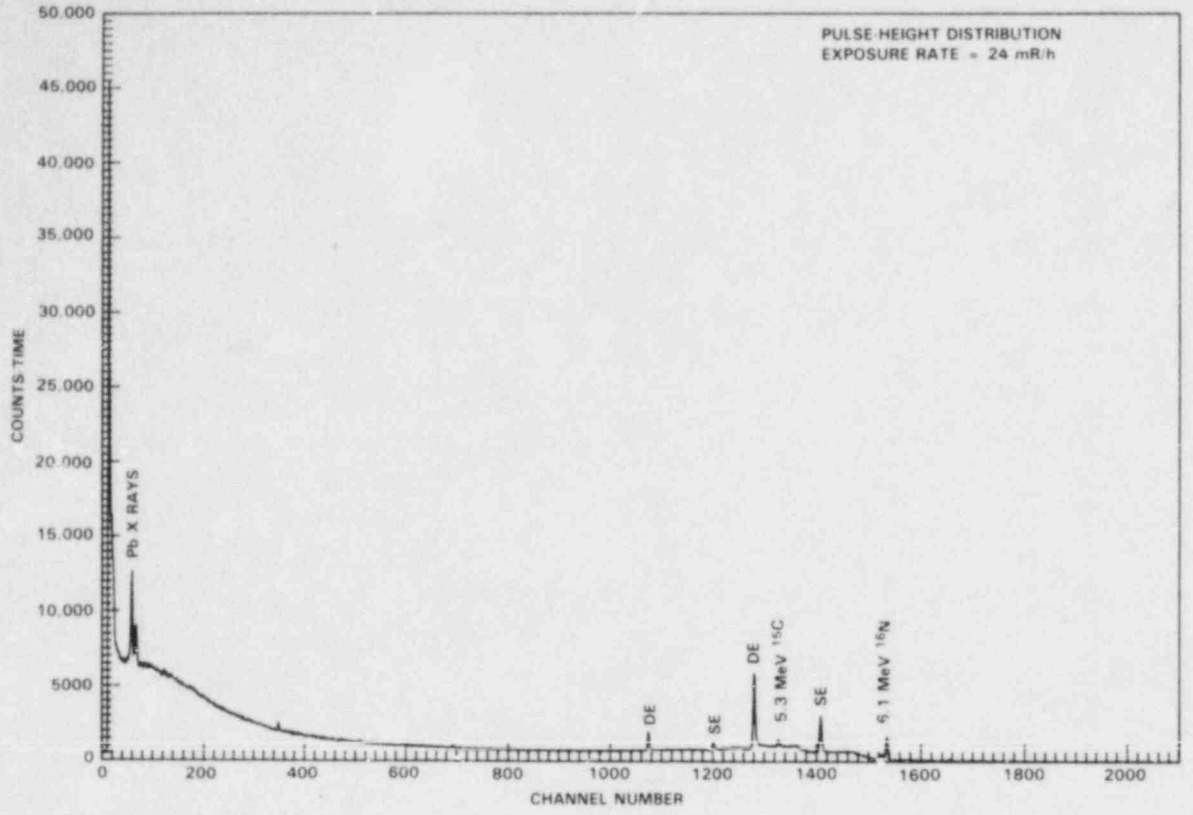

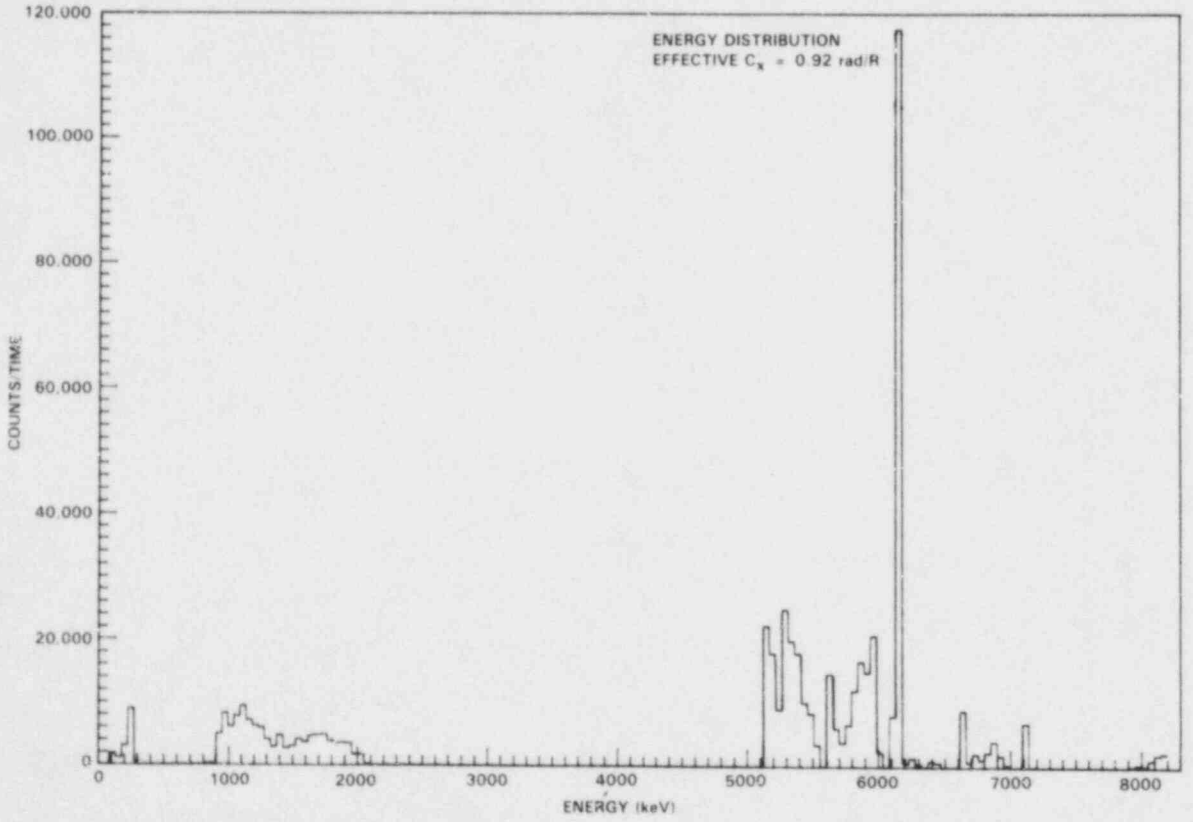

FIGURE A.4.3. Pulse-Height and Photon Energy Distributions, Operating BWR, Turbine Building, Site Q, Location C-Floor 272, NW Corner of Turbine (collimated)

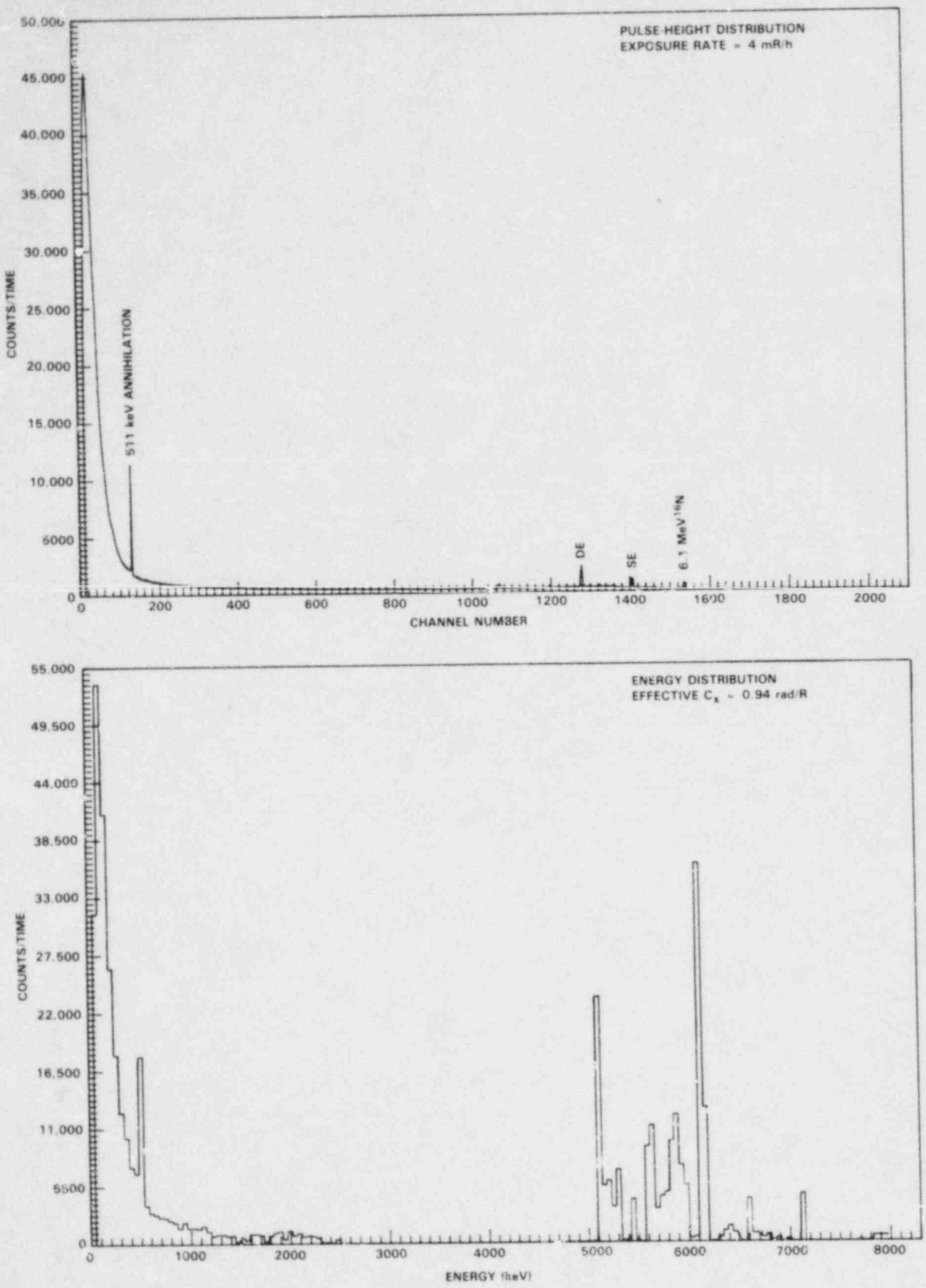

FIGURE A.4.4. Pulse-Height and Photon Energy Distributions, Operating BWR, Turbine Building, Site Q, Location D-Floor 272, SW Corner Behind Shield Wall

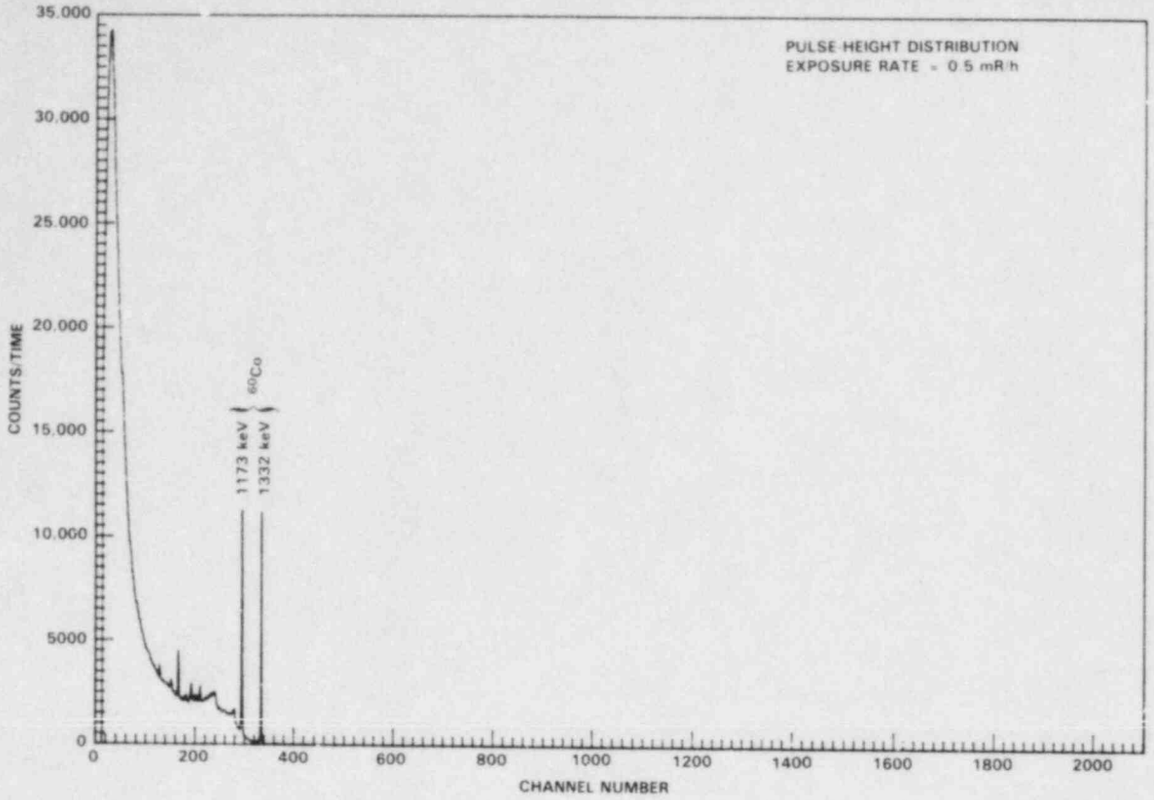

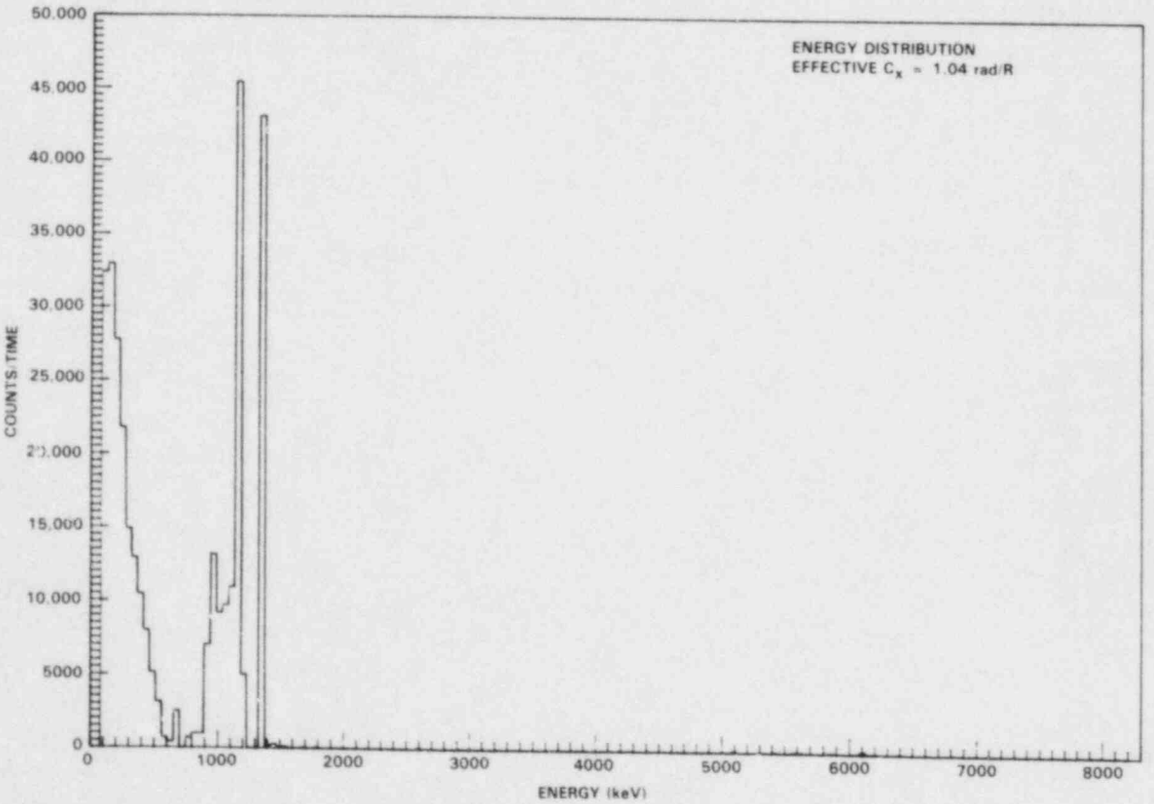

FIGURE A.4.5. Pulse-Height and Photon Energy Distributions, Operating BWR, Turbine Building, Site Q, Location F-Floor 248, Laundry/Turbine Loading Area

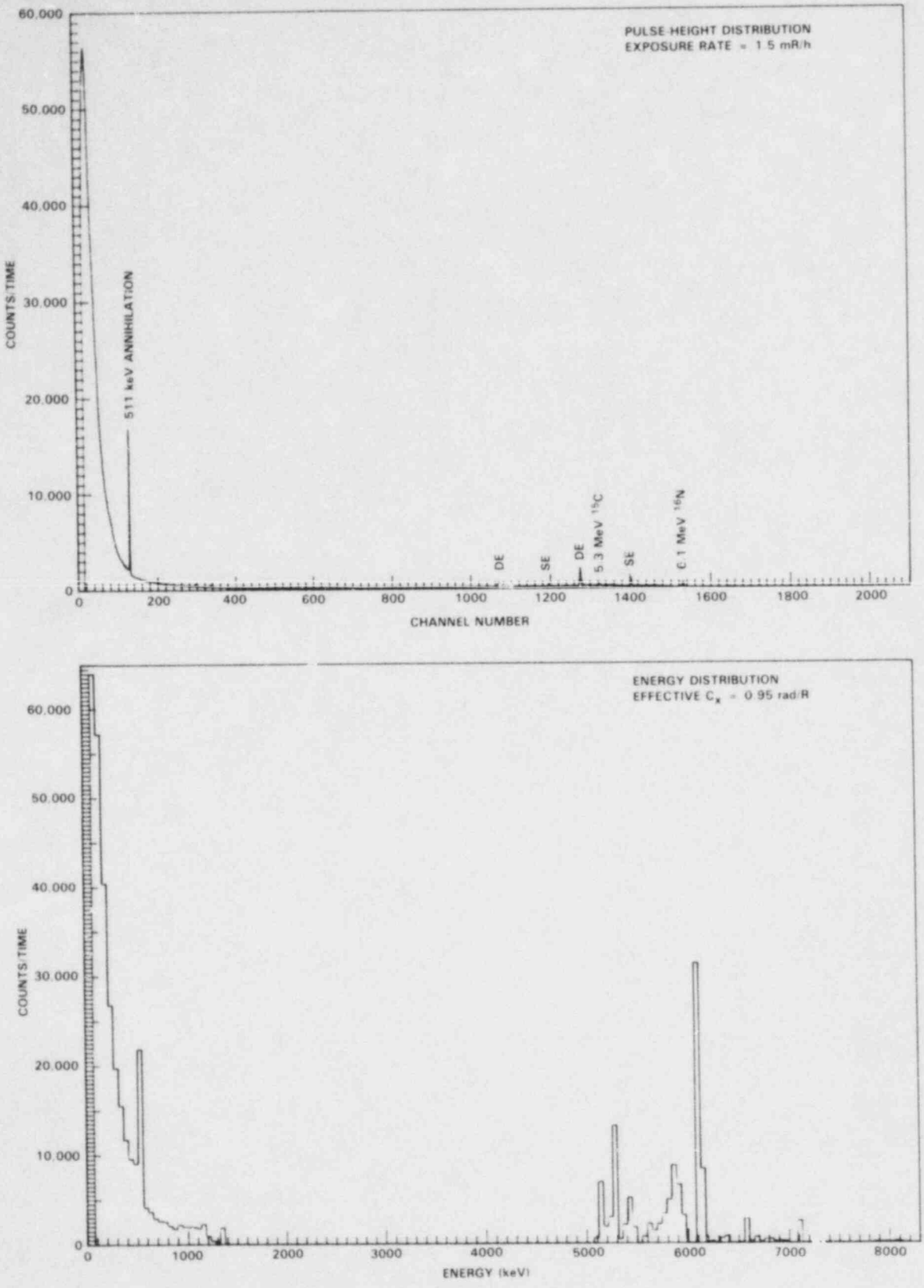

FIGURE A.4.6. Pulse-Height and Photon Energy Distributions, Operating BWR, Turbine Building, Site Q, Location G-Floor 248, Entrance #1 to Turbine Building

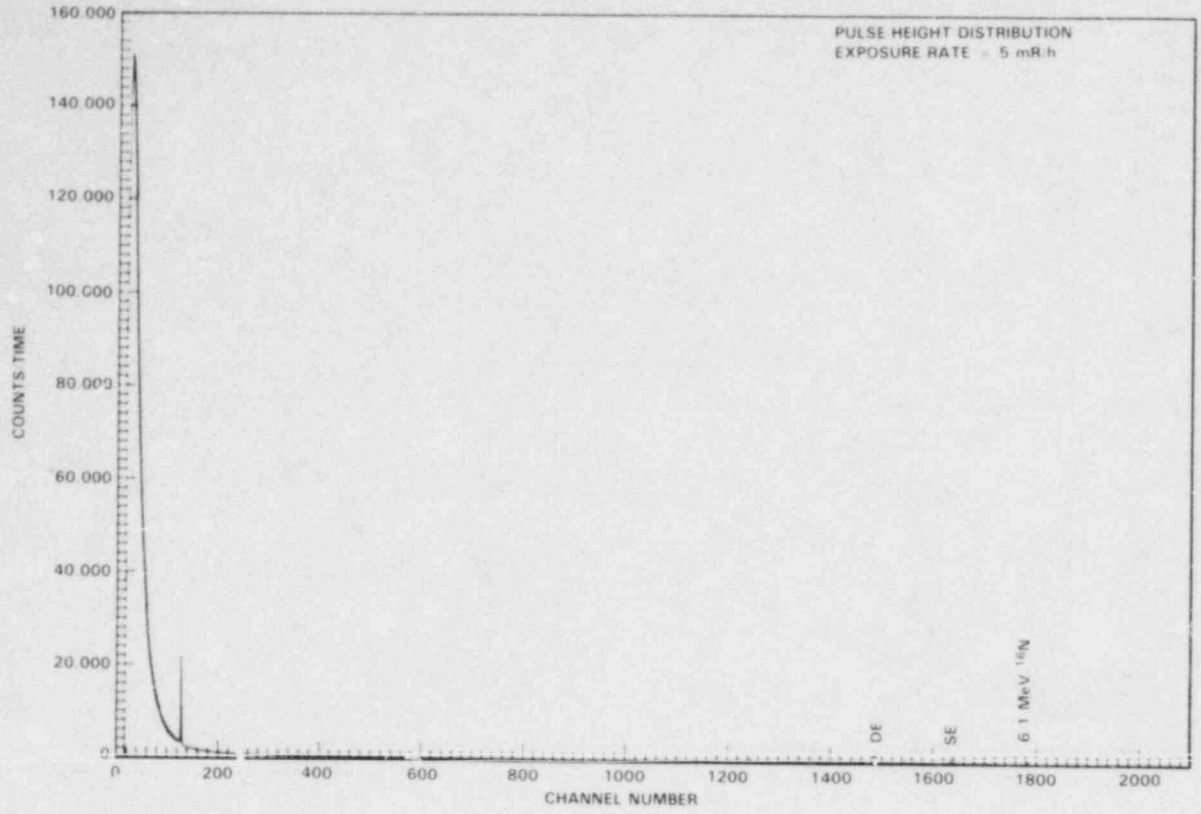

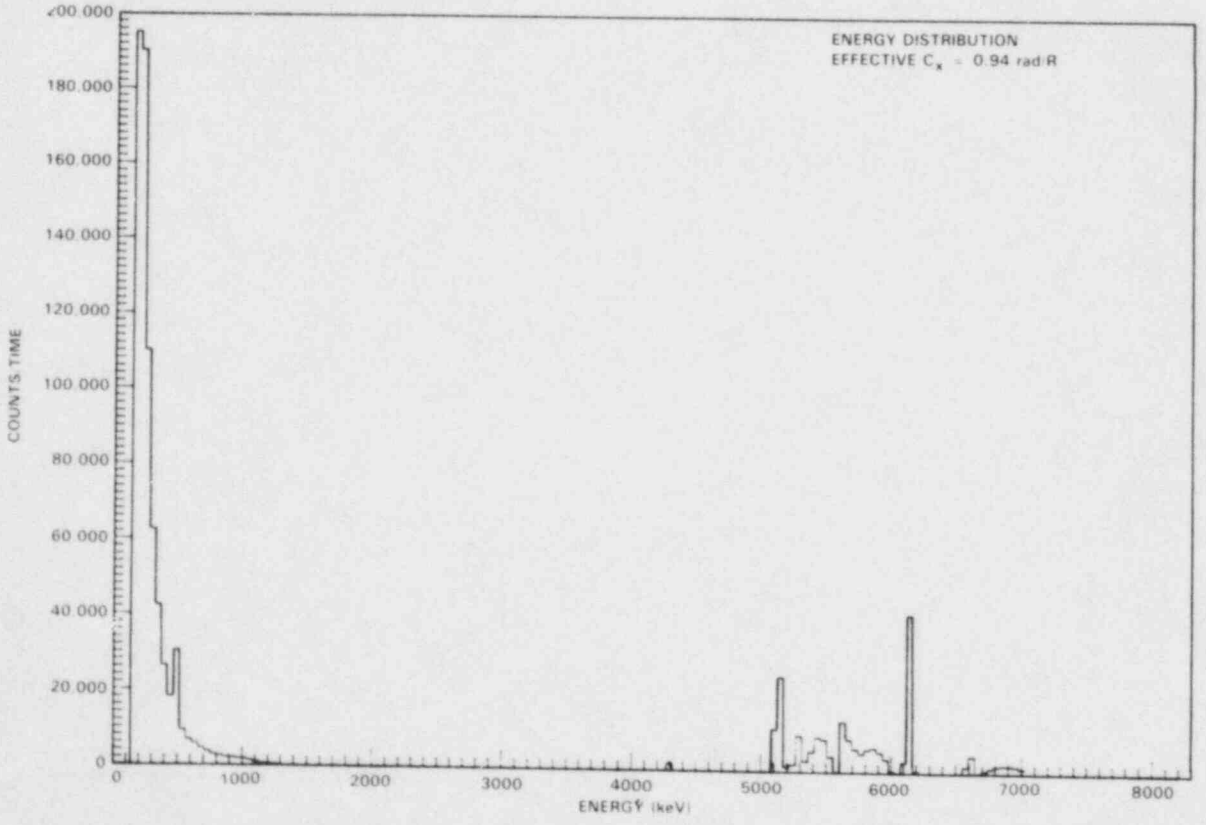

FIGURE A.4.7. Pulse-Height and Photon Energy Distributions, Operating BWR, Turbine Building, Site Q, Location H-Floor 248, Entrance #2 to Turbine Building

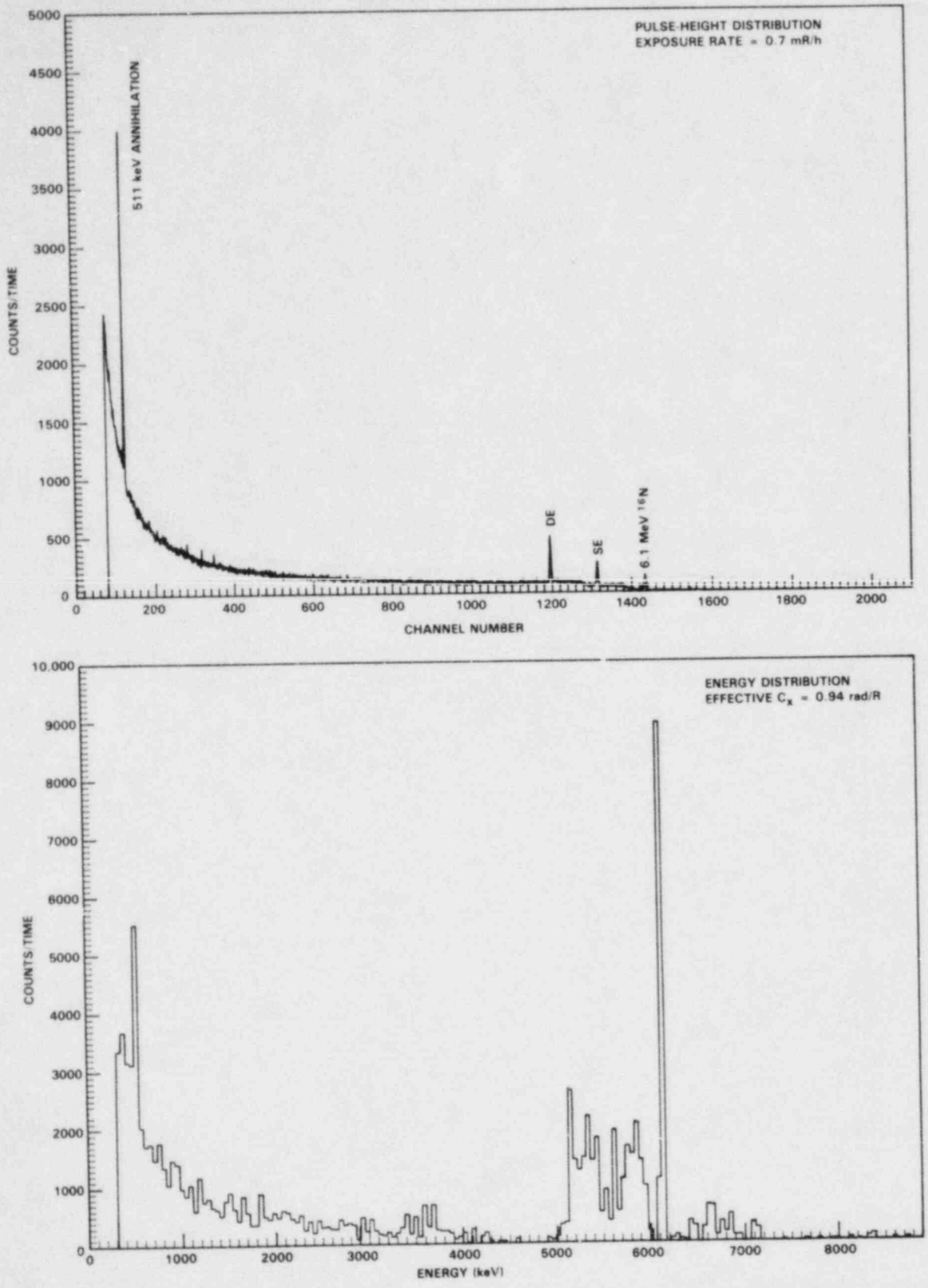

FIGURE A.4.8. Pulse-Height and Photon Energy Distributions, Operating BWR, Turbine Building, Site Q, Location I-Floor 248, General Area

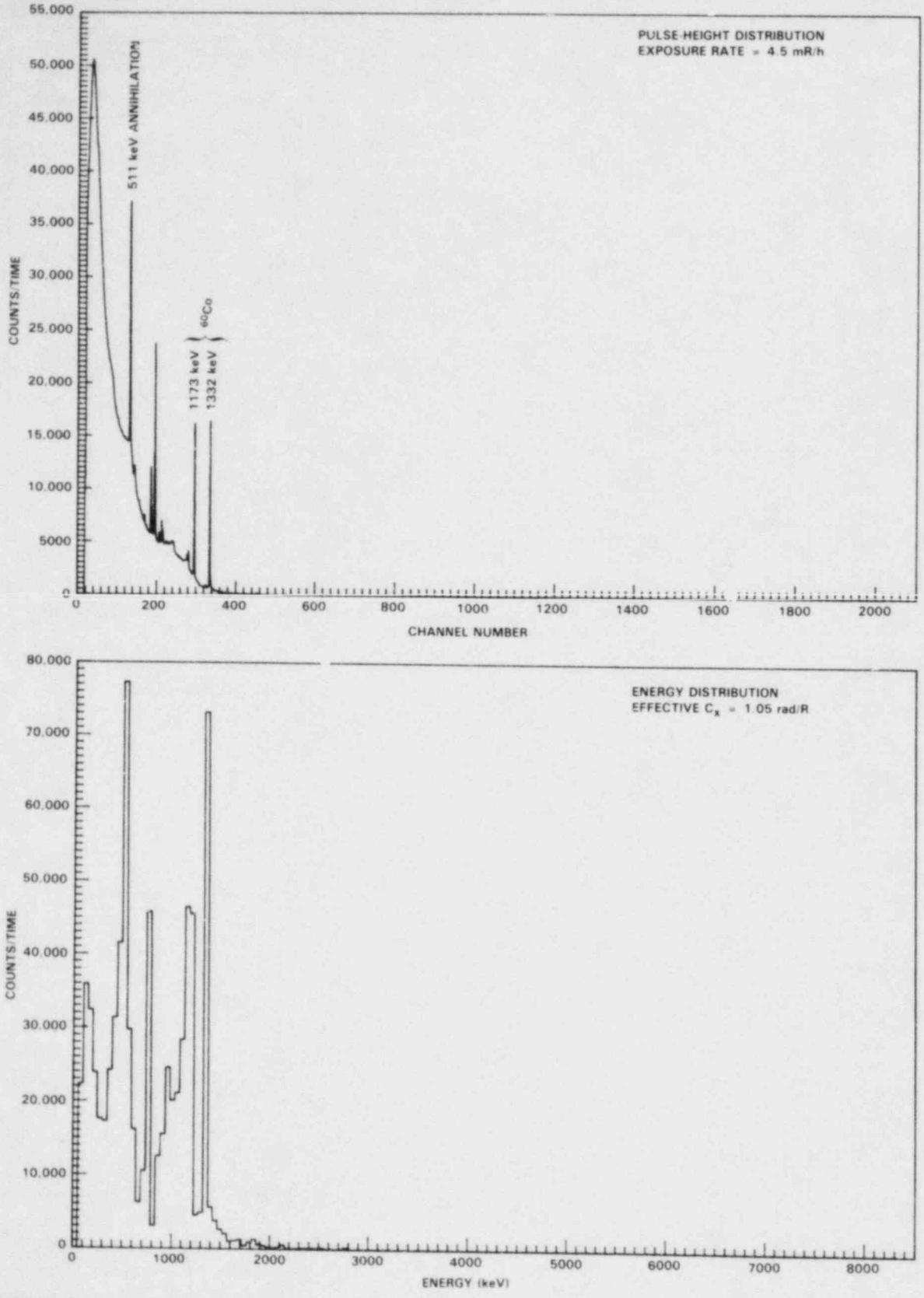

FIGURE A.4.9. Pulse-Height and Photon Energy Distributions, Operating BWR, Site Q, Location J-Reactor Vessel Sampling Station

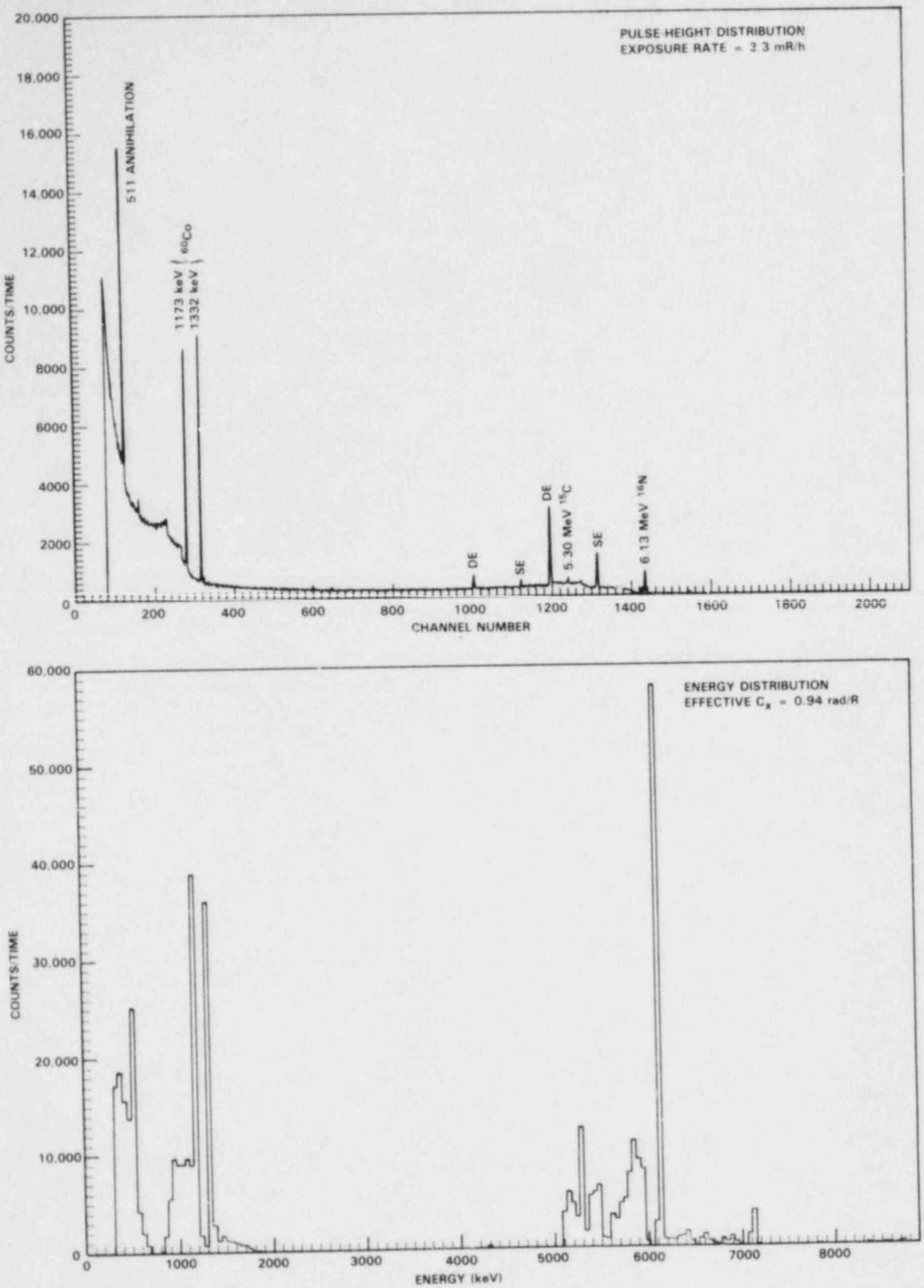

FIGURE A.4.10. Pulse-Height and Photon Energy Distributions, Operating BWR, Site Q, Location K-Spent Fuel Room

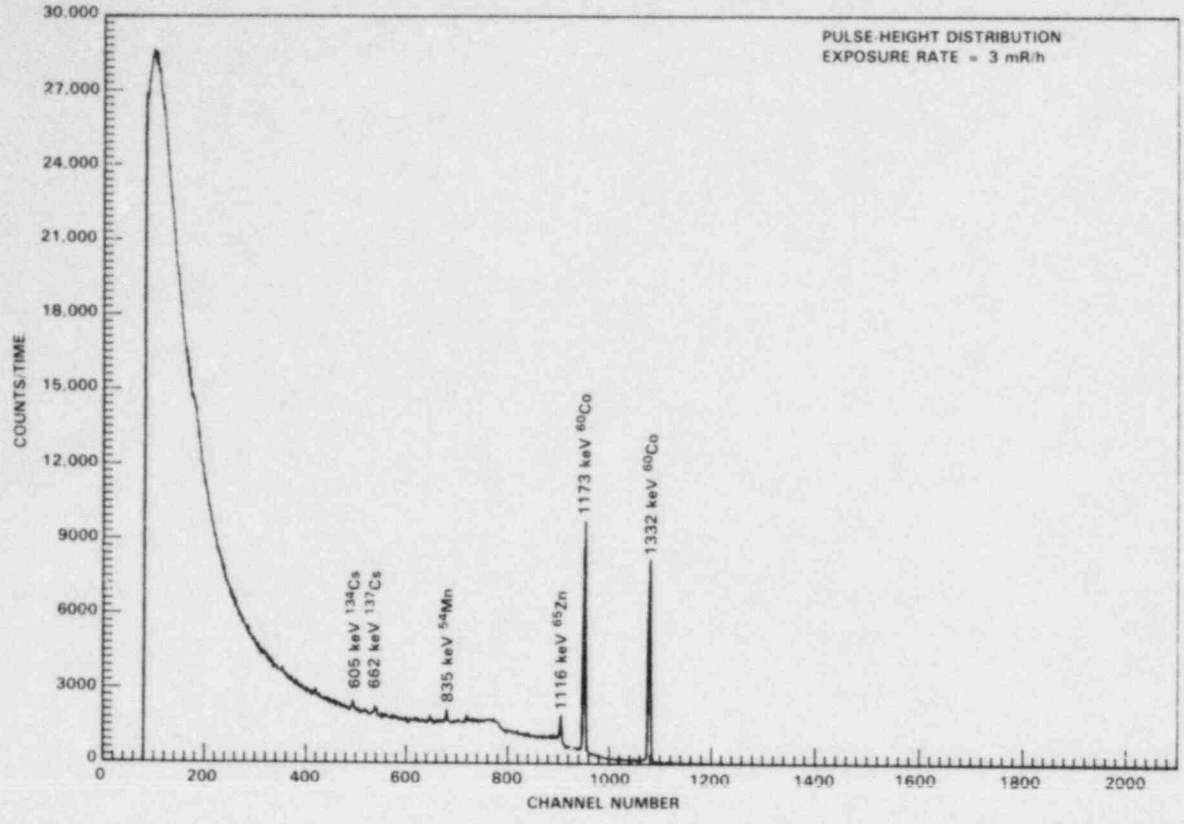

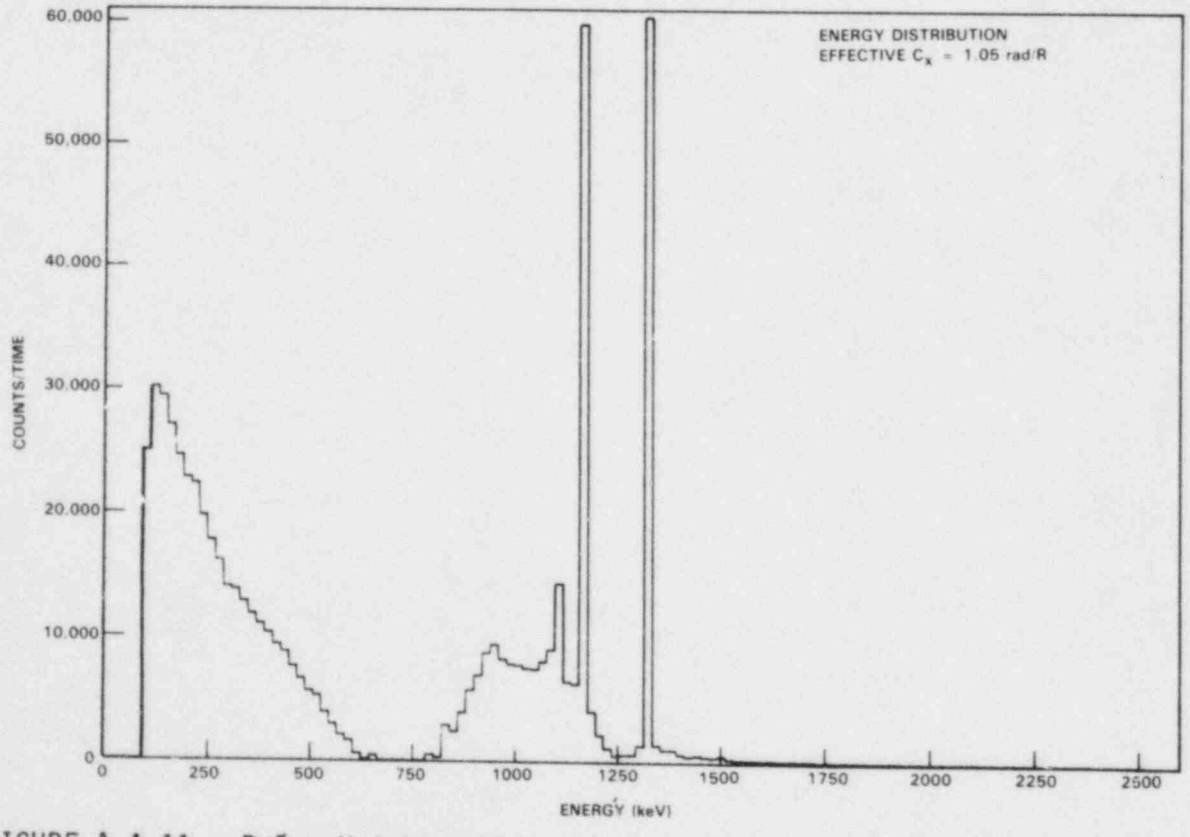

FIGURE A.4.11. Pulse-Height and Photon Energy Distributions, Operating BWR, Site Q, Location L-Waste Storage Area

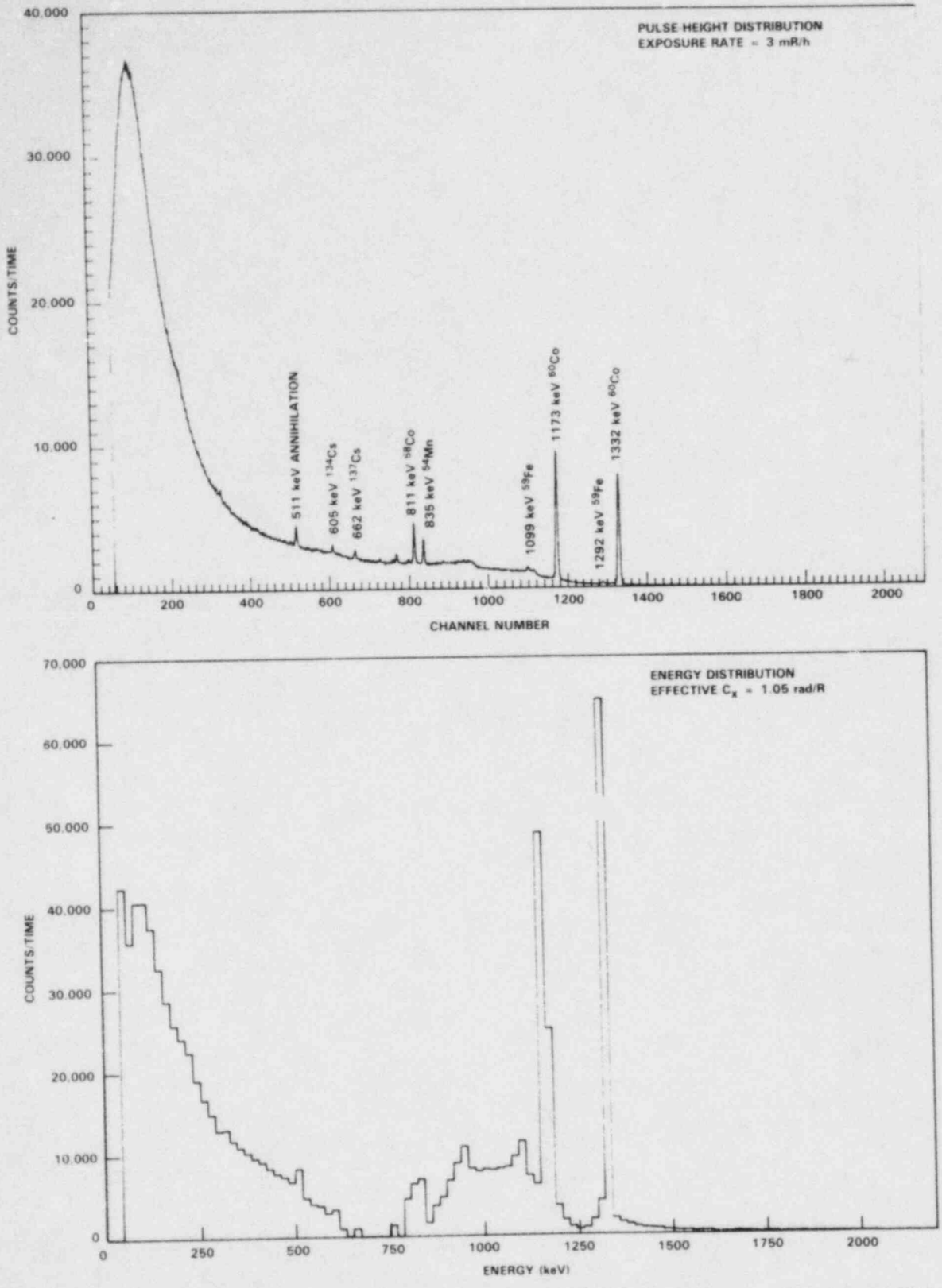

FIGURE A.5.1. Pulse-Height and Photon Energy Distributions, Shutdown PWR, Waste Storage Area, Site P, Location A-Barrel Storage (Outside Waste Disposal Building)

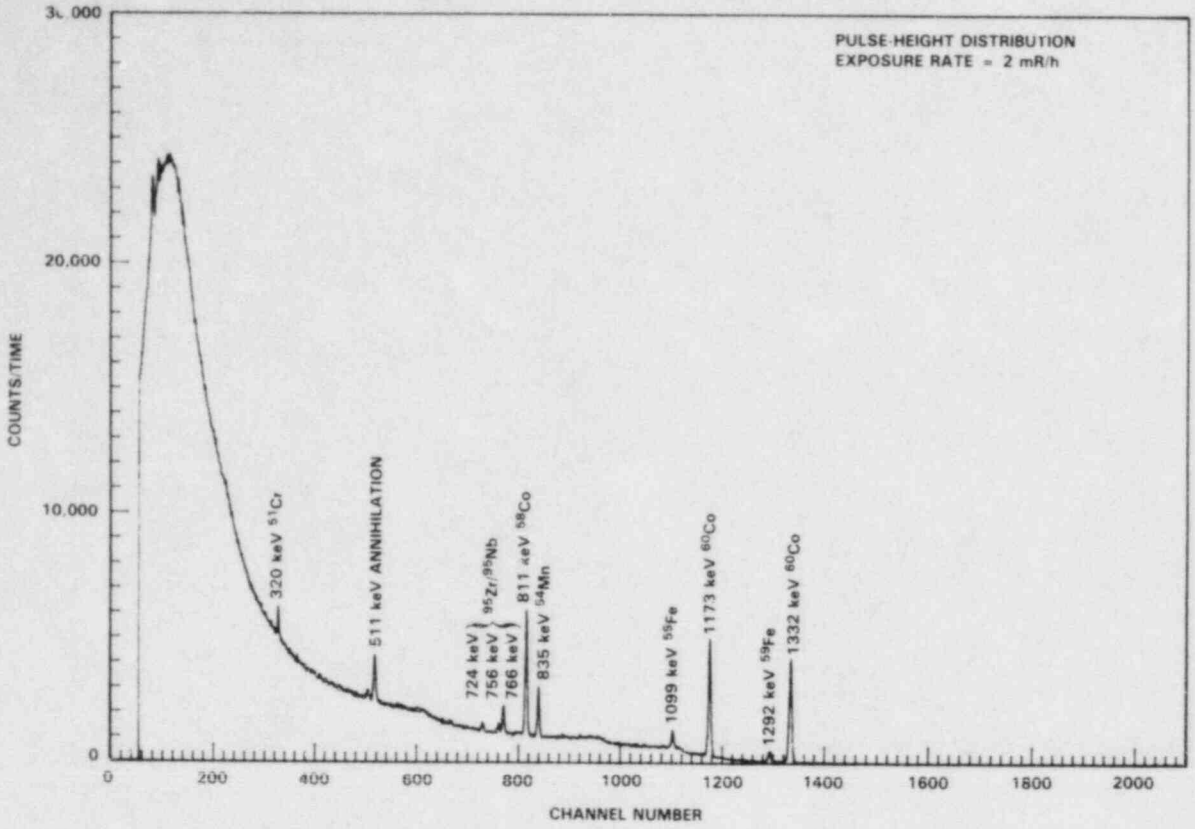

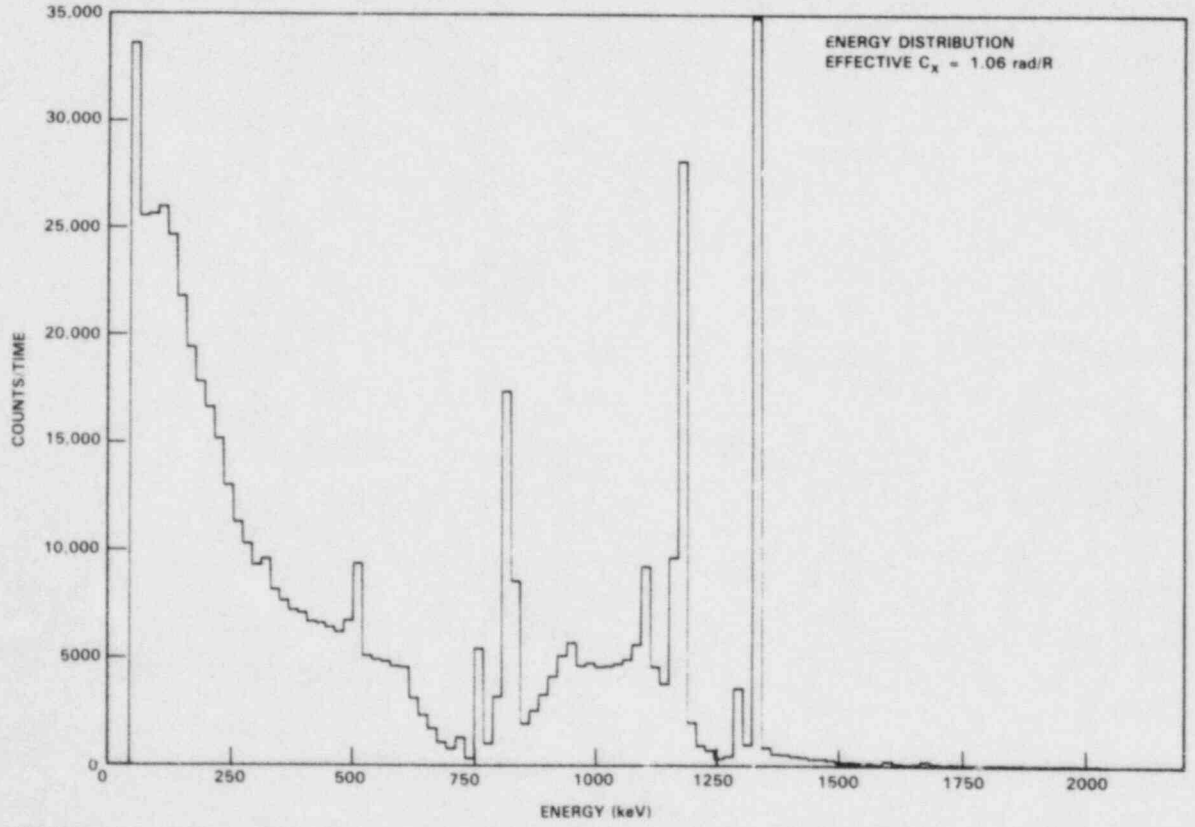

FIGURE A.5.2. Pulse-Height and Photon Energy Distributions, Shutdown PWR, Waste Storage Area, Site P, Location B-Compactor Area (Outside Waste Disposal Building)

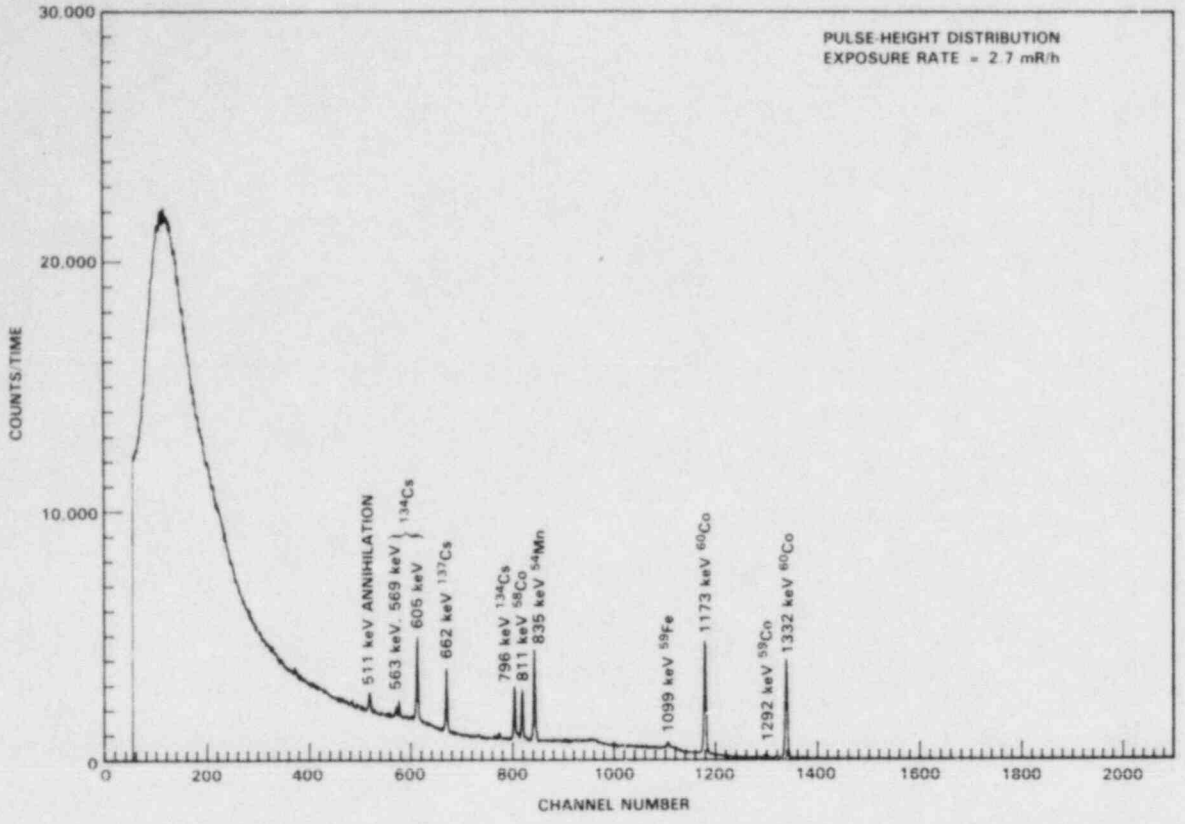

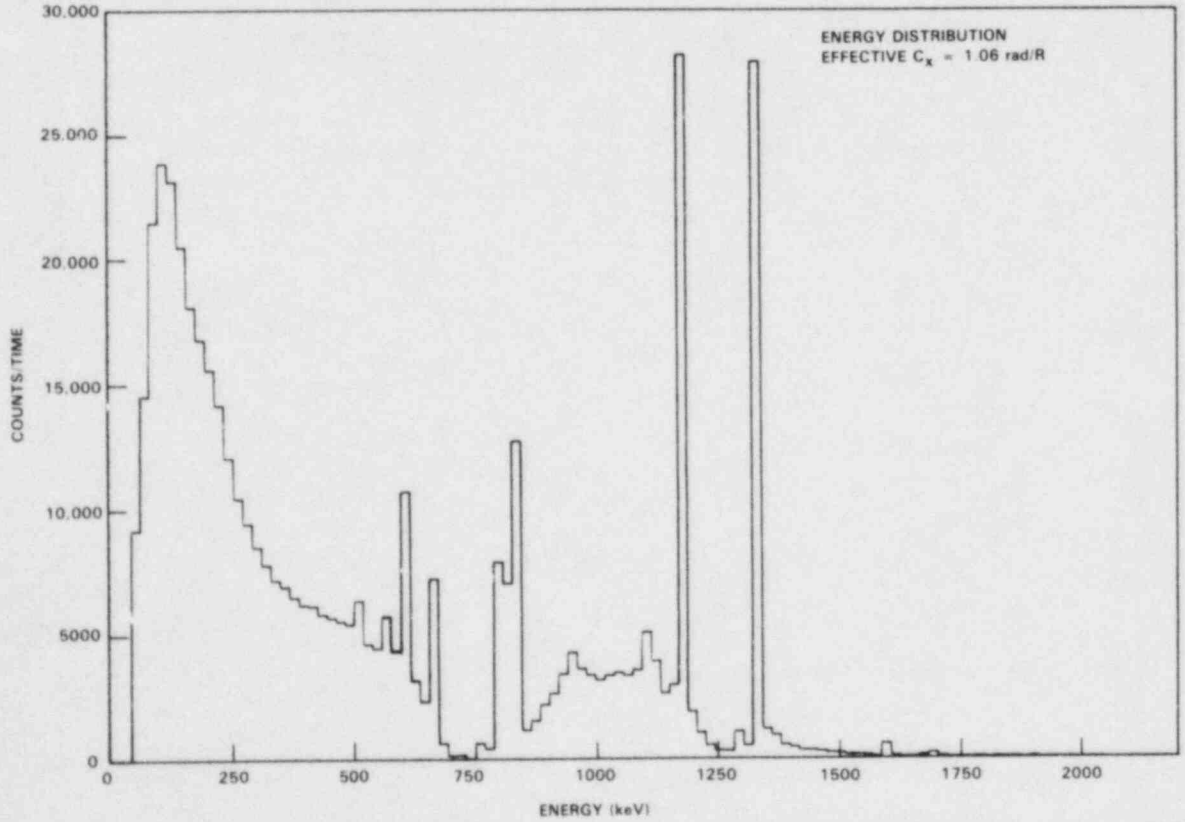

FIGURE A.5.3. Pulse-Height and Photon Energy Distributions, Shutdown PWR, Waste Storage Area, Site P, Location C-Waste Disposal Building

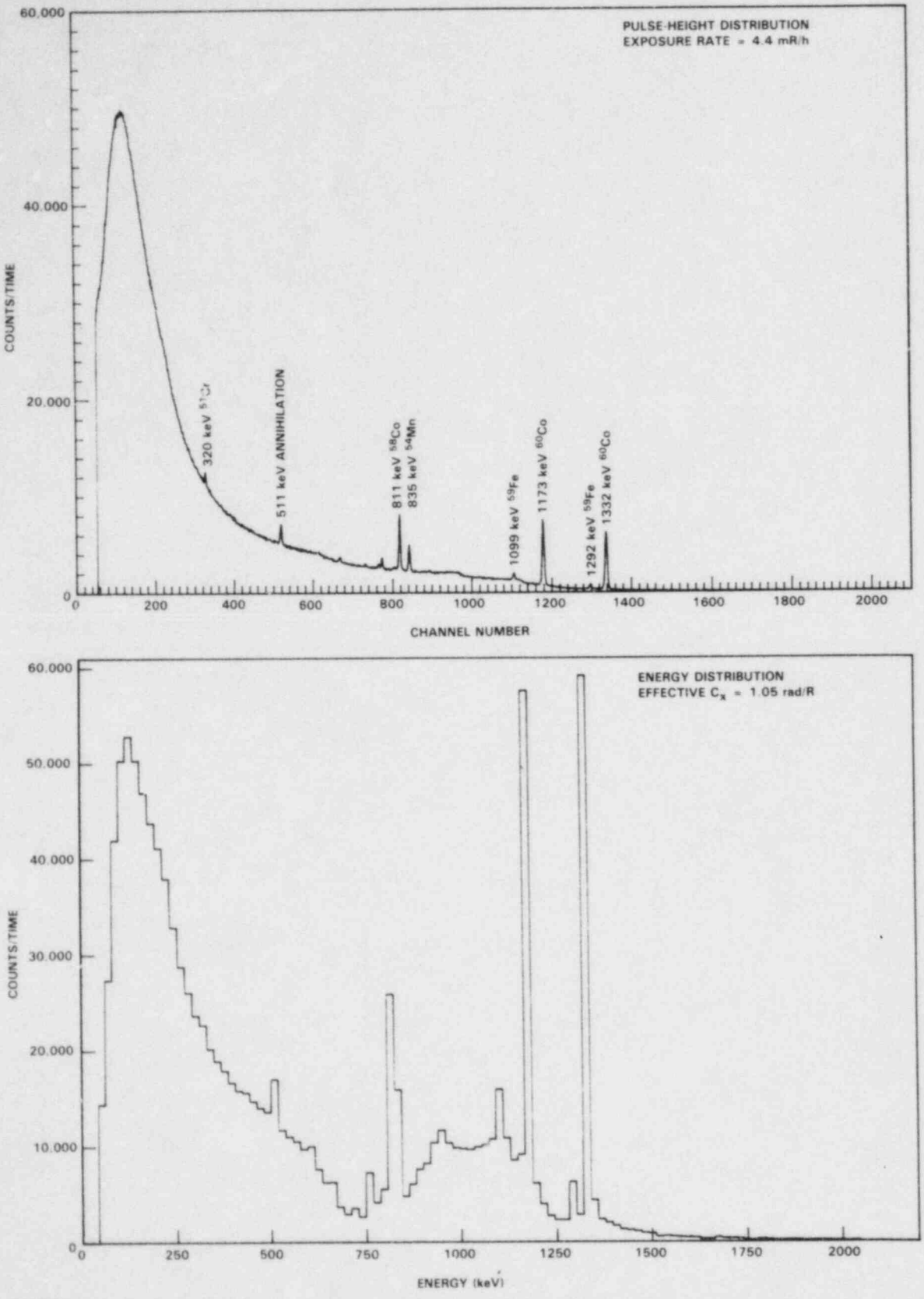

FIGURE A.5.4. Pulse-Height and Photon Energy Distributions, Shutdown PWR, Spent Fuel Pit, Site P, Location D-Heat Exchange

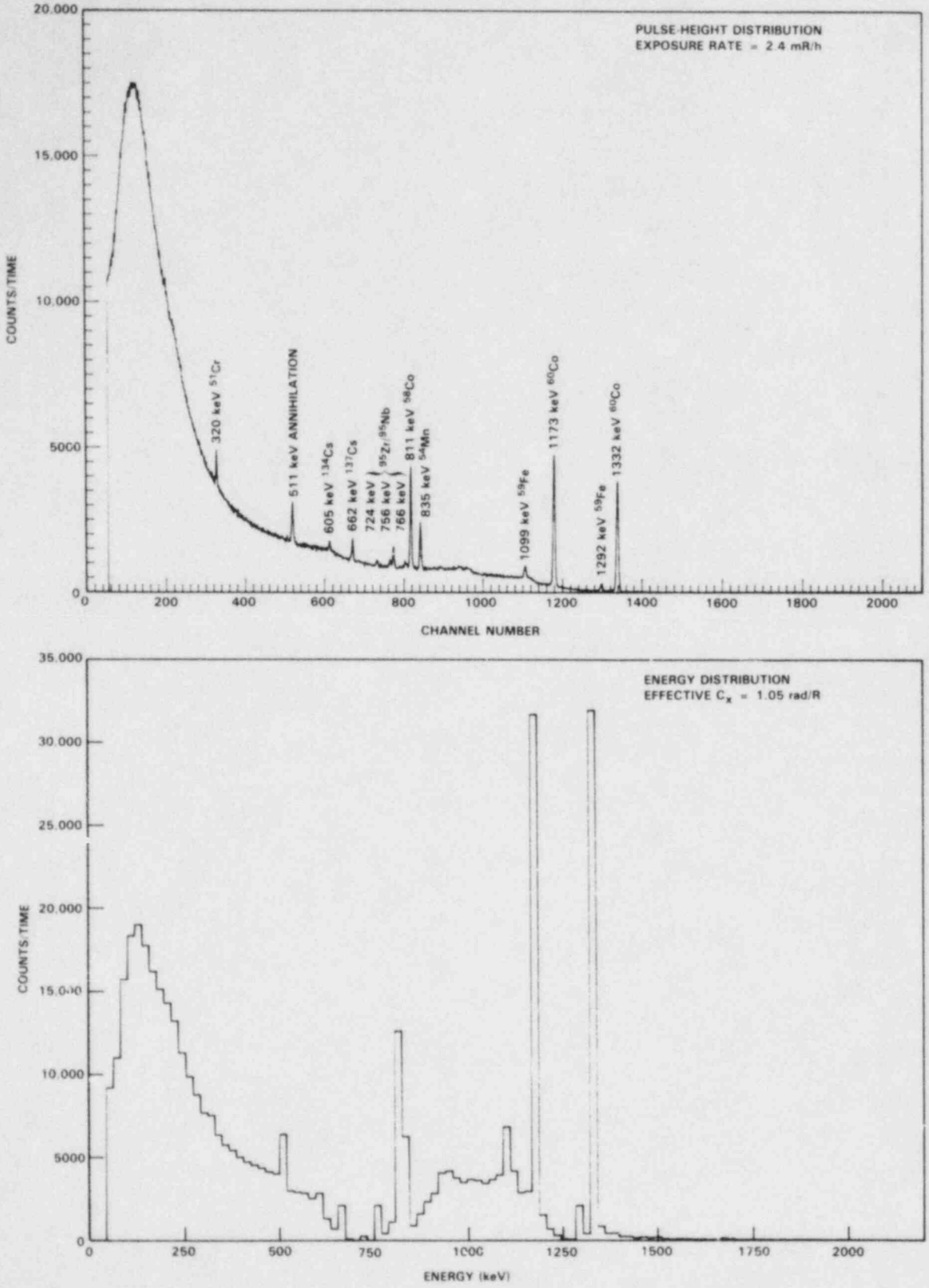

FIGURE A.5.5. Pulse-Height and Photon Energy Distributions, Shutdown PWR, Spent Fuel Pit, Site P, Location E-Ion Exchange Pit

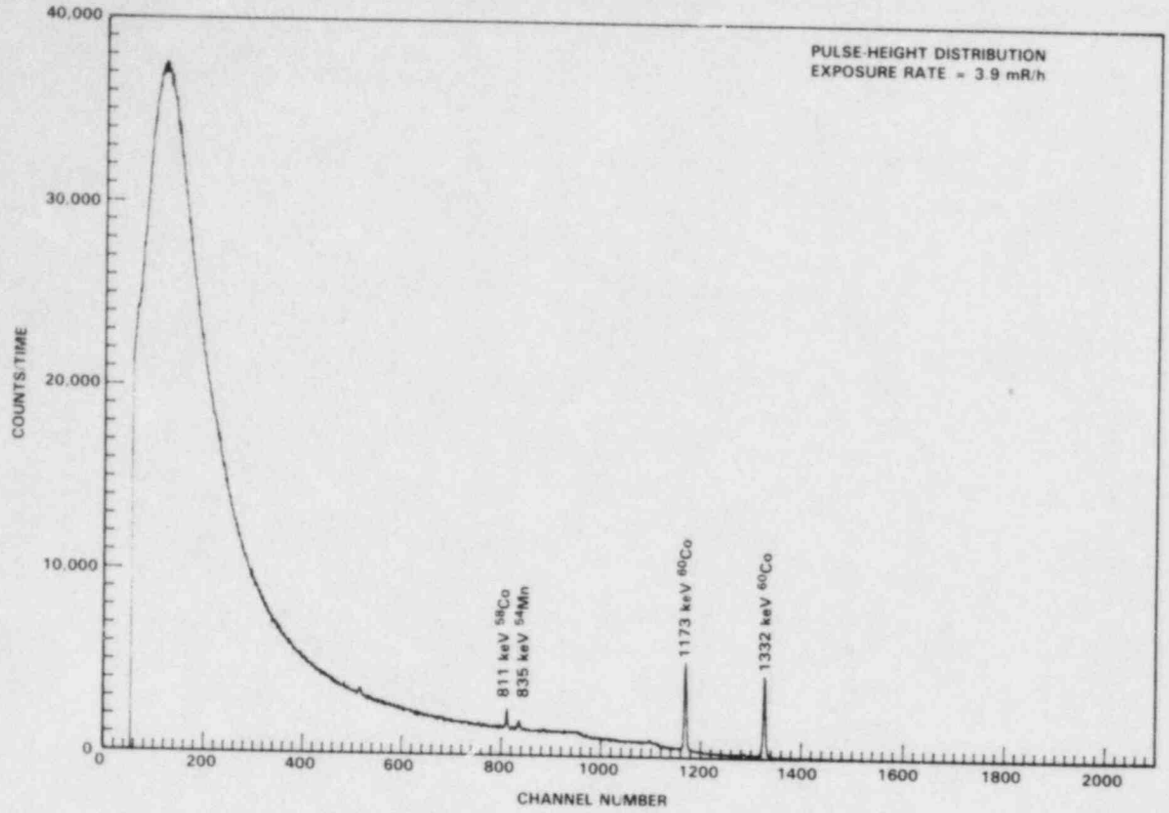

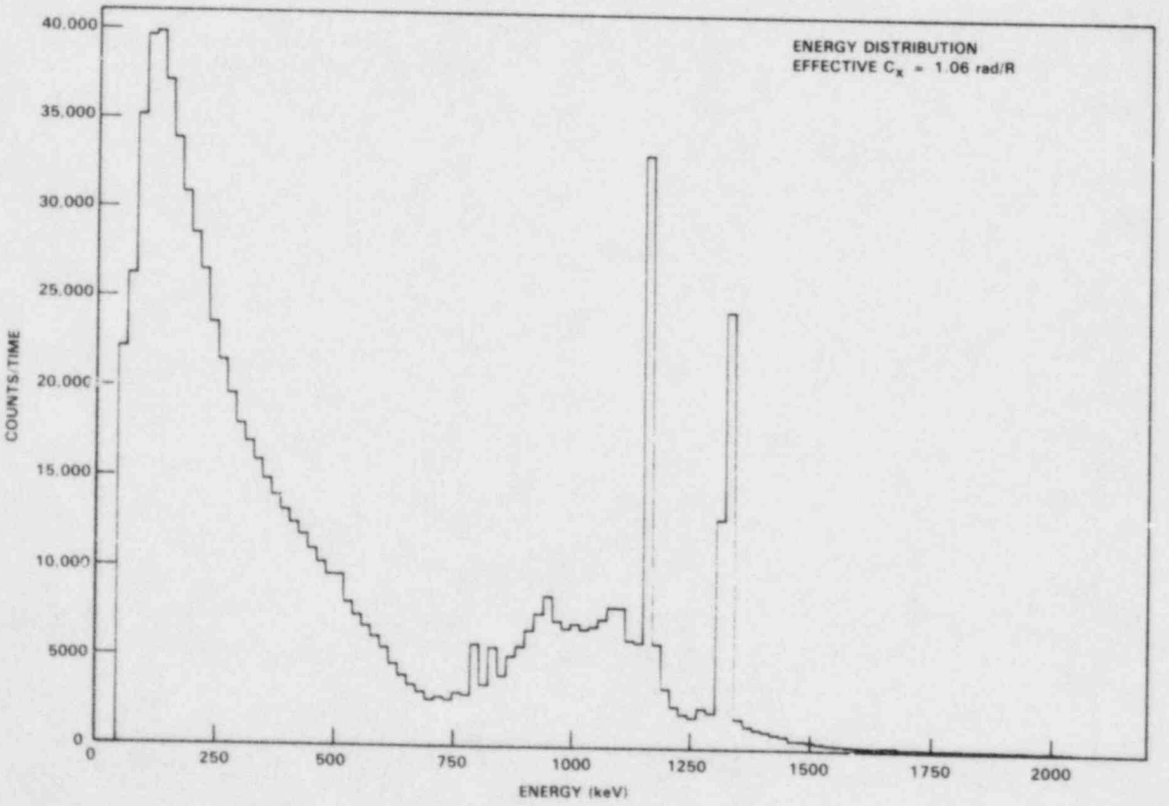

FIGURE A.5.6. Pulse-Height and Photon Energy Distributions, Shutdown PWR, Spent Fuel Pit, Site P, Location F-Fuel Transfer Shoot

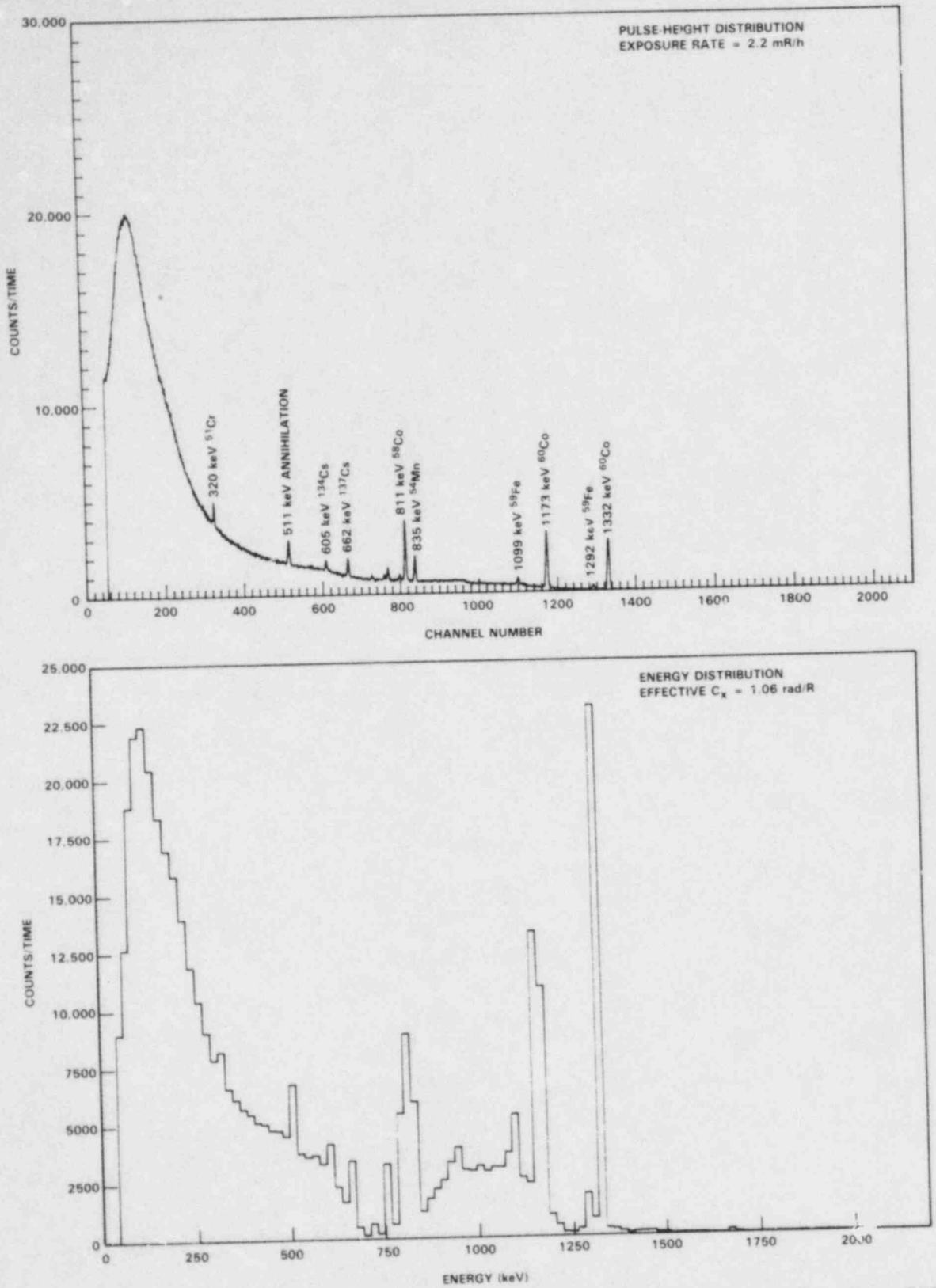

FIGURE A.5.7. Pulse-Height and Photon Energy Distributions, Shutdown PWR, Spent Fuel Pit, Site P, Location G-Spent Fuel Pit

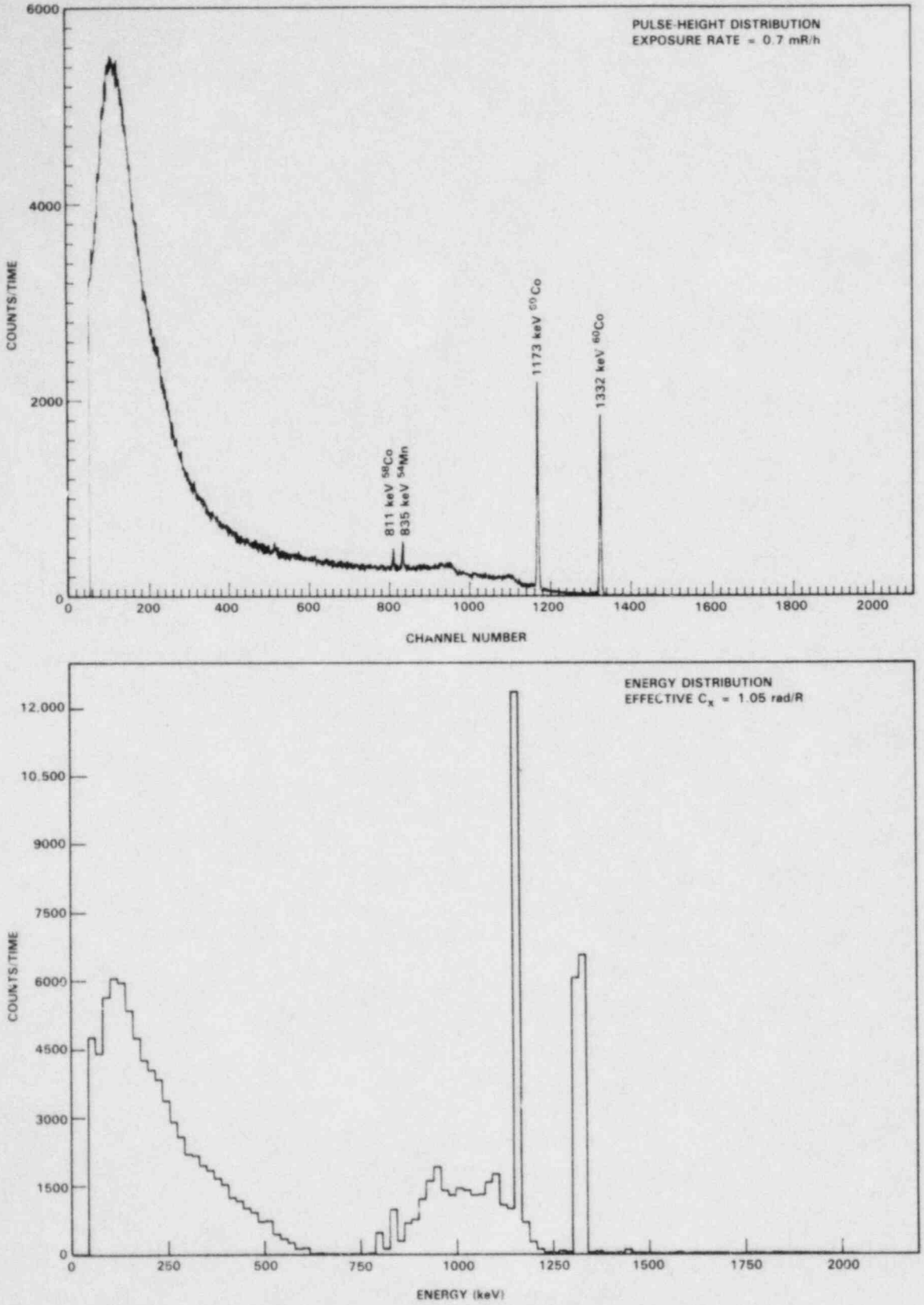

FIGURE A.5.8. Pulse-Height and Photon Energy Distributions, Shutdown PWR, Auxiliary Building, Site P, Location H-Primary Auxiliary Building, General Area

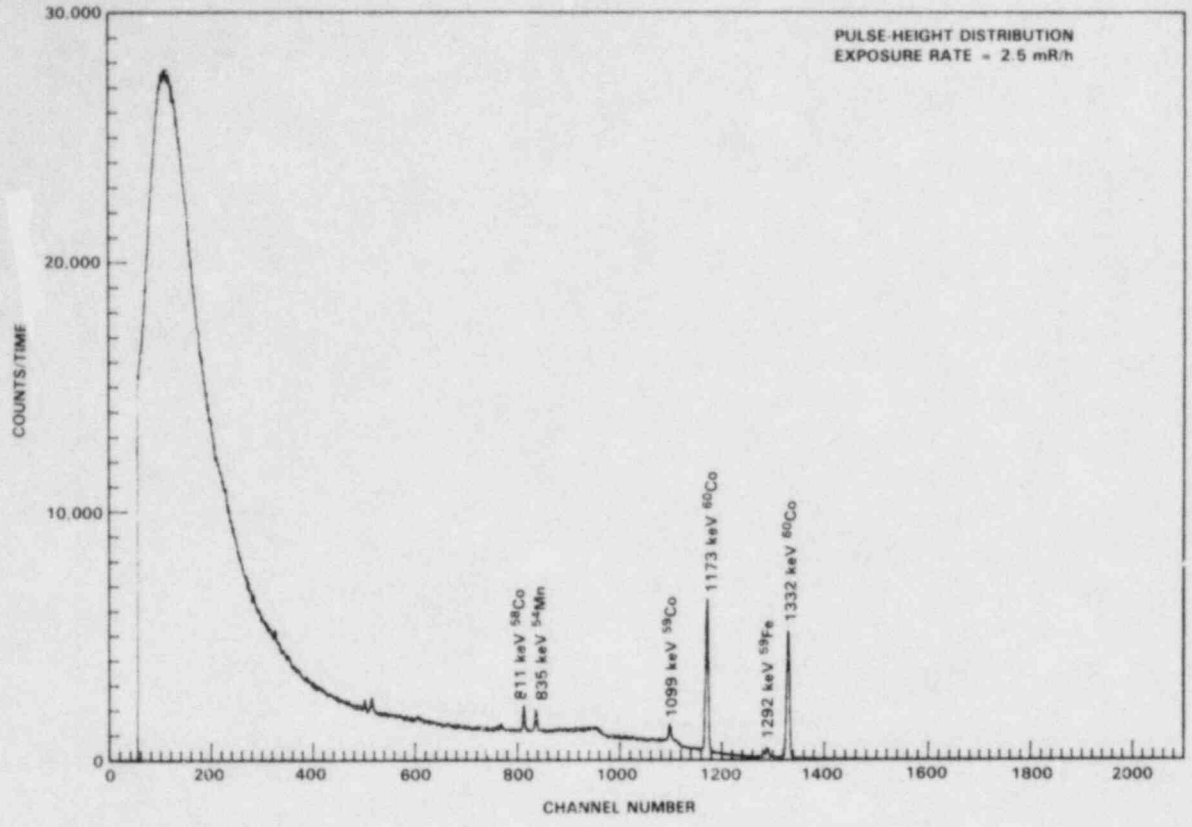

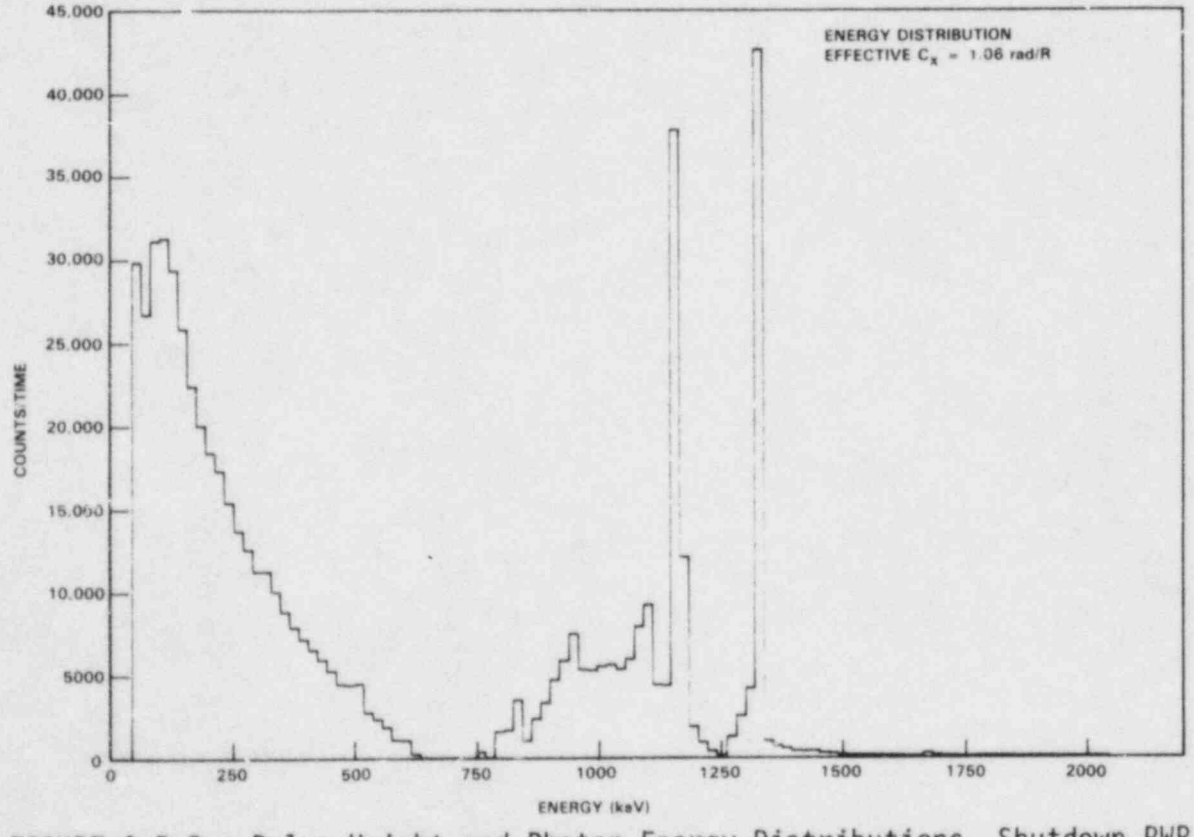

FIGURE A.5.9. Pulse-Height and Photon Energy Distributions, Shutdown PWR, Auxiliary Building, Site P, Location I-Open Surge Line

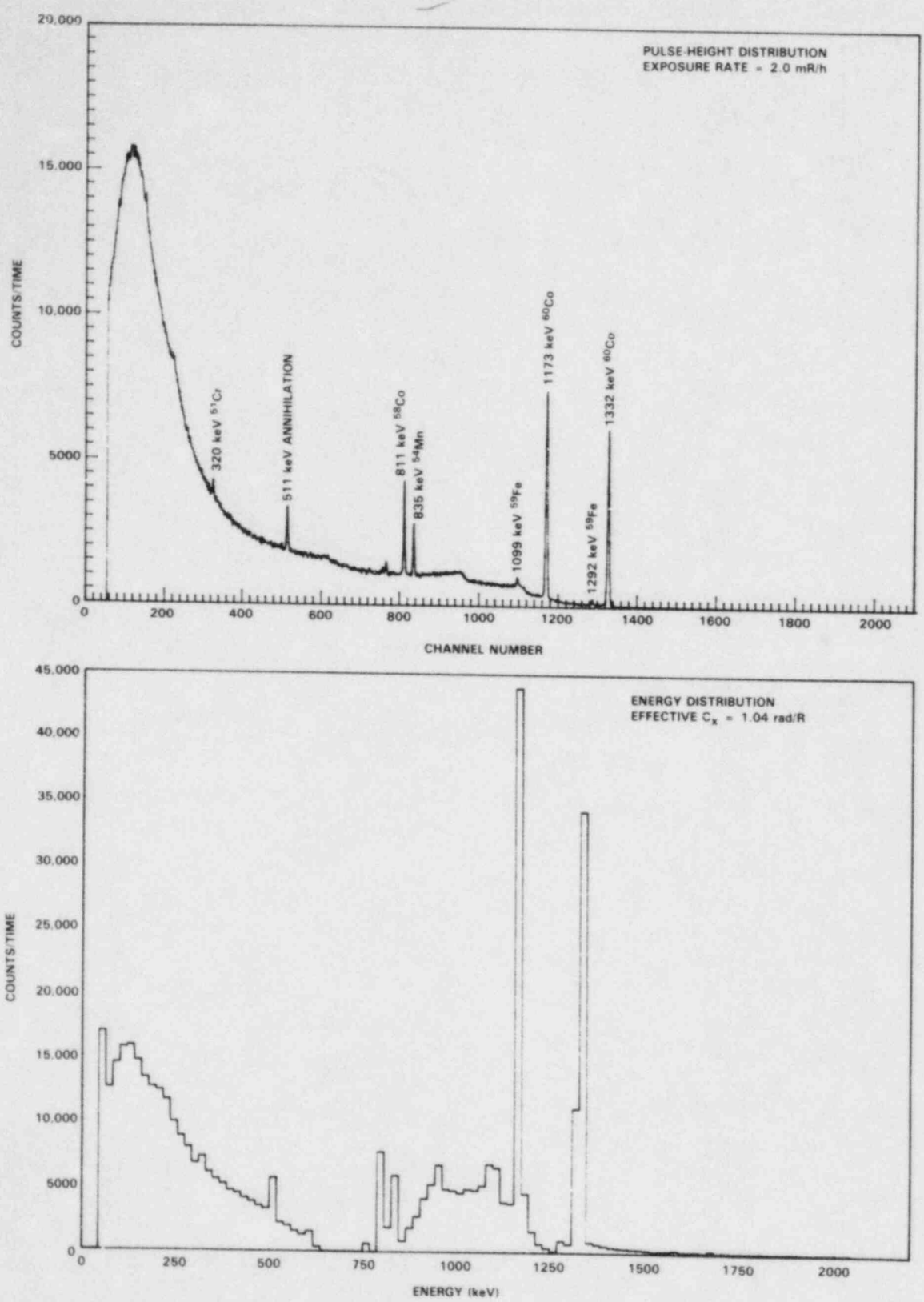

FIGURE A.5.10. Pulse-Height and Photon Energy Distributions, Shutdown PWR, Containment, Site P, Location J-Above Reactor Head Area (Flooded)

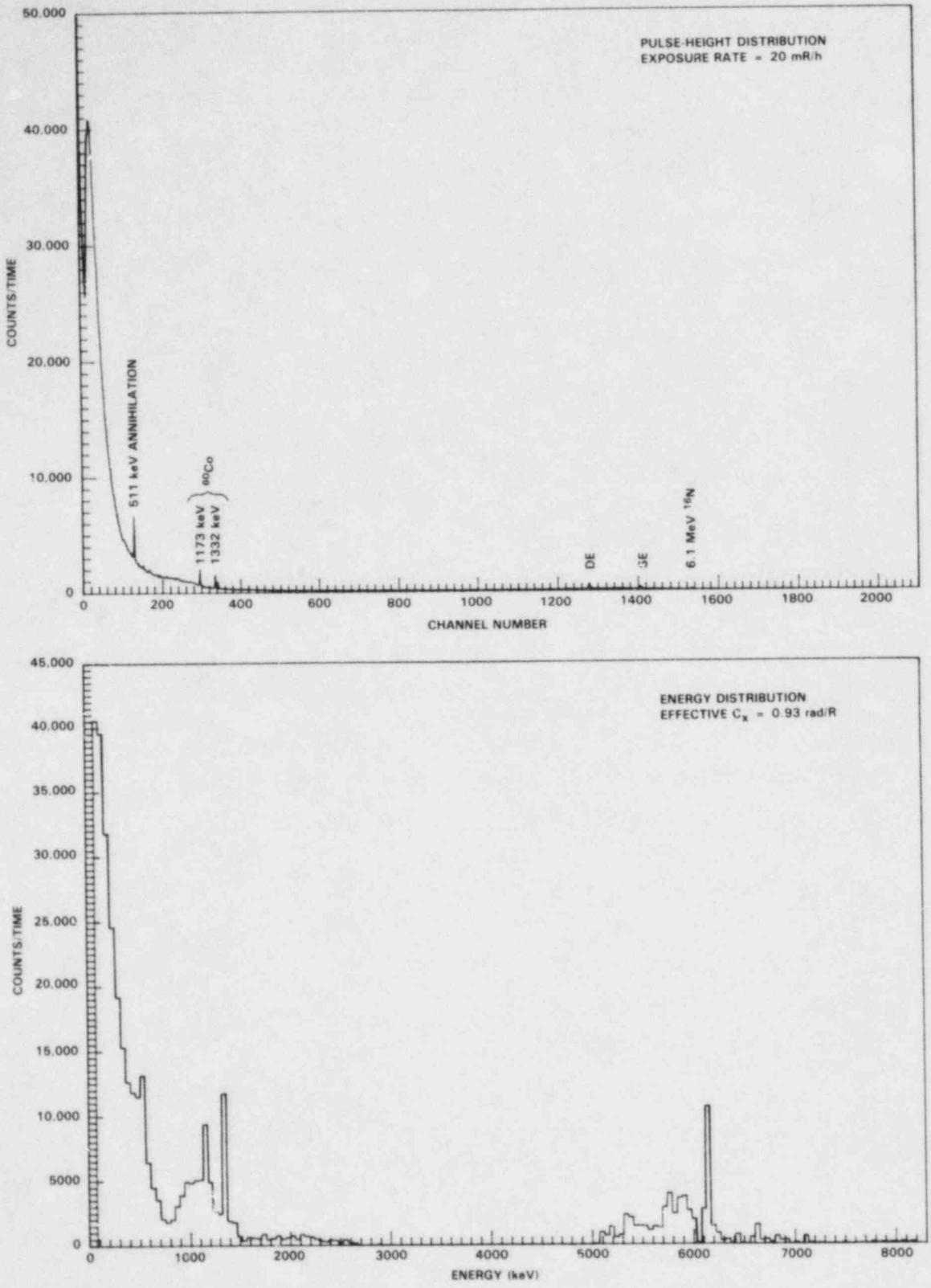

FIGURE A.6.1. Pulse-Height and Photon Energy Distributions, Operating BWR, Site N, Location A-Heater Bay, Entrance

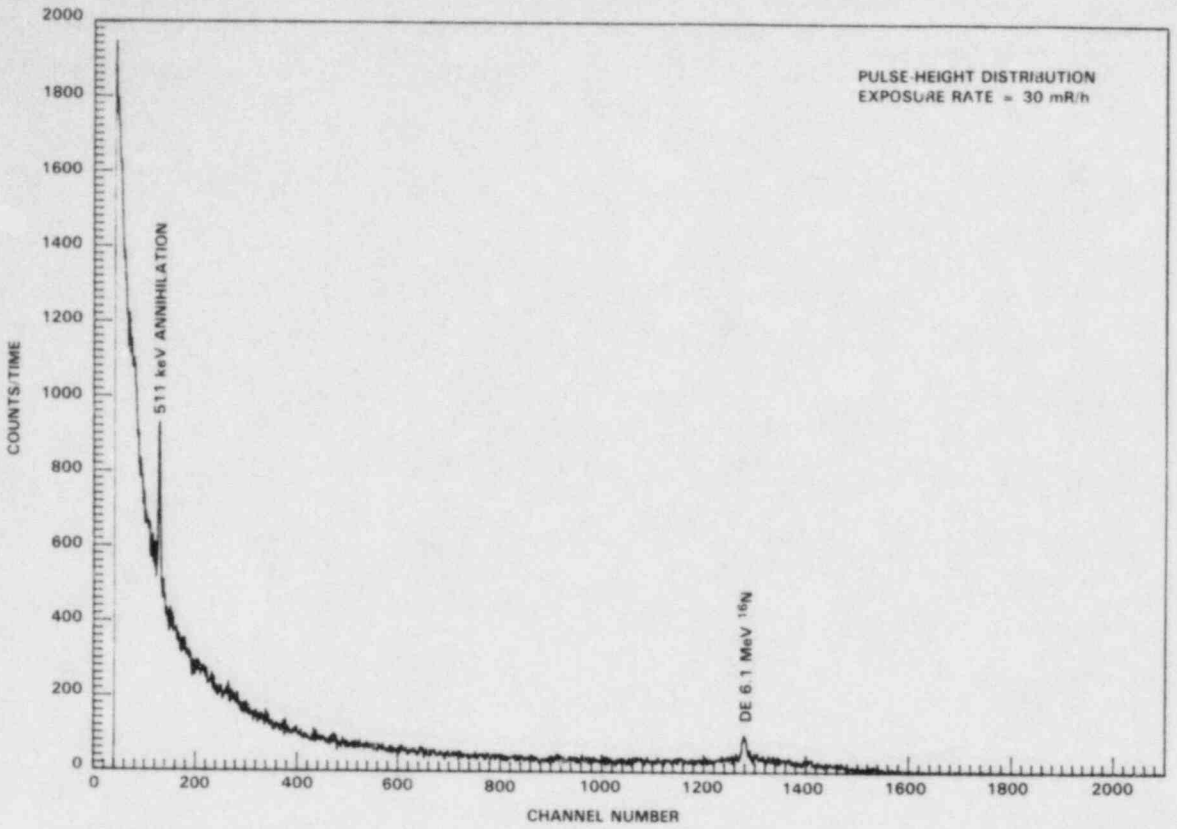

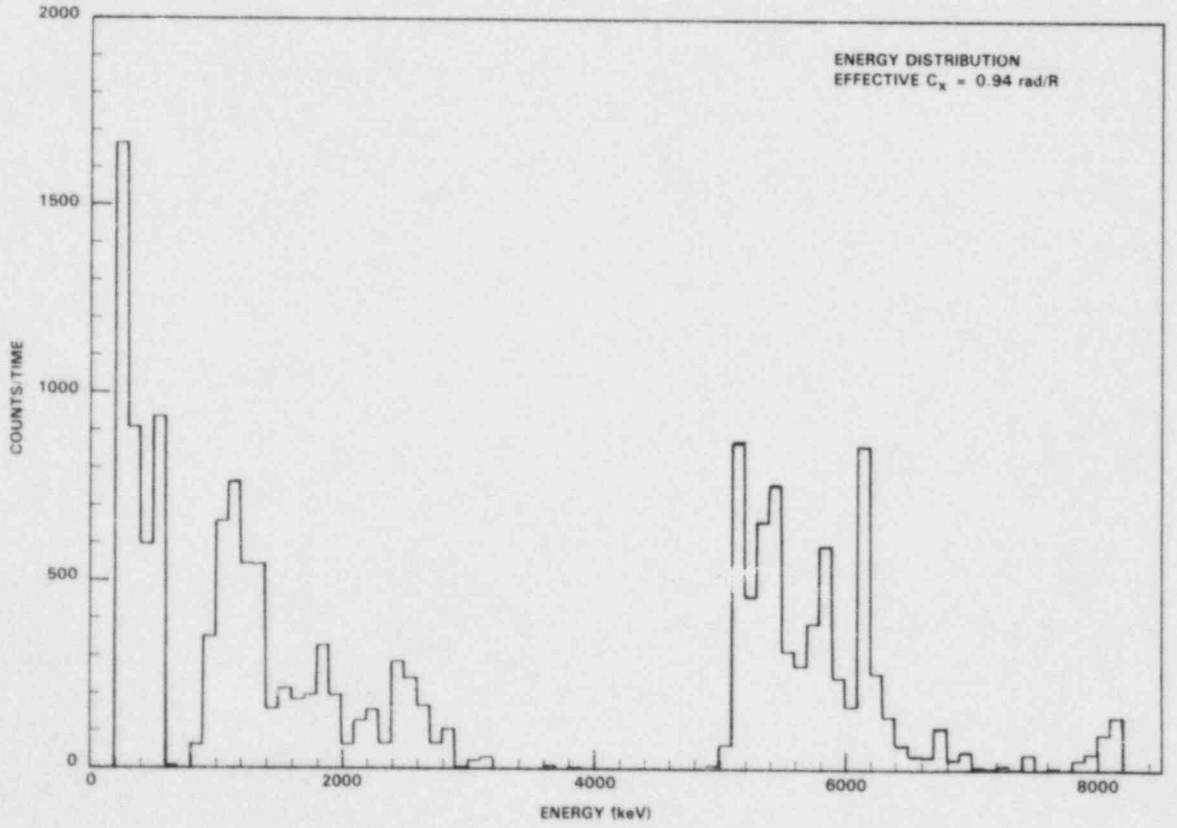

FIGURE A.6.2. Pulse-Height and Photon Energy Distributions, Operating BWR, Site N, Location B-Heater Bay, Near Steam Lines (collimated)

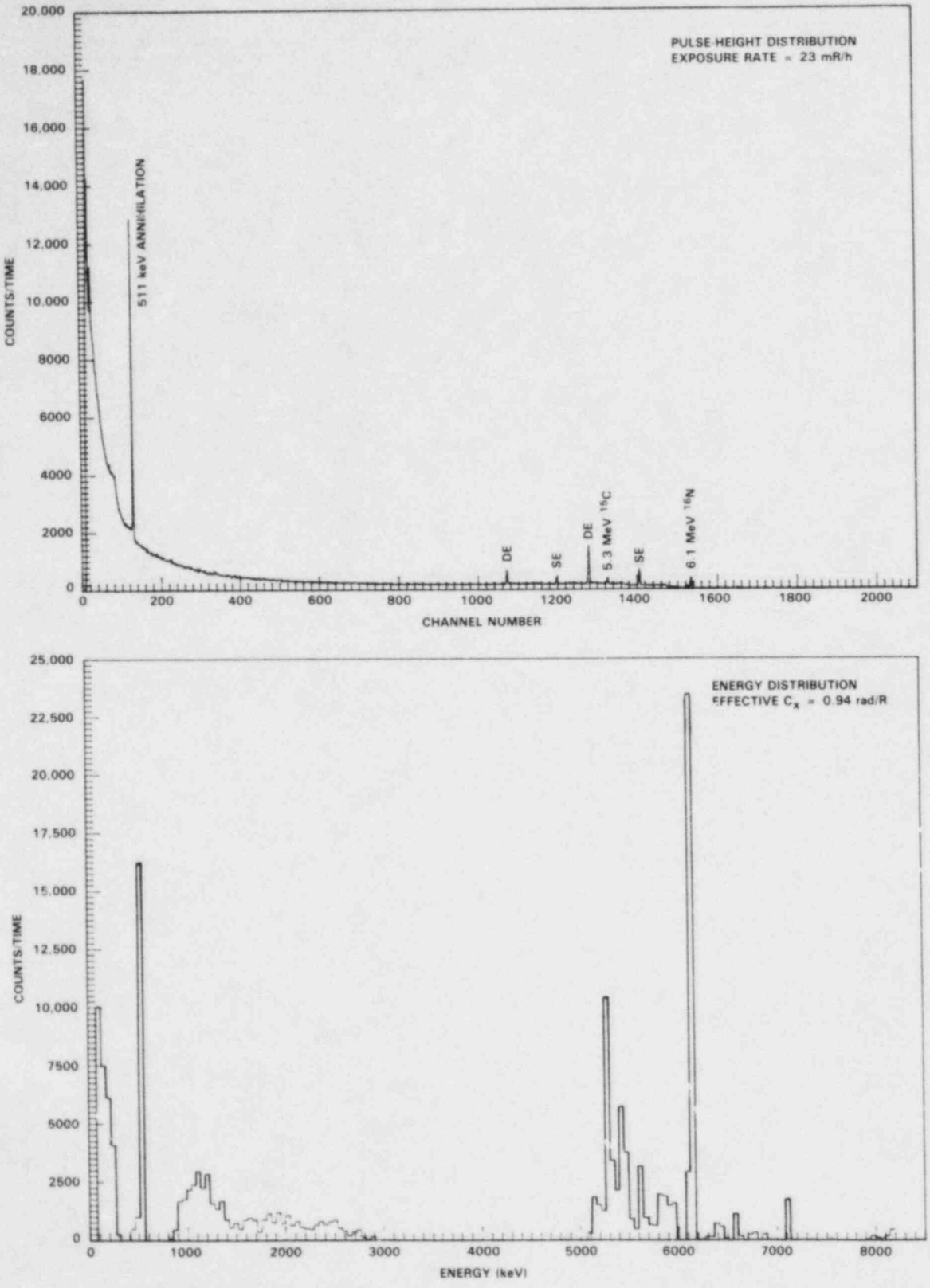

FIGURE A.6.3. Pulse-Height and Photon Energy Distributions, Operating BWR, Site N, Location C-MSIV, Entrance Hallway (collimated)

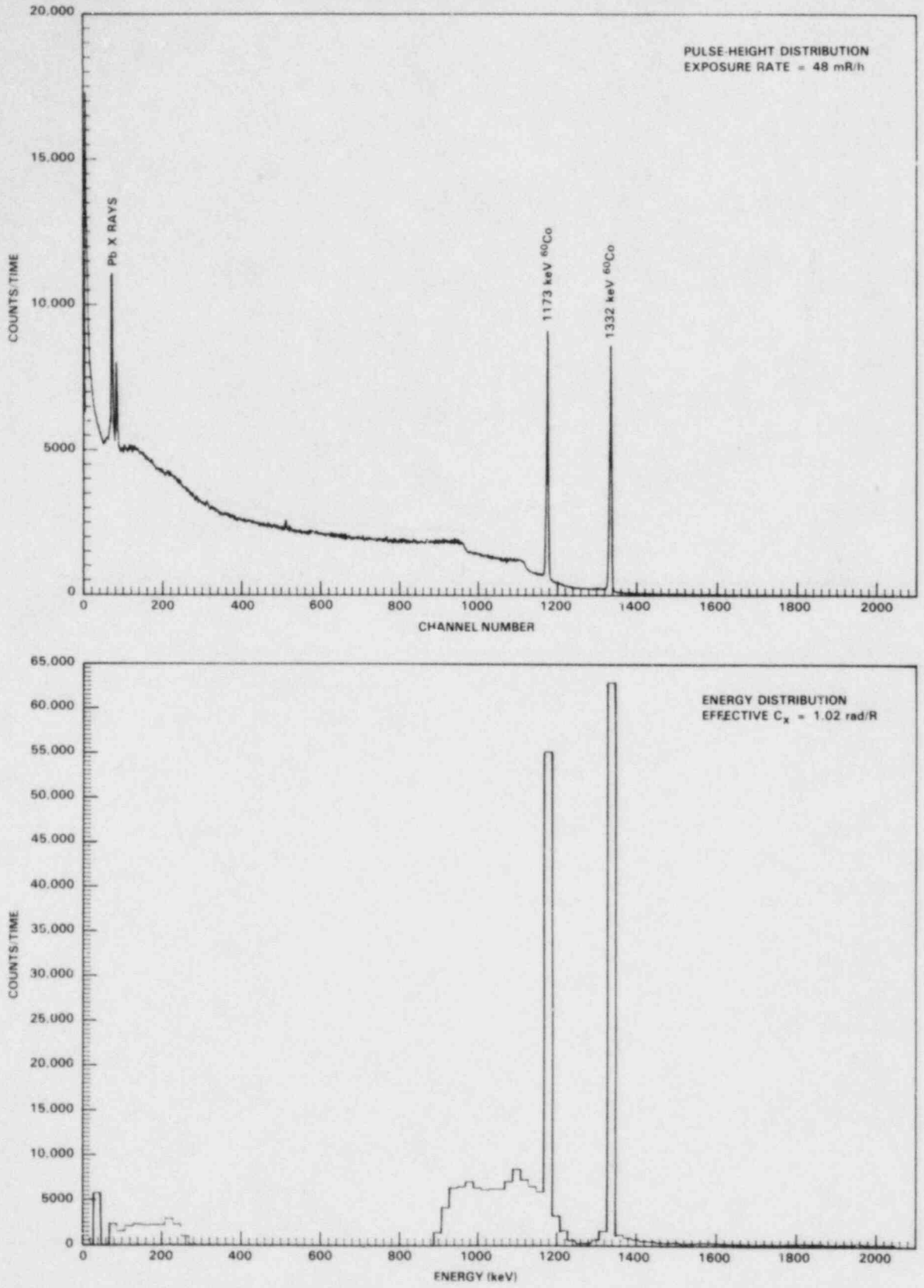

FIGURE A.6.4. Pulse-Height and Photon Energy Distributions, Operating BWR, Site N, Location D-CRD Room (collimated)

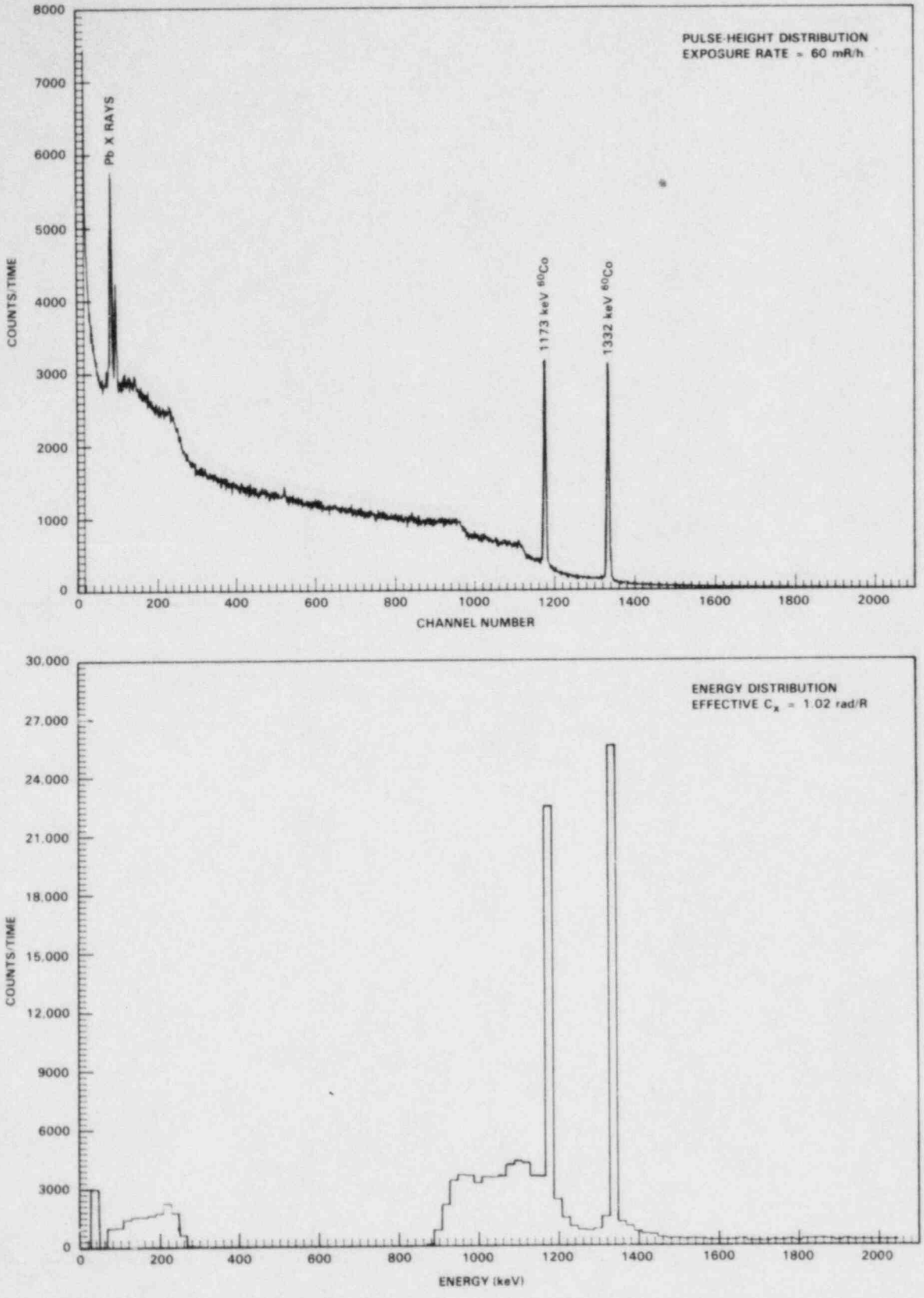

FIGURE A.6.5. Pulse-Height and Photon Energy Distributions, Operating BWR, Site N, Location E-Storage Room, Contaminated Pipe (collimated)

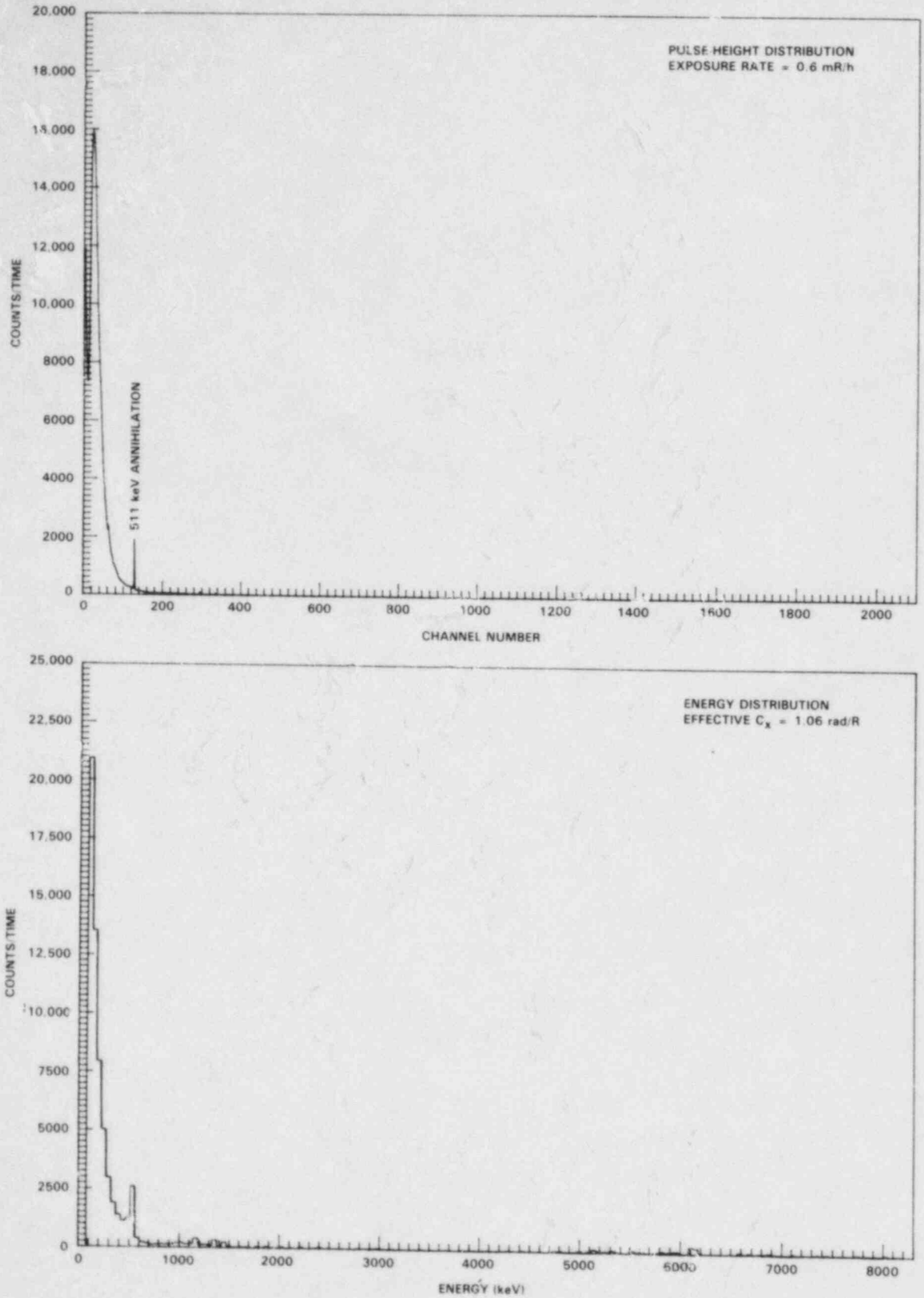

FIGURE A.6.6. Pulse-Height and Photon Energy Distributions, Operating BWR, Site N, Location F-Turbine Floor, Outside Shield Wall

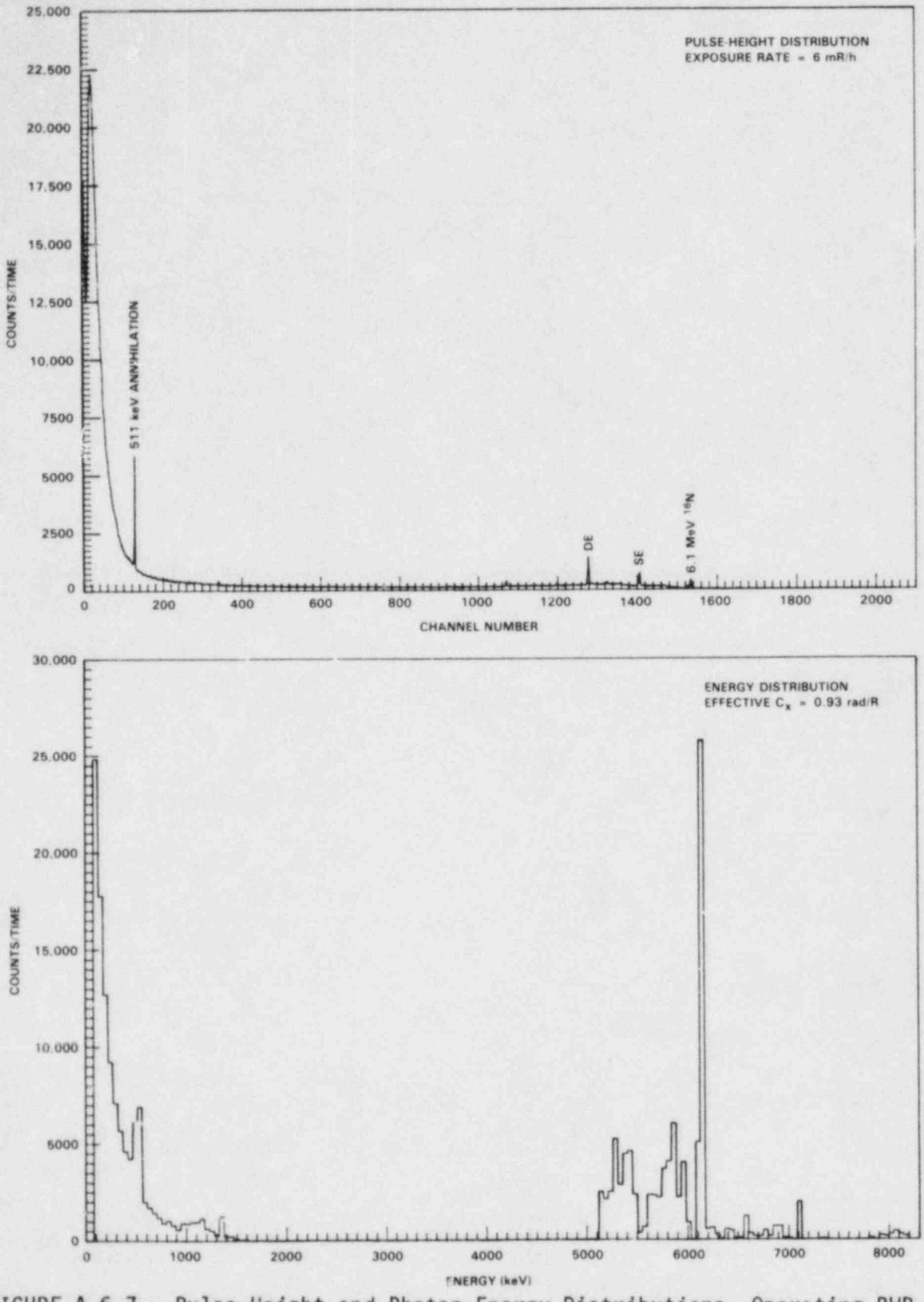

FIGURE A.6.7. Pulse-Height and Photon Energy Distributions, Operating BWR, Site N, Location G-Turbine Floor, Maze Entrance to Turbine Room

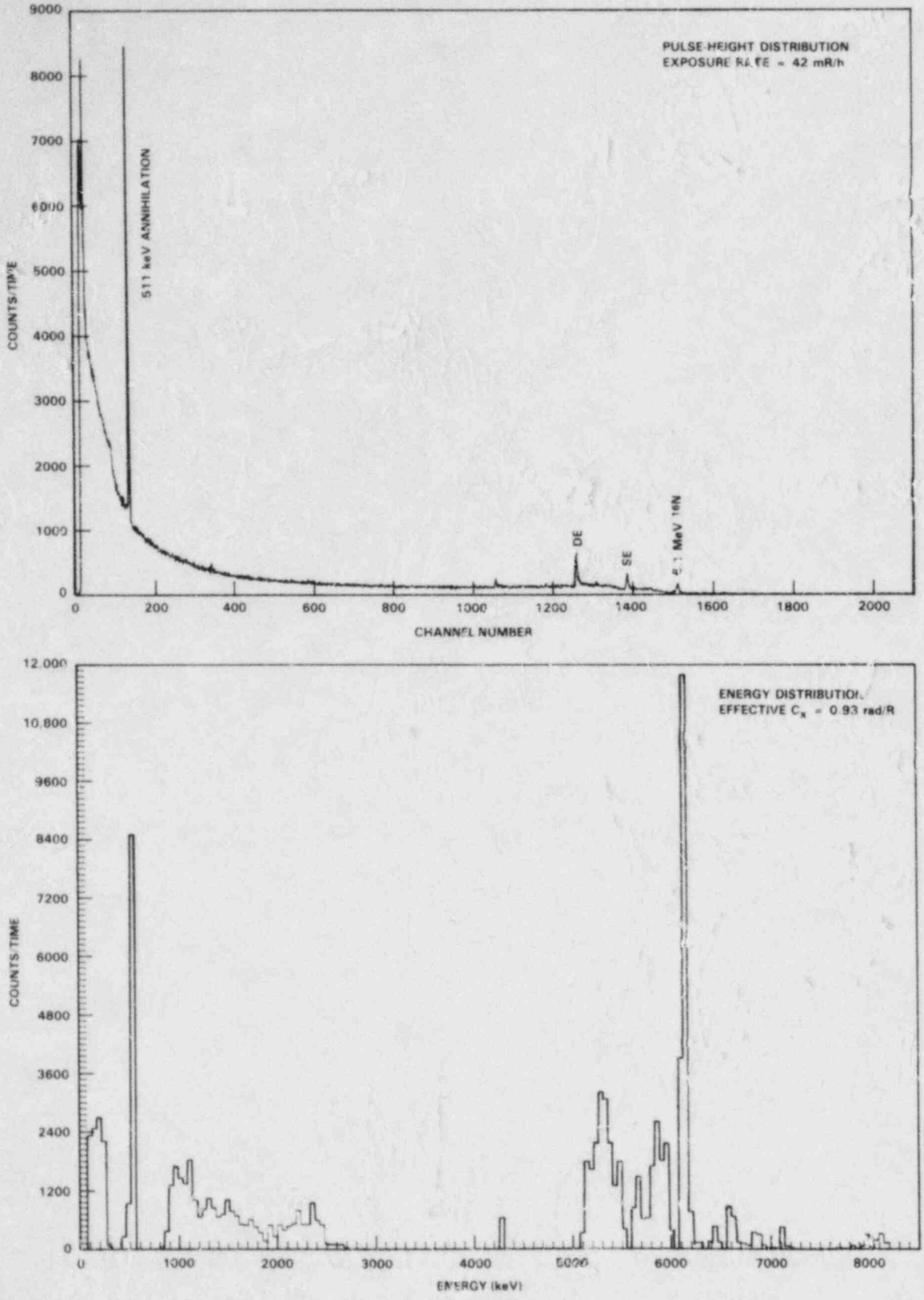

FIGURE A.6.8. Pulse-Height and Photon Energy Distributions, Operating BWR, Site N, Location H-Turbine Floor, Inside Turbine Room (collimated)

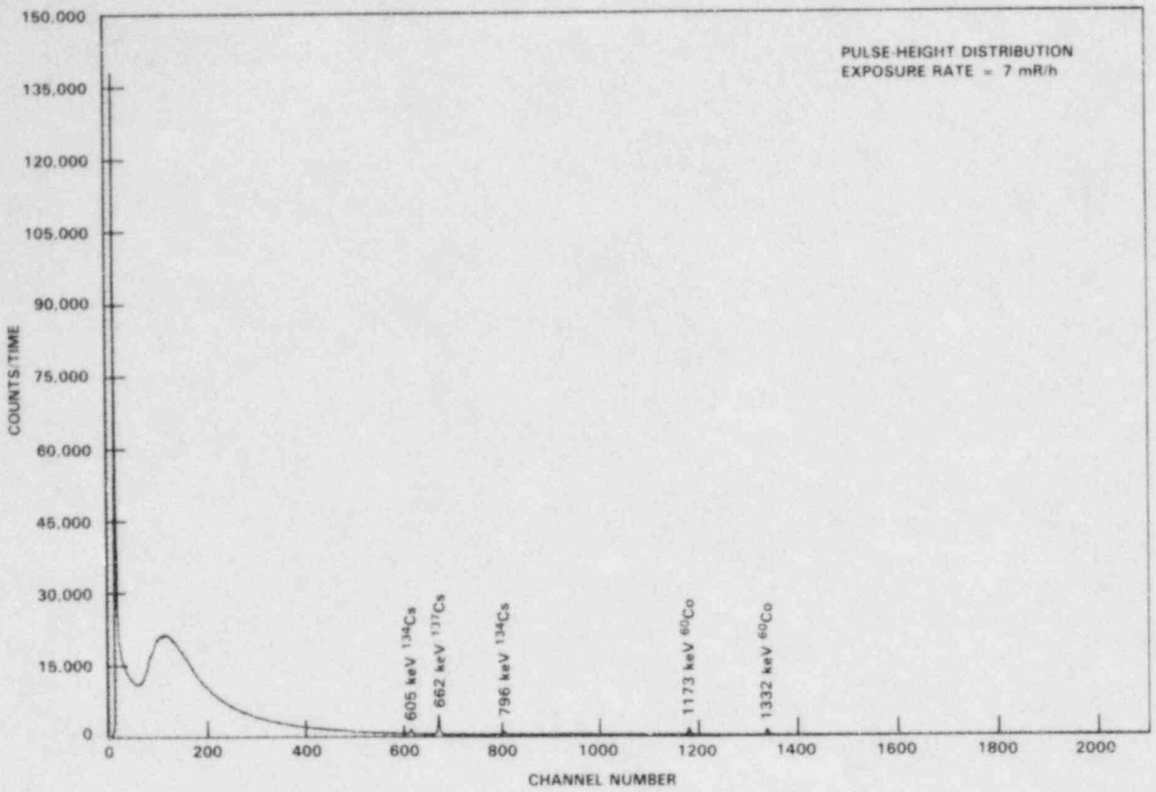

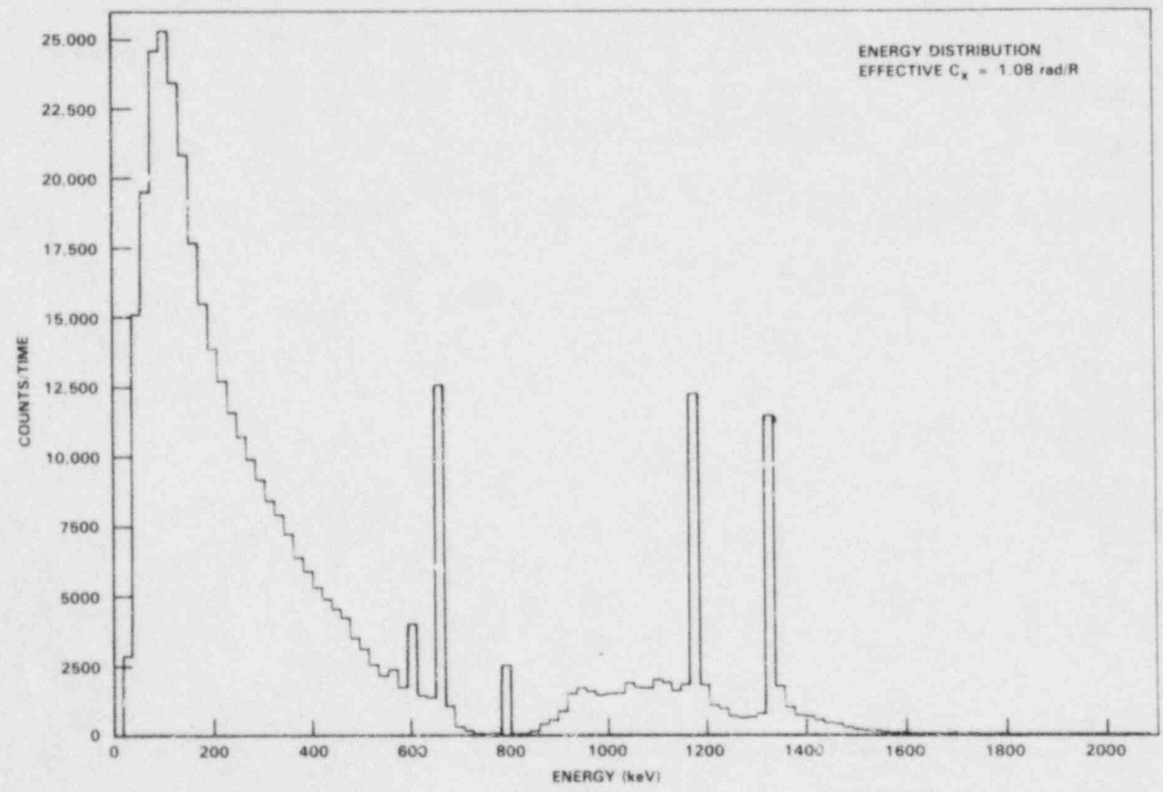

FIGURE A.6.9. Pulse-Height and Photon Energy Distributions, Operating BWR, Site N, Location I-Clean-Up Phase Separation Room Door

APPENDIX B

PHOTON FIELD MEASUREMENT TECHNIQUES

APPENDIX B

PHOTON FIELD MEASUREMENT TECHNIQUES

The preparation time required to conduct photon field surveys in occupational environments can be considerable. A large part of this time is devoted to studying the literature and preparing the computer software for data analysis. The techniques used for this study are described below to help others reduce their initial time investment. Familiarity with the discussions in Section 2 is assumed.

Described here are example data analysis formulae and computer software. (Instructions for the operation of equipment are typically provided by the manufacturer.) An HP-1000 computer with an enhanced version of ANSI FORTRAN X3.9-1966 was used for the programs discussed here and reproduced at the end of this appendix. The computer programs can be adapted to many micro- or larger computers with Fortran capability. The data file handling procedures will probably require modifications.

B.1 PHOTON SPECTROSCOPY

The photon spectrometer manufacturer's demonstrations and literature show methods of collecting data in the form of pulse-height distributions, typically recorded by a multichannel analyzer. To conduct an effective spectral monitoring program, the capability of electronically transferring the data into an analysis computer should be available. Input parameters for the analysis software are obtained from detector calibration spectra.

B.1.1 Efficiency Calibration

The detector can be calibrated using simple sources (e.g., ^{109}Cd, ^{137}Cs, and ^{60}Co) for response function characteristics and using calibrated multinuclide sources for efficiency measurements. Multinuclide sources are commercially available. With additional effort, the efficiency calibration can be performed with individually calibrated sources. The sources are positioned at a distance from the detector to simulate parallel incidence of photons. The calibration sources are moved or the detector is rotated to determine the efficiency at other entrance angles. If a collimator is used, the aperture is placed along the axis of the detector, and the calibration is performed with the source along the same axis. Detector efficiency at each source photon energy is calculated by dividing the number of counts in the full-energy peak by the number of incident photons calculated using the source calibration data and the source-detector geometry.

The semi-empirical formula given in Equation 8 of Hajnal and Klusek (1974) can be used to parameterize the detector efficiency (Σ_m) for germanium detectors. The formula is:

$$\Sigma_m = e^{-\mu_A W} e^{-\mu A_1} \left\{ \frac{1 - e^{-\mu A_2}}{\mu_1} \right\} \left\{ A_3\tau + \left[A_4\sigma_a + A_5\sigma_s \frac{1 - e^{-\mu' A_6}}{\mu'} \left(\tau' + A_7\sigma' e^{-E_2 A_8} \right) \right] e^{-E_1 A_9} + A_{10}\kappa\, e^{-T_2 A_{11}} \right\} \quad \text{(B.1)}$$

where $E_1 = E\sigma_s/\sigma$

$E_2 = E_1\sigma_s'/\sigma'$

and $\ln Q = \sum_{i=1}^{N} a_i [\ln E]^{i-1}$

for $Q = \tau$, σ_{coh}, σ_{inc}, κ for aluminum and τ, σ_{coh}, σ_{inc}, κ for germanium and E_1. The parameters are identified in Table B.1 along with the corresponding variable names used in Subroutine EFF (Program TEST). Many of the parameters are fixed using the detector characteristics. Hajnal and Klusek (1974) explain the meaning of the parameters in detail. Other parameters are varied until an acceptable fit is found. The a_i coefficients are tabulated in Table 1 of Hajnal and Klusek and in Function F of Program TEST. Program TEST, which is used to calculate the efficiency curves, calls Subroutine EFF to calculate Equation B.1. Subroutine EFF requires Function F to calculate the 'Q' parameters. Detector 'ID' = 1 was used to generate the curve in Figure 4 (page 7) of this report.

The highest energy available from the calibration sources used in this work was 1836 keV from ^{88}Y. The extrapolation to 6 MeV using the semi-empirical model was checked using ^{16}N fields at a reactor site. Two locations with radiation fields almost totally due to ^{16}N decay were used. Results for the Ge detector were compared to results for a NaI detector and TL dosimeter measurements. The measured dose rates at depths greater than 3 cm were used to estimate the fluence of 6-MeV photons. The Ge efficiency was low, but the resulting error was smaller than that caused by the use of the simple formula for unfolding the spectra.

TABLE B.1. Efficiency Formula Parameters

Symbol	Unit, Name	FORTRAN Label
τ	barn, photoelectric cross section (Ge)	F(5,E)
σ_a	barn, Compton energy absorption cross section	SA
σ_s	barn, Compton scattering cross section (Ge)	SS
σ	barn, average Compton collision cross section (Ge)	S
κ	barn, pair-production cross section (Ge)	F(8,E)
μ_1	barn, $\mu_1 = \tau + \sigma + \kappa$ (Ge)	XM1
μ	cm^2g^{-1}, mass attenuation coefficient (Ge)	XM
μ_A	cm^2g^{-1}, mass attenuation coefficient (Al)	XMA
E	MeV, primary photon energy	E
E_1, E_2	MeV, the average once- or twice-Compton-scattered photon energy (Ge)	E1, E2
T_2	MeV, average energy of electron/positron (Ge)	T2
W	gcm^{-2}, window thickness (Al)	A(12)
A_i	Parameters of the semi-empirical Equation (8)	A(1)-A(11)
$\Sigma_m(E)$	Semi-empirical efficiency at energy E .	EFM
Σ_T	Total efficiency without scattering loss	EFT

Primed quantities refer to Compton-scattered photons and are denoted by the FORTRAN label followed by a 'P'.

B.1.2 Conversion to Energy Distributions

The efficiency equation (Equation B.1) and the simple model of Seelentag and Panzer (1979) are used to unfold the pulse-height distributions to yield energy spectra. Program HILO is used to calculate the necessary corrections using Subroutine EFF and the parameters developed with Program TEST.

The parameterization for Compton scattering (see Figure 4 of Seelentag and Panzer) is:

$$H(E,E_i) = \begin{cases} \frac{3h(E_i)}{2}(1 - E/E_c) & 0 < E < E_c/3 \\ h(E_i) & E_c/3 < E < E_c \\ \frac{h(E_i)}{2}(1-3/4\ (E/E_c)) & E_c < E < 4\ E_c/3 \end{cases}$$

where E is the energy channel, E_c is the Compton edge and h is the amplitude. The data are analyzed by correcting the highest energy bin, subtracting the scattered radiation from all lower bins, and repeating the procedure for all lower bins in order. Dividing the data into bins of 20- to 50-keV increments simplifies the analysis. The corrected number of counts in energy bin E is

$$N_c(E) = \frac{N(E) - \frac{6}{7}\sum_{E_i>E} H(E,E_i)}{\Sigma_m(E)}$$

where $h(E_i) = N_c(E_i)(\Sigma_T - \Sigma_m(E_i)$
and N(E) is the original number of counts in energy bin E. These formulae are coded in lines 137 to 175 of Program HILO.

Corrections for pair production effects are required at high energies. The single- and double-escape peaks are subtracted from the spectra using the number of counts in the full-energy peak and the average probability of recording a 511-keV photon that was created inside the detector by the annihilation of a positron and an electron. The 511-keV detection probability factor is determined for each detector using average ratios of the full-energy, single-escape and double-escape peaks. Lines 179 to 200 of Program HILO accomplish this.

Calculations using a collimator can be performed by establishing the difference in detector response functions with and without the collimator. The difference is parameterized and stored in Subroutine LEAD. Each collimator-detector combination may require different variable values. The modifications required for Program HILO are given in Table B.2.

TABLE B.2. Modifications to Program HILO for the Use of a Collimator

Location	Change
After Line 11	insert COMMON COL (2100)
After Line 126	insert CALL LEAD (PEAK(1),PEAK(2))
After Line 151	insert COMPT(II) = COMPT(II)*(1.+COL(II))
After Line 161	insert COMPT(II) = COMPT(II)*(1.+COL(II))
After Line 171	insert COMPT(II) = COMPT(II)*(1.+COL(II))

Although artifacts in the spectra caused by the approximate formulae used are easily seen, these techniques were determined to be adequate for the purpose. Improved formulae for computer corrections at low energies (<300 keV) are found in the literature (Seltzer 1981). Improved methods at high energies would have to be developed.

B.1.3 Calculation of Dosimetry Correction Factors

As indicated in Figure 3 (page 6) of this report, the spectra are used to generate dosimetry correction factors using a conversion from fluence to exposure and a conversion from exposure to dose (C_x). Program CX uses the following formula to calculate effective C_x factors (C_x^{Eff}).

$$C_{x,k}^{Eff} = \frac{\sum_{E_i} C_{x,k}(E_i) N(E_i)/F(E_i)}{\sum_{E_i} N(E_i)/F(E_i)}$$

The 'k' index refers to the type and tissue depth of the C_x factor and $F(E_i)$ is the photon flux per Roentgen. The C_x factors are listed in the DATA statement for Program CX and correspond to the energies in keV in the DATA statement for E. Eight sets of C_x factors are listed consecutively for the maximum and central values at 2.5 cm, 1 cm, 0.3 cm, and 0.007 cm.

Correction factors for an instrument or dosimeter that does not have a flat energy response can be calculated by changing the DATA statement for Program CX. The energy response of the instrument or dosimeter must be known.

B.2 THERMOLUMINESCENCE DOSIMETRY

Thermoluminescent dosimeters can be used to determine the approximate spectral composition of photon and electron fields. The advantages of this technique are that monitoring can be performed fairly inexpensively and will not be limited to a small range of dose rates. The TL material is packaged so that relative magnitudes of dose due to specific energy ranges can be determined. Many (approximately 10) elements are needed to achieve the required sensitivity. Computer analysis of the data can be performed in a manner similar to the TLD-phantom analysis discussed in Subsection 2.3 (page 14). Program POLY uses least-square fitting techniques to determine the optimum linear combination of calibration responses to describe the field data. The multielement TL dosimeter is calibrated using the photon and beta-particle energies that represent the occupational environment. The number of calibration types and energies must be less than the number of elements in the dosimeter. It is important to design the multielement dosimeter to respond uniquely to each energy of interest.

Some of the calculations in Program POLY apply specifically to the analysis of the TLD-phantom data. For example, inverse-distance-squared corrections are made to remove geometry-phantom effects for the least-square fitting. For a different design, the data statement in Subroutine GCORR can be changed.

```
T6      I=00004 IS ON CR00026 USING 00018 BLKS R-0000

0001    FTN4X,L
0002          PROGRAM TEST
0003    C-----------------------------------------------------------------
0004    C--THIS PROGRAM CALCULATES DETECTOR EFFICIENCIES FOR GE OR GELI
0005    C--DETECTORS.
0006    C-----------------------------------------------------------------
0007          DIMENSION EN(7),EE(40),EF(40)
0008          DATA EN/59.5,88.03,122.1,511.,661.6,1173.2,2754.1/
0009          WRITE(1,'("ENTER DETECTOR NUMBER OR CHOOSE PARAMETERS (ID=5)")')
0010          WRITE(1,'("ID = ")')
0011          READ(1,'(I1)')ID
0012          DO 10 I=1,7
0013          E=EN(I)/1000.
0014          CALL EFF(E,ID,EFM,EFT)
0015          WRITE(1,'(3F10.4)') E,EFM,EFT
0016          WRITE(6,'(3F10.4)') E,EFM,EFT
0017    10    CONTINUE
0018          E=0.020
0019          DO 30 I=1,40
0020          E=E*1.189207
0021          CALL EFF(E,ID,EFM,EFT)
0022          EE(I)=E
0023          EF(I)=EFM
0024    30    CONTINUE
0025          WRITE(6,'(4(2E10.4,5X))')(EE(I),EF(I),I=1,40)
0026          STOP
0027          END
0028          SUBROUTINE EFF(E,ID,EFM,EFT,PE,CO,PP)
0029    C...DETECTOR EFFICIENCY BASED ON HAJNAL AND KLUSEK,NIM 122,559(1974).
0030    C.....
0031          DIMENSION A(12),AA(12,4)
0032          DATA AA/.4,15.,.96,.30,.56,3.25,8.27,7.57,1.15,.111,1.19,.3,
0033         X,1.20,.9,.45,.3,5.2,.9,9.5,1.5,.1,.6,.14,
0034         X0.0,21.4,.9,.45,.3,5.2,.9,9.5,1.5,.1,.6,.2,
0035         X ,3226, 42.23,.06180,.1743,.1521, 5.158,90.11, 9.507, 1.493,
0036         X7.458, 2.993,.1370/
0037          DO 4 I=1,9
0038          A=F(I,E)
0039    4     CONTINUE
0040          IF(ID.EQ.-1)GO TO 7
0041          IF(ID.NE.5)GO TO 6
0042          ID=-1
0043          WRITE(1,'("SPECIFY DETECTOR PARAMETERS(12)")')
0044          READ(1,'(F10.3)') A
0045          WRITE(1,'("RUNNING")')
0046          GO TO 7
0047
0048    6     CONTINUE
0049          DO 5 I=1,12
0050    5     A(I)=AA(I,ID)
0051    7     CONTINUE
0052
0053    C.....
0054    C...ABSORBING MULTIPLIERS
0055    C.....
0056          XM1=F(5,E)+F(6,E)+F(7,E)+F(8,E)
0057          XMA=(F(1,E)+F(2,E)+F(3,E)+F(4,E))*.02232
0058          XM=XM1*.008297
0059          EX = 1.-EXP(-XM*A(2))
0060
0061          AI =EXP(-XMA*A(12))*EXP(-XM*A(1))
0062          EFT=AI*EX
0063    C.....
0064    C...PHOTOELECTRIC
0065    C.....
0066          PE=A(3)*F(5,E)*EX/XM1
0067    C.....
0068    C...COMPTON
0069    C.....
0070          S=F(7,E)
0071          E1=F(9,E)
0072          E2=F(9,E1)
0073          S5=S*E1/E
0074          SA=S-S5
0075          XM1P=F(5,E1)+F(6,E1)+F(7,E1)+F(8,E1)
0076          XMP=XM1P*.008297
0077          SP=         F(7,E1)
0078
```

```
0079          C=          A(5)*55*(1.-EXP(-XMP*A(6)))/XM1P
0080          C=C*(F(5.E1)+A(7)*SP*EXP(-E2*A(8))) +A(4)*SA
0081          CO=C*EXP(-E1*A(9))*EX/XM1
0082    C.....
0083    C...PAIR PROD
0084    C.....
0085          T2=(E-1.022)/2.
0086          PP=A(10)*F(8.E)*EXP(-T2*A(11))*EX/XM1
0087    C.....
0088    C...TOTAL
0089    C.....
0090          EFM=AT*(PE+CO+PP)
0091          IF(E.GT.0.08) RETURN
0092          IF(EFM.LT.0.1) EFM=0.1
0093          RETURN
0094          END
0095          FUNCTION F(I,E)
0096          DIMENSION A(9,9)
0097          DATA A/-6.80487,-2.29488,.647210,.255878,-.0798018,-.127118,
0098         X-.0499159,-.0084875,-.000540104,-4.98287,-2.01556,.0101226,
0099         X.00444688,-.00310911,.000227534,.000093797,-.00000879574,
0100         X-.00000130512,1.00878,-.491853,-.0545706,-.000213763,-.00043142,
0101         X.000290897,.000002166O7,-.00000500136,-.0000000730006,
0102         X-9.01182,16.3696,-18.7053,13.6747,-6.31765,1.85838,-.326402,
0103         X.0322528,-.00135773,-2.61505,-2.18328,.417284,.00613371,
0104         X-.0343345,.000321599,.00209723,-.0000208088,.0000524518,
0105         X-2.73228,-2.00133,.00684719,.00147381,-.00217007,.000428610,
0106         X.0000230333,-.0000102334,.000000057240B,1.90842,-.488624,
0107         X-.0573383,.000524148,-.000558472,.000383555,-.0000157282,
0108         X-.00000808485,.000000642804,-7.04492,15.4097,-17.4141,12.5903,
0109         X-5.75616,1.65932,-.292118,.0286337,-.00119563,
0110         X-.579831,.755106,-.0146638,.00544192,.000281432,-.0000732701,
0111         X0,,0,,0,/
0112
0113          FL=A(1,I)
0114          DO 10 J=2,9
0115    10    FL=A(J,I)*ALOG(E)**(J-1) + FL
0116          F=EXP(FL)
0117          RETURN
0118          END
```

```
T4      I=00004 IS ON CR00026 USING 00036 BLKS R-0000

0001    FTN4X,L
0002    $FILES(2,2)
0003    $EMA(LARGE,0)
0004          PROGRAM HILO(),ANALYZE A HI-LO GAMMA SPECTRUM
0005    C-------------------------------------------------------------------------
0006    C--THIS PROGRAM CONVERTS PULSE HEIGHT DISTRIBUTION TO AN ENERGY SPECTRUM.
0007    C-------------------------------------------------------------------------
0008          INTEGER NAME(6),ITITLE(36),CLEAR(2),LCRSR,LOCK,UNLOCK
0009          INTEGER ICHAN(8200)
0010          DIMENSION FX(5),CKEV(5,2),PEAK(4),AA(4,12)
0011          COMMON/LARGE/DATA(8200),ICHAN,COMPT(8200)
0012          DATA CLEAR/15550B,15512B/
0013          DATA LCRSR/15507B/
0014          DATA LOCK/15554B/
0015          DATA UNLOCK/15555B/
0016    C-------------------------------------------------------------------------
0017    C--GET THE DATA FILE NAME
0018    C-------------------------------------------------------------------------
0019          WRITE(1,'(2A2,/,T25,"HI-LO GAMMA SPECTRUM ANALYSIS",/)') CLEAR
0020          WRITE(1,'(A2)') LOCK
0021     100  WRITE(1,'("ENTER FILE NAME (SIX CHARACTERS MAX):  ")')
0022          READ(1,'(6A2)') NAME
0023          OPEN(80,FILE=NAME,IOSTAT=IOS,ERR=200)
0024    C-------------------------------------------------------------------------
0025    C--READ THE TITLE OF THE FILE
0026    C-------------------------------------------------------------------------
0027          READ(80,'(36A2)') ITITLE
0028          WRITE(1,'(2A2,36A2,/)') CLEAR,ITITLE
0029          WRITE(1,'("IS THIS THE FILE YOU WANT??  ")')
0030          READ(1,'(A2)') IANS
0031          IF(IANS.NE.2HNO) GOTO 110
0032          CLOSE(80)
0033          WRITE(1,'("TRY AGAIN?  ")')
0034          READ(1,'(A2)') IANS
0035          IF(IANS.NE.2HNO) GOTO 100
0036          WRITE(1,'("A2)') UNLOCK
0037          STOP
0038    C-------------------------------------------------------------------------
0039    C--READ THE DATA FROM THE FILE AND TOTAL THE COUNTS
0040    C-------------------------------------------------------------------------
0041     110  WRITE(1,'(2A2,/,6A2,/,36A2,/,A2)') CLEAR,NAME,ITITLE,LOCK
0042          WRITE(1,'("GETTING DATA FROM FILE: "6A2)') NAME
0043          TOTAL=0
0044          DO 120 I=1,8500
0045            READ(80,*,END=130) ICHAN(I),DATA(I)
0046            WRITE(1,'(I4,A2," ")') ICHAN(I),LCRSR
0047            IF(),LE,2) GOTO 120
0048            TOTAL=TOTAL+DATA(I)
0049     120  CONTINUE
0050     130  I=I-1
0051          WRITE(1,'("DATA POINTS:",I5,/,"TOTAL COUNTS:",F8,2,/)') I,TOTAL
0052          CLOSE(80)
0053    C-------------------------------------------------------------------------
0054    C--GET NAME OF OUTPUT STORAGE FILE
0055    C-------------------------------------------------------------------------
0056     140  WRITE(1,'("DATA STORAGE FILE NAME:  ")')
0057          READ(1,'(6A2)') NAME
0058          OPEN(81,FILE=NAME,IOSTAT=IOS,ERR=140)
0059          WRITE(81,'(36A2)') ITITLE
0060          DATA(1)=0.
0061          DATA(2)=0.
0062    C-------------------------------------------------------------------------
0063    C--CHOOSE DETECTOR
0064    C-------------------------------------------------------------------------
0065          WRITE(1,155)
0066     155  FORMAT("DETECTOR: 1, 31cc"/,T11"2, 48cc"/,T11"3, 59cc"/,T11,
0067         +"4, TEST",/,T9,"?? ")
0068          READ(1,'(I1)') IDQ
0069    C-------------------------------------------------------------------------
0070    C--CALCULATE keV/CHANNEL FOR SPECTRUM  (Y=MX+b)
0071    C-------------------------------------------------------------------------
0072     156  WRITE(1,'("ENTER CHANNEL NUMBER,keV IN CHANNEL(-99=END INPUT)")')
0073          KQ=0
0074          KR=0
0075          MAX=5
0076          SUMX=0.
0077          SUMX2=0.
0078          SUMY=0.
```

```
0079          SUMXY=0.
0080          DO 157 K=1,MAX
0081            READ(1,*) CKEV(K,1),CKEV(K,2)
0082            IF(CKEV(K,1).EQ.-99) GOTO 158
0083            SUMX=SUMX+CKEV(K,1)
0084            SUMX2=SUMX2+(CKEV(K,1)**2)
0085            SUMY=SUMY+CKEV(K,2)
0086            SUMXY=SUMXY+CKEV(K,1)*CKEV(K,2)
0087   157    CONTINUE
0088   158    K=K-1
0089          A1=(SUMXY-((SUMX*SUMY)/K))/(SUMX2-(SUMX**2)/K)
0090          A0=(SUMY/K)-(A1*(SUMX/K))
0091          WRITE(1,'("Y="F5.2" X+"F5.2)') A1,A0
0092    C-------------------------------------------------------------------
0093    C CALCULATE THE NUMBER OF CHANNELS/BLOCK FOR GIVEN keV/BLOCK
0094    C-------------------------------------------------------------------
0095    159    WRITE(1,'("TOTAL keV/BLOCK:  ")')
0096          READ(1,*) KEVB
0097          ICHBK=IFIX(KEVB/A1)
0098          WRITE(1,'(F7.2," keV/BLOCK = "I5" CHANNELS -- OK .")') KEVB,ICHBK
0099          READ(1,'(A2)') IANS
0100          IF(IANS.NE.2HNO) GOTO 160
0101          WRITE(1,'("TRY AGAIN?  ")')
0102          READ(1,'(A2)') IANS
0103          IF(IANS.NE.2HNO) GOTO 159
0104          GOTO 300
0105    C-------------------------------------------------------------------
0106    C CALCULATE THE NUMBER OF BLOCKS/SPECTRUM
0107    C-------------------------------------------------------------------
0108    160    NBK=I/ICHBK
0109    C-------------------------------------------------------------------
0110    C CALCULATE THE AVERAGE COUNTS AND CENTER keV IN THE HIGHEST BLOCK
0111    C-------------------------------------------------------------------
0112          N=1
0113    800    IB=NBK-N
0114          SUM=0.
0115          FIRST=I-(N*ICHBK)+1
0116          LAST=FIRST+ICHBK-1
0117          DO 900 K=FIRST,LAST
0118            SUM=SUM+DATA(K)
0119    900    CONTINUE
0120          AVE=SUM/ICHBK
0121          PEAK(1)=((FIRST*A1+A0)+(LAST*A1+A0))/2.
0122          PEAK(2)=(FIRST+LAST)/2.
0123          E=PEAK(1)/1000.
0124          CALL EFF(E,IDQ,EFM,EFT,PE,CO,PP)
0125          WRITE(1,'(" FIRST  LAST      SUM        AVE, CHANNEL")')
0126          WRITE(1,'(2I6,2X,F7.2,2X,F7.2)') FIRST,LAST,SUM,AVE
0127    C-------------------------------------------------------------------
0128    C--CALCULATE THE COMPTON EDGE
0129    C-------------------------------------------------------------------
0130          PEAK(3)=PEAK(1)-PEAK(1)/(1.+(2.*PEAK(1)/511.))
0131          PEAK(4)=(PEAK(3)-A0)/A1
0132          WRITE(1,'("PEAK ENERGY*PEAK CHANNEL*EDGE ENERGY*EDGE CHANNEL")')
0133          WRITE(1,'(4(F7.3,5X))') PEAK
0134    C-------------------------------------------------------------------
0135    C--SUBTRACT COMPTON BACKGROUND
0136    C-------------------------------------------------------------------
0137    185    DO 186 IK=1,8200
0138            COMPT(IK)=0.
0139    186    CONTINUE
0140          INEXT=IFIX(PEAK(4))
0141          P=PEAK(1)
0142          IF(KK.GT.0)GO TO 188
0143          KK=1
0144          WRITE(1,'("CHOOSE COMPTON CORRECTION COEFFICIENT(DEF=1.)")')
0145          READ(1,*) CCOEFF
0146          IF(CCOEFF.LE.0.001) CCOEFF=1.0
0147    188    H=SUM*(EFT/EFM-1.)/PEAK(4)*.86*CCOEFF
0148          WRITE(1,'("AVERAGE H=",F7.1)') H
0149          N1=INEXT/3.
0150          DO 190 II=N1,INEXT
0151            COMPT(II)=H
0152            DATA(II)=DATA(II)-(COMPT(II))
0153            IF(DATA(II).LT.0) DATA(II)=0
0154    190    CONTINUE
0155          H2=H/2.
0156          N2=4.*INEXT/3.
0157          SLOPE=(H2-0)/(INEXT-N2)
0158          WRITE(1,'("FIRST SLOPE="F7.3)') SLOPE
```

```
0159          N1=INEXT+1
0160          DO 191 II=N1,N2
0161            COMPT(II)=H2+(SLOPE*(II-N1))
0162            IF(COMPT(II).LT.0) COMPT(II)=0
0163            DATA(II)=DATA(II)-(COMPT(II))
0164            IF(DATA(II).LT.0) DATA(II)=0.
0165   191    CONTINUE
0166          N2=(INEXT/3.)-1
0167          H3=3.*H/2.
0168          SLOPE=(H3-H)/(1-N2)
0169          WRITE(1,'("SECOND SLOPE=",F7.3)') SLOPE
0170          DO 192 II=3,N2
0171            COMPT(II)=H3+(SLOPE*II)
0172            IF(COMPT(II).LT.0) COMPT(II)=0
0173            DATA(II)=DATA(II)-(COMPT(II))
0174            IF(DATA(II).LT.0) DATA(II)=0.
0175   192    CONTINUE
0176  C-------------------------------------------------------------------------
0177  C---SUBTRACT SE AND DE PEAKS
0178  C-------------------------------------------------------------------------
0179          IF(E.LT.1.022) GO TO 1910
0180          IF(KQ.GT.0) GO TO 1909
0181          KQ=1
0182          WRITE(1,'("S11 DETECTION PROBABILITY FACTOR:  ")')
0183          READ(1,*) PS11
0184   1909   R=PP/(PE+CO+PP)*1.3
0185          ESE=2.*(1.-PS11)/PS11*R
0186          EDE=((1.-PS11)/PS11)**2 *R
0187          DO 1907 K=FIRST,LAST
0188            IS=IFIX(511./A1)
0189            ID=IFIX(1022./A1)
0190            ISE=K-IS
0191            IDE=K-ID
0192            DATA(ISE)=DATA(ISE)-DATA(K)*ESE
0193            DATA(IDE)=DATA(IDE)-DATA(K)*EDE
0194   1907   CONTINUE
0195          WRITE(1,'(2I10,3F20.5)')ISE,IDE,ESE,EDE,AVE
0196   1910   DO 901 K=FIRST,LAST
0197            DATA(K)=AVE/EFM
0198   901    CONTINUE
0199          N=N+1
0200          IF(N.LT.NBK) GOTO 800
0201  C-------------------------------------------------------------------------
0202  C--ZERO OUT FIRST CHANNELS--NOT A FULL BLOCK AND STORE DATA
0203  C-------------------------------------------------------------------------
0204          DO 777 KK=1,FIRST-1
0205            DATA(KK)=0
0206   777    CONTINUE
0207   193    DO 194 JK=1,I
0208            ICHAN(JK)=IFIX(ICHAN(JK)*A1+A0)
0209   194    CONTINUE
0210          WRITE(1,'("STORING ",I5," DATA CHANNELS")') I
0211          DO 195 JK=1,I
0212            WRITE(81,*) ICHAN(JK),DATA(JK)
0213   195    CONTINUE
0214          GOTO 300
0215   200    WRITE(1,'("READ ERROR "I4" ON FILE "6A2" OPEN = ")') IOS,NAME
0216   300    CLOSE(81)
0217          WRITE(1,'(T25,"PROGRAM IS FINISHED")')
0218          WRITE(1,'(A2)') UNLOCK
0219          STOP
0220          END
```

SUBROUTINE LEAD

```
T3      T=00004 IS ON CR00026 USING 00006 BLKS R=0000

0001          SUBROUTINE LEAD(E,C)
0002    C---SUBROUTINE TO SUBTRACT LEAD COLLINATOR SCATTER
0003          COMMON COL(2100)
0004          DIMENSION MU(12),EMU(12),RANGE(40)
0005          REAL MU,MUCO
0006          DATA MU/5.2,.95,.22,.12,.086,.069,.06,.051,.045,.042,.043,.047/
0007          DATA EMU/150.,300.,500.,700.,900.,1200.,1400.,1750.,2500.,5500.,
0008         X        6500.,10000./
0009          DATA RANGE/1.9,2.1,1.5,1.6,1.6,1.6,1.5,1.8,2.2,2.2,2.2,2.2,2.4,2.3,
0010         X 2.1,2.4,2.3,2.1,2.0,2.1,1.9,2.0,1.8,1.8,1.7,1.7,1.6,1.6,1.4,1.4,
0011         X 1.3,1.25,1.25,1.3,1.3,1.3,1.3,1.25,1.25,1.3,1.3,1.3/
0012    C-------------------------------------------------------------------
0013    C--CALCULATE NET TRANSMISSION THRU COLLINATOR - 31.8G/CM**2
0014    C--DATA IS NORMALIZED TO CO-60
0015    C-------------------------------------------------------------------
0016          MUCO=0.06
0017          T=31.8
0018          IBF=30
0019          DO 10 I=1,10
0020          IF(E.LT.EMU(I)) GO TO 20
0021       10 CONTINUE
0022       20 NET=MU(I)-MUCO
0023          AB=EXP(-NET*T)
0024          DO 40 I=1,2100
0025          EC=I/C*E
0026          ED=EC/IBF
0027          J=IFIX(ED)
0028          IF(J.GT.38) GO TO 35
0029          COL(I)=AB*(RANGE(J)-1.)
0030          GO TO 40
0031       35 COL(I)=AB*0.3
0032       40 CONTINUE
0033          RETURN
0034          END
```

```
T1      T=00004 IS ON CR00026 USING 00024 BLKS R=0000

$001    FTN4X,L
0002    $FILES(2,2)
0003    $EMA(LARGE,0)
$004          PROGRAM CX(),CALCULATES EFFECTIVE CX VALUES FOR THE ICRU SPHERE
0005    C-------------------------------------------------------------------------
0006    C--DATA INTERPOLATED FROM DIMBYLOW AND FRANCIS,1979, A CALCULATION OF THE
0007    C-----PHOTON DEPTH-DOSE DISTRIBUTIONS IN THE ICRU SPHERE FOR A BROAD PARALLEL
0008    C-----BEAM.A POINT SOURCE AND AN ISOTROPIC FIELD.NAT RAD PROT BOARD,NRPB 92,
0009    C-----HARWELL,ENGLAND.
0010    C-------------------------------------------------------------------------
0011          INTEGER NAME(6),ITITLE(36),CSCRN(2),LCRSR,LOCK,UNLOCK
0012          INTEGER ICHAN(8200)
$013          DIMENSION F(5),CKEV(5,2),E(31),FL(31),CX(31,8),C(8),CT(8)
0014          COMMON/LARGE/DATA(8200),ICHAN,COMPT(2100)
0015          DATA CSCRN/15550B,15512B/
0016          DATA LCRSR/15507B/
0017          DATA LOCK/15554B/
0018          DATA UNLOCK/15555B/
0019          DATA E/15.,20.,30.,40.,50.,60.,70.,80.,90.,100.,110.,120.,130.,
0020         X140.,150.,200.,300.,400.,500.,600.,1000.,1500.,2000.,3000.,
0021         X4000.,5000.,6000.,7000.,8000.,9000.,10000./
0022          DATA FL/29.6,54.6,125.,212.,279.,304.,303.,277.,250.,226.,206.,
0023         X187.,169.,153.,139.,97.1,60.5,44.4,35.4,29.5,18.7,13.7,11.2,
0024         X8.38,6.92,5.92,5.19,4.69,4.19,3.84,3.49/
$025          DATA CX/.0,.2,.82,1.18,1.40,1.44,1.47,1.45,1.43,1.41,1.38,1.36,
0026         X1.33,1.32,1.3,1.22,1.11,1.06,1.04,1.,1.,.99,.99,.97,.95,.92,.91,
0027         X.91,.7,.89,.87,
$028         X.28,.58,1.00,1.28,1.46,1.47,1.45,1.43,1.41,1.39,1.37,
$029         X1.35,1.33,1.32,1.30,1.22,1.12,1.08,1.06,1.03,1.02,1.00,1.00,.98,
0030         X.95,.92,.91,.91,.9,.89,.87,
0031         X.67,.79,1.07,1.29,1.46,1.47,1.45,1.43,1.41,1.39,1.37,
$032         X1.35,1.33,1.32,1.30,1.22,1.12,1.08,1.06,1.03,1.02,1.00,0.99,.93,
0033         X.88,.83,.84,.85,.84,.83,.82,
0034         X.90,.94,1.11,1.34,1.50,1.52,1.5,1.48,1.45,1.43,1.4,
$035         X1.36,1.34,1.32,1.3,1.22,1.12,1.08,1.06,1.03,1.00,0.95,0.85,0.81,
0036         X.80,.79,.78,.78,.77,.76,.76,
0037         X.0,.2,.82,1.18,1.4,1.44,1.47,1.45,1.43,1.41,1.38,1.36,1.33,1.32,
0038         X1.3,1.22,1.11,1.06,1.04,1.,1.,.99,.99,.97,.95,.92,.91,.91,.85,
0039         X.75,.65,
0040         X.28,.58,1.,1.28,1.46,1.47,1.45,1.43,1.41,1.39,1.37,1.35,1.33,
0041         X1.32,1.3,1.22,1.12,1.08,1.06,1.03,1.02,1.,1.,.97,.91,.84,.75,
0042         X.63,.5,.37,.25,
0043         X.67,.79,1.07,1.29,1.46,1.47,1.45,1.43,1.41,1.39,1.37,1.35,1.33,
0044         X1.32,1.3,1.22,1.12,1.08,1.06,1.03,.95,.65,.41,.36,.32,.28,.25,
0045         X.21,.17,.13,.1,
$046         X.9,.94,1.11,1.34,1.5,1.52,1.5,1.47,1.42,1.37,1.32,1.25,1.21,1.15
0047         X.1.09,.92,.67,.54,.39,.25,.17,.13,.12,.11,.11,.1,.09,.08,.07,.06
0048         X,.05/
0049    C-------------------------------------------------------------------------
0050    C--GET THE DATA FILE NAME AND LU
0051    C-------------------------------------------------------------------------
0052          WRITE(1,'(2A2,/,T25,"SPECTRUM ANALYSIS PROGRAM",/)') CSCRN
0053          WRITE(1,'(A2)') LOCK
0054     100  WRITE(1,'("ENTER FILE NAME (SIX CHARACTERS MAX):  ")')
0055          READ(1,'(6A2)') NAME
0056          OPEN(80,FILE=NAME,IOSTAT=IOS,ERR=200)
$057    C-------------------------------------------------------------------------
0058    C--READ THE TITLE OF THE FILE
0059    C-------------------------------------------------------------------------
0060          READ(80,'(36A2)') ITITLE
0061          WRITE(1,'(2A2,36A2,/)') CSCRN,ITITLE
0062          WRITE(1,'("IS THIS THE FILE YOU WANT?? ")')
0063          READ(1,'(A2)') IANS
0064          IF(IANS.NE.2HNO) GOTO 110
0065          CLOSE(80)
0066          GOTO 100
0067    C-------------------------------------------------------------------------
0068    C--READ THE DATA FROM THE FILE
0069    C-------------------------------------------------------------------------
0070     110  WRITE(1,'("GETTING DATA FROM FILE: "6A2)') NAME
$071          DO 120 I=1,8500
$072            READ(80,*,END=130) ICHAN(I),DATA(I)
$073            WRITE(1,'(I4,5X,F7.0,A2," ")') ICHAN(I),DATA(I),LCRSR
0074     120  CONTINUE
0075     130  I=I-1
$076          WRITE(1,'(I5," DATA ITEMS READ")') I
0077          CLOSE(80)
0078    C-------------------------------------------------------------------------
```

```
0079  C--CALCULATE CX VALUES
0080  C-------------------------------------------------------------------
0081        RT=0.
0082        DO 8 K=1,8
0083   8    CT(K)=0.
0084        DO 30  J=3,2048
0085        EN=ICHAN(J)
0086        DO 10 I=1,31
0087        IF(EN.LT.E(I))GO TO 20
0088   10   CONTINUE
0089   20   IG=I
0090        IF(IG.LT.2)GO TO 30
0091        EI=(E(IG)-EN)/(E(IG)-E(IG-1))
0092        F=-(FL(IG)-FL(IG-1))*EI + FL(IG)
0093        DO 25 K=1,8
0094   25   C(K)=CX(IG,K)-(CX(IG,K)-CX(IG-1,K))*EI
0095        R=   DATA(J)/F
0096        RT=RT+R
0097        DO 28 K=1,8
0098   28   CT(K)=CT(K)+R*C(K)
0099   30   CONTINUE
0100        DO 32 K=1,8
0101   32   C(K)=CT(K)/RT
0102        WRITE(1,'("CX FACTORS FOR THE ICRU SPHERE, PLANE PARALLEL INCIDENC
0103       XE.",/,"VALUES INTERPOLATED FROM DINBYLOW AND FRANCIS.")')
0104        WRITE(1,'(/"MAXIMUM VALUES: 2.5CM = ",F5.2,/,16X,"DEEP  = ",
0105       XF5.2,/,16X,"0.3CM = ",F5.2,/,16X,"SHALL = ",F5.2,//"CENTRAL VALUES
0106       X: 2.5CM = ",F5.2,/,16X,"DEEP  = ",F5.2,/,16X,"0.3CM = ",F5.2,/,
0107       X16X,"SHALL = ",F5.2)') C
0108        WRITE(1,'(/"TOTAL EXPOSURE = ",E10.4,"  10**-8 R*CM**2")')RT
0109        GO TO 300
0110   200  WRITE(1,'("READ ERROR "I4" ON FILE "6A2" OPEN = ")') IOS,NAME
0111   300  CLOSE(80)
0112        WRITE(1,'(/,T25,"PROGRAM IS FINISHED")')
0113        WRITE(1,'(A2)') UNLOCK
0114        STOP
0115        END
0116
```

```
T2      T=00004 IS ON CR00026 USING 00042 BLKS R-0000

0001   FTN4,L
0002   $FILES(3,4)
0003         PROGRAM POLY( ), PHANTOM DATA ANALYSIS
0004   C
0005   C     THIS PROGRAM ANALYSES DATA FROM THE PLEXIGLASS TLD PHANTOM.
0006   C     TLD DATA IS ENTERED ALONG WITH THE CALIBRATION AND BACKGROUND;
0007   C     IF THE GEOMETRY IS A POINT SOURCE, AN INVERSE R2 CORRECTION
0008   C     IS APPLIED.  THE PROGRAM THEN FITS EXISTING CALIBRATIONS FOR
0009   C     THE PHANTOM TO THE DATA, TO DETERMINE THE RELATIVE CONTRIBUTIONS
0010   C     OF THE  COMPONENTS.
0011   C
0012   C     NOTE: AN OPTION ALLOWS OMISSION OF ANY TWO COMPONENTS.
0013   C
0014         REAL X,D(11),SKIP(11)
0015         REAL T(11,5),R(11),CXS(5),CXD(5),C(11,11),A(6,7),FRAC(5),DIST
0016         INTEGER EN(6,3),TITLE,ICNT,GEOM,NAME(3),ANS,MODE,SCAL,TYPE,TNUM
0017         INTEGER SCAL1
0018         DATA D/0.0,0.48,0.95,1.43,1.91,3.02,5.08,7.14,0.48,1.91,7.14/
0019   C
0020   C     ENTER DATA
0021         WRITE (1,10)
0022      10 FORMAT ("1",///,T15,"PLEXIGLASS TLD PHANTOM DATA ANALYSIS",///)
0023         WRITE (1,500)
0024         MODE=2                !DEFAULT VALUE
0025     500 FORMAT (//,T7,"PHANTOM DATA OR MODIFIED TMI DOSIMETER?",/,
0026        +    T7,"  (ENTER 2 FOR PHANTOM, 1 FOR MODIFIED TMI)      ")
0027         READ (1,'(I1)') MODE
0028         TNUM=8
0029         IF (MODE.EQ.2) WRITE (1,520)
0030     520 FORMAT (//,T7,"TLD-700 ONLY (ENTER 1)",
0031        +    " OR BOTH TLD-700 AND TLD-400 (ENTER 2) ?    ")
0032         READ (1,*) TYPE
0033         IF (TYPE.EQ.2) TNUM=TNUM+3     !11 READINGS IF CaF:Mn INCLUDED
0034   C
0035         MODE=MODE+2             !NUMBER OF ENTRIES PER LINE
0036         WRITE (1,11)
0037      11 FORMAT (//,T7,"IS DATA IN A FILE?     ")
0038         READ (1,12) ANS
0039      12 FORMAT (A1)
0040         IF (ANS.NE.1HY) GO TO 19
0041   C
0042   C     DATA IN A FILE
0043         WRITE (1,13)
0044      13 FORMAT (///T7,"ENTER 6 CHARACTER FILE NAME     ")
0045         READ (1,14) (NAME(I),I=1,3)
0046      14 FORMAT (3A2)
0047         OPEN (89,FILE=NAME)
0048         READ (89,12) ANS          !IGNORE FILE HEADING
0049         DO 16 J=1,TNUM
0050         READ (89,*) (T(J,K),K=1,MODE)
0051      16 CONTINUE
0052         CLOSE (89)
0053         GO TO 28
0054   C
0055   C     DATA FROM TERMINAL
0056      19 WRITE (1,20)
0057      20 FORMAT (///,T7,"ENTER OBSERVED TLD READINGS (FOUR) FOR EACH "
0058        +    "DEPTH.",/,T7,"(NOTE: VALUES OF ZERO WILL BE IGNORED)",/)
0059         DO 27 J=1,TNUM
0060         WRITE (1,25) J
0061      25 FORMAT (T7,"POSITION ",I1,":     ")
0062      27 READ (1,*) (T(J,K),K=1,MODE)
0063   C
0064   C     AVERAGE VALUES FOR EACH POSITION
0065      28 DO 40 J=1,TNUM
0066         SUM=0.
0067         CNT=1.0*MODE
0068         DO 30 K=1,MODE
0069         SUM=SUM+T(J,K)
0070         IF (T(J,K).EQ.0.) CNT=CNT-1.0     !IGNORE ZERO VALUES
0071      30 CONTINUE
0072         IF (CNT.EQ.0.) CNT=CNT+1.0     !(NO DIVISION BY ZERO)
0073         R(J)=SUM/CNT
0074      40 CONTINUE
0075         WRITE (1,50)
0076      50 FORMAT (//,T7,"ENTER TLD BACKGROUND  NC(700,400):    ")
0077         READ (1,*) BKG,BKG4
0078         BK=BKG
```

```
0079          WRITE (1,'(////,T7,"BACKGROUND SUBTRACTED VALUES",//)')
0080          DO 60 J=1,INUM                                    !SUBTRACT BACKGROUND
0081          IF(J.GT.8)BK=BKG4
0082          R(J)=R(J)-BK
0083          IF (R(J).LT.0.0) R(J)=0.
0084          WRITE (1,*) R(J)
0085       60 CONTINUE
0086  C
0087  C       CORRECT FOR SOURCE GEOMETRY
0088  C
0089          WRITE (1,62)
0090       62 FORMAT (///,T7,"OPTIONAL GEOMETRY CORRECTION:",
0091         +          //,T9,"1.  NO CORRECTION (UNIFORM FIELD)",
0092         +           /,T9,"2.  1/R CORRECTION (LINE SOURCE)",
0093         +           /,T9,"3.  1/R**2 CORRECTION (POINT SOURCE)",
0094         +          //,T7,"ENTER OPTION DESIRED (1,2 OR 3)    ")
0095          READ(1,64) GEOM
0096       64 FORMAT(I1)
0097          IF(GEOM.EQ.0)GEOM=1    !DEFAULT
0098          IF (GEOM.EQ.1) GO TO 68
0099          WRITE (1,66)
0100       66 FORMAT (//,T7,"ENTER DISTANCE FROM SOURCE TO PHANTOM (CM)     ")
0101          READ (1,*) DIST
0102          CALL GEOMR(R,DIST,GEOM,INUM)
0103       68 CONTINUE
0104  C
0105  C       NORMALIZE TO 0.5 CM AND DISPLAY TLD RESULTS
0106          WRITE (1,'(////)')
0107          DO 72 J=1,INUM
0108          X=R(J)/R(2)
0109          WRITE (1,*) D(J),R(J),X
0110       72 CONTINUE
0111  C
0112  C       READ CALIBRATION VALUES FROM FILE
0113  C
0114  C       OPTION TO IGNORE A CALIBRATION
0115          WRITE (1,1070)
0116     1070 FORMAT (//,T7,"ENTER CALIBRATIONS TO BE SKIPPED (/E FOR NONE)    ")
0117          READ (1,'(2A2)')  SCAL,SCAL1
0118  C
0119          IF (MODE.EQ.3) THEN
0120          OPEN (12,FILE='TCALIB')
0121          ELSE
0122          OPEN (12,FILE='PCAL')
0123          ENDIF
0124          READ (12,70) TITTLE                               !FILE HEADING
0125       70 FORMAT (A1)
0126          ICNT=0
0127          DO 90 I=1,5
0128          READ (12,80,END=100) (EN(I,L),L=1,3)      !READ CALIBRATION SOURCE
0129       80 FORMAT (3A2)
0130          IF ((EN(I,1).EQ.SCAL).OR.(EN(I,1).EQ.SCAL1)) THEN  !OPTION TO SKIP CALIB
0131          READ (12,*) CS,CD                                 !IGNORE DATA IF SKIPPED
0132          READ (12,*) (SKIP(J),J=1,INUM)
0133          ELSE
0134          ICNT=ICNT+1
0135          READ (12,*) CXS(I),CXD(I)                         !SHALLOW AND DEEP CX
0136          READ (12,*) (C(ICNT,J),J=1,INUM)                  !TLD READINGS FOR 1R OR 1 RAD
0137          DO 88 L=1,3
0138       88 EN(ICNT,L)=EN(I,L)
0139          ENDIF
0140       90 CONTINUE
0141    100 CONTINUE
0142  C
0143  C       DETERMINE CROSS PRODUCTS
0144  C       AND SET UP MATRIX FOR SIMULTANEOUS EQUATION SOLUTION
0145  C       BY GAUSSIAN ELIMINATION.
0146  C
0147  C       THE INPUT MATRIX HAS DIMENSIONS ICNT BY ICNT+1, WHERE
0148  C         ICNT IS THE NUMBER OF CALIBRATIONS
0149  C
0150          N=ICNT+1
0151  C       SET MATRIX TO ZERO
0152          DO 120 I=1,ICNT
0153          DO 110 J=1,N
0154    110   A(I,J)=0.0
0155    120   CONTINUE
0156  C       CALCULATE CROSS PRODUCTS
0157          DO 180 I=1,ICNT          ! I=ROW NUMBER
0158          DO 160 J=1,ICNT          ! J=COLUMN NUMBER
```

```
0159          DO 140 L=1,TNUM          ! L=DEPTH (POSITION IN PHANTOM)
0160          A(I,J)= A(I,J) + C(I,L)*C(J,L)
0161      140 CONTINUE
0162      160 CONTINUE
0163      180 CONTINUE
0164  C
0165          DO 200 I=1,ICNT              !LAST COLUMN OF MATRIX
0166          DO 190 L=1,TNUM
0167      190 A(I,N)=A(I,N)+R(L)*C(I,L)
0168      200 CONTINUE
0169  C
0170  C       PRINT INTERMEDIATE VALUES
0171          DO 205 L=1,ICNT
0172          WRITE (1,*) (A(L,LL),LL=1,N)
0173      205 CONTINUE
0174          CLOSE (12)
0175  C
0176  C       SOLVE FOR COEFFICIENTS
0177          CALL MATRX(ICNT,A)              !ANSWERS ARE NOW IN LAST COLUMN OF A
0178  C
0179  C       DISPLAY RESULTS
0180          WRITE (1,'(///)')
0181          DO 230 L=1,ICNT
0182      230 WRITE (1,240) (EN(L,J),J=1,3),A(L,N)
0183      240 FORMAT (I7,3A2,2X,F6.3,/)
0184          END
0185  C
0186  C
0187          SUBROUTINE GCORR(R,DIST,GEOM,TNUM)
0188          REAL R(11),DIST,D(11)
0189          INTEGER GEOM,EXP,TNUM
0190          DATA D/0.0,0.48,0.95,1.43,1.91,3.02,5.08,7.14,0.48,1.91,7.14/
0191          EXP=GEOM-1
0192          DO 10 I=1,TNUM
0193          R(I)=R(I)*(((DIST+D(I))/(DIST))**EXP)
0194       10 CONTINUE
0195          IF (TNUM.EQ.8) WRITE (1,20) (R(I),I=1,8)
0196          IF (TNUM.EQ.11) WRITE (1,25) (R(I),I=1,11)
0197       20 FORMAT (//,T7,"CORRECTED READINGS: ",/,T9,8(F5.0,1X))
0198       25 FORMAT (//,T7,"CORRECTED READINGS: ",/,T9,11(F5.0,1X))
0199          RETURN
0200          END
0201  C
0202  C
0203          SUBROUTINE MATRX(M,A)
0204          REAL A(6,7)
0205          INTEGER N,M
0206  C*****************************************************************************
0207  C                                                                            *
0208  C       G O D D A R D   C O M P U T E R   S C I E N C E   I N S T I T U T E  *
0209  C                                                                            *
0210  C       (1) SUBROUTINE NAME,          SIMULTANEOUS EQUATION SOLVER           *
0211  C       (2) CALLING NAME,             SIMEQ                                  *
0212  C       (3) STATUS/CHANGE LEVEL,      PGM.= GCSL013, PCR.= 00-10-65          *
0213  C       (4) PROGRAMMED BY,            GRETCHEN PHILLIPS                      *
0214  C       (5) ADAPTED TO HP FORMAT      ROLAND JAHN 02-70                      *
0215  C                                                                            *
0216  C            SUPPORTED IN PART BY GRANT NO. FR00197 BY THE                   *
0217  C            SPECIAL RESEARCH RESOURCES BRANCH, NIH-USPHS.                   *
0218  C                                                                            *
0219  C*****************************************************************************
0220  C                                                                            *
0221  C            SUPPORTED IN PART BY GRANT NO. FR00197 BY THE                   *
0222  C            SPECIAL RESEARCH RESOURCES BRANCH, NIH-USPHS.                   *
0223  C                                                                            *
0224  C*****************************************************************************
0225  C       INSTRUCTIONS FOR USE:
0226  C          This program will handle a maximum of 22 equations. The number
0227  C       of coefficients per equation must be equal to the (number of
0228  C       equations + 1); i.e. an augmented matrix. The input data may be
0229  C       entered in any form subject to the ordering restriction; the
0230  C       format being specified by the user in his/her program. The
0231  C       ordering restriction is that the input coefficients of the ith
0232  C       equation must (a) be placed in ascending sequence, A(1,J),....
0233  C       A(I,J),... and (b) the coefficients for the (I+1)th equation
0234  C       must begin on a new line.
0235  C
0236  C       The array A contains the input coefficients and is passed in
0237  C       COMMON. The number of equations (N) is passed to the subroutine
0238  C       by the call statement- CALL SSIME(M) (M (or=22). The resultant
```

```
0239  C      values are found in the (M+1)th elements of the array A; i.e.,
0240  C      variable 1 = (1,M+1), variable 2 = (2,M+1), variable M = (M,M+1).
0241  C-----------------------------------------------------------------------
0242  C
0243         N=M+1
0244         I1=1
0245      10 I3=I1
0246         SUM=ABS(A(I1,I1))
0247         DO30I=I1,M
0248         IF(SUM-ABS(A(I,I1)))20,30,30
0249      20 I3=I
0250         SUM=ABS(A(I,I1))
0251      30 CONTINUE
0252         IF(I3-I1)40,60,40
0253      40 DO 50J=1,N
0254         SUM=-A(I1,J)
0255         A(I1,J)=A(I3,J)
0256      50 A(I3,J)=SUM
0257      60 I3=I1+1
0258         DO70I=I3,M
0259      70 A(I,I1)=A(I,I1)/A(I1,I1)
0260      80 J2=I1-1
0261         I3=I1+1
0262         IF(J2)90,110,90
0263      90 DO100J=I3,N
0264         DO100I=1,J2
0265     100 A(I1,J)=A(I1,J)-A(I1,I)*A(I,J)
0266         IF(I1-M)110,130,110
0267     110 J2=I1
0268         I1=I1+1
0269         DO120I=I1,M
0270         DO120J=1,J2
0271     120 A(I,I1)=A(I,I1)-A(I,J)*A(J,I1)
0272         IF(I1-M)10,80,10
0273     130 DO150I=1,M
0274         J2=M-I
0275         I3=J2+1
0276         A(I3,N)=A(I3,N)/A(I3,I3)
0277         IF(J2)140,160,140
0278     140 DO150J=1,J2
0279     150 A(J,N)=A(J,N)-A(I3,N)*A(J,I3)
0280     160 RETURN
0281         END
```

DISTRIBUTION

No. of Copies

OFFSITE

10 R. B. Neel
Occupational Radiation Protection Branch
Office of Nuclear Regulatory Research
ML-5650
U.S. Nuclear Regulatory Commission
Washington, DC 20555

U.S. Nuclear Regulatory Commission
Division of Technical Information and Document Control
7920 Norfolk Ave.
Bethesda, MD 20014

K. L. Holbrook
265 El Dorado Blvd., No. 713
Webster, TX 77598

No. of Copies

ONSITE

50 Pacific Northwest Laboratory

J. L. Baer
L. W. Brackenbush
F. M. Cummings
G. W. R. Endres
R. A. Fox
W. A. Glass
D. L. Haggard
G. R. Hoenes
J. C. McDonald
L. A. Rathbun
P. L. Roberson (33)
Technical Information (5)
Publishing Coordination (2)

NRC FORM 335 (11-81)

U.S. NUCLEAR REGULATORY COMMISSION

BIBLIOGRAPHIC DATA SHEET

1. REPORT NUMBER (Assigned by DDC)
NUREG/CR-3569
PNL-4915

4. TITLE AND SUBTITLE (Add Volume No., if appropriate)
Spectral and Dosimetric Measurements of Photon Fields at Commercial Nuclear Sites

2. (Leave blank)

3. RECIPIENT'S ACCESSION NO.

7. AUTHOR(S)
PL Roberson RA Fox KL Holbrook
GWR Endres DL Haggard LA Rathbun

5. DATE REPORT COMPLETED
MONTH: December YEAR: 1983

9. PERFORMING ORGANIZATION NAME AND MAILING ADDRESS (Include Zip Code)
Pacific Northwest Laboratory
Richland, WA 99352

DATE REPORT ISSUED
MONTH: August YEAR: 1984

6. (Leave blank)

8. (Leave blank)

12. SPONSORING ORGANIZATION NAME AND MAILING ADDRESS (Include Zip Code)
Division of Facility Operations
Office of Nuclear Regulatory Research
U.S. Nuclear Regulatory Commission
Washington, DC 20555

10. PROJECT/TASK/WORK UNIT NO.

11. FIN NO.
NRC FIN No. B2419

13. TYPE OF REPORT
Research Report

PERIOD COVERED (Inclusive dates)

15. SUPPLEMENTARY NOTES

14. (Leave blank)

16. ABSTRACT (200 words or less)

Spectral and dosimetric measurements of photon fields were performed at seven commercial nuclear reactor sites. Revisions to 10 CFR 20 that specify exposure-to-dose conversion factors (C_x) much greater than unity for photons between 40 keV and 200 keV could impact personnel monitoring practices. Monitoring at effective depths of 1 cm of tissue and shallower could underestimate doses received from high-energy photon fields (>3 MeV).

No locations with large C_x factors (approximately 1.5 rad/R) were found. The most significant production of low-energy photons was found to be due to photon scattering. The scatter continuum has an effective C_x factor of approximately 1.2 rad/R. One location was found with a nearly pure scatter spectrum. Other locations contained significant contributions from medium-energy photons due primarily to radioactive decay of cobalt and cesium isotopes. Monitoring requirements at 0.007-cm and 1.0-cm depths in tissue were found to be adequate for estimating dose received in radiation fields containing high-energy photons. Enhanced surface doses attributed to high-energy knock-on electrons were measured in all locations monitored. Personnel monitoring techniques may provide inaccurate results in high-energy fields.

17. KEY WORDS AND DOCUMENT ANALYSIS

17a. DESCRIPTORS

Photons, Gamma ray, Dosimetry
Radiation measurement, Gamma Spectrometers

17b. IDENTIFIERS/OPEN-ENDED TERMS

18. AVAILABILITY STATEMENT
Unlimited

19. SECURITY CLASS (This report)
Unclassified

21. NO. OF PAGES

20. SECURITY CLASS (This page)
Unclassified

22. PRICE
$

NRC FORM 335 (11-81)

UNITED STATES
NUCLEAR REGULATORY COMMISSION
WASHINGTON, D.C. 20555

120555078877 1 1AN
US NRC
ADM-DIV OF TIDC
POLICY & PUB MGT BR-PDR NUREG
W-501
WASHINGTON DC 20555